THE DEVELOPMENT AND APPLICATION OF ANALYTICAL METHODS BASED ON MULTI-COLLECTOR INDUCTIVELY COUPLED PLASMA-MASS SPECTROMETRY (MC-ICP-MS) FOR HIGH-PRECISION ISOTOPIC ANALYSIS OF Fe IN HUMAN BLOOD AND SERUM APPLICABLE TO BIOMEDICAL INVESTIGATIONS

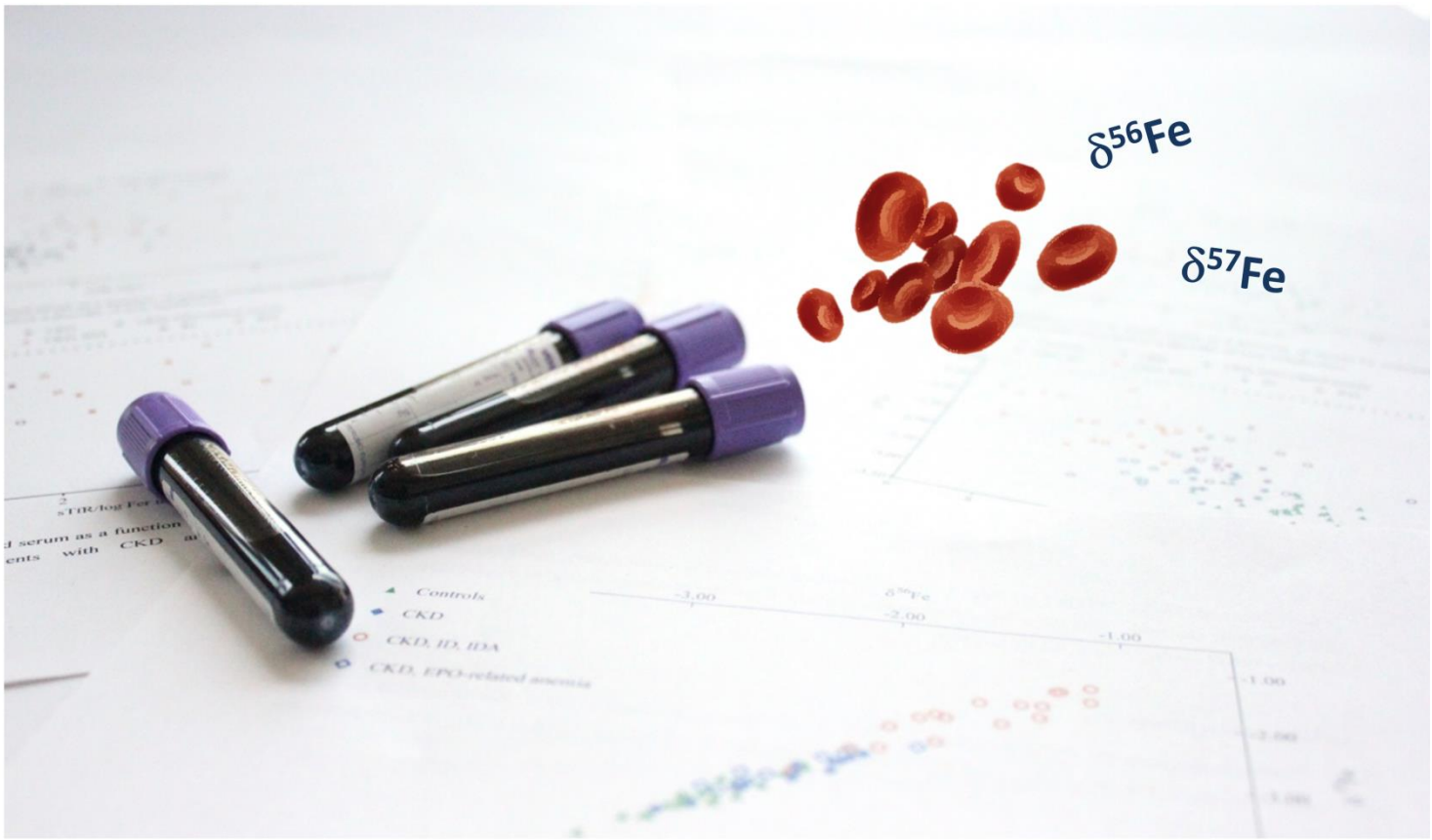

Yulia Anoshkina

Supervisor:
Prof. Dr. Frank Vanhaecke

FACULTY OF SCIENCES

DEPARTMENT OF ANALYTICAL CHEMISTRY
ATOMIC AND MASS SPECTROMETRY (A&MS)

THE DEVELOPMENT AND APPLICATION OF ANALYTICAL METHODS BASED ON MULTI-COLLECTOR INDUCTIVELY COUPLED PLASMA-MASS SPECTROMETRY (MC-ICP-MS) FOR HIGH-PRECISION ISOTOPIC ANALYSIS OF Fe IN HUMAN BLOOD AND SERUM APPLICABLE TO BIOMEDICAL INVESTIGATIONS

Yulia Anoshkina
Student number: 01302310

Supervisor: Prof. Dr. Frank Vanhaecke

A dissertation submitted to Ghent University in partial fulfilment of the requirements for the degree of Doctor of Science: Chemistry

Academic year: 2016 - 2017

GHENT UNIVERSITY

TABLE OF CONTENTS

List of abbreviations 1

Aim and outline 5

Doelstelling en overzicht 9

Impact and scientific outcomes 13

Chapter 1 General Introduction 17

1.1 Human iron metabolism 17

1.1.1 Intestinal iron absorption 19

1.1.2 Erythroid iron metabolism 21

1.1.3 Iron homeostasis in the liver 22

1.1.4 Disorders of iron metabolism 25

1.2 Principles of ICP-mass spectrometry 29

1.2.1 Principle design of ICP-MS 29

1.2.2 Multi-collector ICP-MS 41

1.2.3 Correction for instrumental mass discrimination 42

1.2.4 Overcoming spectral interferences 44

1.3 Iron isotopic variability in a biomedical context 48

1.4 References 53

Chapter 2 Iron isotopic analysis of human whole blood by sector-field inductively coupled plasma-mass spectrometry for iron absorption studies with a stable isotopic tracer 63

2.1 Introduction 65

2.2 Experimental 67

2.2.1 Materials and reagents 67

2.2.2 Samples and sample preparation 68

2.2.3 Instrumentation and measurements 69
2.3 Results and discussion 71
2.3.1 Iron isotope ratios *via* SF-ICP-MS 71
2.3.2 Iron isotope ratios *via* MC-ICP-MS 73
2.3.3 Study of the iron absorption via SF-ICP-MS 76
2.4 Conclusions 81
2.5 References 81
Chapter 3 High-precision iron isotopic analysis of whole blood for biomedical purposes without prior isolation of the target element 85
3.1 Abstract 86
3.2 Introduction 87
3.3 Experimental 89
3.3.1 Reagents and standards 89
3.3.2 Instrumentation and measurements 89
3.3.3 Samples and sample preparation 91
3.4 Results and discussion 92
3.4.1 Evaluation of the effect of concomitants using synthetic solutions 92
3.4.2 Optimization of experimental conditions using actual whole blood 94
3.4.3 Application to human blood samples 96
3.5 Conclusions 98
3.6 Acknowledgements 98
3.7 References 98
Chapter 4 Iron isotopic analysis of finger-prick and venous blood by multi-collector inductively coupled plasma-mass spectrometry after volumetric absorptive microsampling 101
4.1 Abstract 102
4.2 Introduction 103
4.3 Experimental 105
4.3.1 Materials and reagents 105
4.3.2 Samples and sample preparation 106
4.3.3 Instrumentation and measurements 107
4.4 Results and discussion 109
4.4.1 Iron determination 109

4.4.2 Iron isotopic analysis 111
4.4.3 Stability of blood samples in the VAMS device 114
4.4.4 Finger-prick *versus* venous blood 114
4.5 Conclusions 116
4.6 Acknowledgements 118
4.7 References 118
4.8 Supplementary information 121
Chapter 5 Natural iron isotope fractionation in an intestinal Caco-2 cell line model 123
5.1 Abstract 124
5.2 Introduction 125
5.3 Experimental 127
5.3.1 Reagents and standards 127
5.3.2 Cell culture and sample harvesting 128
5.3.3 Sample preparation 128
5.3.4 Instruments and measurements 130
5.4 Results and discussion 132
5.4.1 Optimization of the *in vitro* enterocyte model 132
5.4.2 Natural iron isotope fractionation accompanying iron fluxes through the cells 135
5.4.3 Presence/absence of apo-Tf in the basal compartment 139
5.4.4 Natural iron isotope fractionation of the specific non-heme iron uptake pathway 141
5.5 Conclusions 142
5.6 Acknowledgements 142
5.7 References 142
5.8 Supplementary information 146
Chapter 6 Iron isotopic composition of age-separated erythrocytes 147
6.1 Introduction 149
6.2 Experimental 150
6.2.1 Materials and reagents 150
6.2.2 Samples and sample preparation 151
6.2.3 Instrumentation and measurements 154
6.3 Results and discussion 156

6.3.1 Analytical method validation 156
6.3.2 Iron isotopic composition of erythrocytes 158
6.4 Conclusions 160
6.5 References 160
Chapter 7 Iron isotopic composition of blood serum in anemia of chronic kidney disease ... 163
7.1 Abstract 164
7.2 Introduction 165
7.3 Experimental 167
7.3.1 Materials and reagents 167
7.3.2 Samples 168
7.3.3 Sample preparation 168
7.3.4 Instrumentation and measurements 169
7.3.5 Statistical Methods 170
7.4 Results and discussion 171
7.4.1 Method validation 171
7.4.2 Fe isotopic composition in serum samples 171
7.4.3 Correlations with clinical parameters 174
7.5 Conclusions 178
7.6 Acknowledgements 178
7.7 Author contributions 178
7.8 References 179
7.9 Supplementary information 183
Summary and conclusions 191
Acknowledgements 195
Appendix A: The main biomedical indicators of iron status and kidney function 199

LIST OF ABBREVIATIONS

AAS	Atomic Absorption Spectrometry
AC	Alternating Current
ACD	Anemia of Chronic Disease
CKD	Chronic Kidney Disease
CRP	C-Reactive Protein
DC	Direct Current
Dcytb	Duodenal Ferrireductase Enzyme
DMT-1	Divalent Metal Ion Transporter-1
DRC-ICP-MS	Dynamic Reaction Cell Inductively Coupled Plasma-Mass Spectrometry
eGFR	Estimated Glomerular Filtration Rate
EPO	Erythropoietin
ETV	Electro-Thermal Vaporization
ESA	Erythropoiesis Stimulating Agent
ESRD	End-Stage Renal Disease
Fer	Ferritin
FID	Functional Iron Deficiency
Hb	Hemoglobin

HCP1	Heme Carrier Protein 1
HCT	Hematocrit
HH	Hereditary Hemochromatosis
HSCs	Hematopoietic Stem Cells
ICP	Inductively Coupled Plasma
ICP-MS	Inductively Coupled Plasma-Mass Spectrometry
ICP-OES	Inductively Coupled Plasma-Optical Emission Spectrometry
ID	Iron Deficiency
IDA	Iron Deficiency Anemia
IRMM	Institute for Reference Materials and Measurements
KDIGO	Kidney Disease: Improving Global Outcomes
LA	Laser Ablation
MC-ICP-MS	Multi-Collector Inductively Coupled Plasma-Mass Spectrometry
NICE	National Institute for Health and Clinical Excellence
NTBI	Non-transferrin bound iron
PFA	Perfluoroalkoxy
Q-MS	Quadrupole Mass Spectrometer
RBC	Red Blood Cells
RE	Reticuloendothelial
RF	Radio Frequency
RSD	Relative Standard Deviation
SCr	Serum Creatinine

SEM	Secondary Electron Multiplier
SF-ICP-MS	Sector-Field Inductively Coupled Plasma-Mass Spectrometry
SSB	Sample-Standard Bracketing
sTfR	Soluble Transferrin Receptor
Tf	Transferrin
TfR	Transferrin Receptor
TIBC	Total Iron-Binding Capacity
TIMS	Thermal Ionization Mass Spectrometry
TOF-MS	Time-of-Flight Mass Spectrometer
TSAT	Transferrin Saturation
VAMS	Volumetric Absorptive Microsampling
WHO	World Health Organization

AIM AND OUTLINE

Essential mineral elements show natural variations in their isotopic composition as a result of isotope fractionation accompanying physical processes and/or (bio)chemical reactions, *i.e.* isotopes of the same element do not take part with exactly the same extent to these processes/reactions. For tracing down and quantifying the resulting small differences in isotopic composition, multi-collector inductively coupled plasma-mass spectrometry (MC-ICP-MS) is the preferred technique. MC-ICP-MS combines a highly efficient ion source, with simultaneous monitoring of the isotopes of interest, thus providing highly precise isotope ratio data (relative standard deviation down to 0.002%).

Currently, high-precision isotopic analysis of essential mineral elements, in particular iron (Fe), is gaining attention as a potential tool for providing insight into metabolism and for tracing down related diseases. Therefore, the overall aim of this work has been to contribute to the development of analytical methods based on ICP-mass spectrometry for iron isotopic analysis of human whole blood and serum for biomedical applications. Specifically, the possibility to simplify the sample preparation by analyzing whole blood samples without prior chromatographic separation of iron from the blood matrix, as well as, the potential use of a novel whole blood volumetric absorptive microsampling (VAMS) technique followed by a miniaturized chromatographic iron isolation procedure were investigated. Another part of this work focused on obtaining an improved insight into the mechanism of natural isotope fractionation accompanying intestinal absorption of iron using enterocyte-like cells *in vitro* and into the possible effect of the aging process of erythrocytes (separated according to their density) on their iron isotopic composition. Finally, high-precision serum iron isotopic analysis was assessed as a potential tool to distinguish different disorders related to iron metabolism in patients with renal insufficiency. For the ease of reading, the chapters were placed in order of analytical development and application rather than in chronological order.

In **Chapter 1**, a brief introduction on iron metabolism and related disorders is provided. The literature on the iron isotopic composition of human body fluids, and the use of animal models for the understanding of iron metabolism is presented. The principles of ICP-MS and, particularly, of MC-ICP-MS instrumentation, are also provided.

Iron isotopic analysis is valuable for nutritional studies, *e.g.*, for studies focused on the development of novel types of iron supplements. In general, isotopically labeled supplements are used to decipher the actual iron intestinal absorption. In **Chapter 2**, the iron isotopic analysis of whole blood by single-collector sector-field ICP-MS in the context of a human absorption study is described. It has been demonstrated that, although the precision obtained using SF-ICP-MS is lower than that achieved with MC-ICP-MS, iron isotope ratios obtained *via* SF-ICP-MS show a precision that is adequate to be used in this context, even when sample preparation is limited to acid digestion and adequate dilution. The isotopic composition of iron in whole blood obtained using both techniques were in a good agreement. However, SF-ICP-MS cannot replace MC-ICP-MS for measurements of natural Fe isotope variations due to significantly lower precision.

As described in Chapter 1, a clear link between the Fe isotopic composition of whole blood and an individual's iron status has been established. Thus, the Fe isotopic composition provides valuable clinical information and to fully exploit this, the development of simple and reliable methodologies for the high-precision isotopic analysis of biological fluids, providing high sample throughput, are required. In general, the reference procedure for sample preparation prior to Fe isotopic analysis *via* MC-ICP-MS consists of acid digestion and the chromatographic isolation of the target analyte from the blood matrix. This procedure is laborious, time-consuming and costly. In **Chapter 3**, the possibility of Fe isotopic analysis of whole blood by MC-ICP-MS without isolation of the analyte element, *i.e*. directly after acid digestion and adequate dilution of the sample digest, was evaluated. The influence of the main mineral matrix elements and the effect of potentially remaining organic compounds were systematically evaluated. The results obtained for whole blood samples analyzed directly after acid digestion compared well to those after chromatographic Fe isolation. This approach can be suggested for specific clinical applications that require a prompt response.

Routine use of the approach proposed in Chapter 3, can result in overburdening of the MC-ICP-MS instrument. Therefore, in **Chapter 4**, an alternative approach to increase sample throughput has been proposed, based on the use of a novel whole blood volumetric absorptive

microsampling technique (VAMS), which overcomes the issues associated with the hematocrit level and sample inhomogeneity that occur in dried blood spots analysis. This fast, inexpensive, minimally invasive and straightforward sample collection technique allows to facilitate sample acquisition by self-collection and shipping of finger-prick whole blood samples by the patients, with the possibility to store the VAMS tips at different temperatures for a reasonable time without effect on the Fe isotope ratios. In order to simplify and optimize the sample preparation preceding high-precision Fe isotope ratio measurements, a miniaturized chromatographic isolation protocol has been developed. It provided quantitative recovery of the target element, thus avoiding any effect from on-column fractionation, and resulted in a significant reduction in the consumption of expensive ultrapure acids and proved beneficial in terms of time. The suitability of the VAMS device for high-precision Fe isotopic analysis and quantitative iron assay after storage under different conditions was studied. Results for simultaneously collected finger-prick and venous whole blood samples compared well, thus demonstrating the possibility of using VAMS for high-precision isotopic analysis of iron with the final aim of clinical use.

In vitro experiments using the Caco-2 cell line are well-established to date for the study of the iron bioavailability and absorption. This model has been used to study the mechanisms of natural Fe isotope fractionation occurring during intestinal absorption at a cellular level. The intestinal enterocytes act as a first metabolic barrier where iron uptake from the intestinal lumen takes place, followed by the transfer of iron into the peripheral circulation. In **Chapter 5**, the experimental setup developed to optimize the iron uptake through the Caco-2 cells line is described. Moreover, the analytical procedure developed was carefully checked for any source of analytical bias.

In addition to the natural Fe fractionation accompanying the intestinal absorption process, also variations within the life span of erythrocytes could possibly occur. In comparison with transferrin-bound iron, which represents the iron transport compartment, erythrocyte iron represents the Hb-bound iron, which provides information on the functional iron compartment. In **Chapter 6**, variations of the Fe isotopic composition in density-separated fractions of erythrocytes, which correspond to their ages, were evaluated to investigate a possible effect of erythrocyte aging on the whole blood Fe isotopic composition.

The isotopic analysis of blood serum is interesting due to the high iron turnover rate of transferrin as a main carrier of iron (< 5 days) in comparison to the relatively static

compartment of whole blood erythrocytes (~ 120 days). Iron deficiency and anemia of different nature are common complications of chronic kidney disease (CKD). Until now, the management of iron deficiency and anemia of CKD proved to be challenging due to the difficulties in diagnosis using standard markers, such as serum iron, serum total iron-binding capacity, hemoglobin or ferritin. This hampers adequate decisions concerning therapeutic treatment. In **Chapter 7**, blood serum of patients suffering from CKD stage 3 or higher and without chronic inflammation was analysed in order to evaluate the use of the Fe isotopic composition as a potential tool to reveal the Fe-related complications of the disease. Correlation of the Fe isotopic composition with typical parameters used in clinical practice has been evaluated. It has been demonstrated that for patients with renal insufficiency, serum Fe isotopic analysis allows iron deficiency anemia (IDA) and erythropoietin-related (EPO-related) anemia to be distinguished from one another.

DOELSTELLING EN OVERZICHT

Essentiële minerale elementen vertonen natuurlijke variaties in hun isotopische samenstelling als gevolg van fractionatie-effecten. De term isotopenfractionatie geeft aan dat isotopen van een zelfde element niet in exact dezelfde mate deelnemen aan fysische processen en/of (bio)chemische reacties. Om de kleine verschillen in de isotopische samenstelling als gevolg van deze processen te kunnen bepalen, is multi-collector inductief gekoppeld plasma-massaspectrometrie (MC-ICP-MS) de te verkiezen techniek. MC-ICP-MS combineert een hoog-efficiënte ionenbron met de simultane monitoring van de geselecteerde isotopen, waardoor isotopenverhoudingen met zeer hoge precisie kunnen gemeten worden (tot ≤ 0.002% relatieve standaarddeviatie).

De interesse in zeer precieze isotopenanalyse van essentiële minerale elementen, waaronder Fe, neemt geleidelijk aan toe en heeft als doel inzicht verschaffen in het metabolisme van deze elementen en metaal-gerelateerde aandoeningen te diagnosticeren. Bijgevolg was het algemene doel van dit werk gericht op (een bijdrage aan) de ontwikkeling van analytische methoden gebaseerd op ICP-massaspectrometrie voor isotopenanalyse van Fe in humaan volbloed en serum voor biomedische toepassingen. Meer specifiek werd de mogelijkheid om de monstervoorbereiding te vereenvoudigen, door het analyseren van volbloed stalen zonder voorafgaandelijke chromatografische afscheiding van Fe van de matrix, bestudeerd. Eveneens werd ook de mogelijkheid van het gebruik van een nieuwe techniek om bloed te bemonsteren (volumetrisch absorptieve microstaalname - VAMS van bloed verkregen *via* een vingerprik), gevolgd door een geminiaturiseerd chromatografisch procédé voor de isolatie van Fe, onderzocht. Een ander deel van dit werk was gefocusseerd op het verwerven van een beter inzicht in het mechanisme van natuurlijke isotopenfractionatie, die optreedt tijdens de intestinale absorptie van Fe, door middel van *in vitro* experimenten met enterocyt-achtige cellen. Eveneens werd het mogelijke effect van het verouderingsproces van erythrocyten (gescheiden op basis van hun dichtheid) op hun isotopische samenstelling van Fe onderzocht. Tenslotte werden de mogelijkheden van hoog-precieze isotopenanalyse van Fe in serum

onderzocht om een onderscheid te maken tussen verschillende aandoeningen gerelateerd aan het Fe-metabolisme bij patiënten met nierinsufficiëntie Voor het gemak van de lezer werden de hoofdstukken in volgorde van analytische ontwikkeling en toepassing geplaatst en niet in chronologische volgorde.
In **Hoofdstuk 1** wordt een korte introductie over het Fe-metabolisme en Fe-gerelateerde aandoeningen gegeven. Dit hoofdstuk bevat eveneens een samenvatting van de literatuur over de isotopische samenstelling van Fe in humane lichaamsvloeistoffen en het gebruik van diermodellen voor de ontrafeling van het Fe-metabolisme. De principes van ICP-MS in het algemeen en van MC-ICP-MS in het bijzonder worden hier ook behandeld.

Isotopenanalyse van Fe kan ook waardevol zijn voor nutritionele studies, zoals voor studies die gefocust zijn op de ontwikkeling van nieuwe ijzersupplementen. Doorgaans worden isotopisch gemerkte supplementen ingezet om de effectieve intestinale absorptie van ijzer te ontrafelen. In **Hoofdstuk 2** wordt een beschrijving gegeven van isotopenanalyse van Fe in volbloed *via* single-collector sector-veld ICP-MS (SF-ICP-MS) in de context van een humane absorptie studie. Ondanks de minder goede isotopenprecisie geboden door SF-ICP-MS dan door MC-ICP-MS, vertonen de isotopenverhoudingen van Fe bekomen met SF-ICP-MS toch een precisie die adequaat is om in deze context gebruikt te worden, zelfs na zure digestie en adequate verdunning als enige monstervoorbereiding. Eveneens werd er een goede overeenkomst gevonden tussen de isotopenverhoudingen van Fe in volbloed die bekomen werden na analyse *via* beide technieken.

Zoals toegelicht in hoofdstuk 1, werd er een duidelijke link vastgesteld tussen de isotopische samenstelling van Fe in volbloed en de Fe-status. De isotopische samenstelling van Fe verschaft dus waardevolle klinische informatie. Om isotopenanalyse van Fe te kunnen inzetten in klinische studies, is niet alleen de ontwikkeling van eenvoudige en betrouwbare methodes voor zeer-precieze isotopenanalyse in biologische vloeistoffen vereist, maar ook een hoge sample throughput. Doorgaans bestaat de gehele monstervoorbereiding voorafgaand aan isotopenanalyse van Fe in volbloed *via* MC-ICP-MS uit een digestiestap met geconcentreerd zuur en een chromatografische afscheiding van het analietelement. Deze procedure is echter arbeidsintensief, tijdrovend en duur. In **Hoofdstuk 3** wordt de mogelijkheid van isotopenanalyse van Fe in volbloed *via* MC-ICP-MS zonder voorafgaande isolatie van het doelelement, nl. isotopenanalyse volgend op een digestiestap en adequate verdunning, geëvalueerd. De invloed van de belangrijkste matrixelementen en het effect van

mogelijke restanten van organisch materiaal werden systematisch geëvalueerd. De resultaten die bekomen werden voor volbloed na isotopenanalyse volgend op een enkele digestiestap kwamen goed overeen met deze die bekomen werden na isotopenanalyse volgend op een digestiestap en chromatografische afscheiding. Deze monstervoorbereiding zou kunnen ingezet worden voor specifieke klinische toepassingen waarbij een snelle respons vereist is.

Routinematig gebruik van de in hoofdstuk 2 voorgestelde methode kan leiden tot een overbelasting van het MC-ICP-MS instrument. Daarom werd in **Hoofdstuk 4** een alternatieve methode voorgesteld om de sample throughput te verhogen. Deze techniek is gebaseerd op een nieuwe VAMS techniek om bloed te bemonsteren. Deze techniek overwint de problemen geassocieerd met de variaties in de hematocrietwaarde en de inhomogeniteit van de stalen, die de analyse van gedroogde bloedspots bemoeilijken. Deze snelle, goedkope en minimaal invasieve monstername techniek laat toe om de staalname te vereenvoudigen door zelfcollectie (door de patiënt) waarna de VAMS-probe met het gecollecteerde bloed voor analyse kan verzonden worden. In dit hoofdstuk werd eveneens aangetoond dat de VAMS-tips bij verschillende temperaturen gedurende enige tijd bewaard kunnen worden zonder een effect te hebben op de isotopenverhoudingen van Fe. Om de monstervoorbereidingsprocedure voorafgaand aan zeer precieze isotopenanalyse van Fe te vereenvoudigen en te optimaliseren, werd een geminiaturiseerde chromatografische isolatieprocedure ontwikkeld. Deze methode bleek succesvol voor de kwantitatieve herwinning van het doelelement – waardoor het effect van artificiële isotopenfractionatie vermeden werd – en resulteerde in een significante vermindering van het verbruiik van dure ultrazuivere zuren en in een verkorting van de duur van de monstervoorbereiding. De geschiktheid van VAMS voor zeer precieze isotopenanalyse van Fe en kwantitatieve Fe bepaling werd bestudeerd na bewaring van de probes onder verschillende omstandigheden. Om de mogelijkheid van het gebruik van VAMS voor hoog-precieze isotopenanalyse van Fe in klinische studies na te gaan, werd simultaan gecollecteerd vingerprik bloed en veneus volbloed met elkaar vergeleken. De goede overeenkomst tussen de betreffende resultaten toont de inzetbaarheid van de methode aan.

In vitro experimenten met behulp van de Caco-2 cellijn worden vaak gebruikt voor het bestuderen van de biobeschikbaarheid en de absorptie van Fe. Dit model werd gebruikt om de mechanismen van natuurlijke Fe isotopenfractie die optreedt tijdens intestinale absorptie te bestuderen op cellulair niveau. De intestinale enterocyten gedragen zich als een eerste barrière waar de opname van Fe uit het darmlumen plaatsvindt, gevolgd door de overdracht van Fe

naar de perifere circulatie. In **Hoofdstuk 5** wordt de experimentele opstelling, die ontwikkeld werd om de opname van Fe door de Caco-2 cellijn te optimaliseren, beschreven. Eveneens werd de aldus ontwikkelde analytische procedure zorgvuldig bestudeerd om elke bron van mogelijke afwijkingen na te gaan.

Naast het optreden van natuurlijke Fe fractionatie tijdens het intestinale absorptieproces, zouden ook variaties kunnen optreden tijdens de levensduur van erythrocyten. In vergelijking met transferrine-gebonden Fe, wat het Fe transport-compartiment voorstelt, stelt het Fe in de erythrocyten, dat gebonden is in hemoglobine, het functionele Fe compartiment voor. In **Hoofdstuk 6** werd de isotopische samenstelling van Fe in op basis van dichtheid gescheiden fracties van erythrocyten bepaald om het mogelijk effect van de leeftijd van erythrocyten op de isotopische samenstelling van Fe in volbloed te onderzoeken.

De isotopische samenstelling van Fe in serum wekt interesse door de hoge Fe "turnover rate" van transferrine als belangrijkste drager van Fe (~5 dagen) in vergelijking met het relatief statische volbloed compartiment van erythrocyten (~120 dagen). IJzertekort en verschillende soorten van anemie zijn vaak voorkomende complicaties bij chronische nieraandoeningen (CKD). Tot dusver blijkt de behandeling van ijzertekort en anemie veroorzaakt door CKD een uitdaging als gevolg van de moeilijkheden bij de diagnose door middel van de traditionele parameters, zoals, serum ijzerconcentratie, serum totale ijzerbindingscapaciteit, hemoglobine- en ferritineconcentraties. Dit belemmert adequate beslissingen voor therapeutische behandelingen. In **Hoofdstuk 7** worden de resultaten van de isotopenanalyse van Fe in serum van patiënten met CKD in stadium 3 of een verder stadium zonder chronische inflammatie toegelicht. Eveneens wordt de mogelijkheid van de isotopische samenstelling van Fe als hulpmiddel voor het ontrafelen van Fe-gerelateerde complicaties van de ziekte geëvalueerd. Er werden correlaties bestudeerd tussen de isotopische samenstelling van Fe en de klassieke parameters die gebruikt worden in klinisch onderzoek. Er werd aangetoond dat voor patiënten met nierinsufficiëntie, de isotopische samenstelling van Fe toelaat om anemie door ijzertekort te onderscheiden van erythropoëtine-gerelateerde (EPO-gerelateerde) anemie.

IMPACT AND SCIENTIFIC OUTCOMES

The impact of the PhD research is reflected in international peer-reviewed publications:

1. Flórez M R, **Anoshkina Y**, Costas-Rodríguez M, Grootaert Ch, Delanghe J, Van Camp J, Vanhaecke F. Natural Fe isotope fractionation in an intestinal Caco-2 cell line model. *J. Anal. At. Spectrom.* DOI: 10.1039/C7JA00090A (2017)

2. **Anoshkina Y**, Costas-Rodriguez M, Speeckaert M, Van Biesen W, Delanghe J. Iron isotopic composition of blood serum in anemia of chronic kidney disease. *Metallomics* **9,** 517–524 (2017)

3. **Anoshkina Y**, Costas-Rodríguez M, Vanhaecke F. Iron isotopic analysis of finger-prick and venous blood by multi-collector inductively coupled plasma-mass spectrometry after volumetric absorptive microsampling. *J. Anal. At. Spectrom.* **32**, 314-321 (2017)

4. **Anoshkina Y**, Costas-Rodríguez M, Vanhaecke F. High-precision Fe isotopic analysis of whole blood for biomedical purposes without prior isolation of the target element. *J. Anal. At. Spectrom.* **30,** 1816–1821 (2015).

Additional publications in international peer-reviewed journals:

1. Costas-Rodríguez M, **Anoshkina Y**, Lauwens S, Van Vlierberghe H, Delanghe J, Vanhaecke F. Isotopic analysis of Cu in blood serum by multi-collector ICP-mass spectrometry: a new approach for the diagnosis and prognosis of liver cirrhosis? *Metallomics* **7,** 491–498 (2015)

2. Zhang Z, Van Steendam K, Maji S, Balcaen L, **Anoshkina Y**, Zhang Q, Vanluchene G, De Rycke R, Vanhaecke F, Deforce D, Hoogenboom R and De Geest B G. Tailoring cellular uptake of gold nanoparticles *via* the hydrophilic-to-hydrophobic ratio of their (Co)polymer coating. *Adv. Funct. Mater.* **25,** 3433–3439 (2015).

The scientific outcomes of the PhD were presented on international conferences with the following oral presentations:

1. **Anoshkina Y**, Costas-Rodríguez M, Vanhaecke F. Iron isotopic analysis of finger-prick blood *via* multi-collector inductively coupled plasma-mass spectrometry after volumetric absorptive microsampling (VAMS). The European Winter Conference on Plasma Spectrochemistry (EWCPS), Sankt Anton Am Arlberg, Austria, 19th-24th February, 2017
2. Vanhaecke F, **Anoshkina Y**, Costas-Rodríguez M, Florez M R, Lauwens S, Van Vlierberghe H, Speeckaert M, Delanghe J. High-Precision isotopic analysis of essential transition metals in human body fluids for medical diagnosis, prognosis & monitoring. SciX 2016 Conference, Minneapolis MN, USA, 19th-21st September, 2016
3. **Anoshkina Y**, Costas-Rodríguez M, Speeckaert M, Delanghe J and Vanhaecke F. Iron isotopic composition of blood serum in anemia of chronic kidney disease. The 32nd International Conference on Environmental Geochemistry and Health, Brussels, Belgium, 4th-8th July, 2016
4. Costas-Rodriguez M, **Anoshkina Y**, Vanhaecke F. Fast and simple high precision isotopic analysis of Fe in whole blood by MC-ICP-MS for biomedical purposes. Goldschmidt, Yokohama, Japan, 26th June-1st July, 2016
5. Vanhaecke F, **Anoshkina Y**, Balcaen L, Buckle T, Bolea-Fernandez E, Costas-Rodriguez M, Delanghe J, Lauwens S, Speeckaert M, Van Malderen S, Van Vlierberghe H, Van Acker T, Vergucht E, Vincze L. Novel clinical applications of ICP-mass spectrometry. 27th MassSpec Forum Vienna, Austria, 23rd-24th February, 2016
6. Vanhaecke F, **Anoshkina Y**, Balcaen L, Chernonozhkin S, Costas-Rodriguez M, Florez-Garcia M, Lauwens S, Rua-Ibarz A, Goderis S, Claeys P, Delanghe J, Van Vlierberghe H, Maage A. From outer space to within the human body: natural isotope ratios as proxies.Winter Conference on Plasma Spectrochemistry, Tucson, Arizona, USA, 10th-16th January, 2016

7. Vanhaecke F, **Anoshkina Y**, Balcaen L, Costas-Rodríguez M, Bolea-Fernandez E, Rua-Ibarz A, Van Malderen S. ICP-mass spectrometry: a versatile technique for the determination, speciation and isotopic analysis of trace elements. Mass Spectrometry in Food and Feed II, Ghent, Belgium, 15th September, 2015
8. Vanhaecke F, **Anoshkina Y**, Balcaen L, Bolea-Fernandez E, Costas-Rodríguez M, Lauwens S, Van Heghe L, Van Malderen S. Instrument evolution in ICP-mass spectrometry renders the technique ever more useful in biomedical analysis. Colloquium Analytical Atomic Spectroscopy (CANAS), Leipzig, Germany, 8th-10th March, 2015
9. Vanhaecke F; **Anoshkina Y**. Aramendia M, Balcaen L, Bolea Fernandez E, Costas Rodriguez M, Delanghe J, Resano M, Van Malderen S, Van Vlierberghe H. ICP-mass spectrometry as an emerging tool for medical diagnosis. The European Winter Conference on Plasma Spectrochemistry (EWCPS), Munster, Germany, 22nd-26th February, 2015
10. Costas-Rodriguez M, **Anoshkina Y**, Vanhaecke F, Van Vlierberghe H. Isotopic analysis of Cu and Fe in blood serum from patients with liver cirrhosis by multi-collector ICP-mass spectrometry. The European Winter Conference on Plasma Spectrochemistry (EWCPS), Munster, Germany, 22nd-26th February, 2015
11. Vanhaecke F, **Anoshkina Y**, Costas-Rodriguez M, Van Heghe L, Delanghe J, Depyere H, Santens P, et al. Unraveling the Message in Transition Metal Isotope Ratios in Body Fluids - On the Way to "Isotopic Diagnosis"?. Winter Conference on Plasma Spectrochemistry, Amelia Island, Florida, USA, 6th-11th January, 2014

CHAPTER 1

GENERAL INTRODUCTION

1.1 HUMAN IRON METABOLISM

Iron (Fe) is an essential metal for almost all living organisms since it is present in a large number of iron-containing enzymes and proteins.[1,2] These proteins play a vital role in a broad range of biological functions, including oxygen transport, energy production and cell proliferation. Despite its essentiality for a wide variety of metabolic processes, iron can also be toxic for living systems.[3,4] Iron exists in solution in one of two oxidation states, *i.e.* in the ferrous form (Fe^{2+}) or the ferric form (Fe^{3+}), which can relatively easy donate or accept an electron, respectively. This chemical property results in a catalytic role for a multitude of redox reactions which are necessary to support basic metabolic functions. Due to this redox activity, iron is, however, also involved in the formation of harmful oxygen radicals, *e.g.*, *via* the Fenton reaction[5], that can damage the cell structure.[1,3,4,6] Moreover, at physiological pH and oxygen tension, Fe(II) is readily oxidized to Fe(III) in solution, which rapidly forms insoluble $Fe(OH)_3$. Because of this insolubility and potential toxicity, specialized mechanisms and molecules are involved in the uptake, transport, and storage of iron in soluble non-toxic forms.[4]

Daily requirements of iron vary depending on an individual's age, sex and physiological status. The body's total iron content is estimated to be 55 and 45 mg per kg of body weight in adult men and women, respectively.[4,6] A healthy individual absorbs daily approximately 1–2 mg of iron from the diet, which compensates for non-specific iron losses, mainly by normal sloughing of cells in the gastrointestinal tract and the small loss of erythrocytes in urine and feces (~1 mg).[7–9] Menstruation increases the physiological loss of iron in premenopausal females.[8–10] Despite the low intestinal uptake, approximately 20-30 mg of iron are required

daily for the erythropoiesis. Therefore, in contrast to other essential elements, iron is strictly conserved by iron recycling from aging erythrocytes and from other sources.[6,11]

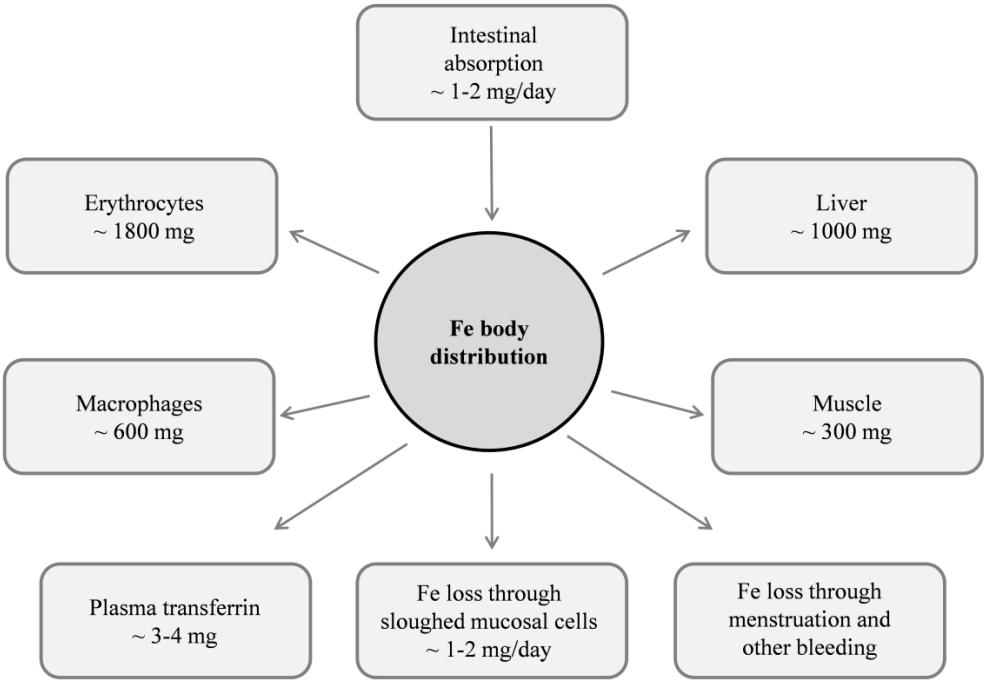

Fig. 1-1 Iron distribution in the adult human body.

The distribution of iron in the adult human body is shown in Fig. 1-1. The majority of the body's iron (~60–70%) is found in the heme groups of hemoglobin (Hb) in circulating erythrocytes (red blood cells, RBCs).[3,11–13] Heme iron is essential for oxygen transport in hemoglobin, oxygen storage in myoglobin, and in the electron transport within the cytochrome C oxidase complex in aerobic respiration. When erythrocytes reach the end of their lifespan, they are phagocytosed by the reticuloendothelial macrophages, which recycle iron from heme.[13] The second largest pool of iron (~20-30 %) is found in its storage form, ferritin.[6] Due to the large size of this protein (450 kDa), ferritin can store up to 4500 iron atoms as hydrous oxide with the ability to gain and release iron according to the physiological need. The majority of iron storage occurs in liver hepatocytes, reticuloendothelial cells (macrophages) and skeletal muscle.[1] The remaining body iron (10-15%) is primarily localized in myoglobin (an iron- and oxygen-binding protein in the muscle tissue), cytochromes (heme-containing proteins participating in electron transport), and a variety of iron-containing enzymes, involved in the oxidative metabolism and many other cell functions.[10]

Iron uptake and transport through the body require special mechanisms to diminish its ability to form active radicals. Iron is transported between sites of absorption, storage, and recycling by the plasma glycoprotein transferrin (Tf).[1] Transferrin-bound iron (Fe^{3+}) is intended to be delivered to the cells by binding to the specific cell surface transferrin receptor (TfR). Each molecule of transferrin can bind two atoms of ferric iron. Although only ~3-4 mg of iron is bound to transferrin (< 0.1% of the total body iron), it is the most important dynamic iron pool in the body with the highest rate of turnover (~25 mg per 24 h). Under healthy conditions, ~80% of this iron is transported to the bone marrow for hemoglobin synthesis in developing erythroid cells. The saturation state of serum transferrin (TSAT) plays a key role in the regulation of iron metabolism and hence, it is one of the indices used clinically to evaluate an individual´s iron status.[4,6] Alterations of overall body iron amounts and/or tissue iron distribution can lead to human iron disorders[14] (further described, section 1.1.4).

The amount of circulating transferrin-bound iron is regulated by three coordinated processes: duodenal iron absorption, macrophage iron recycling, and iron storage. A general description of these processes is presented below.

1.1.1 Intestinal iron absorption

Due to the absence of a regulated active pathway of iron excretion, the body's iron content is precisely controlled by the intestinal absorption. The majority of dietary iron absorption occurs in the duodenum.[15] The absorption of dietary iron is highly regulated and involves its transport across the luminal (apical) membrane of enterocytes in the gut and across the basolateral membrane into the blood plasma.[16] Two forms of dietary iron can be distinguished: heme and non-heme. A normal individual ingests approximately 10-20 mg of iron per day, that is mostly in heme iron form due to its higher absorption efficiency compared to the non-heme iron form.[11,17] However, only approximately 10% (~1-2 mg) of iron is absorbed daily.[2,7] The iron absorption is regulated mainly by the amount of storage iron, hypoxia and the rate of erythropoiesis. Thereby, an increase of the iron stores will lead to a decreased dietary iron absorption.[11,15] The basic mechanism of iron absorption is shown in Fig. 1-2.

At the luminal side of the enterocyte, the ferric iron (Fe^{3+}) of non-heme iron requires to be reduced to ferrous iron (Fe^{2+}) by the duodenal ferrireductase enzyme (Dcytb). The ferrous

iron is then transported into the enterocytes by the divalent metal ion transporter-1 (DMT-1). The dietary heme iron is transported across the enterocyte by heme carrier protein 1 (HCP1).

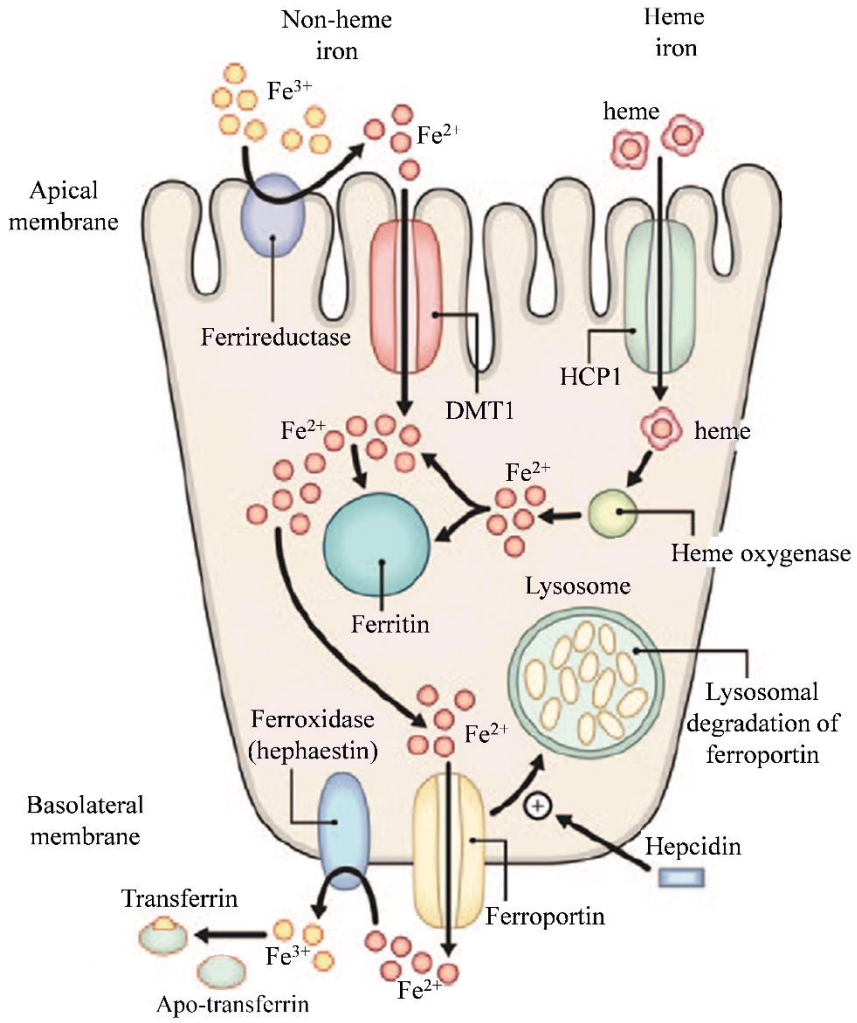

Fig. 1-2 Mechanism of intestinal (enterocyte) iron absorption (adapted from Rizvi and Schoen, 2011).[15]

Inside the enterocyte, ferrous iron Fe^{2+} is released from the protoporphyrin of heme iron by the heme oxygenase to enter in the same labile iron pool (LIP) as the dietary non-heme iron.[18] Depending on the cellular requirements, there are two possible pathways for the ferrous iron inside the cell: i) a part of the ferrous iron is incorporated into ferritin inside the enterocyte (this iron is probably never absorbed and is lost when the enterocytes senescence and are sloughed off into the gut lumen[11]) and ii) another part is transported across the basolateral membrane of the enterocyte by ferroportin. The transported Fe^{2+} is oxidized to the Fe^{3+} form by the ferroxidase (hephaestin) and then, it is incorporated into transferrin in the blood and transported to sites of use and storage,[2,11,15] except when this transporter is saturated. In this case, the ferric iron will bind to other ligands, such as citrate, constituting the non-transferrin

bound iron (NTBI) pool.[2] In a healthy organism, most of the iron will be transported to be involved in the erythroid iron metabolism or will be trapped in available ferritin molecules.[2,19,20]

1.1.2 Erythroid iron metabolism

Erythropoiesis in humans results in the average daily production of about 2×10^{11} erythrocytes (red blood cells, RBCs). In adult humans, erythropoiesis occurs in the bone marrow[21] and involves the entire process by which hematopoietic stem cells (HSCs) differentiate in the bone marrow through several stages into RBCs.[22] The new cells enter into the circulation as reticulocytes where, within about 24 h, they develop into mature erythrocytes that circulate in the blood for about 120 days.[4] Under normal conditions, approximately 1% of the RBCs are synthesized on a daily basis. The rate of erythropoiesis can increase significantly from this baseline level in response to hypoxic stress (hypoxia), which occurs when the body is deprived of adequate oxygen supply at the tissue level. It was observed that erythropoiesis is mainly regulated by the kidney-derived cytokine erythropoietin (EPO).[23] The production of EPO in the kidneys is directly regulated by the tissue oxygen tension (Fig. 1-3, red arrows). In response to a low oxygen level, EPO is released from the kidneys and stimulates the bone marrow to produce more RBCs, which, in turn, increase the oxygen-carrying capacity of the blood.

At the end of the RBC life span, senescent and/or damaged erythrocytes are phagocytosed by macrophages (mainly in the spleen, liver or bone marrow) to recycle the iron (Fig. 1-3). In this process, the heme-groups from hemoglobin are split into ferrous iron and the pigment bilirubin. The released ferrous iron is exported by the transmembrane transporter ferroportin, further oxidized to its ferric form in order to bind to circulating transferrin in the plasma and be exported, to be recycled for various functions.[14,24] The bilirubin, inversely, is secreted into the blood and carried to the liver where it is bound to (conjugated with) glucuronic acid, a derivative of glucose. Some of the conjugated bilirubin is secreted into the blood and the rest is excreted into the bile as bile pigment that passes into the small intestine. The blood normally contains a small amount of free and conjugated bilirubin.[4,24]

Because most of the body's iron is used by the bone marrow for hemoglobinization of the RBCs, it is not surprising that erythropoietic regulation has a dominant function in the control

of iron homeostasis.[12] Moreover, in disorders with ineffective erythropoiesis, the iron absorption is increased independently of the body iron (even when the iron stores are replete).

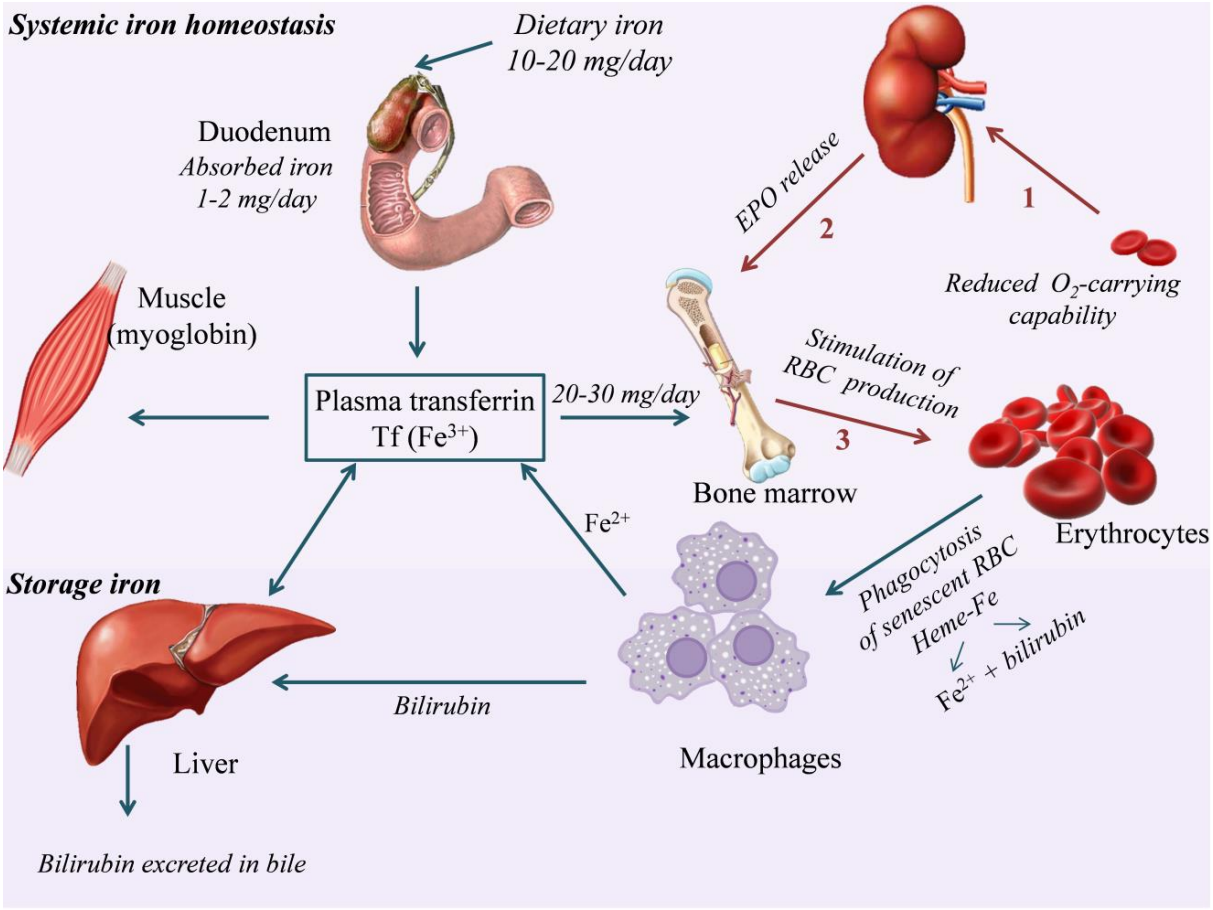

Fig. 1-3 Iron balance in human body. The red arrows indicate the stimulation of RBC production: 1) Detection of a reduced O_2-carrying capability of blood; 2) The kidneys respond by secreting EPO into the blood stream that stimulates erythropoiesis in the bone marrow; 3) Release of RBCs, increasing the O_2-carrying capability that inhibits further EPO secretion.

1.1.3 Iron homeostasis in the liver

Iron enters into the plasma *via* intestinal absorption and macrophage iron recycling in response to various physiological needs. The excess of circulating iron in both transferrin-bound and non-transferrin-bound forms (NTBI) is stored as ferritin and hemosiderin in the liver hepatocytes, which is the major storage location for body iron.[25] The hemosiderin is the product of ferritin breakdown within the lysosomes. It represents a very small fraction of the normal body iron stores but it can increase dramatically under iron overload conditions.[11] An additional fraction of free iron is present in the form of the LIP within cells. The LIP is

biologically active in the intracellular metabolism *via* oxidation–reduction reactions, cell proliferation, and cell signaling, but toxic when present in excess.

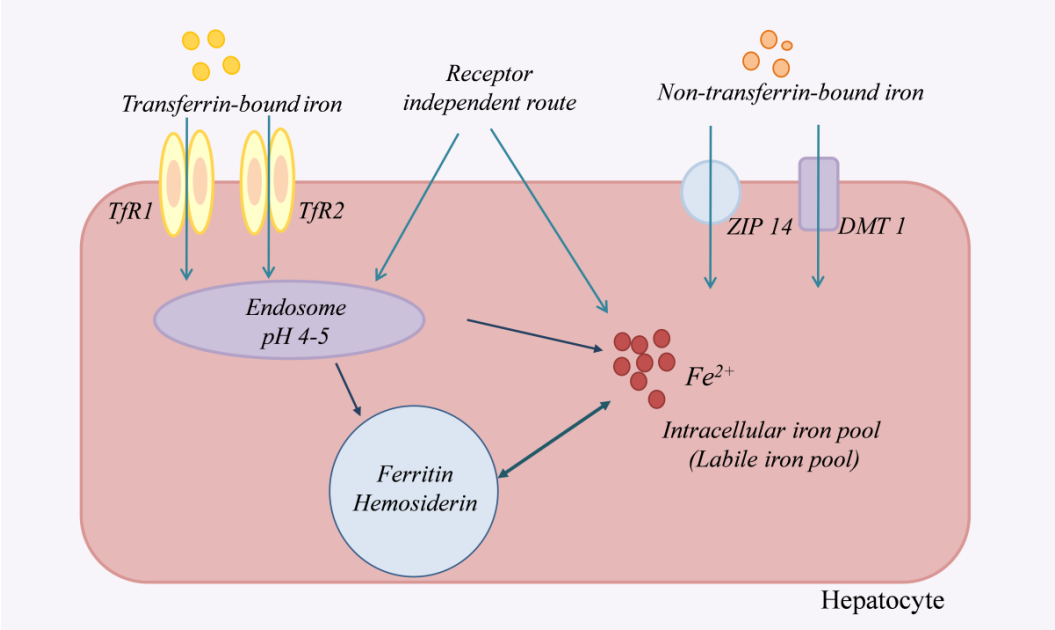

Fig. 1-4 The main pathways for iron uptake by a hepatocyte.

Ferritin is the main form of stored iron in hepatocytes under physiological circumstances. Hepatocytes have essentially two pathways for iron uptake from the circulation: uptake of Tf-bound iron (Fe_2-Tf) under healthy conditions, and of NTBI in case of iron overload, however the mechanism of the iron uptake by the hepatocytes is not fully understood yet.[14] The principle of Fe uptake by the hepatocytes is shown in Fig. 1-4. Transferrin receptor 1 (TfR1) is a classical functional receptor, which bounds Tf-bound iron from the plasma and forms internalized Fe_2Tf-TfR1 complexes. This complex releases iron within the endosome at acidic pH. The resulting apotransferrin-TfR1 complex is then recycled back to the cell surface for reutilization. In an iron overload situation, TfR1 is downregulated in the hepatocytes. Transferrin receptor 2 (TfR2), is highly present on hepatocyte surfaces and has a similar mechanism of recycling. This mechanism is not well known, but likely plays an important role in iron overload states. In normal and iron-loaded conditions, the expression of TfR2 exceeds that of TfR1, which suggests that TfR2 plays an important role in hepatic iron loading in hemochromatosis (*e.g.*, a mutation in TfR2 is responsible for type 3 hemochromatosis). Based on murine studies, there is another Tf-bound iron uptake mechanism in the hepatocytes that is independent of TfR recycling. In iron-overloaded conditions, NTBI appears in the circulation and is taken up through two molecules, DMT1

and ZIP14, in hepatocytes.[11,25] In contrast to iron uptake, likely there is only one mechanism to transport iron out of the hepatocytes by ferroportin: the exported iron is then oxidized by the ceruloplasmin and bound to transferrin.[11]

Another important function of the liver in the systemic iron homeostasis is the production of the hormone hepcidin. In recent years, hepcidin has emerged as a primary regulator of iron homeostasis and it controls iron transport by binding to ferroportin and promoting its internalization and degradation. The loss of ferroportin from the cell membrane leads to cellular iron retention and represses absorption of dietary iron in the intestine, recycling of iron by macrophages, and mobilization of stored iron from hepatocytes. Consequently, the transferrin saturation decreases, resulting in the reduction of the amount of iron available.[26]

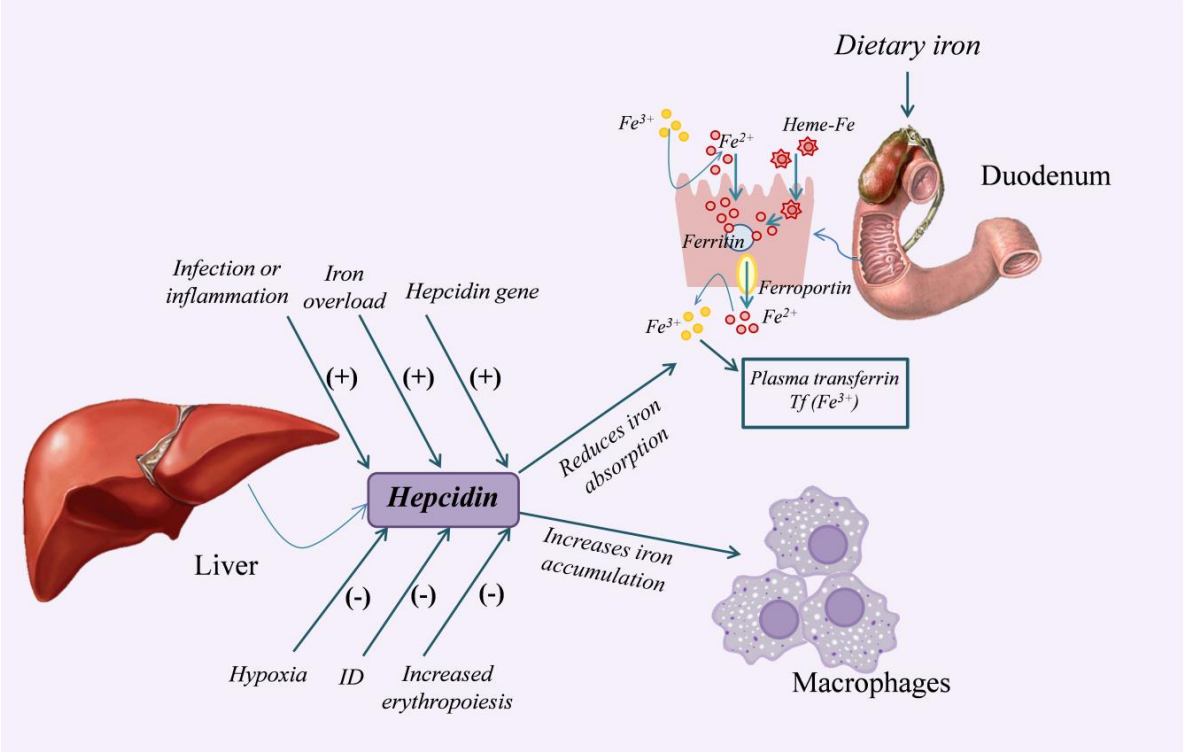

Fig. 1-5 Regulation of circulating iron by hepcidin. (+) is stimulatory effect, (-) is inhibitory effect.

A schematic diagram presenting the regulation of circulating iron by hepcidin is shown as Fig. 1-5. Hepcidin constantly regulates iron uptake to maintain sufficient iron stores for erythropoiesis, while preventing iron overload. Dysregulation of hepcidin production, whether genetic or acquired, causes an iron disorder. In healthy individuals, an increase in body iron would lead to an increased hepcidin expression and therefore to a decreased iron absorption. The level of hepcidin elevates during inflammation, which is the main reason of anemia of

chronic disease (ACD). In patients with hemochromatosis, iron absorption continues leading to iron overload due to an inadequate or ineffective down-regulation of ferroportin by hepcidin. In contrast, the level of hepcidin decreases in conditions of hypoxia, iron deficiency/anemia, and increased erythropoiesis, resulting in an increased iron export into the blood plasma.[2] The nature of the suppressive signal is unknown but there is evidence that it could be a circulating factor produced by the erythroid signal in the bone marrow.[14,16,19,25,27–29] Defective erythropoiesis results in an increased iron export from enterocytes regardless of the liver iron stores status. Consequently, patients with defective erythropoiesis can be anemic and suffer simultaneously from tissue iron-overload.[16,26,29,30] Although the conditions that regulate hepcidin expression are known, its molecular regulation and interactions form an active area of investigation.[26]

1.1.4 Disorders of iron metabolism

Iron plays a vital role in the hemoglobin synthesis and erythrocyte production but its excess can damage human cells. At the same time, iron is also an essential nutrient for germs and microbes that further can cause diseases in the host. Iron metabolism is very complex and strictly controlled by many different genes and proteins. Disturbance of iron homeostasis principally leads to either iron deficiency (ID) or iron overload diseases.[1] In recent years, the identification of hepcidin was a major step forward in the understanding of the iron metabolism. However, early diagnosis and effective treatment of iron metabolism disorders remain a challenge. Disorders of iron homeostasis are invariably chronic, not acute diseases.[31] Iron metabolism disorders in humans can be classified based on four major categories: (i) diseases associated with defective regulation of iron absorption, (ii) diseases caused by the erroneous tissue and/or cellular compartmentalization of iron, (iii) secondary disorders caused by an altered iron content in cells and/or tissues, and (iv) genetic defects which lead to disturbance of iron metabolism.[1]

Generally speaking, iron-overload disease occurs when the amount of absorbed plasma iron exceeds the binding capacity of transferrin, and it arises from the inability to down-regulate the iron absorption appropriately in response to increased iron stores. Iron-overload diseases owing to genetic misregulation of iron acquisition are referred to as primary iron-overload disease or hereditary hemochromatosis (HH).[16] Secondary iron overload is developed as a

result of repeated blood transfusions, which are frequently applied for the treatment of various anemias.[8]

ID is the most common nutrition problem globally, characterized by insufficient iron to maintain the normal physiological function of tissue (blood, brain, and muscles).[32] In developed countries, approximately 10% of the toddlers (due to their rapid growth) and premenopausal women (due to menstrual blood loss) are iron-deficient. In the great majority of cases, the ID is acquired, but it can also come from hereditary etiologies, poorly understood to date.[33] ID can be caused by either inadequate dietary iron absorption (including low dietary availability, high gastric pH, loss or dysfunction of enterocytes, hepcidin fluctuations) or increased iron losses (mainly blood losses) associated with hemodialysis, frequent blood sampling, gastrointestinal bleeding, multiple vascular access surgeries, *etc*.[1,34] At a first step, ID leads to a depletion of iron stores with preservation of erythroid iron, which is reflected in low serum ferritin levels and transferrin saturation (TSAT). The cut-off level of serum ferritin for the diagnosis of ID varies between 12-15 µg L^{-1}.[32] However, due to the association of the ferritin concentration with the inflammatory status (the level of ferritin is elevated in the presence of inflammation), a cut-off value of ≥ 50 µg L^{-1} is used. As a result, the ferritin concentration is not widely used in clinical practice to assess ID. TSAT is another common clinical parameter that indicates the percentage of iron bound to transferrin. In the case of ID, either absolute or functional, this parameter is decreased (typically < 20%). The TSAT is a marker of iron available for erythropoiesis in the circulation and is calculated as follows:

$$TSAT = \frac{serum\ iron\ concentration}{TIBC} \cdot 100 \qquad (1\text{-}1)$$

where TIBC is total iron-binding capacity that indicates the maximum amount of iron needed to saturate plasma or serum transferrin and is calculated from serum transferrin concentration.[35]

According to Wish[34] and Hörl[36], also the TSAT has some acute-phase response because the transferrin level may be elevated in the setting of inflammation, consequently leading to a lowered TSAT. Transferrin may also be low because of decreased transferrin synthesis in the setting of malnutrition and chronic disease, which would raise TSAT if circulating iron is constant. Moreover, TSAT fluctuates widely as a result of diurnal variation in serum iron, and transferrin is affected by the nutritional status. Therefore, due to these sources of variability, many other biochemical indexes are currently explored to evaluate the iron status, such as the

soluble transferrin receptor concentration, the reticulocyte hemoglobin concentration, the percentage of hypochromic red cells, the concentration of erythropoietin (and its relation to the expected values), and the concentration of hepcidin. The soluble transferrin receptor (sTfR) level is one of the most useful, as it is the least influenced by the presence of inflammation, and it correlates well with the concentration of transferrin receptor in the cell plasma membrane. However, in particular groups of patients with increased erythropoiesis due to a variety of disorders, its utility in the clinical setting remains to be proven. The combination of the sTfR and ferritin measurements, as the sTfR/log serum ferritin ratio, provides an increased specificity, but not sensitivity for the diagnosis of ID in such populations.[34,37–42]

Iron deficiency anemia (IDA) is an advanced form of ID caused by a number of factors ranging from dietary deficiency, blood loss, and metabolic lesions and it is characterized by reduced erythropoiesis. The World Health Organization (WHO) estimates that about one third of the world population is anemic, defined as the presence of an insufficient mass of RBCs circulating in the blood. IDA is reflected in hemoglobin concentrations below the recommended thresholds.[32,40] The most common symptoms of anemia conditions result from reduced oxygen transportation by hemoglobin. These symptoms include pallor, fatigue, faintness, shortness of breath, muscle weakness, angina pain, and elevated cardiac output (as compensation for reduced O_2-carrying capacity).[31] The common diagnostic criterion for anemia is based on the hemoglobin concentration although different criteria can be found in the literature. According to the WHO and the Kidney Disease: Improving Global Outcomes (KDIGO) organization developed (2002), the diagnosis of anemia is based on a hemoglobin (Hb) level below 13 g dL^{-1} in men over 15 years, below 12 g dL^{-1} in non-pregnant women over 15 years, and below 11 g dL^{-1} in pregnant women.[32,43,44] The European Renal Best Practice (ERBP) Position Paper uses a Hb value lower than 13.5 g dL^{-1} for male individuals (with a correction to Hb < 13.2 g dL^{-1} for males older than 70 yrs), and lower than 12 g dL^{-1} for female individuals.[44] In 2015, the National Institute for Health and Clinical Excellence (NICE) suggested to diagnose anemia based on a Hb level below 12 g dL^{-1} in men and below 10 g dL^{-1} in premenopausal women.[45]

ID and anemia can occur in absence of each other. ID can exist in absence of IDA if it has not lasted long enough or it has not been severe enough to cause depletion of erythroid iron. However, both ID and anemia have important consequences for human health and child

development: iron deficient and/or anemic women and their infants show a higher risk of dying during the perinatal period; the child's mental and physical development is delayed or impaired by iron deficiency; and the physical work capacity and productivity of manual workers may be reduced. Besides ID, anemia can be also caused by (i) inflammation and infectious diseases such as malaria, hookworm infections and schistosomiasis; (ii) reduced erythropoietin (EPO) production in kidney; (iii) deficiencies of other key micronutrients including folate, vitamin B12, and vitamin A; or (iv) hereditary conditions that affect the RBCs, such as thalassaemia.[32]

The condition termed functional iron deficiency (FID, relative iron deficiency) occurs in the situation of inadequate iron supply to the bone marrow. The physiological rate of RBC production exceeds the ability of transferrin-bound circulating iron to provide adequate substrate for Hb synthesis, which results in low TSAT. At the same time, the serum ferritin, which reflects iron stores, can remain normal or elevated.[34,41,46] The iron balance is fundamentally regulated by the rate of erythropoiesis and the size of iron stores. In IDA, the iron supply depends on the quantity of the body's stored iron, whereas in FID, the iron supply depends on the rate of iron mobilization.[47]

An extreme case of FID is known as reticuloendothelial (RE) blockade and usually occurs in the setting of acute or chronic inflammation/infection. This often correlates with a high C-reactive protein (CRP) level and/or a high erythrocyte sedimentation rate. Due to the inflammatory state and likely mediated hepcidin production (see section 1.1.3), the iron gets "locked up" in RE storage and therefore, it cannot bind to transferrin. Thus, transferrin-bound iron (reflected in the TSAT) is low, despite of a normal or elevated ferritin level. This condition is aggravated by the fact that ferritin is an acute-phase reactant and it increases in the setting of inflammation. Consequently, in such conditions, elevated serum ferritin levels can be due to high iron stores or due to the inflammatory state and therefore, patients have to be treated in different ways.[34] FID is one of the forms of ACD which occurs in response to systemic illness and/or chronic inflammatory diseases, such as autoimmune conditions (rheumatoid arthritis and inflammatory bowel disease), cancer, and end-stage renal failure.[41,47,48] ACD is the second most common form of anemia worldwide, which can mimic or co-exist with other types of anemia.

The anemia can be caused by a variety of physiological conditions, such as an impaired production of EPO, reduced marrow erythroid response to EPO, iron-restricted erythropoiesis,

diminished pool of EPO-responsive cells, and reduced RBCs survival.[48] Many efforts to fight iron deficiency and anemia have been made over the past two decades but, despite these efforts, ID and anemia are still common clinical conditions.[32]

As has been mentioned above, in IDA, the iron supply depends on the quantity of iron storage in the body, while in FID (and consequently ACD) the supply depends on the rate of mobilization of iron from the stores. The diagnosis of both conditions is particularly challenging in patients with acute or chronic inflammatory conditions because most of the biochemical markers for iron metabolism are affected by the acute phase reaction. This is also the case of anemia associated to chronic kidney disease (CKD), where anemia of different types typically occurs.[46]

ID and/or anemia is a common complication of CKD that can be derived from multiple causes. The main factors that contribute to iron deficiency in patients with end-stage renal disease (ESRD) are reduced intake and impaired intestinal absorption of dietary iron, blood losses, chronic inflammation associated with ESRD and/or increased iron requirements during therapy with erythropoiesis-stimulating agents (ESA).[36] The anemia, in turn, can be the result of (i) ID (IDA), (ii) reduced production of EPO due to kidney damage (EPO-related anemia), and (iii) inflammatory conditions (FID and ACD). As has been shown in Fig. 1-3 (section 1.1.2), EPO is produced by the kidney in response to a low tissue oxygen level and stimulates the bone marrow to produce new RBCs.[45] Therefore, an altered EPO production has a significant effect on erythropoiesis. The management of ID and anemia is an important issue for patients with renal insufficiency. However, determining the real cause of anemia and consequently, making adequate decisions concerning the patient's treatment is still a challenge.

1.2 PRINCIPLES OF ICP-MASS SPECTROMETRY

1.2.1 Principle design of ICP-MS

Inductively coupled plasma-mass spectrometry (ICP-MS) is a powerful analytical technique for the determination of trace and ultra-trace concentrations of elements and their isotope ratios in a large variety of applications. An ICP-mass spectrometer consists of the combination of an inductively coupled argon plasma (ICP) as an ion source and a mass

spectrometer for subsequent separation and detection of the ions. This coupling was firstly proposed by Houk *et al.* in 1980.[49] After the commercial introduction of this technique in 1983, ICP-MS rapidly occupied a leading position among the analytical techniques. Nowadays, ICP-MS competes with and displaces other techniques commonly used for elemental determinations, such as atomic absorption spectrometry (AAS) and inductively coupled plasma-optical emission spectrometry (ICP-OES), and isotopic analysis, such as thermal ionization mass spectrometry (TIMS). The main advantages of ICP-MS are the high ionization efficiency of the ICP ion source, the high sensitivity, and low detection limits (down to pg L^{-1}), wide linear dynamic range (up to 12 orders of magnitude), high speed data acquisition in multi-elemental determinations, flexibility of sample introduction (liquid samples *via* pneumatic nebulization and solid samples *via* laser ablation (LA) or electrothermal vaporization (ETV)[50]), and high sample throughput. Moreover, ICP-MS is also used in speciation by coupling it with different separation techniques, *e.g.*, high-performance liquid chromatography or gas chromatography.[51] In spite of the numerous advantages of the ICP-MS, it is not free from drawbacks. The occurrence of interferences is probably the strongest limitation of this technique, although several strategies can be used to overcome them. In general, ICP-MS is relatively expensive and requires reagents of high purity, slightly acidified measurement solutions (typically < 5%), and a total amount of dissolved solids < 0.2%.[52–54]

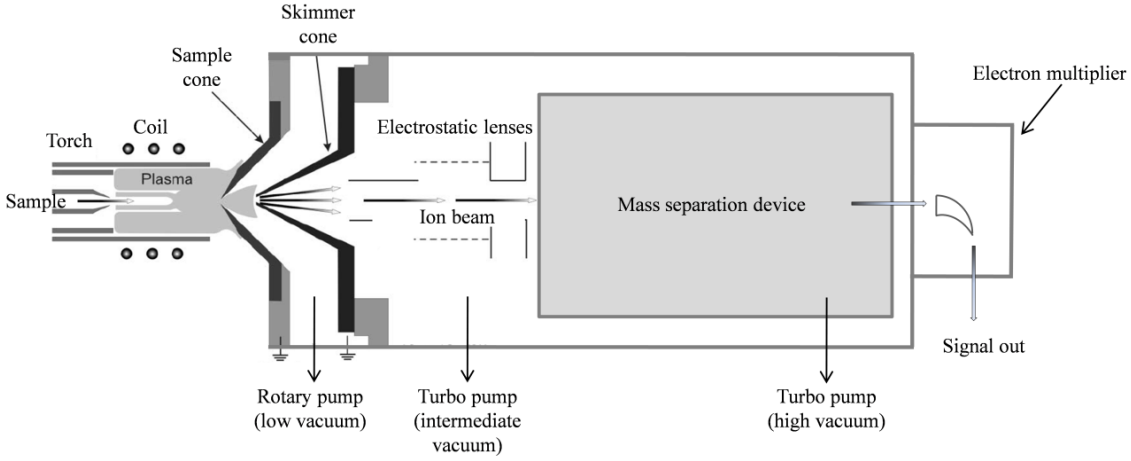

Fig.1-6 Schematic representation of a typical ICP-MS instrument (adapted from Houk 1986).[55]

An ICP-mass spectrometer consists of three principal components: (i) an ionization source (for atomization and ionization); (ii) a mass analyzer (for separation of the ions based on their

mass-to-charge ratios), and (iii) a detector (for converting the ions into a measurable signal). A schematic representation of an ICP-MS instrument is shown in Fig. 1-6.

Nowadays, a number of different ICP-MS designs are available, which can differ from one another in the design of the interface, ion focusing system, and mass separation device.[52] In this PhD, double-focusing sector-field inductively coupled plasma-mass spectrometry (SF-ICP-MS) and multi-collector inductively coupled plasma-mass spectrometry (MC-ICP-MS) were employed. Conventional introduction of a liquid sample is accomplished *via* pneumatic nebulization, where an aerosol is formed through interaction of an accelerated argon flow on the liquid sample surface in the nebulizer (typically of concentric design). The nebulizer is mounted onto a spray chamber (typically of double-pass Scott-type or of cyclonic design) that prevents the large droplets to enter the plasma by gravitational and centrifugal forces, thereby providing stable atomization and ionization in the ICP. The fine aerosol is then transported to the plasma torch, consisting of three concentric tubes, each of which with argon gas flows (Fig. 1-7).

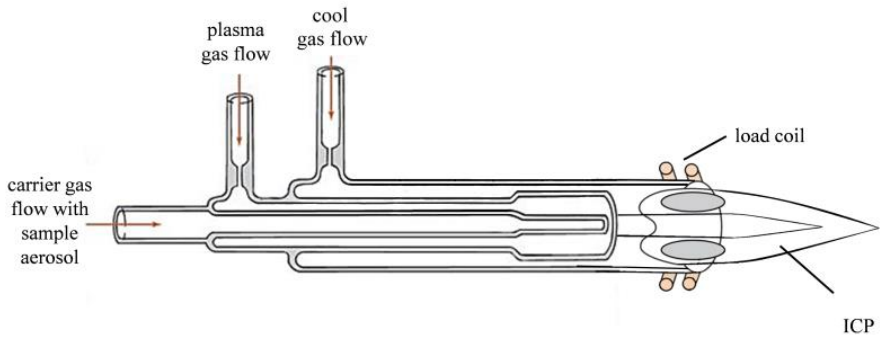

Fig. 1-7 Torch and ICP.

The argon ICP is a plasma ionization source, which can be defined as a gas mixture at high temperature that contains molecules, atoms, ions, and electrons. The plasma torch is surrounded at its top by a water- (or gas-) cooled load coil (usually made of copper) connected to a radio frequency generator (27.12 or 40.68 MHz). When RF power (ranging between 750-2000 W) is applied to the load coil, an alternating current oscillates within the coil at a rate corresponding to the frequency of the generator, thereby creating an intense electromagnetic field at the top of the torch. A high-voltage spark is applied to induce free electrons in the gas stream. These electrons are accelerated in the magnetic field, leading to

the formation of more electrons by collision with argon atoms (electron impact ionization, equation 1-2). The process of ionization of the argon continues in a chain reaction, leading to the formation of more electrons and a self-sustaining plasma.[52,54,56]

$$Ar + e^- \rightarrow Ar^+ + 2e^- \quad (1\text{-}2)$$

At the same time, excited argon atoms are formed (equation 1-3):

$$Ar^+ + e^- \rightarrow Ar^* \quad (1\text{-}3)$$

The ICP is mainly operated in hot plasma conditions, with an RF power of about 1200-1300 W and a plasma temperature (ionization temperature T_{ion}) of about 8000 K (in the center of plasma). At such a temperature, sample aerosol, introduced with the carrier gas stream, is first desolvated and vaporized, and the molecules thus formed subsequently atomized. Analyte atoms *M* are then ionized by means of (i) electron impact ionization (equation 1-4), caused by collision with accelerated electrons; (ii) charge transfer reactions (equation 1-5), caused by collisions between ions and atoms; and (ii) Penning ionization (equation 1-6), caused by collisions between atoms and excited Ar atoms.[54]

Electron impact ionization $M + e^- \rightarrow M^+ + 2e^-$ (1-4)

Charge transfer ionization $M + Ar^+ \rightarrow M^+ + Ar$ (1-5)

Penning ionization $M + Ar^* \rightarrow M^+ + Ar + e^-$ (1-6)

Simultaneously, also excited atoms are formed due to electron excitation of atoms (equation 1-7) and ion–electron radiative recombination (equation 1-8)[54]:

$$M + e^- \rightarrow M^* + e^- \quad (1\text{-}7)$$

$$M^+ + e^- \rightarrow M^* \quad (1\text{-}8)$$

Under such conditions, most of the chemical compounds present in the sample aerosol are decomposed into their atomic constituents and the atoms thus formed are further ionized to a high degree in the plasma. The ionization efficiency α depends on the first ionization energy E_i of the element (the higher E_i, the lower α). The elements with $E_i < 8$ eV are ionized with nearly 100% yield ($\alpha \geq 0.9$), the metalloids ($\alpha \approx 0.3\text{-}0.8$) and nonmetals ($\alpha \approx 0.01\text{-}0.3$) can be ionized with a reasonable ionization efficiency.[56]

Simultaneously with singly charged elemental M^+ ions of the sample and the Ar plasma gas, also a variety of other species are formed, such as doubly charged ions and polyatomic ions, which can interfere with the determination of the target elements at a similar mass-to-charge ratio (m/z) in the mass spectrum. Several approaches can be used to avoid/minimize the occurrence or influence of these species, such as a chemical pre-treatment of the sample prior to ICP-MS measurement, higher mass resolution, the use of a collision/reaction cell, cool plasma conditions and/or mathematical corrections.

The ionization in the ICP, operated at atmospheric pressure, is followed by extraction of analyte ions into the mass spectrometer, which operates under high vacuum conditions (Fig. 1-6). The interface plays a critical role and needs to transport the ions efficiently and with electrical integrity from the plasma into the mass spectrometer.[52] The interface consists of two water-cooled metal cones (typically from Ni or Pt, rarely Al) with a small orifice, sampler and skimmer, which are mounted one after another with an intermediate vacuum (~10^2 Pa) accomplished using a rotary (or fore-vacuum) pump in-between. The ions generated in the plasma pass through the sampler cone first (0.8-1.2 mm orifice) then, travel a short distance to the skimmer cone (0.4-0.8 mm orifice) and subsequently enter the ion optics. The main function of the ion optics is focusing of the ion beam, selecting of positive ions and preventing photons and neutral species from impinging on the detector.[53]

The ion beam, focused through the ion optics, is guided into the mass spectrometer, where the positive ions are separated from one another according to their *m/z* ratio. Quadrupole and sector-field analyzers are the typically used mass separation devices in commercial ICP-MS instrumentation. Resolution, abundance sensitivity, and scan speed are important characteristics of an ICP-MS instrument.

The capability of the mass spectrometer to separate ions with masses m and $m+\Delta m$ is characterized by the mass resolution R (or resolving power), defined as follows:

$$R = \frac{m}{\Delta m} \approx \frac{\left(\frac{m_1 + m_2}{2}\right)}{m_2 - m_1} \qquad (1\text{-}9)$$

Two approaches are used to calculate mass resolution (Fig. 1-8). The 10% valley definition (Fig. 1-8 a) considers two peaks of equal height in a mass spectrum (masses m_1 and m_2). The peaks are considered as resolved if the valley between the peak maxima does not exceed 10%

of the peak heights. The other definition is based on experimentally observed mass width of a single spectral peak at 5% of its maximum (Fig. 1-8 b).[54,56]

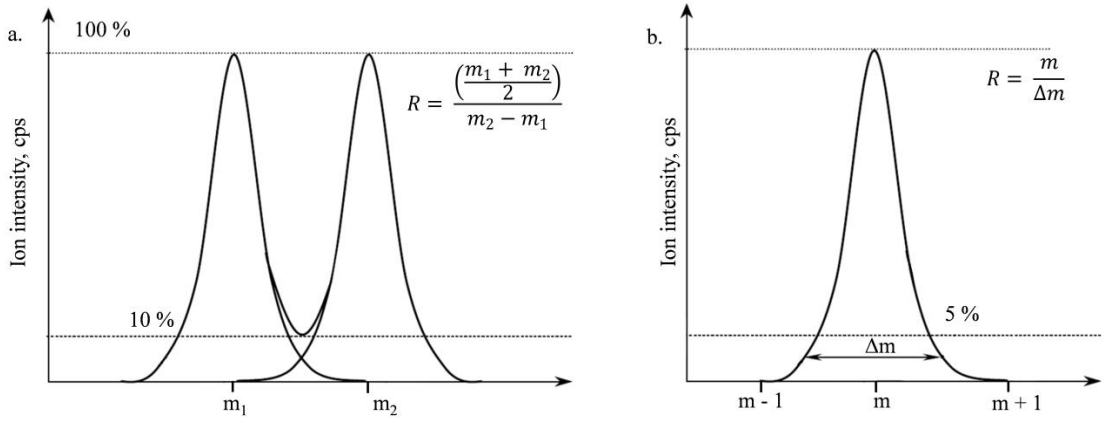

Fig. 1-8 Mass resolution. (a) 10% valley definition: calculation of the resolution required to resolve two adjacent spectral peaks showing a mass difference of $m_2 - m_1$; (b) calculation of the resolution offered by a mass spectrometer on the basis of the width of a spectral peak at 5% peak height (Δm) at mass m (adapted from Vanhaecke and Degryse, 2012 and Becker, 2007).[54,56]

The abundance sensitivity (Fig. 1-9) is a quantitative measure for the contribution of the tail of a neighboring peak to the signal intensity of the target element. This aspect is especially important when a low intensity signal has to be measured next to a high intensity signal peak (large difference between the relative isotopic abundances). The abundance sensitivity is defined by IUPAC as "the ratio of the maximum ion current recorded at a mass m to the ion current arising from the same species recorded at an adjacent mass ($m \pm 1$)".[53,57]

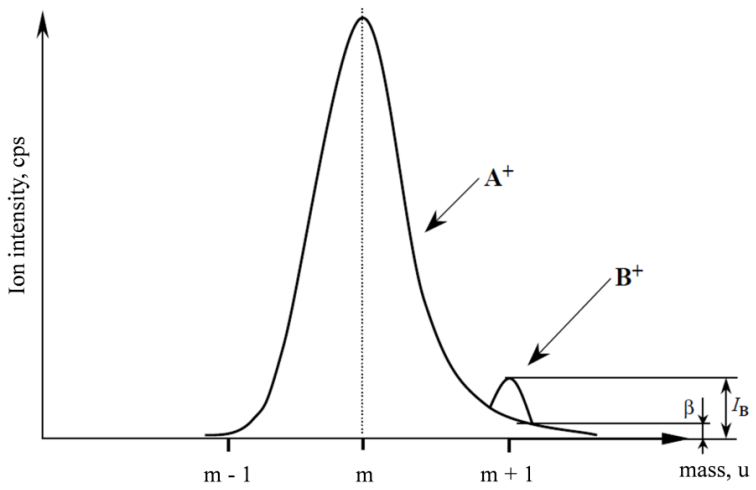

Fig. 1-9 Abundance sensitivity: Influence of peak tailing (β) from the abundant ion peak A^+ at mass m on neighboring ion peak B^+ at mass $m+1$ with low intensity I_B (adapted from Becker, 2007).[54]

The scan speed is an important characteristic in the context of isotope ratio measurements and is the speed with which the mass spectrometer can scan the mass spectrum or switch from one mass to another.[56]

Three types of mass spectrometers are commercially employed in ICP-MS: (i) the quadrupole mass filter (Q-MS), (ii) the double-focusing sector field mass spectrometer (SF-MS), and (iii) the time-of-flight mass spectrometer (TOF-MS).

The quadrupole filter consists of four parallel cylindrical or hyperbolic rods with a direct current (DC) and an alternating current (AC) voltage component applied to them. The diagonally opposed rods are electrically connected, forming two electrode pairs. The voltages applied on both pairs, have the same magnitude but show an opposite charge.[56,58] A schematic representation of the quadrupole is given in Fig. 1-10.

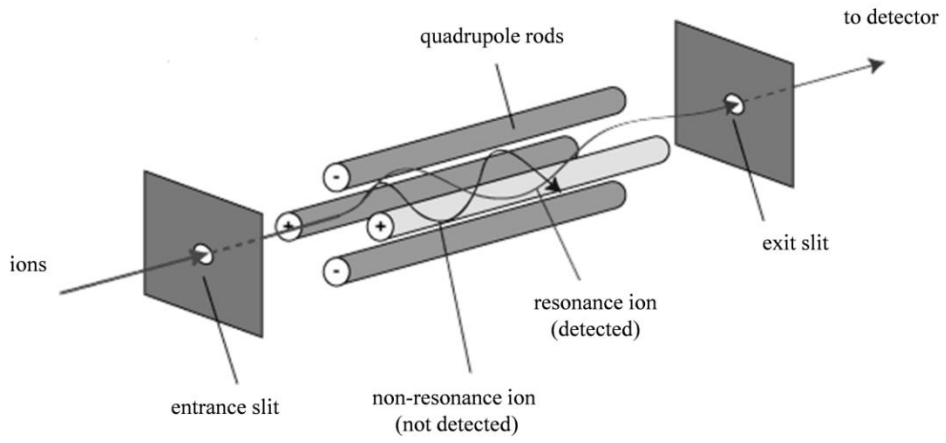

Fig. 1-10 Operation principle of a quadrupole mass filter. (adapted from School of Chemistry, University of Bristol).[59]

The focused ion beam coming from the ion optics is directed into the central channel between the four rods. The positive DC component (+*U*) forces the ions to move towards the axis of the rod and the AC component (*Vsinωt*) focuses the ions to the center during the first half a period and defocuses the ions from the center in the direction of the rods during the second half period. Heavy ions are focused on the central axis and lighter ions are sufficiently accelerated towards the quadrupole rods and removed from the ion beam. The average potential is positive and this pair of the electrodes acts as a high-mass filter. The voltage applied to the other pair of electrodes shows the same magnitude, but the opposite sign. In this case, the pair of electrodes consist of a DC component (-*U*) and an AC component, which

shows a phase difference of 180° ($Vsin(\omega t + \pi)$). The average potential is negative and thus, this pair of electrodes acts as a low-mass filter. In this way, the heavier ions are defocused and removed from the ion beam, while the lighter ions are focused on the central axis. Thus, the combination of the two electrode pairs results in a bandpass filter (Fig. 1-11). The DC and AC voltages are selected in such a way that only the ions within a selected narrow mass-to-charge ratio range can pass through the quadrupole filter, and the heavier and lighter ions collide with the rods and/or are removed. The dynamic selection of masses passing the filter is accomplished by changing the DC and AC voltages in such a way that the ratio of their magnitudes remains constant.[54,56,58] The most notable advantages of the quadrupole mass analyzer are its technical simplicity with rapid scanning, larger tolerance towards the spread of the kinetic energies of ions entering the filter, possibility to operate at higher pressure and, consequently, relatively low cost. The major disadvantage of the quadrupole mass spectrometer is the low mass resolution ($m/\Delta m \approx 300$).

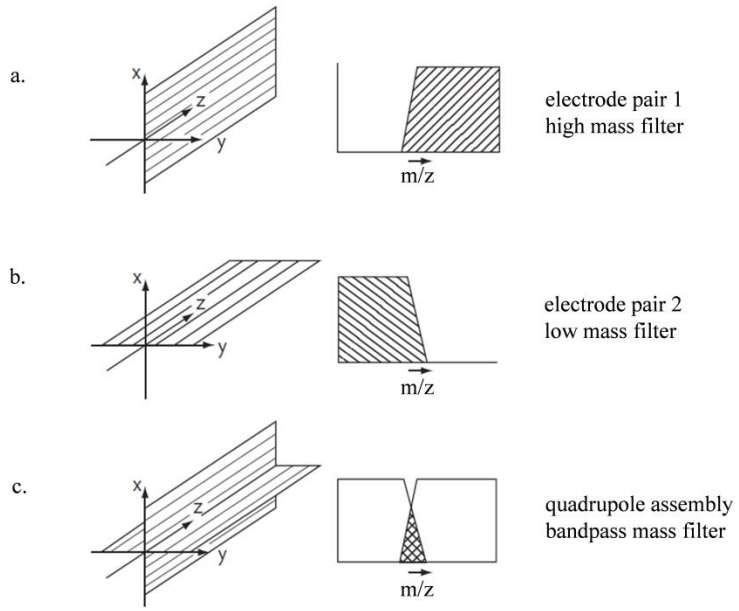

Fig. 1-11 The combination the high-mass (a) and low-mass (b) filters resulting in bandpass filter (c). (adapted from Miller and Denton, 1986).[60]

The sector-field mass spectrometer consists of a combination of a magnetic and an electrostatic sector (Fig. 1-12). Modern mass spectrometers contain the magnetic and electrostatic sectors located one after the other in a double-focusing setup. The ion beam is first accelerated in the ion optics, providing the ions with a high kinetic energy. Subsequently, ions (with mass *m* and charge *z*) are introduced into a magnetic field *B* (Fig 1-12 a). When

ions with velocity *v* are introduced into a magnetic field, they move according to a circular path with radius *r* under Lorentz force:

$$F = \frac{mv^2}{r} = zvB \tag{1-10}$$

The resulting radius of the circular path *r* of the ion depends on its mass-to-charge ratio (*m/z*) at a constant acceleration voltage *V* and constant magnetic field *B*:

$$r = \frac{\sqrt{2Vm}}{B\sqrt{z}} \tag{1-11}$$

The radius of the trajectory of the nuclide of interest need to be altered to allow it to reach the detector. When a single detector is used, the mass-to-charge ratio of the ion can be selected by either adapting the magnetic field strength *B* (magnetic scanning or B-scanning) or the acceleration voltage *V* (electric scanning or E-scanning).[56]

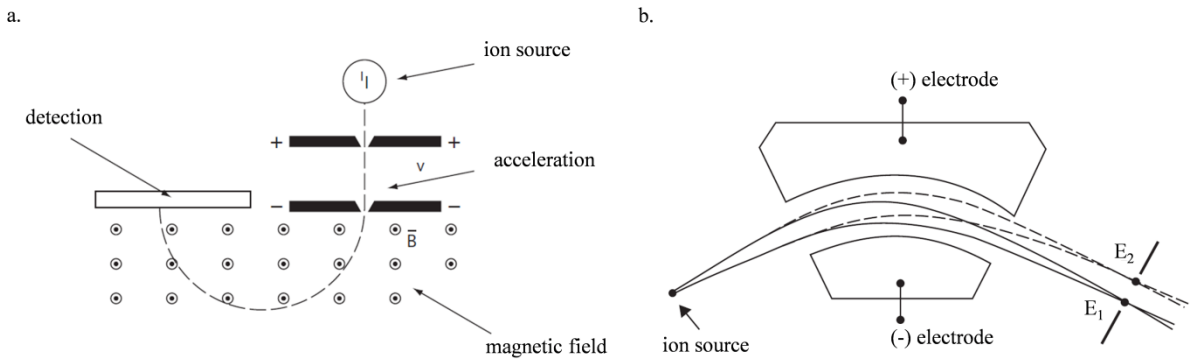

Fig. 1-12 Operation principle of (a) magnetic and (b) electrostatic sectors. (adapted from Vanhaecke and Degryse, 2012).[56]

The electrostatic sector (Fig. 1-12 b) provides energy focusing to improve the mass resolution. An electrostatic sector with strength *E* consists of two bent electrode plates, to which potentials equal in magnitude but opposite in charge are applied. The ions, moving between the positively charged and a negatively charged bent plate, are forced to move along a circular path. The centrifugal force (mv^2/r) required to move ions along a circular path, is provided by the electrostatic force, equal to zE[56]:

$$F = \frac{mv^2}{r} = zE \tag{1-12}$$

As a result, the radius of the circular path of an ion depends on its kinetic energy:

$$r = \frac{mv^2}{zE} = \frac{2E_{kin}}{zE} \tag{1-13}$$

The combination of magnetic and electrostatic sectors radically improves the mass resolution, but lowers the transmission efficiency as less ions eventually reach the detector.[54,56,58] In a double-focusing setup, the electrostatic and magnetic sectors are combined in such a way that the dispersions of the ion beam in both sectors eliminate each other. Thus, ions with a different kinetic energy or direction and the same *m/z* will still be focused at the same point. In Fig. 1-13, three different double-focusing geometries (Mattauch-Herzog, Nier-Johnson and reversed Nier-Johnson geometry) are shown. In the Mattauch-Herzog geometry (Fig. 1-13 a), the electrostatic sector with a specific angle of 30°50´ is followed by an anti-directionally curved magnetic sector of 90°. This arrangement permits the simultaneous monitoring of a relatively large mass spectrum. In the Nier-Johnson geometry (Fig. 1-13 b), the electrostatic sector is followed by the magnetic sector (both at 90°) and in the reversed Nier-Johnson geometry (Fig. 1-13 c) the magnetic sector is followed by the electrostatic sector (both at 90°). In this geometry, only one mass can be focused at the detector at any given time, and the spectrum needs to be measured dynamically, in scanning or peak hopping mode. For single-collector instruments, such as SF-ICP-MS, scanning or peak hopping is accomplished by adapting the magnetic field strength *B* or the acceleration voltage *V*. Sector-field mass analyzers are characterized by a higher mass resolution (up to 10000), low abundance sensitivity, high ion transmission efficiency, and flat-topped peaks with a trapezoidal shape.[54,56]

In a time-of-flight mass spectrometer (TOF), ions are accelerated over an electrical potential *V* and subsequently introduced into a field-free flight tube and thus, all ions acquire the same kinetic energy:

$$E_{kin} = \frac{1}{2}mv^2 = zV \tag{1-14}$$

A time *t* is required to travel the distance to the detector, placed at the end of flight tube with length *L*[56] and velocity *v,* determined from equation 1-15:

$$t = \frac{L}{v} = \frac{L\sqrt{m}}{\sqrt{2zV}} \tag{1-15}$$

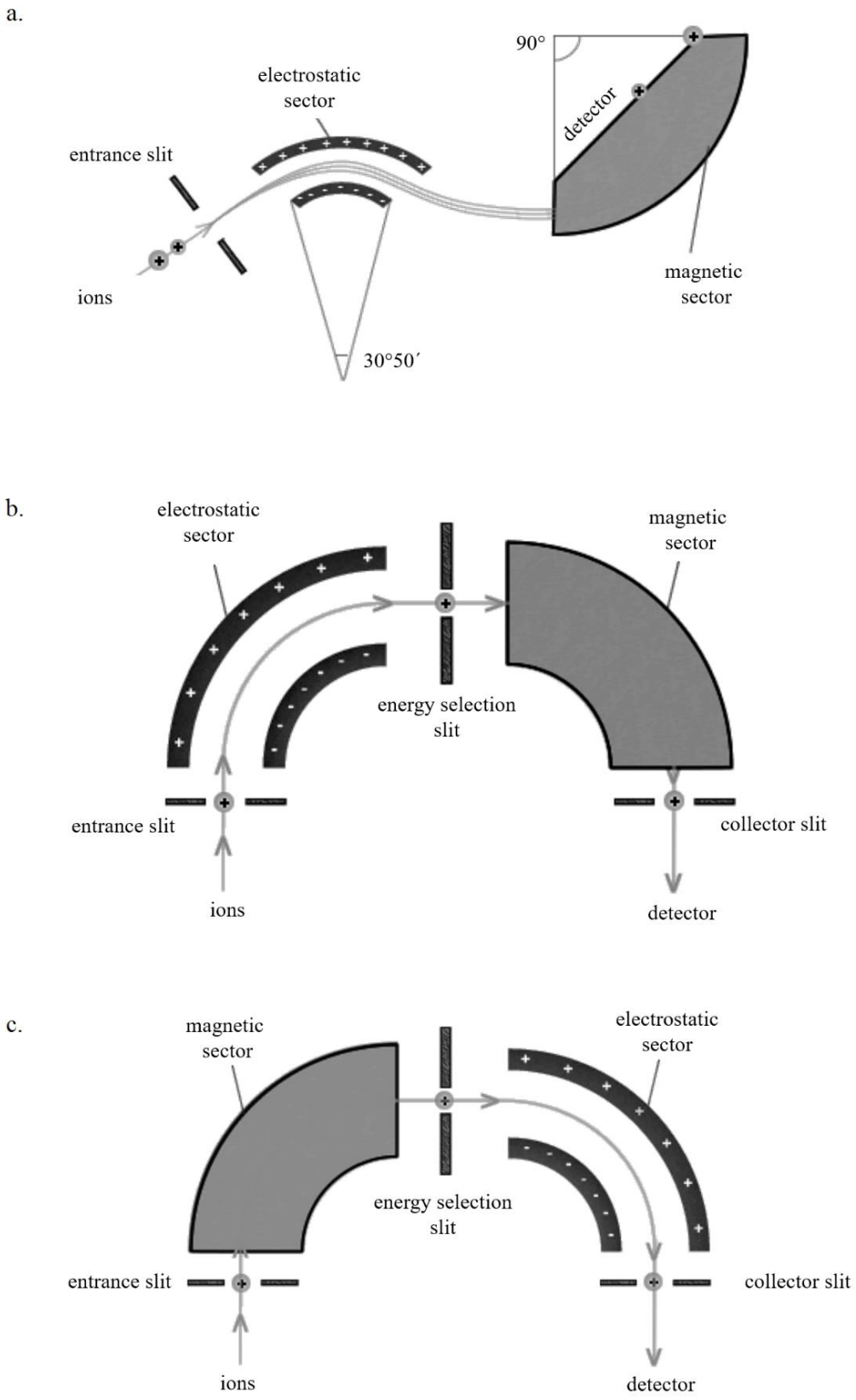

Fig. 1-13 Double-focusing setups: (a) Mattauch-Herzog, (b) Nier-Johnson, and (c) reversed Nier-Johnson geometries (adapted from Wiedenbeck *et al.*, 2012).[61]

The ions are continuously registered at the end of the flight tube and therefore a TOF analyzer provides a complete mass spectrum for each package of ions that is introduced. The combination of a TOF analyzer with an ICP as ion source requires beam modulation, which is typically accomplished by orthogonal acceleration. The high spread in kinetic energy of the introduced ions can be remedied to some extent using an ion mirror to reflect the ions, such that they pass the flight tube twice and the path length is increased. The use of an ion mirror also corrects for differences in kinetic energy, as ions with higher energy are forced to travel a longer distance. TOF currently demonstrates the fastest acquisition rate among the mass analyzers (~ 0.033 ms for full mass spectrum).[56]

The final part of an ICP-MS unit is the ion detection system. The ions that passed the mass analyzer are detected and transformed into a suitable signal, proportional to the abundance of nuclides. Nowadays, two types of detectors are commonly used: the electron multiplier and Faraday cup. The operating principle of an electron multiplier is based on avalanche multiplication of electrons formed due to an ion striking the conversion electrode of a discrete dynode electrode. The electrons thus formed are accelerated towards the back end of the detector due to the potential difference over the detector (negatively charged front end and grounded back end of detector, each subsequent dynode is at a higher potential). This acceleration leads to multiple collisions with subsequent dynodes and whenever an electron collides with a dynode's surface, more electrons are set free. As a result of this multiplication effect, one ion arriving at the detector finally leads to approximately 10^7–10^8 electrons. Each ion is individually detected in pulse counting mode.[56,62]

In a Faraday cup, the ion beam coming from the mass analyzer is directed into a metallic cup, when the ions reach the wall of the cup, they are neutralized by accepting electrons. This leads to a current through the resistor, which is further amplified and detected. This type of detector consists of a thin and deep bucket (cup). In a multi-collector setup, several Faraday cups are fitted onto movable stages. The large depth of the cup helps to ensure that any secondary electrons produced by energetic incident ions cannot escape the detector. The cups are connected to current amplifiers with high-ohmic feedback resistors (modern systems have amplifiers of 10^{10}, 10^{11},10^{12}, and 10^{13} Ω). Faraday cup detection is the most robust, linear, and accurate technology for the measurement of ion currents. However, the main disadvantages of this detector are the low sensitivity, which is limited by the noise of the amplifiers, and a slower response time.

1.2.2 Multi-collector ICP-MS

High-precision isotopic analysis *via* multi-collector inductively coupled plasma-mass spectrometry (MC-ICP-MS) is providing relevant information in the context of geological, cosmochemical, environmental, forensic, and biomedical applications. For such purposes, TIMS was traditionally used. However, nowadays multi-collector ICP-mass spectrometry is preferable for the high-precision isotopic analysis of metals and metalloids from a practical point of view. In TIMS, the element of interest, previously isolated chemically from the sample, is loaded onto a metal filament. Subsequently, the element is ionized under resistive heating in vacuum and thereafter, the ions are separated according to their mass to-charge ratio in the mass analyzer for further detection. Modern MC-ICP-MS provides comparable precision (~0.002% RSD, under ideal circumstances),[63,64] but higher sample throughput. Moreover, the ICP ion source is capable of ionizing elements with high ionization energies (> 7 eV) such as Cu (7.7 eV), Fe (7.9 eV), W (8.0 eV), B (8.3 eV), Sb (8.6 eV), and even the volatile Hg (10.4 eV)[65] at atmospheric pressure. The use of a detector array with multiple Faraday cups permits the simultaneous collection of the separated ion beams thereby ensuring high isotope ratio precision. The simultaneous detection of the isotopes of interest also allows the measurement of transient signals generated by devices, such as gas or liquid chromatographs, laser ablation systems, and on-line chemical reactors, coupled to the MC-ICP-MS unit.[56,66]

MC-ICP-MS instruments are based on a double-focusing sector-field mass analyzer to provide flat-topped peaks, which are necessary for high-precision isotope ratio measurements at low and "pseudo" high mass resolution[67] and static separation of ion beams. The unit in operation at UGhent is equipped with movable faraday cups connected to 10^{10} - 10^{12} Ω amplifiers.[66] The use of "jet" sample cones in combination with a large interface pump allows an improvement in sensitivity by a factor between 4 and 50 compared to the standard interface.[68,69]

In comparison to MC-ICP-MS, the precision of the isotope ratios obtained *via* a quadrupole-based instrumentation or SF-ICP-MS is ≤ 0.05% RSD.[70–72] By increasing the mass resolution (which is necessary for elements as Fe due to the presence of Ar-based interferences) in SF-ICP-MS, the peak shape changes from trapezoidal to almost triangular and therefore, the internal isotope ratio precision is deteriorated (~0.1% RSD under ideal conditions).[73]

Although the precision attainable with this instrumentation is significantly poorer than that obtained *via* MC-ICP-MS or TIMS, it can be sufficient for some applications.

1.2.3 Correction for instrumental mass discrimination

Isotope ratio measurements by MC-ICP-MS are affected by instrumental mass discrimination, principally due to a more efficient transport of the ions of the heavier isotopes of the target analyte. This phenomenon is mainly associated with the supersonic expansion of the ion beam in the interface and space-charge effects (in principle, heavier ions have higher kinetic energy and push the lighter ions away from the center of the ion beam due to electrostatic repulsion).[66,74–77] However, to date, there is still no complete understanding of this phenomenon.[78] The bias between true and measured values for light-mass elements, such as B, is more pronounced in MC-ICP-MS than in TIMS, where the origin of mass fractionation effects (time-dependent mass bias as a result of the finite amount of sample on the filament source and the more efficient thermal ionization of the lighter isotope) is better understood.[56,76] Regardless of the exact origin of the mass discrimination in ICP-MS, this effect has to be carefully corrected for in isotope ratio measurements, in order to obtain precise and accurate results.

Several approaches have been proposed for mass bias correction, typically mathematically based on external correction using a certified isotopic reference material with known isotopic composition, an internal correction using an internal standard (intra- or inter-elemental) or a combination of both. The simplest method is external correction, typically in a sample-standard bracketing (SSB) approach, where the isotope ratio data obtained for a sample is referenced to the ratio obtained for an isotopic standard measured before and after the sample. The SSB approach has two major assumptions: (i) the mass discrimination is supposed to be relatively stable as a function of time and (ii) the external standard and samples show an equal mass discrimination behavior. Therefore, matrix matching of the samples and standard plays a critical role, which in practice is not always possible.[56] Internal standardization using a second isotope pair of the analyte (invariant in nature) can be used to correct the target isotope ratio, containing a radiogenic isotope, for instrumental mass discrimination (intra-element internal standardization).[63,79] This model not only corrects for instrumental mass discrimination, but also for any natural mass-dependent isotope fractionation of the target isotope ratio. However,

the main limitation of intra-elemental internal standardization is the number of isotopes required and the limited applicability. Another approach is based on using the another element, admixed to the sample as an internal standard (IS), for correction of the target element isotope ratios for instrumental mass discrimination (inter-element internal standardization).

Different models for correction of instrumental mass discrimination have been proposed over the years.[63,71,78,80,81] The difference between the measured (R_{exp}) and the true (R_{true}) isotope ratios is usually expressed by the mass bias correction coefficient, K_{ij} (also termed 'mass-bias factor'):

$$R_{true} = R_{exp} \cdot K_{ij} \tag{1-16}$$

The mass-bias correction model, firstly described by Russell *et al.* (equation 1-17)[82] remains the most popular:

$$\frac{R_{true}}{R_{exp}} = \left(\frac{m_i}{m_j}\right)^f \tag{1-17}$$

where m_i and m_j are the nuclide masses, and f_x is fractionation function.

In general, mass-bias correction models express the mass-bias relation between the various isotope pairs of the same (intra-elemental internal standard) or differing (inter-elemental internal standard) elements. Thus, the two mass-bias correction factors are assumed to be proportional to the mass ratio of the nuclides (equation 1-18):

$$f_{sample,IS} = \frac{ln\left(\frac{R_{true}}{R_{exp}}\right)}{ln\left(\frac{m_i}{m_j}\right)} \tag{1-18}$$

Woodhead suggested to use the best-fitting straight line through data for the target isotope ratio (f_{sample}) plotted against those for an IS (f_{IS}), calculated according to equation 1-18, to deduce the correction factor.[80] This model was further revised by Baxter *et al.*[83] using a linear regression line between $ln(R_{sample})$ and $ln(R_{IS})$ to establish the correlation between the correction factors for the analyte and the internal standard:

$$lnR_{sample} = a + b \cdot lnR_{IS} \tag{1-19}$$

Both approaches (Woodhead and Baxter) provide equivalent results. Particularly for Fe isotope ratio data, SSB combined with internal correction (using Ni as an IS) by means of the Russell law, using a regression line to establish the correlation between the correction factors (f_{Fe} is plotted against those for an IS f_{Ni}) or revised Russell law, using a regression line to establish the correlation between the logarithm of uncorrected isotope ratio for Fe plotted versus that of Ni, were used in this PhD.

Instrumental mass discrimination can also be corrected for by using the double spike approach, where a spike enriched in two isotopes and with known isotopic composition of the target element is added to the sample.[56,84,85] Therefore, the target element needs to have at least four isotopes. This method provides accurate and precise isotope ratio data and allows to correct for sample loss in any sample preparation step, which can lead to artificial isotope fractionation. However, next to the number of isotopes required, the double spike technique also has other disadvantages such as the high cost of high-purity isotopically enriched materials, potential memory effects and lower sample throughput.

1.2.4 Overcoming spectral interferences

Spectral interferences are generally classified into three major groups depending on the type of ion at the origin of the problem: an isobaric atomic ion, a multiply charged ion (mostly doubly charged ion), or a polyatomic (molecular) ion. Isobaric interferences occur when nuclides from different elements have the same nominal mass, *e.g.*, ^{58}Fe and ^{58}Ni. However, each element of the periodic table, except indium, has at least one isotope free from isobaric interference, although these nuclides are not always the most abundant. Doubly charged ions are formed when an ion is generated with a double positive charge and produces a spectral peak at half its mass. The level of doubly charged species is related to the ionization conditions of the plasma and can be minimized by optimization of the nebulizer gas flow, RF power, and torch position.[52] Polyatomic or molecular ions consist of two or more atoms and typically contain Ar, and/or elements from the sample matrix, the solvent and/or the surrounding air. Moreover, the signals of neighboring ions with very high intensity, for instance derived from the matrix elements, can alter the analytical signal of the target element with lower intensity as a result of the signal "tails" of the neighboring peaks when the abundance sensitivity is not sufficient.

A variety of strategies can be used to overcome spectral interferences, such as high mass resolution in sector-field instruments, chemical or energy resolution using a reaction/collision cell, cold plasma conditions, mathematical corrections, and chemical separation of the target analyte from the sample matrix.[100] A compilation of the isobaric and polyatomic interferences affecting iron isotopes and common strategies to overcome them are presented in the Table 1-1.

Table 1-1. Interferences affecting the monitoring of the Fe isotopes[86] and strategies to overcome them in ICP-MS.

Isotope	**Relative isotopic abundance, %**	**Interfering Species**	**Strategies**
^{54}Fe	5.82	$^{54}Cr^+$, $^{38}Ar^{16}O^+$, $^{36}Ar^{18}O^+$, $^{40}Ar^{14}N^+$, $^{40}Ar^{18}O^+$, $^{38}Ar^{18}O^+$, $^{40}Ar^{14}N^+$, $^{39}K^{15}N^+$, $^{24}Mg^{16}O^{14}N^+$, $^{38}Ar^{15}N^1H^+$, $^{37}Cl^{16}O^1H^+$, $^{35}Cl^{18}O^1H^+$, $^{36}Ar^{17}O^1H^+$, $^{37}Cl^{17}O^+$, $^{36}S^{18}O^+$	Desolvating nebulizer system to eliminate influence of polyatomic interferences such as ArN^+, ArO^+ or $ArOH^+$.[87–89] Use of reactive gases (*e.g.*, NH_3, CO, H_2 and N_2) in a collision/reaction cell in Q-ICP-MS and triple-quadrupole ICP-MS.[90–94] Use of a non-reactive gas (*e.g.*, He) in a collision cell combined with kinetic energy discrimination.[95] Chemical separation of isobaric interferences.[87,88,96] High mass resolution.[92,97] Cold plasma conditions to suppress polyatomic ions such as $^{40}Ar^{14}N^+$ and $^{40}Ar^{16}O^+$.[89,98,99]
^{56}Fe	91.66	$^{40}Ar^{16}O^+$, $^{40}Ca^{16}O^+$, $^{40}Ar^{15}N^1H^+$, $^{38}Ar^{18}O^+$, $^{38}Ar^{17}O^1H^+$, $^{37}Cl^{18}O^1H^+$	
^{57}Fe	2.19	$^{40}Ar^{16}O^1H^+$, $^{40}Ca^{16}O^1H^+$, $^{40}Ar^{17}O^+$, $^{38}Ar^{18}O^1H^+$, $^{38}Ar^{19}F^+$, $^{40}Ar^{18}O^+$, $^{40}Ar^{17}O^1H^+$, $^{41}K^{16}O^+$, $^{39}K^{18}O^+$, $^{43}Ca^{14}N^+$	
^{58}Fe	0.33	$^{58}Ni^+$, $^{40}Ar^{18}O^+$, $^{40}Ar^{17}O^1H^+$, $^{44}Ca^{14}N^+$	

The measurement of iron signal intensities or isotope ratios in ICP-MS is usually performed at medium or high mass resolution due to the presence of spectral interferences, as a result of the presence of ArN^+, ArO^+, and $ArOH^+$ species, which interfere with the signals of the iron nuclides at masses 54, 56, 57 and 58.[86] Quantification of iron, for instance, can be performed successfully *via* SF-ICP-MS using "full" medium or high resolution (Fig. 1-14 b). In case of

Fe isotope ratio measurement *via* MC-ICP-MS, "pseudo" mass resolution is used, according to which the peaks from the analyte and the interferent are not entirely resolved, but there is a significantly wide window, wherein only the analyte ion contributes to the signal intensity and where the signal is flat (Fig. 1-14 c). An improved isotope ratio precision is obtained under these conditions compared to that obtained at "full" high mass resolution.[64,67]

The collision/reaction cell is a universal and flexible strategy to reduce spectral interferences in ICP-MS equipped with a quadrupole mass spectrometer. The cell, containing a multipole under a radio frequency potential, is positioned between the interface and the mass analyzer and filled with a selected gas. The analyte ion can be separated *via* selective ion-chemical reactions of the interfering ion with the reaction gas in the cell with subsequent neutralization or change in its *m/z* ratio and therefore, reducing its contribution to the spectrum. Newly formed species, as a result of the reactions, can be eliminated by kinetic energy discrimination using a deceleration voltage. Alternatively, the target ion can be involved in a selective reaction and measured under a form of reaction product ion. Another approach is based on using an inert collision gas (He or H_2) in combination with energy discrimination. As a result, a decelerating voltage may be applied to discriminate selectively against the polyatomic ions.[56,101] Triple-quadrupole ICP-MS (ICP-QQQ) is a recently introduced type of instrument, equipped with an octopole or quadrupole collision cell located between two quadrupole mass filters and it offers the potential to improve the removal of spectral interferences compared to conventional quadrupole ICP-MS with a collision/reaction cell. The tandem mass spectrometer configuration provides two separate mass selection steps, which provides full control over the ion/molecule chemistry that occurs in the cell.[102] Particularly for Fe, the precision obtained *via* QQQ-ICP-MS is in the order of 0.1% RSD for $^{56/54}$Fe, 0.15 % RSD for $^{57/54}$Fe and 0.5 % RSD for $^{58/54}$Fe. Self-evidently, the precision is worse than that achieved with MC-ICP-MS, but it is equal to or better than that of SF-ICP-MS. This confirms that QQQ-ICP-MS can be considered as a suitable technique for the routine determination of induced changes in the isotopic composition of Fe as encountered in studies on human iron absorption and the evaluation of the efficacy of Fe supplementation, but of course, it cannot replace MC-ICP-MS for the measurement of natural Fe isotope ratio variations due to its significantly lower isotope ratio precision.

Cool plasma conditions are obtained by reducing the RF power of the ICP and increasing the sample gas flow rate. Under these conditions, molecules such as NO and O_2 are not

a.

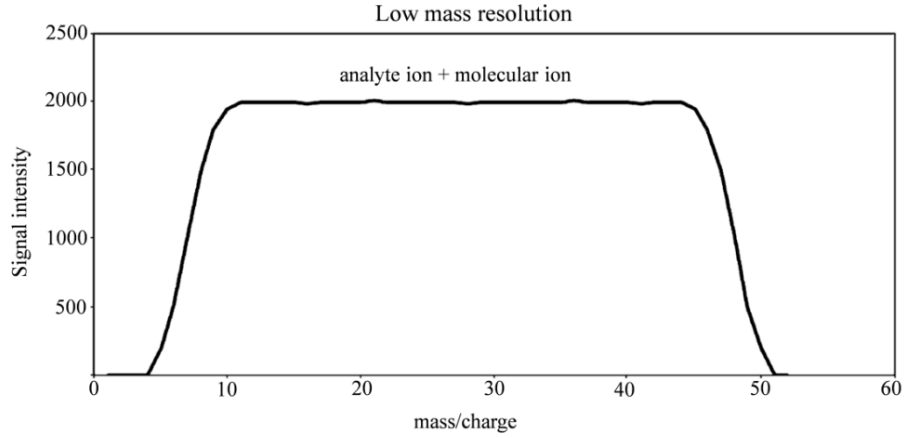

b.

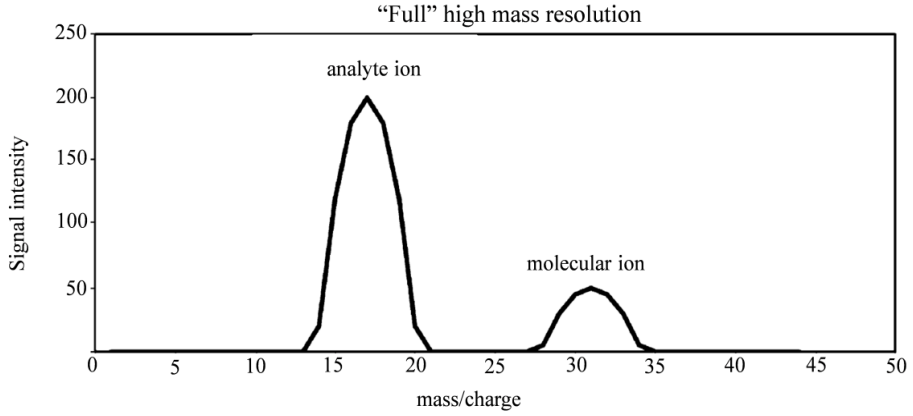

c.

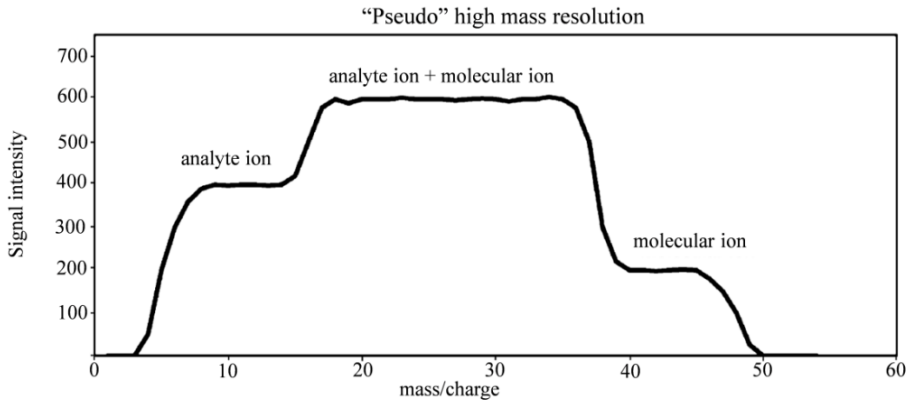

Fig. 1-14 Appearance of mass spectral peak subject to overlap at (a) low mass resolution, (b) (full) high mass resolution, and (c) pseudo high resolution with multi-collector ICPMS (adapted from Vanhaecke and Moens, 2004).[67]

completely atomized and charge transfer from Ar-containing ions to these species is then significantly lowering the signal intensity of interfering ions (such as $^{40}Ar^{16}O^{+}$ and $^{40}Ar^{14}N^{+}$).[56,89,103]

Another way to eliminate spectral interferences is *via* chemical separation of the target element from sample matrix prior to ICP-MS measurement. Ion exchange chromatography is typically used for such purpose. Ion exchange chromatography can induce mass-dependent isotope fractionation (artificial fractionation), but the effect of on-column isotope fractionation on the final results is avoided when the recovery of the target element is quantitative.[104] In case of a non-quantitative recovery, the double spike approach is recommended. Another possible disadvantage is the presence of organic material stripped from the resin in the pure fraction of the analyte. Pietruszka and Reznik[105] observed a significant effect on Mo isotope ratio measurement results due to the organic material released from the resin.

1.3 IRON ISOTOPIC VARIABILITY IN A BIOMEDICAL CONTEXT

Natural variations in the isotopic composition of elements with two or more isotopes can occur due to the isotope fractionation that is accompanying (bio)chemical reactions and/or physical processes. Isotopes of the same element may take part in such reactions or processes to slightly different extents. The lighter of two isotopes reacts slightly faster (kinetic effect) and the heavier one shows a slight preference for the strongest bond (thermodynamic or equilibrium effect).[106,107]

Light elements, such as H, C, N, O or S, have been analyzed for their isotope ratios because of their large isotopic variations in nature, due to the large relative mass difference between the isotopes. In a biomedical context, for instance, the ^{13}C-urea breath test is used in gastroenterology practice to measure small-bowel bacterial overgrowth and for the diagnosis of Helicobacter pylori infection of the stomach in an indirect way *via* gas source isotope ratio mass spectrometry of the $^{13}C/^{12}C$ ratio in exhaled breath.[108] The ^{13}C-glucose breath methodology relies on measuring the $^{13}CO_2/^{12}CO_2$ isotope ratio with high-precision *via* laser-based high-resolution cavity-enhanced absorption spectroscopy and can also be used for the accurate real-time monitoring of individuals with small intestinal bacterial overgrowth.[109]

Recently, considerable effort has been made to obtain precise and accurate isotope ratio data for heavier elements, such as Fe, Cu, Zn, and Ca, in this context in order to extend the applicability of stable isotopic analysis.[110] For such purpose, MC-ICP-MS is nowadays the preferred technique for tracing down isotope fractionation processes occurring during biological processes. As has been described before, the combination of a highly efficient ion source with simultaneous detection of all isotope signals allows the typically unstable signal intensities to be counteracted, thus realizing high isotope ratio precision.[87,110,111]

A variety of studies have already demonstrated that iron shows natural variations in its isotopic composition as a result of isotope fractionation accompanying physical processes and/or biochemical reactions.[56,112] As a result of the small variations, the isotopic composition is typically expressed in delta notation (*i.e*. as the relative difference between the isotope ratio of the sample and that of a standard, in ‰)[56,63]:

$$\delta^{x}Fe_{sample} = \left(\frac{{}^{x}Fe/{}^{54}Fe_{sample}}{{}^{x}Fe/{}^{54}Fe_{IRMM-014}} - 1 \right) \qquad (1\text{-}20)$$

where *x* is 56 or 57.

Beard *et al.*[113] demonstrated that the Fe isotopic composition of ferrous iron produced by iron-reducing bacteria was lighter than that of the ferrihydrite substrate and pointed out as a first time that natural isotopic fractionation can occur due to biological effects. Over the last decade, iron isotopic analysis of human fluids and tissues gained increasing attention. Walczyk and von Blanckenburg[114] were the first who showed that human whole blood and muscle tissue have a similar iron isotopic composition, while that of liver is heavier. The authors hypothesized that natural iron isotope variations in human blood are primarily related to the dietary iron absorption. They also demonstrated that gender is as an important source of variability in the Fe isotopic composition. Men show a greater proportion of the lighter iron isotopes in whole blood than women.[114,115] The same result was later observed by Van Heghe *et al.*[116,117] in whole blood, Ohno *et al.*[87], and Jaouen and Balter[118] in RBCs and Albarede *et al.*[119] in whole blood, RBCs and serum. Later on, the menstruation and the associated iron loss and the body's reaction to replenish the iron store were identified as the underlying reason of gender-related Fe isotope ratio variations.[118,120] For post-menopausal women and those with a Mirena® (an intra-uterine contraceptive device), a significant shift to lighter Fe isotopic signatures (overlapping with those for the male reference population) was observed

compared to menstruating women. Between post-menopausal women and women with a Mirena®, no differences were observed in the whole blood Fe isotopic composition.[120] At the same time, Jaouen and Balter came to the same conclusion, indicating that Fe isotopic composition of RBC from newly post-menopausal women is similar to pre-menopausal individuals and an isotopic shift becomes visible 5 years after the menopause.[118]

Walczyk and von Blanckenburg observed that (i) the iron in the biosphere (including plants, animals and humans) shows an $^{56}Fe/^{54}Fe$ ratio lower by 2-3‰ than the iron in the geosphere and (ii) the Fe isotopic composition changes along the human food chain.[115] Further, in a study on isotope fractionation along mammal trophic chains, Jaouen *et al.*, this observation was confirmed by demonstration that the second trophic step (as documented by the difference in the isotopic composition of Fe between bones of herbivores and bones of carnivores) is characterized by a ^{56}Fe-depletion of about 0.6‰.[121] Thus, Fe becomes enriched in the lighter isotope along the human food chain.[115,121]

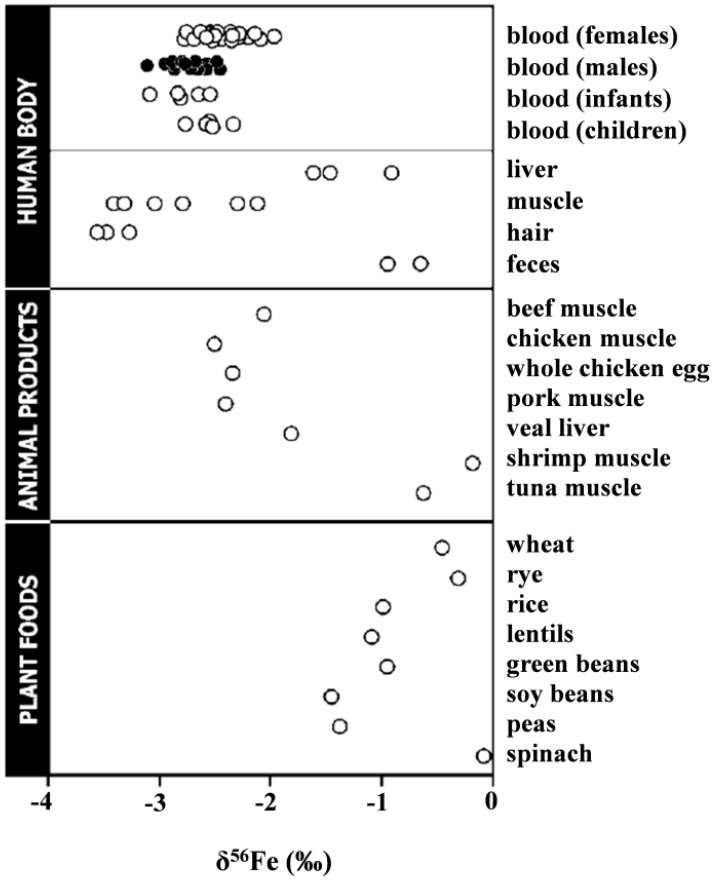

Fig. 1-15 Fe isotope ratio variations in the human body and different food samples covering the most relevant dietary Fe sources. Data are plotted relative to an isotopic reference material (IRMM-014, $\delta = 0$). (adapted from Walczyk and von Blanckenburg).[114]

By using a pig model, Hotz *et al.* identified the preferential uptake of light iron isotopes in the intestine and the extent of dietary iron absorption efficiency as key factors governing the whole blood Fe isotopic composition.[122,123] Comparison of the isotopic composition of Fe in whole blood and tissues from humans,[114] as well as in animal models[122,124] demonstrated that Fe is systematically isotopically lighter in all organs and biofluids than in the diet (Fig. 1-15). Walczyk and von Blanckenburg[114,115] reported a difference of 1.7‰ between the whole blood and diet Fe isotopic composition. Isotopic analysis of different food products showed that animal products show a δ^{56}Fe value of around -2‰, while plant products are characterized by a value of around -0.7 ‰ to 0 ‰.[125] Van Heghe *et al.*,[116] however, demonstrated that whole blood from supposedly healthy subjects following different diets, *i.e.* omnivores and vegetarians of the same gender, do not show a significant difference in Fe isotopic composition. This finding supported the conclusion of Walczyk and von Blanckenburg,[114] who stated that the isotopic composition of Fe in blood is not primarily determined by the diet, but by the favoured uptake of the lighter isotopes in the intestine. Von Blanckenburg *et al.* [125] hypothesized that heme-bound Fe passes through the intestinal mucosa without ligand exchange and therefore without fractionation, while Fe originating from vegetables (mostly in ferric form) is reduced in the intestine and is fractionated in the process.

The heavier Fe isotopic composition of liver and spleen, as main Fe store sites, and the higher fraction of lighter iron isotopes in whole blood were demonstrated first by Walczyk and von Blanckenburg.[114,115] Later, Balter *et al.*[124] observed the same trend in organs and body fluids of mice and sheep.

Current researches are focused on the study of diseases related with iron metabolism to reveal the possible occurrence of a significant effect on the isotopic composition. In first studies, in patients with hereditary hemochromatosis (HH), which leads to ironoverload, the whole blood δ^{56}Fe was shown to be shifted to higher values.[126,127] Krayenbuehl *et al.* found an altered Fe isotopic composition of whole blood of patients with HH compared to assumed healthy individuals. The heavier whole blood Fe isotopic composition of HH patients was explained by the upregulated intestinal iron absorption and therefore, the preferential transfer of lighter isotopes was less emphasized.[127] Later on, in HH patients under phlebotomy treatment, it was observed that this effect is further enhanced by remobilization of iron from the storage tissues, which is characterized by a heavier isotopic composition than iron in the blood.[117,128] In contrast, ACD had a contrary effect on the Fe isotopic composition as a consequence of a

downregulated iron uptake, transfer of a larger amount of iron to the storage sites and no mobilization of storage iron to the circulation.[117] Fig. 1-16 provides a general indication of how the Fe status affects the whole blood and serum delta Fe values. At low iron status, the production of hepcidin is downregulated to increase intestinal iron absorption, and only a small portion (if any) of the iron taken up is deposited in hepatocytes. The iron store and the macrophages recycling iron from senescent red blood cells are activated thus stimulating hemoglobin synthesis. At high iron status, in contrast, the iron absorption is downregulated due to increased production of hepcidin as a result of inflammation or genetic predisposition, or low bioavailability of dietary iron

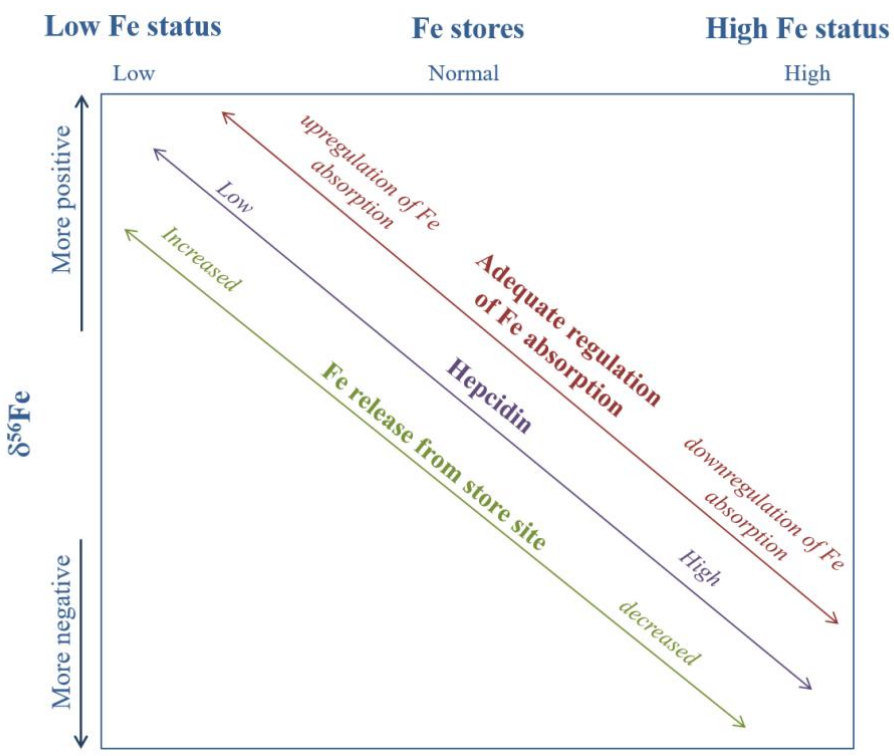

Fig.1-16 General indication of effect of iron status on whole blood and serum delta Fe values.

Von Blanckenburg *et al.*[129] compared the isotopic composition of human erythrocytes and plasma. The Fe isotopic composition in blood plasma is more variable than in erythrocytes and shows a higher fraction of the heavier iron isotopes. Ferritin was indicated as a key player that can induce isotope fractionation by release and uptake of iron involving redox processes.

Since there is a clear association between the whole blood Fe isotopic composition and an individual's iron status,[117,123] high-precision Fe isotopic analysis turns out to be a potentially

interesting approach for assessing iron depletion or overload in clinical practice. However, the main carrier of iron in whole blood is hemoglobin in erythrocytes with a lifespan of 110 - 120 days, and thus are not an ideal measure of immediate iron stores. In turn, serum, with transferrin as a main carrier of iron with highest turnover (the protein undergoes cycling between holo- and apo-states more than 10 times per day, thus cycling around 30 mg of iron), can provide more accurate information on current iron status.

The precision attainable in isotopic analysis is the decisive factor when it comes to the question of which instrument type to be employed in studies of element metabolism. In comparison to MC-ICP-MS (~0.002% RSD, under ideal circumstances), the precision of Fe isotope ratios obtained *via* quadrupole-based or SF-ICP-MS instrumentation is about 0.05% RSD under ideal circumstances. Thus, these instruments cannot be recommended for tracing down the small changes and quantifying the resulting small differences in isotopic composition accompanying physical processes and/or (bio)chemical reactions, however, they can be considered as a suitable technique for the routine determination of iron absorption in human iron supplementation studies with stable isotopic tracers.

1.4 REFERENCES

1. Lieu, P. T., Heiskala, M., Peterson, P. A. & Yang, Y. The roles of iron in health and disease. *Mol. Aspects of Med.* **22,** 1–87 (2001).
2. Crichton, R. R., Wilmet, S., Legssyer, R. & Ward, R. J. Molecular and cellular mechanisms of iron homeostasis and toxicity in mammalian cells. in *J. Inorg. Biochem.* **91,** 9–18 (2002).
3. Ponka, P. Cellular iron metabolism. *Kidney Int. Suppl.* **69,** S2–S11 (1999).
4. Ponka, P. Iron metabolism: Physiology and pathophysiology. *J. Trace Elem. Exp. Med.* **13,** 73–83 (2000).
5. Winterbourn, C. C. Toxicity of iron and hydrogen peroxide: the Fenton reaction. *Toxicol. Lett.* **82–83,** 969–974 (1995).
6. Ross, A. C. *Modern nutrition in health and disease.* (Wolters Kluwer Health/Lippincott Williams & Wilkins, 2014).
7. Institute of Medicine (US) Panel on Micronutrients. *Dietary Reference Intakes for Vitamin A, Vitamin K, Arsenic, Boron, Chromium, Copper, Iodine, Iron, Manganese, Molybdenum, Nickel, Silicon, Vanadium, and Zinc*. (National Academies Press, 2001). doi:10.17226/10026
8. Papanikolaou, G. & Pantopoulos, K. Iron metabolism and toxicity. *Toxicol. Appl. Pharmacol.* **202,** 199–211 (2005).

9. Crichton, R. *Iron Metabolism: From Molecular Mechanisms to Clinical Consequences, 3rd Edition*. (John Wiley & Sons, Ltd, 2009).

10. Abbaspour, N., Hurrell, R. & Kelishadi, R. Review on iron and its importance for human health. *J. Res. Med. Sci.* **19,** 164–74 (2014).

11. Muñoz, M., Villar, I. & García-Erce, J. A. An update on iron physiology. *World J. Gastroenterol.* **15,** 4617–4626 (2009).

12. Andrews, N. C. Disorders of iron metabolism. *N. Engl. J. Med.* **341,** 1986–95 (1999).

13. Andrews, N. C. Iron homeostasis: insights from genetics and animal models. *Nat. Rev. Genet.* **1,** 208–217 (2000).

14. Wrighting, D. M. & Andrews, N. C. Iron Homeostasis and Erythropoiesis. *Cur. Top. Dev. Biol.* **82,** 141–167 (2008).

15. Rizvi, S. & Schoen, R. E. Supplementation with oral vs. intravenous iron for anemia with IBD or gastrointestinal bleeding: is oral iron getting a bad rap? *Am. J. Gastroenterol.* **106,** 1872–9 (2011).

16. De Domenico, I., McVey Ward, D. & Kaplan, J. Regulation of iron acquisition and storage: consequences for iron-linked disorders. *Nat. Rev. Mol. Cell Biol.* **9,** 72–81 (2008).

17. Morgan, E. H. & Oates, P. S. Mechanisms and regulation of intestinal iron absorption. *Blood Cells. Mol. Dis.* **29,** 384–399 (2002).

18. West, A. R. & Oates, P. S. Mechanisms of heme iron absorption: Current questions and controversies. *World J. Gastroenterol.* **14,** 4101–4110 (2008).

19. Tandara, L. & Salamunic, I. Iron metabolism: current facts and future directions. *Biochem Med* **22,** 311–28 (2012).

20. Scheers, N. Regulatory effects of Cu, Zn, and Ca on Fe absorption: The intricate play between nutrient transporters. *Nutrients* **5,** 957–970 (2013).

21. Prem, P. & Sheftel, A. D. in *Iron Physiology and Pathophysiology in Humans* (eds. Anderson, G. J. & McLaren, G. D.) 191–209 (Humana Press, 2012).

22. Neildez-Nguyen, T. M. A. *et al.* Human erythroid cells produced ex vivo at large scale differentiate into red blood cells in vivo. *Nat. Biotechnol.* **20,** 467–472 (2002).

23. Hattangadi, S. M., Wong, P., Zhang, L., Flygare, J. & Lodish, H. F. From stem cell to red cell: regulation of erythropoiesis at multiple levels by multiple proteins, RNAs, and chromatin modifications. *Blood* **118,** 6258–6268 (2011).

24. Chung, J., Chen, C. & Paw, B. H. Heme metabolism and erythropoiesis. *Curr. Opin. Hematol.* **19,** 156–62 (2012).

25. Kohgo, Y., Ikuta, K., Ohtake, T., Torimoto, Y. & Kato, J. Body iron metabolism and pathophysiology of iron overload. *Int. J. Hematol.* **88,** 7–15 (2008).

26. Ganz, T. & Nemeth, E. Hepcidin and iron homeostasis. *Biochim. Biophys. Acta* **1823,** 1434–43 (2012).

27. Donovan, A., Roy, C. N. & Andrews, N. C. The ins and outs of iron homeostasis. *Physiology (Bethesda).* **21,** 115–123 (2006).

28. Wang, J. & Pantopoulos, K. Regulation of cellular iron metabolism. *Biochem. J.* **434,**

365–81 (2011).

29. Kautz, L. *et al.* Identification of erythroferrone as an erythroid regulator of iron metabolism. *Nat. Genet.* **46,** 678–84 (2014).

30. Pak, M., Lopez, M. A., Gabayan, V., Ganz, T. & Rivera, S. Suppression of hepcidin during anemia requires erythropoietic activity. *Blood* **108,** 3730–5 (2006).

31. Hare, D., Ayton, S., Bush, A. & Lei, P. A delicate balance: Iron metabolism and diseases of the brain. *Front. Aging Neurosci.* **5,** 34 (2013).

32. *Assessing the iron status of populations: including literature reviews. Report of a Joint World Health Organization/Centers for Disease Control and Prevention Technical Consultation on the Assessment of Iron Status at the Population Level*. (World Health Organization, 2007). at <http://www.who.int/nutrition/publications/micronutrients/anaemia_iron_deficiency/9789241596107/en/>. Last accessed on 25/07/0217.

33. Andrews, N. C. Iron metabolism: Iron Deficiency and Iron Overload. *Annu. Rev. Genomics Hum. Genet.* **1,** 75–98 (2000).

34. Wish, J. B. Assessing iron status: beyond serum ferritin and transferrin saturation. *Clin. J. Am. Soc. Nephrol.* **1,** S4–S8 (2006).

35. Yamanishi, H., Iyama, S., Yamaguchi, Y., Kanakura, Y. & Iwatani, Y. Total iron-binding capacity calculated from serum transferrin concentration or serum iron concentration and unsaturated iron-binding capacity. *Clin. Chem.* **49,** 175–178 (2003).

36. Hörl, W. H. Clinical aspects of iron use in the anemia of kidney disease. *J. Am. Soc. Nephrol.* **18,** 382–93 (2007).

37. Lee, E. J., Oh, E.-J., Park, Y.-J., Lee, H. K. & Kim, B. K. Soluble Transferrin Receptor (sTfR), Ferritin, and sTfR/Log Ferritin Index in Anemic Patients with Nonhematologic Malignancy and Chronic Inflammation. *Clin. Chem.* **48,** (2002).

38. Beguin, Y. Soluble transferrin receptor for the evaluation of erythropoiesis and iron status. *Clin. Chim. Acta* **329,** 9–22 (2003).

39. Margetic, S., Topic, E., Ruzic, D. F. & Kvaternik, M. Soluble transferrin receptor and transferrin receptor-ferritin index in iron deficiency anemia and anemia in rheumatoid arthritis. *Clin. Chem. Lab. Med.* **43,** 326–331 (2005).

40. Bermejo, F. A guide to diagnosis of iron deficiency and iron deficiency anemia in digestive diseases. *World J. Gastroenterol.* **15,** 4638 (2009).

41. Goddard, A. F., James, M. W., McIntyre, A. S. & Scott, B. B. Guidelines for the management of iron deficiency anaemia. *Gut* **60,** 1309–16 (2011).

42. Castel, R. *et al.* The transferrin/log(ferritin) ratio: a new tool for the diagnosis of iron deficiency anemia. *Clin. Chem. Lab. Med.* **50,** 1343–9 (2012).

43. Locatelli, F. *et al.* Kidney Disease: Improving Global Outcomes guidelines on anaemia management in chronic kidney disease: A European Renal Best Practice position statement. *NDT* **28,** 1346–1359 (2013).

44. Practice Guidelines for Iron Deficiency and Anemia in CKD. *Https://www.compact-renal.com/2016/05/19/practice-guidelines-iron-deficiency-anemia-ckd/*. (2016). at <https://www.compact-renal.com/2016/05/19/practice-guidelines-iron-deficiency-

anemia-ckd/>. Last accessed on 25/07/0217.

45. National Institute for Health and Care Exellence. *Chronic kidney disease: managing anaemia. Guidance and guidelines. NICE*. (NICE, 2015). at <https://www.nice.org.uk/guidance/ng8?unlid=6344784542016101117293 1>. Last accessed on 25/07/0217.

46. Urrechaga, E., Borque, L. & Escanero, J. Assessing iron status in CKD patients: new Laboratory parameters. *Chronic Kidney Dis.* **30,** 225–250 (2012).

47. Thomas, C., Kirschbaum, A., Boehm, D. & Thomas, L. The diagnostic plot: a concept for identifying different states of iron deficiency and monitoring the response to epoetin therapy. *Med. Oncol.* **23,** 23–36 (2006).

48. Cullis, J. O. Diagnosis and management of anaemia of chronic disease: current status. *Br. J. Haematol.* **154,** 289–300 (2011).

49. Houk, R. S. *et al.* Inductively coupled argon plasma as an ion source for mass spectrometric determination of trace elements. *Anal. Chem.* **52,** 2283–2289 (1980).

50. Darke, S. A. & Tyson, J. F. Review of Solid Sample Introduction for Plasma Spectrometry and a Comparison of Results for Laser Ablation, Electrothermal Vaporization, and Slurry Nebulization. *Microchem. J.* **50,** 310–336 (1994).

51. Zoorob, G. K., McKiernan, J. W. & Caruso, J. A. ICP-MS for elemental speciation studies. *Mikrochim. Acta* **128,** 145–168 (1998).

52. Thomas, R. *Practical guide to ICP-MS*. (Marcel Dekker, Inc., New York, U.S.A., 2004).

53. Nelms, S. M. *Inductively coupled plasma mass spectrometry handbook*. (Blackwell Pub., 2005).

54. Becker, J. S. *Inorganic mass spectrometry: principles and applications*. (John Wiley & Sons Ltd, 2007).

55. Houk, R. S. Mass spectrometry of inductively coupled plasmas. *Anal. Chem.* **58,** 97A–105A (1986).

56. Vanhaecke, F. & Degryse, P. *Isotopic Analysis: Fundamentals and Applications Using ICP-MS*. (Wiley-VCH Verlag GmbH & Co. KGaA, 2012).

57. McNaught, A. D., Wilkinson, A. & Jenkins, A. D. *IUPAC compendium of chemical terminology the gold book.* (International Union of Pure and Applied Chemistry, 2006).

58. Hoffmann, E. de. & Stroobant, V. *Mass spectrometry : principles and applications*. (J. Wiley, 2007).

59. Chromatography Mass Spectrometry (GC/MS), University of Bristol. (2017). at <http://www.bris.ac.uk/nerclsmsf/techniques/gcms.html>. Last accessed on 25/07/0217.

60. Miller, P. E. & Denton, M. B. The quadrupole mass filter: Basic operating concepts. *J. Chem. Educ.* **63,** 617 (1986).

61. Wiedenbeck, M. *et al.* GGR Biennial Critical Review: Analytical Developments Since 2010. *Geostand. Geoanalytical Res.* **36,** 337–398 (2012).

62. Koppenaal, D. W. *et al.* MS Detectors. *Anal. Chem.* **77,** 418 A-427 A (2005).

63. Yang, L. Accurate and precise determination of isotopic ratios by MC-ICP-MS: a

review. *Mass Spectrom. Rev.* **28,** 990–1011 (2009).

64. Vanhaecke, F., Balcaen, L. & Malinovsky, D. Use of single-collector and multi-collector ICP-mass spectrometry for isotopic analysis. *J. Anal. At. Spectrom.* **24,** 863 (2009).

65. Albarède, F. *et al.* Precise and accurate isotopic measurements using multiple-collector ICPMS. *Geochim. Cosmochim. Acta* **68,** 2725–2744 (2004).

66. Rehkämper, M., Schönbächler, M. & Stirling, C. H. Multiple Collector ICP-MS: Introduction to Instrumentation, Measurement Techniques and Analytical Capabilities. *Geostand. Geoanalytical Res.* **25,** 23–40 (2001).

67. Vanhaecke, F. & Moens, L. Overcoming spectral overlap in isotopic analysis via single- and multi-collector ICP-mass spectrometry. *Anal.Bioanal. Chem.* **378,** 232–240 (2004).

68. Bouman, C., Deerberg, M. & Schwieters, J. B. *Neptune and Neptune Plus: Breakthrough in Sensitivity using a Large Interface Pump and New Sample Cone*. (2009).

69. Newman, K., Freedman, P. A., Williams, J., Belshaw, N. S. & Halliday, A. N. High sensitivity skimmers and non-linear mass dependent fractionation in ICP-MS. *J. Anal. At. Spectrom.* **24,** 742 (2009).

70. Vanhaecke, F., Moens, L., Dams, R. & Taylor, P. Precise Measurement of Isotope Ratios with a Double-Focusing Magnetic Sector ICP Mass Spectrometer. *Anal. Chem.* **68,** 567–569 (1996).

71. Heumann, K. G., Gallus, S. M., Rädlinger, G. & Vogl, J. Precision and accuracy in isotope ratio measurements by plasma source mass spectrometry. *J. Anal. At. Spectrom.* **13,** 1001–1008 (1998).

72. Bolea-Fernandez, E., Balcaen, L., Resano, M. & Vanhaecke, F. Tandem ICP-mass spectrometry for Sr isotopic analysis without prior Rb/Sr separation. *J. Anal. At. Spectrom.* **31,** 303–310 (2016).

73. Vanhaecke, F., Moens, L., Dams, R., Papadakis, I. & Taylor, P. Applicability of High-Resolution ICP−Mass Spectrometry for Isotope Ratio Measurements. *Anal. Chem.* **69,** 268–273 (1997).

74. Maréchal, C. N., Télouk, P. & Albarède, F. Precise analysis of copper and zinc isotopic compositions by plasma-source mass spectrometry. *Chem. Geol.* **156,** 251–273 (1999).

75. Ingle, C. P., Sharp, B. L., Horstwood, M. S. A., Parrish, R. R. & Lewis, D. J. Instrument response functions, mass bias and matrix effects in isotope ratio measurements and semi-quantitative analysis by single and multi-collector ICP-MS. *J. Anal. At. Spectrom.* **18,** 219–229 (2003).

76. Andrén, H., Rodushkin, I., Stenberg, A., Malinovsky, D. & Baxter, D. C. Sources of mass bias and isotope ratio variation in multi-collector ICP-MS: optimization of instrumental parameters based on experimental observations. *J. Anal. At. Spectrom.* **19,** 1217–1224 (2004).

77. Kivel, N., Günther-Leopold, I., Vanhaecke, F. & Günther, D. Isotope fractionation during ion beam formation in multi-collector inductively coupled plasma mass spectrometry. *Spectrochim. Acta Part B At. Spectrosc.* **76,** 126–132 (2012).

78. Meija, J., Yang, L., Sturgeon, R. & Mester, Z. Mass Bias Fractionation Laws for Multi-

Collector ICPMS: Assumptions and Their Experimental Verification. *Anal. Chem.* **81,** 6774–6778 (2009).

79. Horsky, M., Irrgeher, J. & Prohaska, T. Evaluation strategies and uncertainty calculation of isotope amount ratios measured by MC ICP-MS on the example of Sr. *Anal. Bioanal. Chem.* **408,** 351–67 (2016).

80. Woodhead, J. A simple method for obtaining highly accurate Pb isotope data by MC-ICP-MS. *J. Anal. At. Spectrom.* **17,** 1381–1385 (2002).

81. Baxter, D. C., Rodushkin, I., Engström, E. & Malinovsky, D. Revised exponential model for mass bias correction using an internal standard for isotope abundance ratio measurements by multi-collector inductively coupled plasma mass spectrometry. *J. Anal. At. Spectrom.* **21,** 427–430 (2006).

82. Russell, W. A., Papanastassiou, D. A. & Tombrello, T. A. Ca isotope fractionation on the Earth and other solar system materials. *Geochim. Cosmochim. Acta* **42,** 1075–1090 (1978).

83. Baxter, D. C., Rodushkin, I., Engström, E. & Malinovsky, D. Revised exponential model for mass bias correction using an internal standard for isotope abundance ratio measurements by multi-collector inductively coupled plasma mass spectrometry. *J. Anal. At. Spectrom.* **21,** 427–430 (2006).

84. Galer, S. J. G. Optimal double and triple spiking for high precision lead isotopic measurement. *Chem. Geol.* **157,** 255–274 (1999).

85. Konter, J. G., Pietruszka, A. J. & Hanan, B. B. Evaluation of double and triple spike Fe isotope measurements and results for basaltic lavas. *Am. Geophys. Union* A2102 (2008).

86. May, T. W. & Wiedmeyer, R. H. A table of polyatomic interferences in ICP-MS. *At. Spectrosc.* **19,** 150–155 (1998).

87. Ohno, T., Shinohara, A., Kohge, I., Chiba, M. & Hirata, T. Isotopic analysis of Fe in human red blood cells by multiple collector-ICP-mass spectrometry. *Anal. Sci.* **20,** 617–621 (2004).

88. Benkhedda, K., Chen, H., Dabeka, R. & Cockell, K. Isotope ratio measurements of iron in blood samples by multi-collector ICP-MS to support nutritional investigations in humans. *Biol. Trace Elem. Res.* **122,** 179–192 (2008).

89. Chernonozhkin, S. M., Costas-Rodriguez, M., Claeys, P. & Vanhaecke, F. Evaluation of the use of cold plasma conditions for Fe isotopic analysis via multi-collector-ICP-mass spectrometry: effect on spectral interferences and instrumental mass discrimination. *J. Anal. At. Spectrom.* (2017). doi:10.1039/C6JA00428H

90. Koyanagi, G. K., Baranov, V. I., Tanner, S. D. & Bohme, D. K. An inductively coupled plasma/selected-ion flow tube mass spectrometric study of the chemical resolution of isobaric interferences. *J. Anal. At. Spectrom.* **15,** 1207–1210 (2000).

91. Bandura, D. R., Baranov, V. I. & Tanner, S. D. Inductively coupled plasma mass spectrometer with axial field in a quadrupole reaction cell. *J. Am. Soc. Mass Spectrom.* **13,** 1176–1185 (2002).

92. Vanhaecke, F., Balcaen, L., De Wannemacker, G. & Moens, L. Capabilities of inductively coupled plasma mass spectrometry for the measurement of Fe isotope ratios. *J. Anal. At. Spectrom.* **17,** 933–943 (2002).

93. McCurdy, E. & Woods, G. The application of collision/reaction cell inductively coupled plasma mass spectrometry to multi-element analysis in variable sample matrices, using He as a non-reactive cell gas. *J. Anal. At. Spectrom.* **19,** 607 (2004).

94. Chu, H., Yip, Y., Chan, K. & Sham, W. Determination of iron in plant samples using isotope dilution inductively coupled plasma mass spectrometry with a quadrupole ICP-MS operated in an He/H2 cell mode. *J. Anal. At. Spectrom.* **21,** 1068 (2006).

95. Sakai, K. *Routine soil analysis using an Agilent 8800 ICP-QQQ. Application note.* (2015).

96. Stenberg, A. *et al.* Separation of Fe from whole blood matrix for precise isotopic ratio measurements by MC-ICP-MS: a comparison of different approaches. *J. Anal. At. Spectrom.* **18,** 23–28 (2003).

97. Malinovsky, D. *et al.* Performance of high resolution MC-ICP-MS for Fe isotope ratio measurements in sedimentary geological materials. *J. Anal. At. Spectrom.* **18,** 687–695 (2003).

98. Wollenweber, D., Straßburg, S. & Wünsch, G. Determination of Li, Na, Mg, K, Ca and Fe with ICP-MS using cold plasma conditions. *Fresenius. J. Anal. Chem.* **364,** 433–437 (1999).

99. Dial, A. R., Misra, S. & Landing, W. M. Determination of low concentrations of iron, arsenic, selenium, cadmium, and other trace elements in natural samples using an octopole collision/reaction cell equipped quadrupole-inductively coupled plasma mass spectrometer. *Rapid Commun. Mass Spectrom.* **29,** 707–718 (2015).

100. Lum, T.-S. & Sze-Yin Leung, K. Strategies to overcome spectral interference in ICP-MS detection. *J. Anal. At. Spectrom.* **31,** 1078–1088 (2016).

101. Tanner, S. D., Baranov, V. I. & Bandura, D. R. Reaction cells and collision cells for ICP-MS: a tutorial review. *Spectrochim. Acta Part B At. Spectrosc.* **57,** 1361–1452 (2002).

102. Vanhaecke, F. *Agilent 8800 ICP-QQQ Application Handbook. 2nd addition*. (2015).

103. Tanner, S. D. Characterization of ionization and matrix suppression in inductively coupled 'cold' plasma mass spectrometry. *J. Anal. At. Spectrom.* **10,** 905–921 (1995).

104. Maréchal, C. & Albarède, F. Ion-exchange fractionation of copper and zinc isotopes. *Geochim. Cosmochim. Acta* **66,** 1499–1509 (2002).

105. Pietruszka, A. J. & Reznik, A. D. Identification of a matrix effect in the MC-ICP-MS due to sample purification using ion exchange resin: An isotopic case study of molybdenum. *Int. J. Mass Spectrom.* **270,** 23–30 (2008).

106. Rodushkin, I., Stenberg, A., Andrén, H., Malinovsky, D. & Baxter, D. C. Isotopic Fractionation during Diffusion of Transition Metal Ions in Solution. *Anal. Chem.* **76,** 2148–2151 (2004).

107. Matthews, A., Emmanuel, S., Levi, L., Gvirtzman, H. & Erel, Y. Kinetic fractionation of Fe isotopes during transport through a porous quartz-sand column. *Geochim. Cosmochim. Acta* **72,** 5908–5919 (2008).

108. Gisbert, J. P. & Pajares, J. M. Review article: 13C-urea breath test in the diagnosis of Helicobacter pylori infection - a critical review. *Aliment. Pharmacol. Ther.* **20,** 1001–1017 (2004).

109. Banik, G. D. *et al.* Diagnosis of small intestinal bacterial overgrowth in irritable bowel syndrome patients using high-precision stable 13 CO 2 / 12 CO 2 isotope ratios in exhaled breath. *J. Anal. At. Spectrom.* **29,** 1918–1924 (2014).

110. Costas-Rodríguez, M., Delanghe, J. & Vanhaecke, F. High-precision isotopic analysis of essential mineral elements in biomedicine: Natural isotope ratio variations as potential diagnostic and/or prognostic markers. *TrAC* **76,** 182–193 (2016).

111. Zhu, X. K. *et al.* Mass fractionation processes of transition metal isotopes. *Earth Planet. Sci. Lett.* **200,** 47–62 (2002).

112. Schauble, E. A. Applying Stable Isotope Fractionation Theory to New Systems. *Rev. Mineral. Geochemistry* **55,** 65–111 (2004).

113. Beard, B. L. *et al.* Iron isotope biosignatures. *Science* **285,** 1889–1892 (1999).

114. Walczyk, T. & von Blanckenburg, F. Natural iron isotope variations in human blood. *Science* **295,** 2065–6 (2002).

115. Walczyk, T. & von Blanckenburg, F. Deciphering the iron isotope message of the human body. *Int. J. Mass Spectrom.* **242,** 117–134 (2005).

116. Van Heghe, L., Engström, E., Rodushkin, I., Cloquet, C. & Vanhaecke, F. Isotopic analysis of the metabolically relevant transition metals Cu, Fe and Zn in human blood from vegetarians and omnivores using multi-collector ICP-mass spectrometry. *J. Anal. At. Spectrom.* **27,** 1327–1334 (2012).

117. Van Heghe, L., Delanghe, J., Van Vlierberghe, H. & Vanhaecke, F. The relationship between the iron isotopic composition of human whole blood and iron status parameters. *Metallomics* **5,** 1503–1509 (2013).

118. Jaouen, K. & Balter, V. Menopause effect on blood Fe and Cu isotope compositions. *Am. J. Phys. Anthropol.* **153,** 280–5 (2014).

119. Albarède, F., Telouk, P., Lamboux, A., Jaouen, K. & Balter, V. Isotopic evidence of unaccounted for Fe and Cu erythropoietic pathways. *Metallomics* **3,** 926–33 (2011).

120. Van Heghe, L., Deltombe, O., Delanghe, J., Depypere, H. & Vanhaecke, F. The influence of menstrual blood loss and age on the isotopic composition of Cu, Fe and Zn in human whole blood. *J. Anal. At. Spectrom.* **29,** 478–482 (2014).

121. Jaouen, K., Pons, M.-L. & Balter, V. Iron, copper and zinc isotopic fractionation up mammal trophic chains. *Earth Planet. Sci. Lett.* **374,** 164–172 (2013).

122. Hotz, K., Augsburger, H. & Walczyk, T. Isotopic signatures of iron in body tissues as a potential biomarker for iron metabolism. *J. Anal. At. Spectrom.* **26,** 1347–1353 (2011).

123. Hotz, K. & Walczyk, T. Natural iron isotopic composition of blood is an indicator of dietary iron absorption efficiency in humans. *J. Biol. Inorg. Chem.* **18,** 1–7 (2013).

124. Balter, V. *et al.* Contrasting Cu, Fe, and Zn isotopic patterns in organs and body fluids of mice and sheep, with emphasis on cellular fractionation. *Metallomics* **5,** 1470–82 (2013).

125. von Blanckenburg, F., Noordmann, J. & Guelke-Stelling, M. The iron stable isotope fingerprint of the human diet. *J. Agric. Food Chem.* **61,** 11893–9 (2013).

126. Stenberg, A. *et al.* Measurement of iron and zinc isotopes in human whole blood: preliminary application to the study of HFE genotypes. *J. Trace Elem. Med. Biol.* **19,**

55–60 (2005).

127. Krayenbuehl, P.-A., Walczyk, T., Schoenberg, R., von Blanckenburg, F. & Schulthess, G. Hereditary hemochromatosis is reflected in the iron isotope composition of blood. *Blood* **105,** 3812–3816 (2005).

128. Hotz, K., Krayenbuehl, P.-A. & Walczyk, T. Mobilization of storage iron is reflected in the iron isotopic composition of blood in humans. *J. Biol. Inorg. Chem.* **17,** 301–9 (2012).

129. von Blanckenburg, F. *et al.* An iron stable isotope comparison between human erythrocytes and plasma. *Metallomics* **6,** 2052–61 (2014).

CHAPTER 2

IRON ISOTOPIC ANALYSIS OF HUMAN WHOLE BLOOD BY SECTOR-FIELD INDUCTIVELY COUPLED PLASMA-MASS SPECTROMETRY FOR IRON ABSORPTION STUDIES WITH A STABLE ISOTOPIC TRACER

Parts of this chapter will be included in a publication in collaboration with the MRC Human Nutrition Research group from the University of Cambridge, UK. The manuscript is in preparation and is subject to further changes and modifications.

2.1 INTRODUCTION

Iron deficiency (ID) is the most common nutritional disorder worldwide and it accounts for approximately half of the cases of anemia.[1–4] ID can occur due to malnutrition, decreased intestinal iron absorption, hemodialysis, frequent blood sampling, gastrointestinal bleeding, multiple vascular access surgeries, hepcidin fluctuations, *etc.*[5] Iron deficiency refers to the reduction of iron stores, under the form of ferritin, and transferrin saturation (TSAT) with the hemoglobin level remaining normal until the iron stores get exhausted.[6,7] Iron deficiency can exist in the absence of anemia if it has not lasted long enough or if it has not been severe enough to cause the hemoglobin concentration to fall below the threshold for the specific sex and age group.[8] The highest prevalence of ID is among women and young children and it entails important consequences for human health and child development. According to Umbreit,[9] the occurrence of ID in women aged 16–19 years old is 19% and in 1-2 year old children of both sexes, the prevalence is 7%. Among pregnant women, ID and/or iron deficiency anemia (IDA) can occur during all three trimesters (9%, 14%, and 37% prevalence, respectively). ID and IDA in pregnancy is typically associated with an increased risk of poor pregnancy outcomes, including intra-uterine growth retardation, stillbirth, preterm delivery, low birth weight and delayed or impaired mental and physical development.[10]

Many efforts have been done to avoid ID and IDA over the past two decades but, to date, these conditions are still common.[8] In practice, the treatment of ID is based on iron supplementation, however optimum iron administration is still a challenge due to the low intestinal absorption of the iron supplements. The most common oral iron supplements are in the form of ferrous salts, such as ferrous sulfate (included in the WHO list of essential medicines[11]), ferrous gluconate and ferrous fumarate. The estimated absorption efficiency of the ferrous salts is between 5 and 15% only.[12] Alternatively, ferric iron supplementations (*e.g.*, succinylate protein or polymaltose complex) may be used, but ferric ion compounds are either poorly absorbed (3-4 times less than ferrous forms) or expensive.[13] Due to the low absorption efficiency of iron, a high dosing of iron supplements is typically used to counteract ID. However, high doses of iron supplements may give rise to side effects such as abdominal discomfort, nausea, vomiting, diarrhea and constipation.[14–16]

In nutritional or clinical studies assessing the suitability of iron supplements or food fortificants, an ‘absorption and utilization test’ is performed. Absorption is considered as a systemic uptake across the gut and utilization refers to the incorporation of iron into

hemoglobin. The gold standard test in humans requires the incorporation of isotopically labelled iron in the supplements followed by the measurement of the isotopic enrichment in the hemoglobin 14 days after supplementation relative to the baseline (*i.e.* before the supplementation).[17] Stable isotopes, such as ^{58}Fe and ^{57}Fe, are typically used to avoid any radio-isotopic exposure for the subjects. For a long time, the reference technique used for tracing isotopic changes has been thermal ionization mass spectrometry (TIMS), which provides a high isotope ratio precision (0.001 % relative standard deviation[18,19]), but requires exhaustive sample pre-treatment, resulting in a very low throughput and, consequently, high costs.[20] For iron in particular, the ionization efficiency (conversion into Fe^+) in TIMS is lower than that in ICP-MS.[21,22] Moreover, instrumental mass fractionation has to be appropriately corrected for (*e.g.*, by using the double-spike approach).[21] A precision of 0.07% RSD was obtained for the $^{54/56}Fe$ ratio using a negative ion TIMS approach, in which FeF_4^- ions were measured. The precision thus realized was better than the 0.3% RSD reported for the $^{54/56}Fe$ ratio using positive ion TIMS.[23] Multi-collector inductively coupled plasma mass-spectrometry (MC-ICP-MS) is nowadays preferred for high-precision isotope ratio measurements in clinical samples.[24–28] Like in TIMS, in MC-ICP-MS, an array of Faraday cups is used for ion detection. Faraday cups are robust and stable detectors and their use in an array constellation for simultaneous monitoring of the various ion beams provides an isotope ratio precision equivalent to that of TIMS.[29,30] MC-ICP-MS also requires sample preparation, including the chemical separation of the target element form the matrix, but the sample throughput is still higher than for TIMS.[31] However, both TIMS and MC-ICP-MS are not analytical techniques adapted for routine clinical and nutritional studies.[22] Quadrupole ICP-MS equipped with a collision/reaction cell and sector-field ICP-MS (SF-ICP-MS) techniques have therefore often been preferred in human iron absorption studies.[17,22,32,33] These single-collector instruments are also more robust, such that often blood samples are analyzed without prior chromatographic isolation of iron. Both quadrupole-based and sector-field ICP-MS instruments are equipped with a single secondary electron multiplier (SEM) for detection of positively charged ions.[29,30] A modern SEM can be used in a dual detector mode, whereby a high speed amplifier operates in the pulse counting mode for lower ion currents and in the analogue mode for higher ion currents. For isotope ratio measurement, however, a SEM needs to be deployed in one mode only. When used in pulse counting mode, a SEM requires a dead time correction (particularly if extreme isotope ratios are measured) and typically the precision attainable in the isotope ratio measurements is deteriorated compared to that obtained with MC-ICP-MS, in which the ion beams are monitored simultaneously.[20,29,30,34]

In this study, the potential use of SF-ICP-MS was evaluated for tracing changes in the isotopic composition of Fe in whole blood of individuals participating to a human nutritional study. The whole blood Fe isotopic composition obtained *via* SF-ICP-MS (with and without prior chromatographic Fe isolation) was compared to that obtained *via* high-precision MC-ICP-MS. This work was performed in collaboration with the MRC Human Nutrition Research group of the University of Cambridge (UK).

2.2 EXPERIMENTAL

2.2.1 Materials and reagents

Ultrapure water (resistivity ≥18.2 MΩ cm) was obtained from a Milli-Q Element water purification system (Millipore, France). *Pro analysis* purity level nitric acid (HNO_3, 14 M) used for the digestion and the isolation procedure was purified by sub-boiling distillation in a PFA equipment. *Optima grade* hydrochloric acid (HCl, 12 M) was obtained from Fisher Chemicals (UK) and used as such. Ultrapure hydrogen peroxide (H_2O_2, 9.8 M) was acquired from Sigma-Aldrich (Belgium). Sample preparation was performed in a class-10 clean lab.

The Fe isotopic reference material IRMM-014 (Institute for Reference Materials and Measurements, Belgium) was used for external correction for instrumental mass discrimination in a standard-sample bracketing approach. An elemental iron standard solution (Inorganic Ventures, The Netherlands; lot D2-FE03110) was used as in-house isotopic standard solution (further referred to as A&MS-Fe) for checking the quality of isotope ratio measurements. Single-element standard stock solutions (Inorganic Ventures, the Netherlands) were used for quantification purposes after the isolation procedure. Ga, used as internal standard correcting for instrument instability and matrix effects in SF-ICP-MS elemental determination measurements, was coming from a commercially available 1 g L^{-1} stock solution.

AG MP-1 strong anion exchange resin (100-200 mesh, chloride form) and polypropylene chromatographic columns (Bio-Rad, Belgium) were used for the Fe isolation procedure.

2.2.2 Samples and sample preparation

12 whole blood samples originating from 4 Gambian women were obtained from the MRC Human Nutrition Research group. In this study, two different oral iron supplements containing either ^{57}Fe (60 mg Fe + 14 mg ^{57}Fe) or ^{58}Fe (60 mg Fe + 2 mg ^{58}Fe) were given to the individuals during 2 visits 14 days apart. The samples were collected immediately before the administration of the supplement (time point zero) and at two time points after supplement administration, *i.e.* after 14 and after 28 days.

EDTA vacutainer tubes, suitable for trace element analysis, were used to collect whole blood samples. Samples were stored at -20 ºC until sample preparation. Ethical approval was obtained for using these samples by an independent commission of the Gambian Government / MRC Joint Ethics Committee. The individuals signed an informed consent.

About 1 mL of blood was digested in a closed Teflon Savillex beaker using a mixture of 3 mL of 14 M HNO_3 and 0.75 mL of 9.8 M H_2O_2 at 110 ºC overnight (~16 h). The digest thus obtained was evaporated to dryness and re-dissolved in 5 mL of 8 M HCl + 0.001% H_2O_2 for chromatographic Fe isolation.

The Fe isolation from whole blood matrixes was based on the procedure described by Van Heghe *et al.*[31] In brief, the Bio-Rad Poly-Prep columns were filled with 1 mL of AG MP-1 (100-200 mesh) strong anion exchange resin. A frit was placed as a bed support and a piece of cotton was placed on the top of the resin as a stopper. Prior to Fe isolation from the whole blood matrix, the resin was cleaned with 3 mL of 7 M HNO_3, 10 mL of MQ water and conditioned with 5 mL of 8 M HCl + 0.001% H_2O_2. After sample loading, the matrix was eluted with 3 mL of 8 M HCl + 0.001% H_2O_2. Next, Cu was eluted with 9 mL of 5 M HCl + 0.001% H_2O_2. Finally, Fe was eluted with 7 mL of 0.6 M HCl. The purified Fe fraction was collected in 15 mL Teflon Savillex beakers and evaporated to dryness at 95 ºC to remove residual chlorides and re-dissolved in 14 M HNO_3. This procedure was repeated twice. The final residue was re-dissolved in 0.42 M HNO_3. Procedure blank and A&MS-Fe in-house standard, treated in the same way as the samples, were included in each samples batch. The efficiency of isolation procedure and the recovery of the target element was tested by elemental analysis of the pure fraction *via* SF-ICP-MS.

2.2.3 Instrumentation and measurements

A Thermo Scientific Element XR sector-field ICP-MS instrument (Bremen, Germany) was used for quantification purposes after the isolation procedure and for Fe isotopic analysis

Table 2-1. Instrument settings and data acquisition parameters used for elemental determination (A) and for isotope ratio measurements (B) *via* the SF-ICP-MS Element XR.

Setting/parameter	**Value/Description**
(A) Elemental determination	
RF power (W)	1200
Guard electrode	Connected
Sample and skimmer cones	Ni, 1.1 mm and 0.8 mm orifice diameter
Lens settings	Optimized for maximum Fe^+ signal intensity
Ar flow-rates (L min^{-1}):	
plasma gas	15
auxiliary gas	0.8-0.9
nebulizer gas	1.0-1.1
Sample uptake rate (μ.L min^{-1})	200
Resolution mode	Low, medium, high
Nuclides monitored	^{23}Na (LR), ^{44}Ca (MR), ^{54,56,57,58}Fe (MR), ^{52}Cr (MR), ^{39}K (HR), ^{63,65}Cu (MR), ^{64,66}Zn (MR), ^{60}Ni (MR), ^{69}Ga (LR, MR, HR)
Acquisition mode	E-scan
Dwell time per point (ms)	10
Samples per peak	20
Number of runs	5
Number of passes	5
(B) Isotope ratios	
RF power (W)	1200
Guard electrode	Connected
Sample and skimmer cones	Ni, 1.1 mm and 0.8 mm orifice diameter
Lens settings	Optimized for maximum signal intensity
Ar flow-rates (L min^{-1}):	
plasma gas	15
auxiliary gas	0.8-0.9
nebulizer gas	1.0-1.1
Sample uptake rate (μL min^{-1})	200
Resolution mode	Medium
Nuclides monitored	^{54}Fe, ^{56}Fe, ^{57}Fe, ^{58}Fe
Detector mode	Pulse counting
Dead time (ns)	7
Dwell time (ms)	10
Mass window (%)	5
Integration window (%)	5
Samples per peak	125
Number of runs	5
Number of passes	150

(after Fe isolation and without prior Fe isolation). For the introduction of solutions into the plasma, a 200 μl min^{-1} quartz concentric nebulizer mounted onto a cyclonic spray chamber was used. For the elemental determinations, external calibration (calibration curve) combined with an internal standard (Ga) to correct for matrix effects and instrument instability was used. In Fe isotopic analysis, the Fe isotopic reference material IRMM-014 was used for external mass bias correction in a standard-sample bracketing approach. The instrument settings and data acquisition parameters used for elemental determination (A) and for isotope ratio measurements (B) are summarized in Table 2-1.

A Thermo Scientific Neptune MC-ICP-MS instrument (Germany) was used for reference Fe isotope ratio measurements. A (100 μL min^{-1}) PFA concentric nebulizer and a double spray chamber with cyclonic and Scott-type sub-units were used for the introduction of solution into the plasma. Measurements were performed at medium resolution (pseudo mass resolution[35]), in static collection mode, using four Faraday collectors connected to 10^{11} Ω amplifiers. Instrument settings and data acquisition parameters are shown in Table 2-2.

Table 2-2. Instrument settings and data acquisition parameters for the MC-ICP-MS Neptune.

Setting/parameter	**Value/Description**
RF power (W)	1275
Guard electrode	Connected
Sample and skimmer cones	Jet sampler and X-type skimmer, Ni, 1.1 and 0.8 mm orifice diameter, respectively
Lens settings	Optimized for maximum Fe^+ signal intensity
Ar flow-rates (L min^{-1}):	
plasma gas	15
auxiliary gas	0.75
nebulizer gas	0.9-1.0
Sample uptake rate (μL min^{-1})	100
Resolution mode	Medium
Acquisition mode	Static; multi-collection
Number of blocks	9
Number of cycles	5
Integration time (s)	4.194
Cup configuration	L4: ^{54}Fe; L2: ^{56}Fe; L1: ^{57}Fe; C: ^{58}Fe

In this study, mass bias correction relied only on external correction in a sample-standard bracketing approach (SSB). Mass bias correction using admixed Ni was not used to avoid the isobaric interference on ^{58}Fe.

For both measurements, with SF- and MC-ICP-MS, procedural blanks were measured at the beginning of the measurement session to evaluate their contribution to the Fe^+ signal intensities. An A&MS-Fe in-house standard solution, previously characterized isotopically,[31] was measured every 5 samples to monitor the quality of the isotopic measurements.

2.3 RESULTS AND DISCUSSION

2.3.1 Iron isotope ratios *via* SF-ICP-MS

Dead time of the detector

A critical issue in isotope ratio measurements *via* SF-ICP-MS is related with the dead time of the detector. A certain dead time τ of the detector and its associated electronics has to be taken into account when the electron multiplier is used in pulse counting mode. Depending on the type of electron multiplier used, the detection and electronic handling of every pulse typically takes 5-100 ns and another ion arriving at the detector within a shorter time frame after the first one will not be detected.[32] Consequently, this will lead to a signal loss. This effect is more pronounced when the rate of ions arriving at the detector increases. As a result, isotope ratios data show a bias relative to the corresponding true value.[32] A number of approaches for determining dead time in ICP-MS systems can be found in the literature.[36–40]

In general, appropriate correction for dead time losses of the measured signal intensities should result in a sensitivity which is independent of the signal intensity and therefore, independent of the analyte concentration.[32] In the dead time determination method according to Russ,[41] a series of standard solutions with different concentrations of the target element is measured for a given isotope ratio. Different assumed dead time values are subsequently used for correction. The normalized isotope ratios ($^{56/54}Fe_{experimental}$ / $^{56/54}Fe_{true}$) thus obtained are plotted as a function of the τ value applied for the correction.[37] The values obtained for each concentration level, lay on a line, and the intercept of the lines will provide the experimental detector dead time (x-value). The bias of the corresponding y-value from 1 reflects the extent

of mass discrimination.[32] Fig. 2-1 shows the plot of the normalized isotope ratios *versus* the assumed detector dead time. The experimental dead time obtained was ≈ 7 ns.

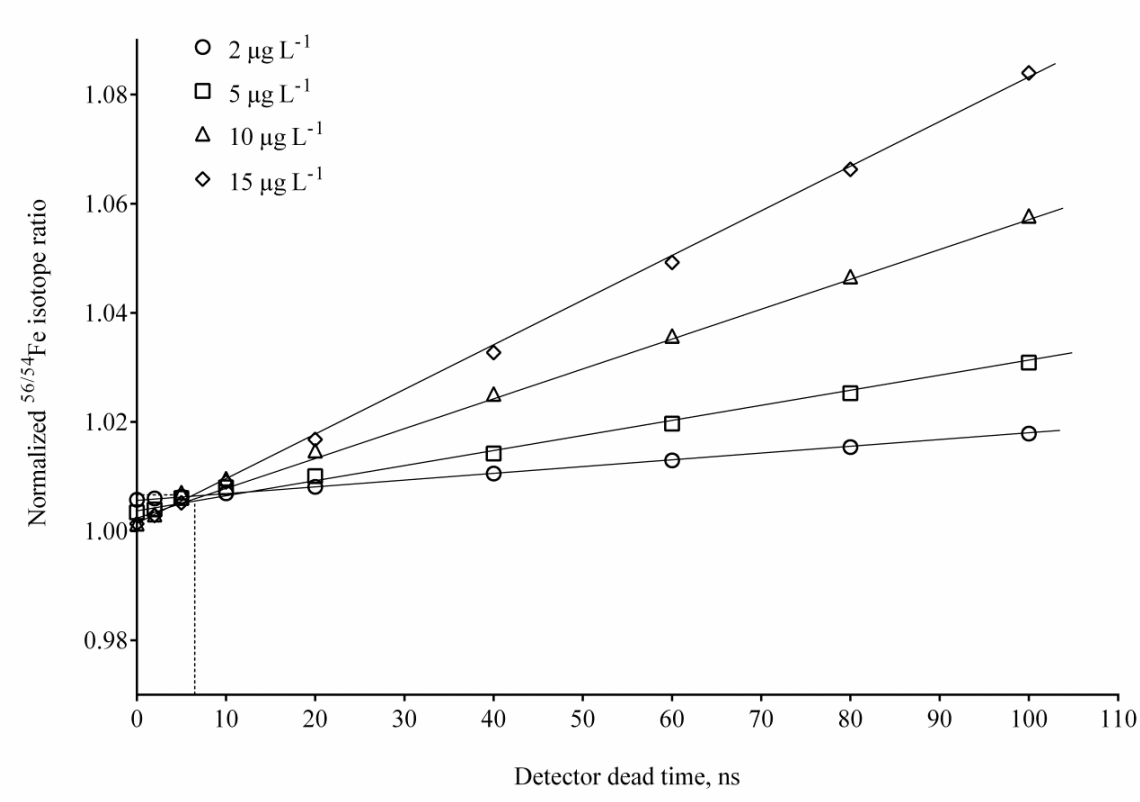

Fig. 2-1 Normalized $^{56/54}$Fe isotope ratio plotted as a function of the dead time value applied for correction.

Iron isotope ratio precision

As a result of isobaric and polyatomic interferences,[42] isotope ratio measurements of Fe *via* SF-ICP-MS requires higher mass resolution. However, at medium and high resolution (~4000 and 10000, respectively[43,44]) the precision on the isotope ratios is compromised due to the absence of a flat top peak and the significant loss in signal intensity (sensitivity).[45] The selection of the optimum Fe concentration is a critical step for isotope ratio measurements *via* SF-ICP-MS in order to obtain accurate and precise isotope ratio data taking into account the automatic switch of the detector mode. This automatic switch between modes of the EM detector of SF-ICP-MS has to be avoided.[46] As a result, a relatively low concentration of Fe is required. Thus, the concentration of Fe in the final solutions was adjusted in order to be able to monitor the signal intensities of all of the nuclides monitored (^{54}Fe, ^{56}Fe, ^{57}Fe, ^{58}Fe) in the pulse counting detector mode. The Fe concentration used was 25 µg L^{-1}.

The precision of the Fe isotope ratios was evaluated as repeatability (the precision of within-run replicates) and reproducibility (the precision of between-run replicates). The repeatability, expressed as relative standard deviation (RSD, %), of the A&MS-Fe in-house standard solution obtained within one measurement session after external mass bias correction using the IRMM-014 reference material was 0.2% for the $^{56/54}$Fe ratio, 0.4% for the $^{57/54}$Fe ratio, and 1.3% for the $^{58/54}$Fe ratio (n = 10). The results obtained in this study agreed with previously reported data (0.2, 0.4 and > 1% for $^{54/56}$Fe, $^{57/56}$Fe and $^{58/56}$Fe, respectively, *via* SF-ICP-MS and ≤ 0.2% for $^{54/56}$Fe, $^{57/56}$Fe and 0.2-0.4% for $^{58/56}$Fe *via* collision/reaction ICP-QMS).[47]

When the concentration of the target element was increased to 150 μg L^{-1}, the RSD obtained for the $^{57/54}$Fe and $^{58/54}$Fe ratios was 0.07% and 1%, respectively. However, when using this concentration, the signal of ^{56}Fe could not be monitored in the pulse counting detector mode. The reproducibility obtained for a period of 1 month is presented in Fig. 2-2. The RSD obtained was 0.3% for $^{56/54}$Fe, 0.5% for $^{57/54}$Fe and 1.5% for $^{58/54}$Fe.

2.3.2 Iron isotope ratios *via* MC-ICP-MS

The relative standard deviations for the Fe isotope ratios obtained for the A&MS-Fe in-house isotopic standard solution at an iron concentration of 500 μg L^{-1} *via* MC-ICP-MS (after correction of mass discrimination) were 0.003% RSD for $^{56/54}$Fe, 0.008% RSD for $^{57/54}$Fe and 0.08% RSD for $^{58/54}$Fe (n = 7). The repeatability obtained in one measurement session is presented in Fig. 2-3. This improved precision is the result of simultaneous measurement of the signal intensities for the ^{54}Fe, ^{56}Fe, ^{57}Fe and ^{58}Fe isotopes and the fact that a flat-topped peak shape is preserved at medium mass resolution.

The low natural abundance and consequently low intensity signal for ^{58}Fe (~ 0.05 V) explains the higher relative standard deviation for the $^{58/54}$Fe ratio. Increasing the concentration of Fe up to 2 mg L^{-1}, and therefore the signal intensity for ^{58}Fe (~ 0.3 V), allowed the RSD for the $^{58/54}$Fe ratio to be improved to 0.02% (n = 5). However, under these conditions the signal for ^{56}Fe would give rise to detector saturation and thus, it was not monitored.

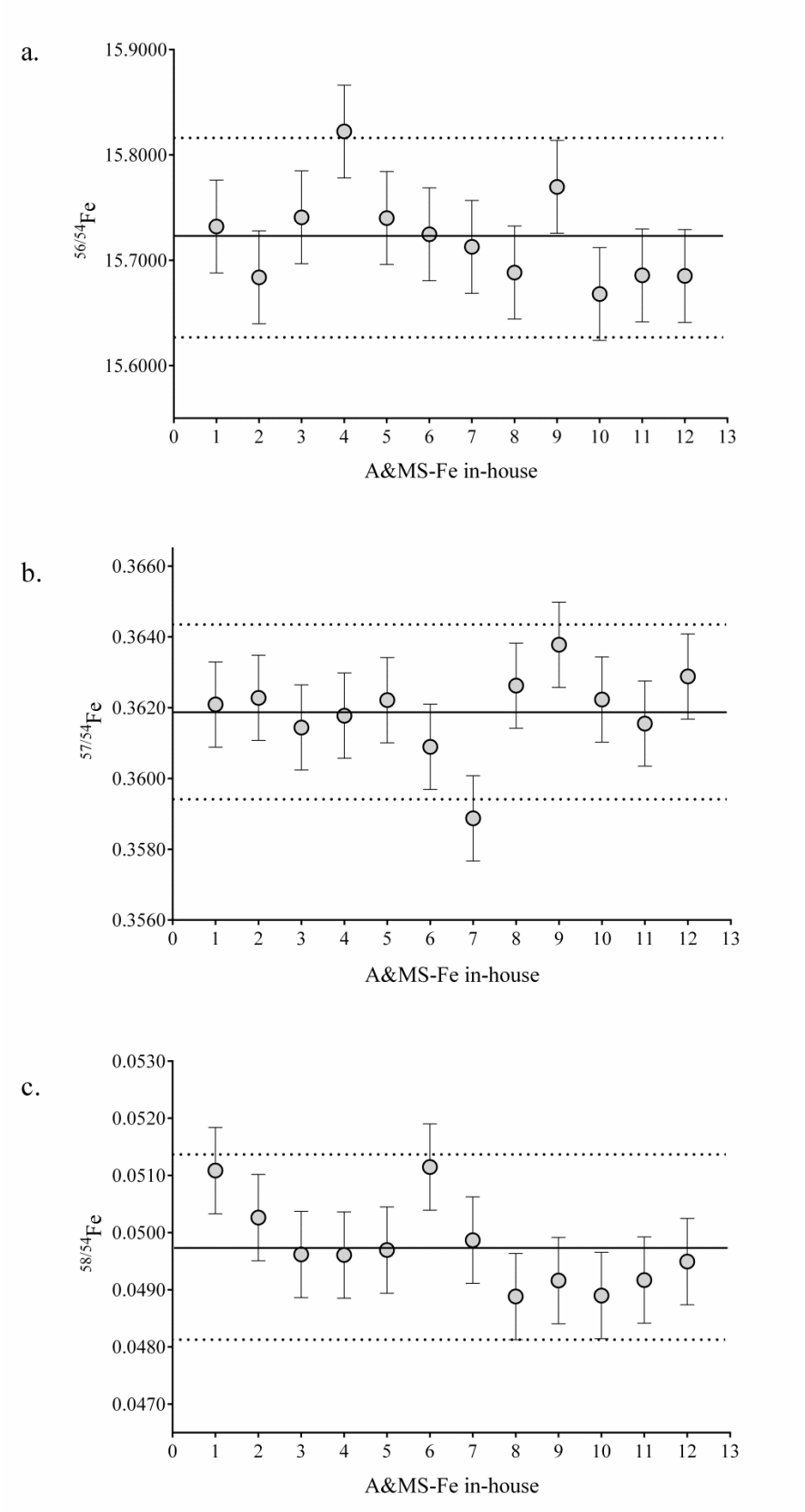

Fig. 2-2 Reproducibility for Fe isotope ratios measured *via* SF-ICP-MS during a period of 1 month using the A&MS-Fe in-house standard. The solid line represents the average ratio and the dashed lines represent 2 times the standard deviation.

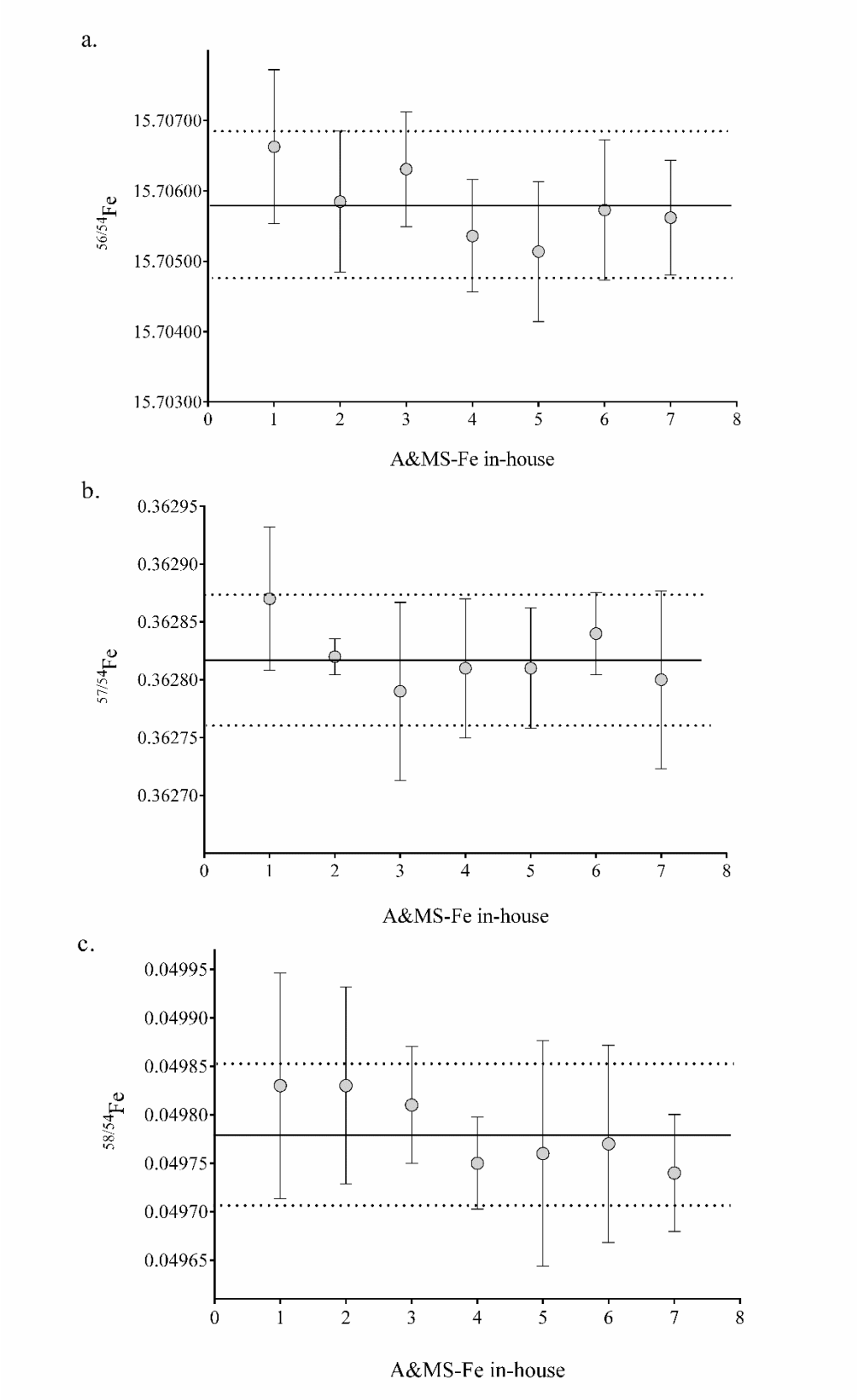

Fig. 2-3 Repeatability obtained over one measurement session for the A&MS-Fe in-house standard with MC-ICP-MS. The solid line represents the average ratio and the dashed lines represent 2 times the standard deviation.

A series of isotope ratio measurements of the A&MS-Fe in-house standard solution was performed over a longer period to evaluate the reproducibility of Fe isotope ratios. The graphical visualization of the $^{56/54}$Fe ratios obtained is presented in Fig. 2-4. The relative standard deviation over 3 years of measurements with MC-ICP-MS was 0.004% RSD for $^{56/54}$Fe and 0.008 % RSD for $^{57/54}$Fe (n = 238). The RSD for $^{58/54}$Fe based on measurements spread over 1 year was 0.09 % (n = 45).

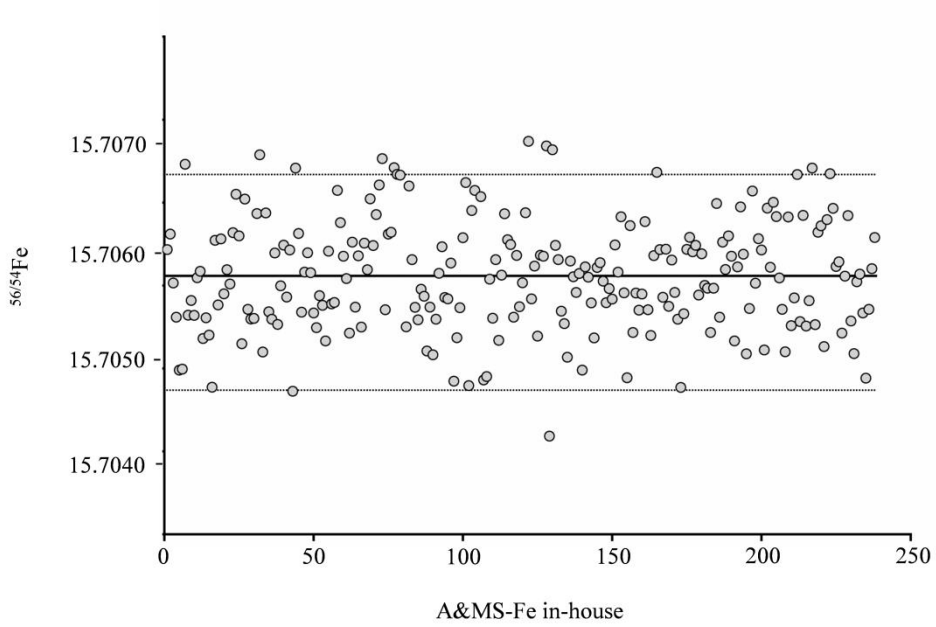

Fig. 2-4 $^{56/54}$Fe isotope ratio of the A&MS-Fe in-house standard solution obtained over a 3 years period *via* MC-ICP-MS. The solid line indicates the average value and the dashed lines 2 times the standard deviation (15.70581 ± 0.00104).

2.3.3 Study of the iron absorption *via* SF-ICP-MS

In order to evaluate the possibility of using SF-ICP-MS for iron absorption studies, the iron isotope ratios were measured in 12 whole blood samples from individuals under supplementation labeled with stable ^{57}Fe or ^{58}Fe isotopes by SF-ICP-MS and MC-ICP-MS.

Prior the Fe isotope ratio measurements by both techniques, elemental concentrations were determined by SF-ICP-MS before and after the chromatographic separation of the target element from the sample matrix to verify that on-column fractionation effects that can occur during the chromatographic separation did not affect the final isotope ratio results.[48] The recoveries of Fe were quantitative in all cases (100 ± 4%, n = 13), thus avoiding any influence

from on-column isotope fractionation. The presence of matrix elements, which can potentially give rise to interfering ions or affect the isotope ratio measurements[49] (such as Cr, Ca, Na and K), were monitored in the purified Fe fraction. After isolation, the presence of matrix elements was negligible. In addition, the level of Fe in the procedural blanks, treated in the same way as the samples, was 0.1% and therefore no blank correction of the isotope data was needed.

Table 2-3 compiles the Fe isotope ratios obtained using SF-ICP-MS and MC-ICP-MS for the whole blood samples from the supplemented individuals. As can be seen in Table 2-3, the results obtained using both techniques were in good agreement. In human absorption studies by using supplements labeled with stable iron isotopes, the high precision attainable with MC-ICP-MS is not required due to the relatively large induced changes in the target element's isotopic composition and thus, SF-ICP-MS could be useful for this purpose.

The Bland-Altman plots[50] (Fig. 2-5) show that the iron isotope ratios obtained by SF-ICP-MS, expressed as enrichment, *i.e.* the change in the ratio from the baseline (time point zero) at day 14 or day 28, were in good agreement with the corresponding MC-ICP-MS results. All data were within a narrow range of 1% for ^{57}Fe and 1.7% for ^{58}Fe enrichment difference and no significant bias throughout the entire data range in the Bland-Altman analysis was evidenced.

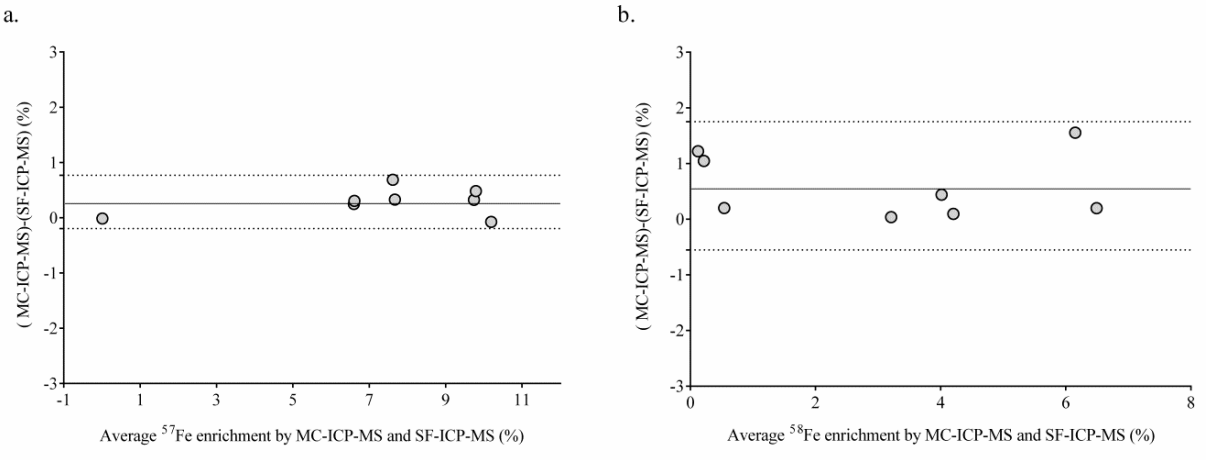

Fig. 2-5 Bland-Altman plots showing the differences between the SF-ICP-MS and MC-ICP-MS results as a function of the average ^{57}Fe (a) and ^{58}Fe (b) enrichment. The solid line represents the average differences between techniques and the dashed lines correspond to the 95% confidence intervals.

Table 2-3. Iron isotope ratios in whole blood samples obtained *via* SF-ICP-MS and MC-ICP-MS (both after chromatographic isolation of Fe). The data have been corrected for instrumental mass discrimination using external correction in a sample-standard bracketing approach. The absolute deviation between two SF-ICP-MS measurement values was ≤ 0.0007 for $^{56/54}$Fe, ≤ 0.0003 for $^{57/54}$Fe and ≤ 0.0010 for $^{58/54}$Fe. The absolute deviation between two MC-ICP-MS measurement values was ≤ 0.00005 for $^{56/54}$Fe, ≤ 0.00004 for $^{57/54}$Fe and ≤ 0.00002 for $^{58/54}$Fe.

Subject	**Sample collection time, days**	**SF-ICP-MS**			**MC-ICP-MS**		
		$^{56/54}$Fe	**$^{57/54}$Fe**	**$^{58/54}$Fe**	**$^{56/54}$Fe**	**$^{57/54}$Fe**	**$^{58/54}$Fe**
1	0	15.71396	0.36184	0.04896	15.66871	0.36160	0.04803
	14	15.66397	0.39650	0.04918	15.66843	0.39745	0.04852
	28	15.73055	0.39885	0.05082	15.66910	0.39835	0.05020
2	0	15.70888	0.36269	0.04842	15.66521	0.36144	0.04800
	14	15.66802	0.36276	0.04997	15.66527	0.36146	0.04960
	28	15.71049	0.39732	0.05044	15.66601	0.39774	0.05013
3	0	15.71062	0.36182	0.04883	15.66539	0.36148	0.04801
	14	15.63921	0.38897	0.04868	15.66556	0.38982	0.04840
	28	15.62071	0.38813	0.05145	15.66535	0.39022	0.05140
4	0	15.69772	0.36262	0.04787	15.66699	0.36156	0.04802
	14	15.68860	0.38609	0.04886	15.66719	0.38584	0.04835
	28	15.69915	0.38604	0.05093	15.66744	0.38602	0.05121

The difference between the ^{57}Fe and ^{58}Fe enrichments as obtained by SF-ICP-MS and MC-ICP-MS was 0.3% and 0.6%, respectively. Fig. 2-6 shows the linear correlation between the iron enrichment obtained using both techniques (R^2 = 0.9950, $p < 0.0001$ and 0.9502, $p < 0.0001$ for ^{57}Fe and ^{58}Fe, respectively). Thus, results obtained using SF-ICP-MS are consistent with those obtained using MC-ICP-MS.

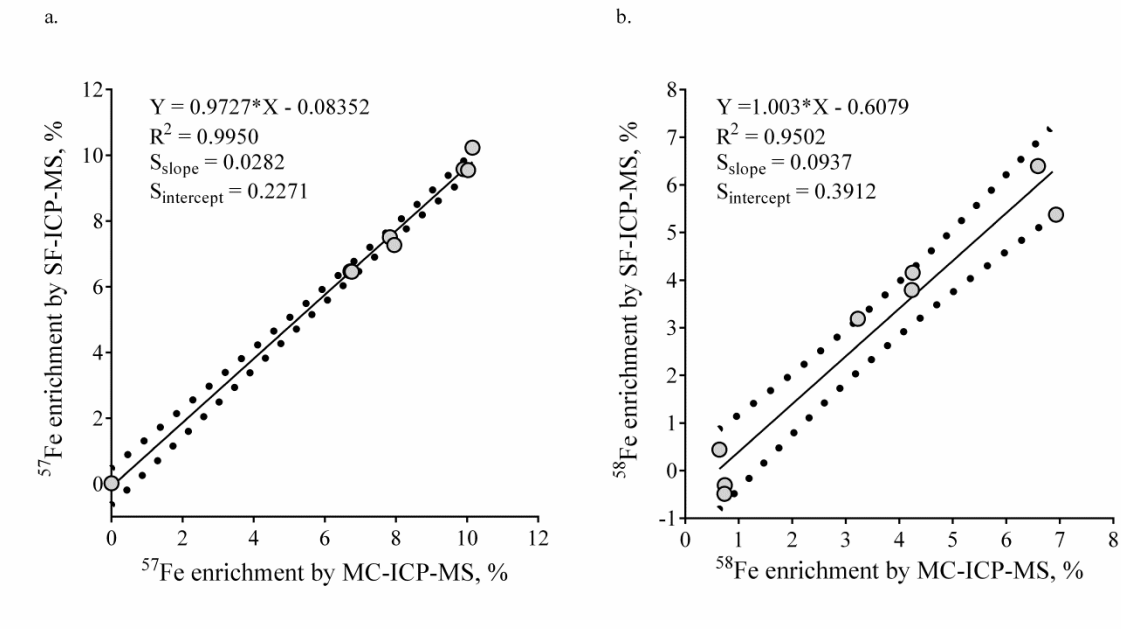

Fig. 2-6 Enrichment of ^{57}Fe (a) and ^{58}Fe (b) in whole blood samples as obtained by SF-ICP-MS and MC-ICP-MS (both after chromatographic isolation of Fe). The dashed lines correspond to the 95% confidence intervals.

Analysis of the whole blood samples after digestion and dilution only were performed to verify whether acceptable results would also be obtained under these conditions, which would increase the overall sample throughput considerably. As can be seen in Table 2-4, the results obtained in digested whole blood *via* SF-ICP-MS are in good agreement with data obtained *via* SF-ICP-MS in the pure iron fractions obtained upon chromatographic isolation. Fig. 2-7 illustrates the linear correlation between the iron enrichments obtained *via* SF-ICP-MS without prior isolation of Fe and that obtained *via* high-precision MC-ICP-MS after Fe isolation from blood matrix (R^2 = 0.9927, $p < 0.0001$ and 0.9749, $p < 0.0001$ for ^{57}Fe and ^{58}Fe, respectively). Thus, Fe isotopic analysis of human whole blood by SF-ICP-MS for Fe absorption studies without prior Fe isolation from the blood matrix is also providing reliable results, while significantly improving sample throughput compare to MC-ICP-MS.

Table 2-4. Iron isotope ratios in whole blood samples obtained *via* SF-ICP-MS after digestion and dilution and *via* SF-ICP-MS after isolation of Fe from blood matrix. The data have been corrected for instrumental mass discrimination using external correction in a sample-standard bracketing approach. The absolute deviation between two SF-ICP-MS measurement values was ≤ 0.0008 for $^{57/54}$Fe and ≤ 0.0009 for $^{58/54}$Fe. The absolute deviation between two MC-ICP-MS measurement values was ≤ 0.00004 for $^{57/54}$Fe and ≤ 0.00002 for $^{58/54}$Fe.

Subject	Sample collection time, days	SF-ICP-MS in digested blood		SF-ICP-MS in pure fraction	
		$^{57/54}$Fe	$^{58/54}$Fe	$^{57/54}$Fe	$^{58/54}$Fe
1	0	0.36111	0.04870	0.36184	0.04896
	14	0.39713	0.04883	0.39650	0.04918
	28	0.39809	0.05046	0.39885	0.05082
2	0	0.36110	0.04758	0.36269	0.04842
	14	0.36045	0.04934	0.36276	0.04997
	28	0.39692	0.04994	0.39732	0.05044
3	0	0.36087	0.04812	0.36182	0.04883
	14	0.38972	0.04840	0.38897	0.04868
	28	0.38759	0.05189	0.38813	0.05145
4	0	0.36154	0.04830	0.36262	0.04787
	14	0.38418	0.04860	0.38609	0.04886
	28	0.38595	0.05151	0.38604	0.05093

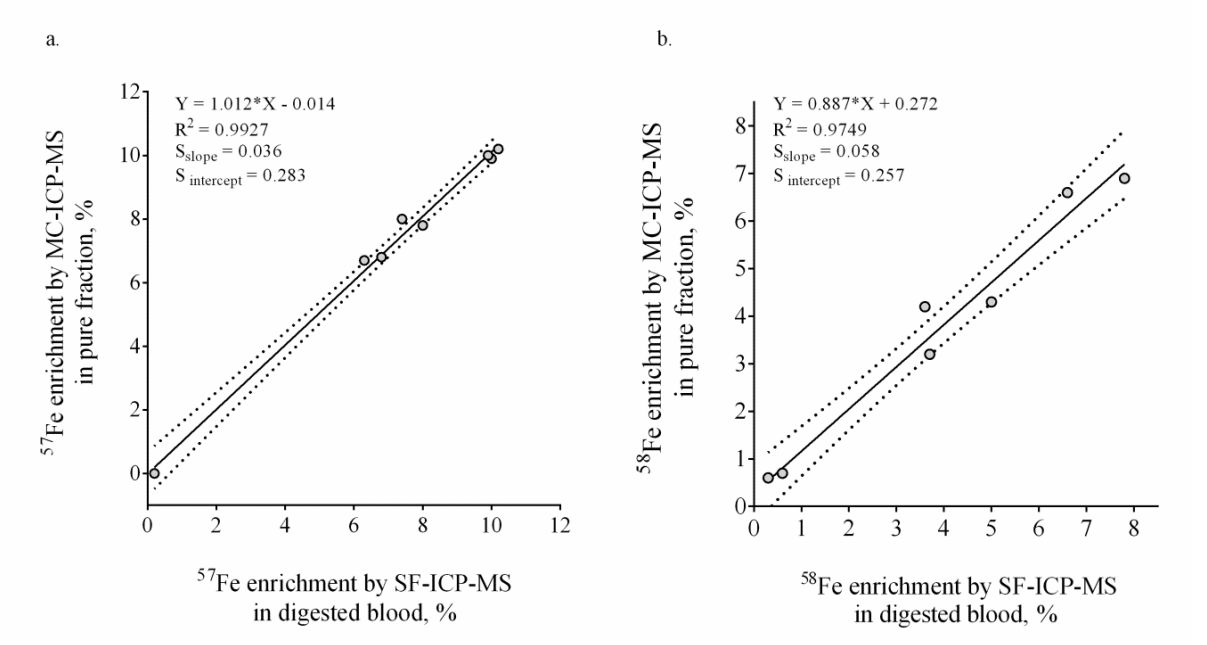

Fig. 2-7 Enrichment of ^{57}Fe (a) and ^{58}Fe (b) in whole blood samples as obtained by SF-ICP-MS after digestion and dilution of whole blood and MC-ICP-MS for the pure Fe fraction. The dashed lines correspond to the 95% confidence intervals.

2.4 CONCLUSIONS

Although MC-ICP-MS provides a superior precision for isotope ratio measurements, the results evidenced that SF-ICP-MS can be used to determine the $^{57/54}$Fe and $^{58/54}$Fe ratios in whole blood samples of supplemented individuals sufficiently accurately and precise and also to detect the ratio of increase in ^{57}Fe and ^{58}Fe for absorption studies. It has been demonstrated that SF-ICP-MS can track ^{57}Fe and ^{58}Fe enrichments down to 0.3% and 0.6%, respectively. The changes observed *via* SF-ICP-MS were in good agreement with those obtained *via* MC-ICP-MS. Since a minimum 5% oral iron absorption is expected for any worthwhile supplementation strategy, SF-ICP-MS can be considered as a suitable technique for the routine determination of iron absorption in human iron supplementation studies. Moreover, isotopic analysis of digested and diluted whole blood samples without prior Fe isolation from whole blood matrix results in an increased sample throughput and decreased cost compared to MC-ICP-MS.

2.5 REFERENCES

1. Stoltzfus, R. J. Iron deficiency: Global prevalence and consequences. *Food Nutr. Bull.* **24,** S99-103 (2003).
2. Johnson-Wimbley, T. D. & Graham, D. Y. Diagnosis and management of iron deficiency anemia in the 21st century. *Therap. Adv. Gastroenterol.* **4,** 177–84 (2011).
3. Miller, J. L. Iron deficiency anemia: A common and curable disease. *Cold Spring Harb. Perspect. Med.* **3,** (2013).
4. Short, M. W. & Domagalski, J. E. Iron deficiency anemia: Evaluation and management. *Am. Fam. Physician* **87,** 98–104 (2013).
5. Wish, J. B. Assessing iron status: beyond serum ferritin and transferrin saturation. *Clin. J. Am. Soc. Nephrol.* **1,** S4–S8 (2006).
6. Hörl, W. H. Clinical aspects of iron use in the anemia of kidney disease. *J. Am. Soc. Nephrol.* **18,** 382–93 (2007).
7. Camaschella, C. Iron-Deficiency Anemia. *N. Engl. J. Med.* **372,** 1832–1843 (2015).
8. *Assessing the iron status of populations: including literature reviews. Report of a Joint World Health Organization/Centers fo r Disease Control and Prevention Technical Consultation on the Assessment of Iron Status at the Population Level*. (World Health Organization, 2007). at <http://www.who.int/nutrition/publications/micronutrients/anaemia_iron_deficiency/9789241596107/en/> Last accessed on 25/07/0217.
9. Umbreit, J. Iron deficiency: A concise review. *Am. J. Hematol.* **78,** 225–231 (2005).

10. Weyers, R., Coetzee, M. J. & Nel, M. Iron status determination in pregnancy using the Thomas plot. *Int. J. Lab. Hematol.* **38,** 119–124 (2016).

11. *WHO Model List of Essential Medicines 19th List*. (2015). at <http://www.who.int/medicines/publications/essentialmedicines/en/>

12. Liu, T.-C., Lin, S.-F., Chang, C.-S., Yang, W.-C. & Chen, T.-P. Comparison of a combination ferrous fumarate product and a polysaccharide iron complex as oral treatments of iron deficiency anemia: a Taiwanese study. *Int. J. Hematol.* **80,** 416–20 (2004).

13. Santiago, P. Ferrous versus Ferric Oral Iron Formulations for the Treatment of Iron Deficiency: A Clinical Overview. *Sci. World J.* **2012,** 1–5 (2012).

14. Rimon, E. *et al.* Are we giving too much iron? Low-dose iron therapy is effective in octogenarians. *Am. J. Med.* **118,** 1142–1147 (2005).

15. Alleyne, M., Horne, M. K. & Miller, J. L. Individualized Treatment for Iron-deficiency Anemia in Adults. *Am. J.Med.* **121,** 943–948 (2008).

16. Low, M. S. Y., Speedy, J., Styles, C. E., De-Regil, L. M. & Pasricha, S.-R. in *Cochrane Database of Systematic Reviews* (ed. Pasricha, S.-R.) **4,** CD009747 (John Wiley & Sons, Ltd, 2016).

17. Faria, N. *et al.* Development of DRC-ICP-MS methodology for the rapid determination of 58Fe erythrocyte incorporation in human iron absorption studies. *J. Anal. At. Spectrom.* **26,** 1648 (2011).

18. Albarède, F. *et al.* Precise and accurate isotopic measurements using multiple-collector ICPMS. *Geochim. Cosmochim. Acta* **68,** 2725–2744 (2004).

19. Yang, L. Accurate and precise determination of isotopic ratios by MC-ICP-MS: a review. *Mass Spectrom. Rev.* **28,** 990–1011 (2009).

20. Barshick, C. M., Duckworth, D. C. & Smith, D. H. (David H. *Inorganic mass spectrometry : fundamentals and applications*. (Marcel Dekker, Inc, 2000).

21. Johnson, C. M. & Beard, B. L. Correction of instrumentally produced mass fractionation during isotopic analysis of fe by thermal ionization mass spectrometry. *Int. J. Mass Spectrom.* **193,** 87–99 (1999).

22. Chen, Z., Griffin, I. J., Plumlee, L. M. & Abrams, S. A. High resolution inductively coupled plasma mass spectrometry allows rapid assessment of iron absorption in infants and children. *J. Nutr.* **135,** 1790–5 (2005).

23. Walczyk, T. Iron isotope ratio measurements by negative thermal ionisation mass spectrometry using FeF4− molecular ions. *Int. J. Mass Spectrom. Ion Process.* **161,** 217–227 (1997).

24. Walczyk, T. & von Blanckenburg, F. Natural iron isotope variations in human blood. *Science* **295,** 2065–6 (2002).

25. Walczyk, T. & von Blanckenburg, F. Deciphering the iron isotope message of the human body. *Int. J. Mass Spectrom.* **242,** 117–134 (2005).

26. Krayenbuehl, P.-A., Walczyk, T., Schoenberg, R., von Blanckenburg, F. & Schulthess, G. Hereditary hemochromatosis is reflected in the iron isotope composition of blood. *Blood* **105,** 3812–3816 (2005).

27. Van Heghe, L., Delanghe, J., Van Vlierberghe, H. & Vanhaecke, F. The relationship

between the iron isotopic composition of human whole blood and iron status parameters. *Metallomics* **5,** 1503–1509 (2013).

28. Costas-Rodríguez, M., Delanghe, J. & Vanhaecke, F. High-precision isotopic analysis of essential mineral elements in biomedicine: Natural isotope ratio variations as potential diagnostic and/or prognostic markers. *TrAC* **76,** 182–193 (2016).
29. Becker, J. S. *Inorganic mass spectrometry: principles and applications*. (John Wiley & Sons Ltd, 2007).
30. Vanhaecke, F. & Degryse, P. *Isotopic Analysis: Fundamentals and Applications Using ICP-MS*. (Wiley-VCH Verlag GmbH & Co. KGaA, 2012).
31. Van Heghe, L., Engström, E., Rodushkin, I., Cloquet, C. & Vanhaecke, F. Isotopic analysis of the metabolically relevant transition metals Cu, Fe and Zn in human blood from vegetarians and omnivores using multi-collector ICP-mass spectrometry. *J. Anal. At. Spectrom.* **27,** 1327–1334 (2012).
32. Vanhaecke, F., Balcaen, L. & Malinovsky, D. Use of single-collector and multi-collector ICP-mass spectrometry for isotopic analysis. *J. Anal. At. Spectrom.* **24,** 863 (2009).
33. Dronov, M. & Schram, J. A method for increasing the precision of isotope ratio analysis on a Quadrupole ICP-MS based on measurements of lead and strontium. *J. Anal. At. Spectrom.* **28,** 1796 (2013).
34. Nelms, S. M. *Inductively coupled plasma mass spectrometry handbook*. (Blackwell Pub., 2005).
35. Vanhaecke, F. & Moens, L. Overcoming spectral overlap in isotopic analysis via single- and multi-collector ICP-mass spectrometry. *Analytical and Bioanalytical Chemistry* **378,** 232–240 (2004).
36. van Heuzen, A. A., Hoekstra, T. & van Wingerden, B. Precision and accuracy attainable with isotope dilution analysis applied to inductively coupled plasma mass spectrometry: theory and experiments. *J. Anal. At. Spectrom.* **4,** 483 (1989).
37. Vanhaecke, F. *et al.* Dependence of detector dead time on analyte mass number in inductively coupled plasma mass spectrometry. *J. Anal. At. Spectrom.* **13,** 567–571 (1998).
38. Held, A. & Taylor, P. D. P. A calculation method based on isotope ratios for the determination of dead time and its uncertainty in ICP-MS and application of the method to investigating some features of a continuous dynode multiplier. *J. Anal. At. Spectrom.* **14,** 1075–1079 (1999).
39. Appelblad, P. K. & Baxter, D. C. A model for calculating dead time and mass discrimination correction factors from inductively coupled plasma mass spectrometry calibration curves. *J. Anal. At. Spectrom.* **15,** 557–560 (2000).
40. Rameback, H., Berglund, M., Vendelbo, D., Wellum, R. & Taylor, P. D. P. On the determination of the true dead-time of a pulse-counting system in isotope ratio mass spectrometry. *J. Anal. At. Spectrom.* **16,** 1271–1274 (2001).
41. Russ, G. P. in *Applications of inductively coupled plasma mass spectrometry* ch. 4, p. 90 (Blackie, Glasgow and London, 1989).
42. May, T. W. & Wiedmeyer, R. H. A table of polyatomic interferences in ICP-MS. *At. Spectrosc.* **19,** 150–155 (1998).

43. Weyer, S. & Schwieters, J. B. High precision Fe isotope measurements with high mass resolution MC-ICPMS. *Int. J. Mass Spectrom.* **226,** 355–368 (2003).

44. Castro, W., Trejos, T., Naes, B. & Almirall, J. R. Comparison of high-resolution and dynamic reaction cell ICP-MS capabilities for forensic analysis of iron in glass. *Anal. Bioanal. Chem.* **392,** 663–72 (2008).

45. Becker, J. S. State-of-the-art and progress in precise and accurate isotope ratio measurements by ICP-MS and LA-ICP-MS. *J. Anal. At. Spectrom.* **17,** 1172–1185 (2002).

46. Vanhaecke, F., Moens, L., Dams, R. & Taylor, P. Precise Measurement of Isotope Ratios with a Double-Focusing Magnetic Sector ICP Mass Spectrometer. *Anal. Chem.* **68,** 567–569 (1996).

47. Vanhaecke, F., Balcaen, L., De Wannemacker, G. & Moens, L. Capabilities of inductively coupled plasma mass spectrometry for the measurement of Fe isotope ratios. *J. Anal. At. Spectrom.* **17,** 933–943 (2002).

48. Maréchal, C. N., Télouk, P. & Albarède, F. Precise analysis of copper and zinc isotopic compositions by plasma-source mass spectrometry. *Chem. Geol.* **156,** 251–273 (1999).

49. Anoshkina, Y., Costas-Rodríguez, M. & Vanhaecke, F. High-precision Fe isotopic analysis of whole blood for biomedical purposes without prior isolation of the target element. *J. Anal. At. Spectrom.* **30,** 1816–1821 (2015).

50. Martin Bland, J. & Altman, D. Statistical methods for assessing agreement between two methods of clinical measurement. *Lancet* **327,** 307–310 (1986).

CHAPTER 3

HIGH-PRECISION IRON ISOTOPIC ANALYSIS OF WHOLE BLOOD FOR BIOMEDICAL PURPOSES WITHOUT PRIOR ISOLATION OF THE TARGET ELEMENT

Based on publication:

Yulia Anoshkina, Marta Costas-Rodríguez and Frank Vanhaecke, Journal of Analytical Atomic Spectrometry, 2015, Vol. 30, Issue 8, P. 1816-1821

3.1 ABSTRACT

Recently, it has been documented that Fe isotopic analysis of whole blood and serum by means of multi-collector ICP-mass spectrometry (MC-ICP-MS) is providing promising results in a biomedical context and thus, there is a demand for simple, fast and reliable methodologies, providing high sample throughput. In this work, the possibility of Fe isotopic analysis by MC-ICP-MS directly in acid-digested whole blood and thus, without prior Fe isolation was evaluated. The influence of the main mineral matrix elements and the effect of potentially remaining organic compounds were first systematically evaluated using synthetic solutions. The Fe isotopic composition was biased low in the presence of matrix elements such as Na and K, while it was biased high for glucose concentrations ≥ 1% (w/v). Nevertheless, after dilution of the whole blood sample digest to 0.75-1.5 mg L^{-1} of Fe, followed by adequate correction for instrumental mass discrimination using a combination of internal (with admixed Ni) and external correction, MC-ICP-MS isotope ratio measurements provided accurate and precise results. For actual samples, the Fe isotopic data obtained agree well with those using the reference procedure, based on prior chromatographic isolation of Fe out of acid-digested blood.

3.2 INTRODUCTION

Recently, several research groups have demonstrated that isotopic analysis of iron (Fe) in whole blood or serum might reveal potentially very useful clinical information. Van Heghe *et al.* have established a clear link between an individual's whole blood Fe isotopic composition and his/her iron status.[1] Hotz *et al.* have identified the extent of mobilization of storage iron (liver) and the dietary iron absorption efficiency as governing factors.[2,3] It was also demonstrated that patients suffering from hereditary hemochromatosis (HH)[1,4] or anemia of chronic disease (ACD)[1] show an altered Fe isotopic composition in whole blood compared to healthy subjects. The HH and ACD populations investigated by Van Heghe *et al.* show a difference in $^{56}Fe/^{54}Fe$ isotope ratio in whole blood of +0.5‰ and -0.3‰ compared to the reference population, respectively.[1,5–7] The number of patient samples was too low to assess gender-based differences. For tracing down and quantifying such small differences, a high isotope ratio precision is mandatory, making multi-collector ICP-mass spectrometry (MC-ICP-MS) the preferable technique. However, Fe isotope ratio data with MC-ICP-MS can be compromised by instrumental mass discrimination and spectral interference, mainly from $^{54}Cr^+$, $^{58}Ni^+$ and Ar- and Ca-based molecular ions.[8,9]

To overcome spectral overlap, medium or high mass resolution, potentially in combination with aerosol desolvation, can be used with MC-ICP-MS.[10–15] With the standard sample introduction system, relatively high concentrations of the target analyte, *i.e.* $\geq$ 1 mg L^{-1} are typically preferred to minimize the effect of spectral interference.[16]

Correction for instrumental mass discrimination can be accomplished *via* external correction in a sample-standard bracketing (SSB) approach, or a combination of such external correction with internal correction using Ni or Cu as an admixed internal standard. Both methods have been proven suitable for high-purity iron solutions.[10,17] The double spike ^{57}Fe-^{58}Fe approach, combined with SSB, was also used, mainly in the context of environmental and geological studies.[18–20] However, it needs to be stressed that both the matrix composition and the target element concentration affect the extent of mass discrimination. Such effects can obscure the small, natural isotope ratio differences that need to be revealed.[21] The origin of mass discrimination is still poorly understood, although several contributions, such as a shift in the ionization equilibrium, collisional scatter, energy consumption for matrix decomposition, space-charge effects and ambipolar diffusion, have been suggested.[9,22–27]

As a result, the sample preparation procedure preceding isotopic analysis of whole blood iron is a critical issue. Typically, whole blood is first digested with HNO_3 or a mixture of HNO_3 and H_2O_2 to set the iron free (predominantly from hemoglobin) in ionic form, followed by the chemical isolation of the target element from the concomitant matrix and residual organic components that potentially affect the extent of mass discrimination. Anion exchange chromatographic methods, based on the high affinity (and thus, partition coefficients) of Fe-chloride complexes towards an anion exchange resin, such as AG MP-1, are the most frequently used for the isolation of Fe from biological samples.[7,10,13,28] Since on-column fractionation effects occur due to the slightly different elution behavior of the different Fe-isotopes on the column, the recovery of iron needs to be quantitative.[28] Chromatographic isolation of Fe is effective and provides better recoveries and a more effective target element / matrix separation than the more conventional iron precipitation methodology. However, the chromatographic approach is labor-intensive and time-consuming, thus reducing the sample throughput. Relatively large amounts of highly pure acid (about 20 mL of concentrated HCl per sample) and additional evaporation / re-dissolution steps are required to make the final matrix suited for isotope ratio measurements with MC-ICP-MS.

Stenberg *et al.*[14] have compared different sample preparation procedures for the isotopic analysis of Fe in Seronorm whole blood reference material by MC-ICP-MS, including microwave-assisted acid digestion with and without Fe isolation *via* anion exchange chromatography and *via* selective iron precipitation with different reagents. Although no differences in the Fe isotopic composition were found following the approaches mentioned, the authors recommended precipitation of iron with NH_3 based on practical considerations, *e.g.*, high sample throughput. Based on the high concentration of iron in whole blood samples (~ 350 mg L^{-1}, healthy subjects) we decided to perform and evaluate the Fe isotopic analysis of whole blood by MC-ICP-MS without matrix separation, *i.e.* directly after acid digestion and dilution of the sample digest. Synthetic solutions were used to systematically investigate the effect of concomitant matrix components on the Fe isotope ratio results. The MC-ICP-MS instrument settings were optimized using an actual whole blood sample. Eleven whole blood samples were analyzed directly (digestion & dilution) and after chromatographic Fe isolation, and the results obtained were compared to one another.

3.3 EXPERIMENTAL

3.3.1 Reagents and standards

Ultrapure water (resistivity > 18.2 MΩ cm) was obtained from a Milli-Q Element water purification system (Millipore, France). *Pro analysis* purity level nitric acid (14 M) was used after sub-boiling distillation. *Optima* grade hydrochloric acid (12 M) was obtained from Fisher Chemical (UK) and used as such. Ultrapure hydrogen peroxide 9.8 M was acquired from Sigma-Aldrich (Belgium). All sample manipulations were carried out in a class-10 clean laboratory.

The Fe isotopic reference material IRMM-014 from the Institute for Reference Materials and Measurements (IRMM, Belgium) was used for external correction in a sample-standard bracketing approach. A single-element Fe standard solution acquired from Inorganic Ventures (The Netherlands; lot D2-FE03110) was used as in-house isotopic standard solution (further referred to as A&MS-Fe) for preliminary experiments and for validating the isotope ratio measurements. Single-element standard stock solutions (1 g L^{-1}) acquired from Inorganic Ventures were used for the preparation of synthetic solutions, for mass discrimination correction using an internal standard (Ni) and for quantification of the target element. Also glucose (Merck, Germany) was used for the preparation of synthetic solutions.

AG MP-1 strong anion exchange resin (100-200 mesh, chloride form) and polypropylene chromatographic columns (Bio-Rad, Belgium) were used for the Fe isolation procedure.

3.3.2 Instrumentation and measurements

A Thermo Scientific Neptune MC-ICP-MS instrument (Germany) was used for the Fe isotope ratio measurements. A PFA concentric nebulizer (100 μL min^{-1}) and double spray chamber, with a cyclonic and a Scott-type sub-unit, were used for the introduction of the solutions into the plasma. Measurements were performed in medium resolution, in static collection mode and using six Faraday collectors connected to 10^{11} Ω amplifiers. Instrument settings and data acquisition parameters are shown in Table 3-1.

Ni was used as an internal standard at the same concentration as the target element Fe. The Fe isotope ratios were calculated off-line after removal of outliers using a 2s-test. Mass bias

correction was performed by means of (i) external correction in a sample-standard bracketing approach (SSB) and (ii) a combination of internal correction (with Ni) by means of the revised Russell's law (using a regression line to establish the correlation between the correction factors for Fe and Ni) and SSB.[29] The isotopic composition is expressed in delta notation (δ^{56}Fe, δ^{57}Fe, ‰), calculated against the isotopic reference material IRMM-014 following eqn.3-1, where x is 56 or 57.

$$\delta^{x}Fe_{sample} = \left(\frac{{}^{x}Fe/{}^{54}Fe_{sample}}{{}^{x}Fe/{}^{54}Fe_{IRMM-014}} - 1 \right) \quad (3\text{-}1)$$

Table 3-1. Instrument settings and data acquisition parameters for the Neptune MC-ICP-MS.

RF power (W)	1275
Guard electrode	Connected
Sampling cone and skimmer	Ni standard sampling cone 1.1 mm aperture diameter Ni H-type skimmer, 0.8 mm orifice diameter
Lens settings	Optimized for maximum signal intensity
Ar flow-rates (L min^{-1})	
plasma gas	15
auxiliary gas	0.75
nebulizer gas	0.9-1.0
Sample uptake rate (μL min^{-1})	100
Resolution mode	Medium
Acquisition mode	Static; multi-collection
Number of blocks	9
Number of cycles	5
Integration time (s)	4.194
Cup configuration	L4: ^{54}Fe; L2: ^{56}Fe; L1: ^{57}Fe; C: ^{58}(Fe + Ni); H1: ^{60}Ni; H3: ^{62}Ni

Elemental concentrations were determined using an Element XR single-collector sector-field ICP-MS instrument (Thermo Scientific). For the introduction of solutions into the ICP, a combination of a 200 μL min^{-1} quartz concentric nebulizer and a cyclonic spray chamber was used. Ga was used as internal standard to correct for matrix effects and instrumentation instability.

A Shimadzu UVmini-1240 UV-Vis spectrophotometer was used to assess the presence of organic matter in the sample.

3.3.3 Samples and sample preparation

Whole blood samples of 11 individuals, provided by the Ghent University Hospital (Belgium), were analyzed. One of these samples (from a hemochromatosis patient and available in a large quantity) was used to optimize the analytical protocol and to evaluate its analytical performance. Synthetic samples were also analyzed to evaluate matrix effects. These were prepared using the A&MS-Fe standard and major, minor and trace elements (Cu, Zn, Mn, Mg, Ni, Ca, Br, P, S, Na and K), mixtures of these elements and/or glucose as an organic compound.

About 3 mL of blood was digested in a closed Teflon Savillex beaker using a mixture of 7 mL of HNO_3 and 1.5 mL of H_2O_2. The digestion was carried out at 110 ºC overnight (~16 h). The digest thus obtained was evaporated to dryness and re-dissolved in 2 mL of concentrated HNO_3. Then, two aliquots of 1 mL were separated for a second evaporation step. After that, one aliquot was re-dissolved in 0.42 M HNO_3 for direct Fe isotope ratio measurement and the other one was re-dissolved in 5 mL of 8 M HCl + 0.001% H_2O_2 for chromatographic Fe isolation.

Chromatographic isolation of Fe was carried out according to Van Heghe *et al.*[7] For this purpose, 5 mL of the sample aliquot were loaded onto the column containing 2 mL of previously cleaned AG MP-1 anion exchange resin. The matrix was eluted with 8 mL of 8 M HCl + 0.001% H_2O_2, followed by Cu, eluted with 12 mL of 5 M HCl + 0.001% H_2O_2. Finally, Fe was eluted with 10 mL of 0.6 M HCl. The purified Fe solution was evaporated to dryness at 95 ºC twice to remove residual chloride. The final residue was re-dissolved in 0.42 M HNO_3 for the isotope ratio measurements. Procedural blanks, treated in the same way as the samples, were also included.

Ethical approval was obtained for using these samples by an independent commission connected to the Ghent University Hospital. Patients and individuals forming the reference population signed an informed consent.

3.4 RESULTS AND DISCUSSION

3.4.1 Evaluation of the effect of concomitants using synthetic solutions

Fe isotope ratio measurements *via* MC-ICP-MS are potentially adversely affected by the presence of matrix components, as these might affect the ion transmission efficiencies of the target nuclides.[9,16] Even after chemical isolation, residual matrix may alter the extent of mass bias.[11] To evaluate the effect of blood matrix components, synthetic solutions containing the A&MS-Fe standard (500 μg L^{-1}), individual matrix elements (Cu, Zn, Mn, Mg, Ni, Ca, Br, P, S, Na and K) and combinations of these were used. The average Fe isotopic composition of the pure A&MS-Fe standard obtained during a period of 1 year is: 0.46 ± 0.07 ‰ for δ^{56}Fe and 0.69 ± 0.10 ‰ for δ^{57}Fe (n = 25). The δ^{56}Fe values in the synthetic solutions after correction for mass discrimination using the combined internal & external correction approach are presented in Fig. 3-1. As can be seen, among the elements studied, Na and K showed the highest influence on the Fe isotope ratio results. The presence of these easily ionizable elements alters the plasma conditions, *i.e.* temperature and electron density, which might explain the effect on the extent of mass discrimination. Shifts of -0.11, -0.17 and -0.13 ‰ were observed in the presence of 1 mg L^{-1} of Na, of K and of a mixture of Na, K, S, P and Br (at 1 mg L^{-1} each), respectively. Levels higher than 2 mg L^{-1} of S (characterized by a high ionization energy and thus, low ionization efficiency) also led to significantly deviating δFe values, but in this case towards higher values.

In contrast, the presence of the other elements studied, whether assessed individually or together, did not generate any deviation of the δ^{56}Fe value outside of the 0.07‰ experimental uncertainty. It had also been previously pointed out that matrix elements should not affect the accuracy of Fe isotope ratio data for an element/Fe ratio < 2.[10,30] However, a deterioration in the precision was reported for increasing concentrations of the matrix elements due to instability of the instrumental mass bias.[30] This effect can be alleviated *via* correction for mass discrimination using the combined approach of internal & external correction for mass discrimination.

A synthetic solution simulating the mineral composition of whole blood after the acid digestion was prepared by addition of the following components to A&MS-Fe standard solution containing 500 μg L^{-1} of Fe : 2 mg L^{-1} of Na, 1.5 mg L^{-1} of K and S, 200 μg L^{-1} of P

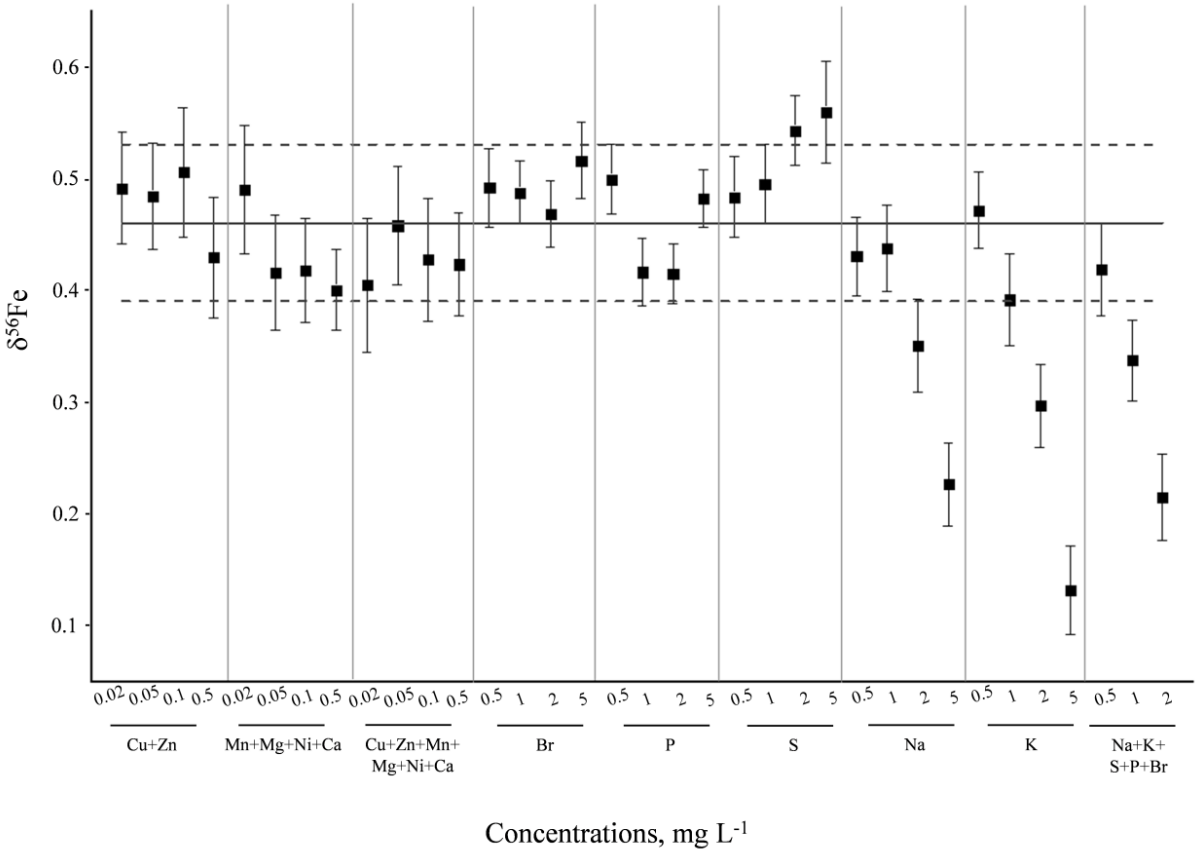

Fig. 3-1 Influence of concomitant elements present in whole blood on the δ^{56}Fe measurement results studied using synthetic solutions. The solid line indicates the average value and the dashed lines 2 times the standard deviation for the A&MS-Fe in-house standard. Error bars indicate the standard deviation for 3 measurements.

and 20 µg L^{-1} of Cu, Zn, Br, Mg, Mn, Ca and Ni. For this mixture, the δ^{56}Fe value was 0.12 ± 0.06 ‰ after SSB correction and 0.53 ± 0.04 ‰ after the combined correction approach with ^{62}Ni/^{60}Ni and SSB (n = 4). This synthetic solution was also admixed with different amounts of glucose to assess the effect of potentially remaining organic components. The δ^{56}Fe values obtained for the synthetic blood solutions with different amounts of glucose are shown in Fig. 3-2. An increasing concentration in organic C concentration led to an increasing bias in the δFe values. The influence of organic substance shifted the isotope ratio results in the opposite direction than did Na and K, *i.e.* the δ^{56}Fe value was shifted by 0.15‰ after the SSB correction, and by 0.08‰ after the combined internal & SSB correction in the presence of 1% (w/v) of glucose. The experimental δ^{56}Fe value for the synthetic solution containing all expected matrix components and 1 % (w/v) of glucose was 0.31‰. This value corresponds well with that expected based on the individual extents of bias observed, *i.e.* 0.27‰ (compensation of effects).

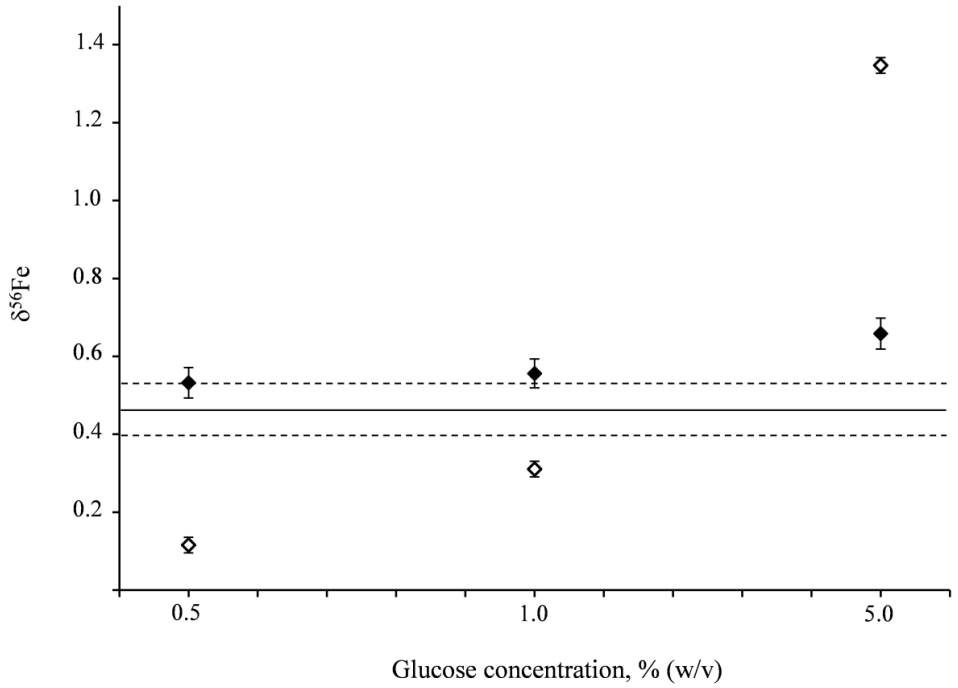

Fig. 3-2 Influence of the glucose content on the δ^{56}Fe measurement results for a synthetic solution also containing the whole blood matrix elements. The solid line indicates the average value and the dashed lines 2 times the standard deviation for the A&MS-Fe standard. Open symbols indicate the data obtained after SSB correction and filled symbols after the combined (internal & SSB) correction. Error bars indicate the standard deviation of 2 measurements.

3.4.2 Optimization of experimental conditions using actual whole blood

Fe isotope ratio measurements were performed in a whole blood sample (obtained from a hemochromatosis patient and available in a large quantity) after acid digestion. Instrument settings, such as gas flow rates, sampling depth and RF power, affect the properties of the plasma, especially the temperature, and consequently, the vaporization rate and atomization and ionization efficiencies.[31–33] Thus, these settings were optimized using the acid-digested whole blood (Table 3-1).

Different sample dilutions were performed. The results obtained after mass discrimination correction using the combination of internal correction & SSB are shown in Table 3-2. The isotopic composition of this sample, obtained following the reference procedure, *i.e* after sample digestion and chromatographic Fe isolation (n = 6), is also included in this table. Two-way ANOVA at a 5% significance level was applied using JMP statistical software (version

12.1.0, SAS Institute Inc., Cary, NC, USA) for the evaluation of the effects of two parameters, *i.e.* the sample dilution and the method of mass discrimination correction, on the delta value. The outcome showed that both factors have a statistically significant effect on the response investigated. Moreover, an interaction between the two factors was also revealed by two-way ANOVA, meaning that the outcome of the methods for mass discrimination correction will be significantly different depending on the dilution of the sample. The reference values (*i.e.* after sample digestion and chromatographic Fe isolation) obtained using the two different approaches of mass discrimination correction were not found to be significantly different from each other. Only the results for a concentration range between 0.75 and 1.5 mg L^{-1} Fe and corrected using the combined correction approach were not significantly different from the reference values obtained.

For higher dilution, the results deviated by about -0.35 ‰ and -0.14 ‰ from the reference values when using SSB alone and the combined correction approach, respectively. This deviation can be tentatively explained by vaporization fractionation and analyte losses from the zone of efficient ion sampling from the ICP by diffusion.[16] Thus, 1 mg L^{-1} of Fe was selected as the optimum concentration for isotopic analysis in acid-digested whole blood. As the concentration of the internal standard Ni used for the mass discrimination correction is also of importance, especially when matrix components are present, the effect of the Fe/Ni ratio was evaluated. A 1:1 ratio provided the most precise results and thus, 1 mg L^{-1} of Ni was further used for the mass discrimination correction.

Table 3-2. Isotopic analysis of Fe in whole blood without Fe isolation at different dilution factors.

[Fe], mg L^{-1}	**SSB**		**SSB and exponential law**	
	$\delta^{56}Fe$	**$\delta^{57}Fe$**	**$\delta^{56}Fe$**	**$\delta^{57}Fe$**
0.30	-2.83 ± 0.08	-4.12 ± 0.11	-2.62 ± 0.06	-3.78 ± 0.10
0.50	-2.85 ± 0.04	-4.17 ± 0.07	-2.64 ± 0.04	-3.87 ± 0.07
0.75	-2.96 ± 0.14	-4.29 ± 0.18	-2.47 ± 0.03	-3.57 ± 0.06
1.00	-3.28 ± 0.06	-4.86 ± 0.21	-2.45 ± 0.03	-3.59 ± 0.05
1.50	-3.35 ± 0.27	-4.93 ± 0.39	-2.44 ± 0.02	-3.58 ± 0.04
Reference value	*-2.50 ± 0.05*	*-3.71 ± 0.09*	*-2.49 ± 0.05*	*-3.72 ± 0.11*

The organic matter present in the measurement solutions, as estimated using the UV absorption at 254 nm, was a factor of 30 higher in the digested sample than in the chromatographically purified iron fractions. After SSB correction, the delta values deviated from the 'true' value, but correction with the combined approach provides accurate results up to a level of 1% of organic C.

Solutions of isotopic reference material IRMM-014, used as external standard (external correction for mass discrimination) and as wash solution used in-between two measurements were also matrix-matched *via* addition of matrix elements (simulated blood concentrations) to minimize changes in the ICP conditions. Every sample was measured 10 times. Although a slight improvement was obtained using matrix-matched IRMM-014 when relying on SSB correction only, the results still deviated from the reference value by about 0.5‰. However, with the combined mass discrimination correction, accurate and precise results were obtained using either matrix-matched or non-matrix-matched IRMM-014 standard. For reasons of simplicity, the non-matrix-matched IRMM-014 standard was used in all further work for SSB correction.

3.4.3 Application to human blood samples

To prove the concept of the study, 10 samples of human whole blood were analyzed with and without Fe analyte isolation. The δ^{56}Fe values obtained for the digested samples and for the purified iron fractions are illustrated in Fig. 3-3. The samples were measured in duplicate. All sample results fall on the normal mass-dependent fractionation line, *i.e.* $\delta^{57}\text{Fe} = 1.47\ \delta^{56}\text{Fe}$. No significant differences at a 95% confidence level were observed between the results obtained using both methods. In all cases, the experimental $|t|$ values were < the critical value.

The precision was evaluated as repeatability (internal and external precision) and reproducibility. The internal precision, expressed as the standard deviation within one measurement (45 subsequent cycles), was 0.04 ‰ for δ^{56}Fe and 0.07 ‰ for δ^{57}Fe. The external precision, expressed as standard deviation for 10 measurements of the whole blood sample measured in one measurement session (one day), was 0.02 ‰ for δ^{56}Fe and 0.03 ‰

for δ^{57}Fe. This is similar to the external precision obtained for the samples after Fe isolation (0.02 ‰ for δ^{56}Fe and 0.04 ‰ for δ^{57}Fe).

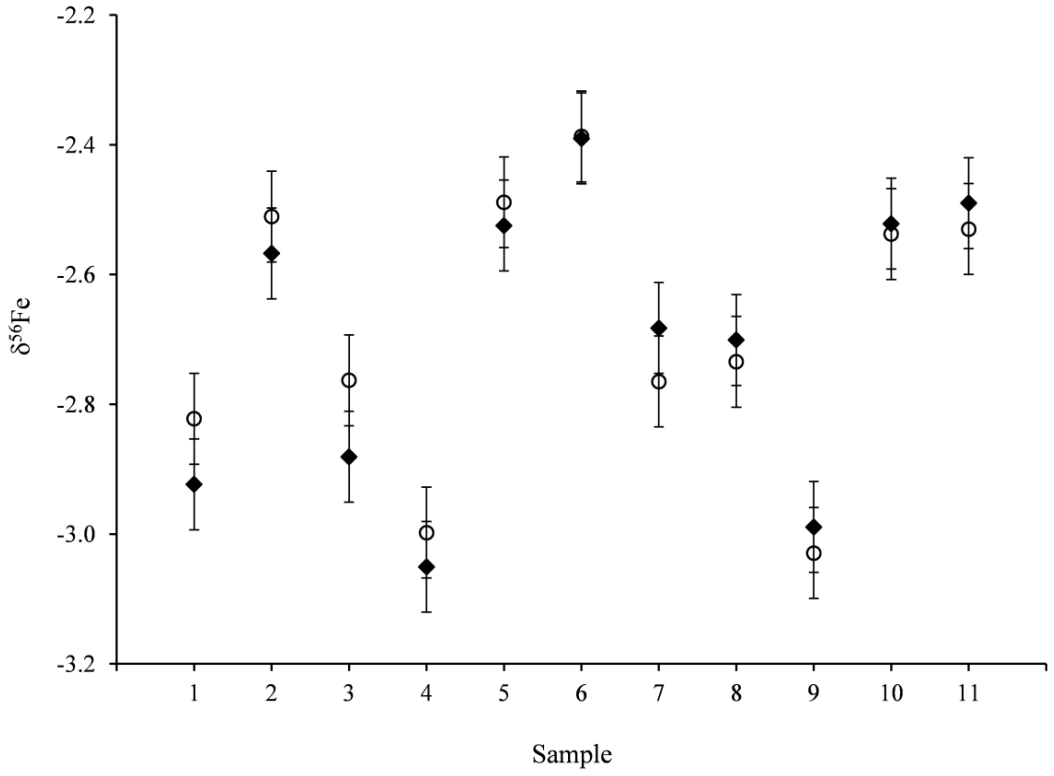

Fig. 3-3 Delta Fe results for actual whole blood samples with and without Fe isolation. Open circles indicate the results obtained after Fe isolation and filled diamonds those without Fe isolation. Error bars represent the external precision as 2 times the standard deviation (0.07‰ for δ^{56}Fe).

The reproducibility obtained, as standard deviation of the sample measured 8 times on different days within 4 months, was 0.03 ‰ for δ^{56}Fe and 0.06 ‰ for δ^{57}Fe. In addition, no decrease in the sensitivity was observed after 3 measurement sessions (measurement days) in a row and the condition of the cones was still adequate. Thus, accurate and precise results were obtained for the Fe isotopic composition in whole blood after acid digestion followed by the adequate dilution of the sample under the conditions described and provided that instrumental mass discrimination was corrected for using a combination of internal correction *via* the revised Russell's law and SSB.

3.5 CONCLUSIONS

It was shown that direct isotopic analysis of whole blood Fe is possible after acid digestion and adequate dilution (0.75-1.5 mg L^{-1} of Fe) provided that instrumental mass discrimination is corrected for using a combination of internal correction using $^{62}Ni/^{60}Ni$ and external correction *versus* IRMM-Fe isotopic reference material in a standard-sample bracketing approach. As a result, chromatographic Fe isolation preceding the MC-ICP-MS Fe isotope ratio measurement can be avoided. Similar results were obtained following this approach and following the reference procedure (including chromatographic Fe isolation) for actual whole blood samples. This simple methodology allows to increase the sample throughput and reduce the amount of acids, cost and time required. Further routine use of the method without Fe isolation will have to reveal long-term robustness and the burden on the instrument. At least, the suggested approach can be relevant for specific clinical applications that require a prompt response.

3.6 ACKNOWLEDGEMENTS

The Special Research Fund of UGent (BOF-UGent) is acknowledged for financial support through research project B/13458/01. The Flemish Research Foundation FWO-Vlaanderen is acknowledged for financial support through research project "G023014N". Marta Costas-Rodríguez thanks FWO-Vlaanderen for her postdoctoral grant.

3.7 REFERENCES

1. Van Heghe, L., Delanghe, J., Van Vlierberghe, H. & Vanhaecke, F. The relationship between the iron isotopic composition of human whole blood and iron status parameters. *Metallomics* **5,** 1503–1509 (2013).
2. Hotz, K., Augsburger, H. & Walczyk, T. Isotopic signatures of iron in body tissues as a potential biomarker for iron metabolism. *J. Anal. At. Spectrom.* **26,** 1347–1353 (2011).
3. Hotz, K. & Walczyk, T. Natural iron isotopic composition of blood is an indicator of dietary iron absorption efficiency in humans. *J. Biol. Inorg. Chem.* **18,** 1–7 (2013).
4. Krayenbuehl, P.-A., Walczyk, T., Schoenberg, R., von Blanckenburg, F. & Schulthess, G. Hereditary hemochromatosis is reflected in the iron isotope composition of blood. *Blood* **105,** 3812–3816 (2005).

5. Van Heghe, L., Deltombe, O., Delanghe, J., Depypere, H. & Vanhaecke, F. The influence of menstrual blood loss and age on the isotopic composition of Cu, Fe and Zn in human whole blood. *J. Anal. At. Spectrom.* **29,** 478–482 (2014).

6. Costas-Rodríguez, M., Van Heghe, L. & Vanhaecke, F. Evidence for a possible dietary effect on the isotopic composition of Zn in blood via isotopic analysis of food products by multi-collector ICP-mass spectrometry. *Metallomics* **6,** 139–146 (2014).

7. Van Heghe, L., Engström, E., Rodushkin, I., Cloquet, C. & Vanhaecke, F. Isotopic analysis of the metabolically relevant transition metals Cu, Fe and Zn in human blood from vegetarians and omnivores using multi-collector ICP-mass spectrometry. *J. Anal. At. Spectrom.* **27,** 1327–1334 (2012).

8. Vanhaecke, F. & Degryse, P. *Isotopic Analysis: Fundamentals and Applications Using ICP-MS*. (Wiley-VCH Verlag GmbH & Co. KGaA, 2012).

9. Agatemor, C. & Beauchemin, D. Matrix effects in inductively coupled plasma mass spectrometry: A review. *Anal. Chim. Acta* **706,** 66–83 (2011).

10. Schoenberg, R. & von Blanckenburg, F. An assessment of the accuracy of stable Fe isotope ratio measurements on samples with organic and inorganic matrices by high-resolution multicollector ICP-MS. *Int. J. Mass Spectrom.* **242,** 257–272 (2005).

11. Arnold, G. L., Weyer, S. & Anbar, A. D. Fe Isotope Variations in Natural Materials Measured Using High Mass Resolution Multiple Collector ICPMS. *Anal. Chem.* **76,** 322–327 (2004).

12. Benkhedda, K., Chen, H., Dabeka, R. & Cockell, K. Isotope ratio measurements of iron in blood samples by multi-collector ICP-MS to support nutritional investigations in humans. *Biol. Trace Elem. Res.* **122,** 179–192 (2008).

13. Ohno, T., Shinohara, A., Kohge, I., Chiba, M. & Hirata, T. Isotopic analysis of Fe in human red blood cells by multiple collector-ICP-mass spectrometry. *Anal. Sci.* **20,** 617–621 (2004).

14. Stenberg, A. *et al.* Measurement of iron and zinc isotopes in human whole blood: preliminary application to the study of HFE genotypes. *J. Trace Elem. Med. Biol.* **19,** 55–60 (2005).

15. Vanhaecke, F. & Moens, L. Overcoming spectral overlap in isotopic analysis via single- and multi-collector ICP-mass spectrometry. *Anal. Bioanal. Chem.* **378,** 232–240 (2004).

16. Malinovsky, D. *et al.* Performance of high resolution MC-ICP-MS for Fe isotope ratio measurements in sedimentary geological materials. *J. Anal. At. Spectrom.* **18,** 687–695 (2003).

17. Weyer, S. & Schwieters, J. B. High precision Fe isotope measurements with high mass resolution MC-ICPMS. *Int. J. Mass Spectrom.* **226,** 355–368 (2003).

18. Pietruszka, A. J. & Reznik, A. D. Identification of a matrix effect in the MC-ICP-MS due to sample purification using ion exchange resin: An isotopic case study of molybdenum. *Int. J. Mass Spectrom.* **270,** 23–30 (2008).

19. Millet, M.-A., Baker, J. A. & Payne, C. E. Ultra-precise stable Fe isotope measurements by high resolution multiple-collector inductively coupled plasma mass spectrometry with a 57Fe–58Fe double spike. *Chem. Geol.* **304–305,** 18–25 (2012).

20. Konter, J. G., Pietruszka, A. J. & Hanan, B. B. Evaluation of double and triple spike Fe isotope measurements and results for basaltic lavas. *Am. Geophys. Union* A2102 (2008).

21. Barling, J. & Weis, D. Influence of non-spectral matrix effects on the accuracy of Pb isotope ratio measurement by MC-ICP-MS: implications for the external normalization method of instrumental mass bias correction. *J. Anal. At. Spectrom.* **23,** 1017–1025 (2008).

22. Heumann, K. G., Gallus, S. M., Rädlinger, G. & Vogl, J. Precision and accuracy in isotope ratio measurements by plasma source mass spectrometry. *J. Anal. At. Spectrom.* **13,** 1001–1008 (1998).

23. Tanner, S. D. Space charge in ICP-MS: calculation and implications. *Spectrochim. Acta Part B At. Spectrosc.* **47,** 809–823 (1992).

24. Kivel, N., Günther-Leopold, I., Vanhaecke, F. & Günther, D. Isotope fractionation during ion beam formation in multi-collector inductively coupled plasma mass spectrometry. *Spectrochim. Acta Part B At. Spectrosc.* **76,** 126–132 (2012).

25. Gregoire, D. C. The effect of easily ionizable concomitant elements on non-spectroscopic interferences in inductively coupled plasma-mass spectrometry. *Spectrochim. Acta Part B At. Spectrosc.* **42,** 895–907 (1987).

26. Kivel, N., Potthast, H.-D., Günther-Leopold, I., Vanhaecke, F. & Günther, D. Variable aperture extraction lens for ion beam investigation in inductively coupled plasma-mass spectrometry. *J. Anal. At. Spectrom.* **30,** 1329–1335 (2015).

27. Chan, C. M. & Hieftje, G. M. Investigation of plasma-related matrix effects in inductively coupled plasma-atomic emission spectrometry caused by matrices with low second ionization potentials—identification of the secondary factor. *J. Int. Bus. Stud.* **37,** 642–665 (2006).

28. Maréchal, C. N., Télouk, P. & Albarède, F. Precise analysis of copper and zinc isotopic compositions by plasma-source mass spectrometry. *Chem. Geol.* **156,** 251–273 (1999).

29. Baxter, D. C., Rodushkin, I., Engström, E. & Malinovsky, D. Revised exponential model for mass bias correction using an internal standard for isotope abundance ratio measurements by multi-collector inductively coupled plasma mass spectrometry. *J. Anal. At. Spectrom.* **21,** 427–430 (2006).

30. Dauphas, N., Pourmand, A. & Teng, F.-Z. Routine isotopic analysis of iron by HR-MC-ICPMS: How precise and how accurate? *Chem. Geol.* **267,** 175–184 (2009).

31. Fontaine, G. H., Hattendorf, B., Bourdon, B. & Günther, D. Effects of operating conditions and matrix on mass bias in MC-ICPMS. *J. Anal. At. Spectrom.* **24,** 637–648 (2009).

32. Andrén, H., Rodushkin, I., Stenberg, A., Malinovsky, D. & Baxter, D. C. Sources of mass bias and isotope ratio variation in multi-collector ICP-MS: optimization of instrumental parameters based on experimental observations. *J. Anal. At. Spectrom.* **19,** 1217–1224 (2004).

33. Vanhaecke, F., Balcaen, L., De Wannemacker, G. & Moens, L. Capabilities of inductively coupled plasma mass spectrometry for the measurement of Fe isotope ratios. *J. Anal. At. Spectrom.* **17,** 933–943 (2002).

CHAPTER 4

IRON ISOTOPIC ANALYSIS OF FINGER-PRICK AND VENOUS BLOOD BY MULTI-COLLECTOR INDUCTIVELY COUPLED PLASMA-MASS SPECTROMETRY AFTER VOLUMETRIC ABSORPTIVE MICROSAMPLING

Based on publication:

Yulia Anoshkina, Marta Costas-Rodríguez and Frank Vanhaecke, Journal of Analytical Atomic Spectrometry, 2017, Vol. 32, Issue 2, P. 314-321

4.1 ABSTRACT

High-precision isotopic analysis of iron (Fe) in blood is currently assessed as a complementary approach to achieve a better understanding of human iron metabolism and for diagnosis of diseases. Volumetric absorptive microsampling (VAMS) is a recently introduced technique that allows the straightforward collection of a well-defined volume of blood by dipping an absorbent polymeric tip into it. In this work, the use of VAMS was evaluated for high-precision isotopic analysis of whole blood iron by multi-collector inductively coupled plasma mass spectrometry (MC-ICP-MS). Iron concentrations in whole blood sampled using VAMS were determined by single-collector sector-field ICP-MS. A variety of solvents were evaluated for extraction of iron from the VAMS-device (Mitra^{TM}). Iron was quantitatively extracted from the absorbent using 1 mL of Milli-Q water. The extracted material was subsequently subjected to acid digestion and to a miniaturized chromatographic procedure for isolation of iron from the blood matrix. The Fe isotopic compositions and concentrations of paired finger-prick and venous blood samples collected at the same time from six individuals were compared. No significant differences were found between the two blood types. The proposed methodology significantly increases the sample throughput and facilitates sample acquisition for Fe isotopic analysis in clinical applications.

4.2 INTRODUCTION

High-precision iron (Fe) isotopic analysis of biological fluids *via* multi-collector ICP-mass spectrometry (MC-ICP-MS) is nowadays assessed as a potential tool to achieve a better understanding of human iron metabolism and for the diagnosis of disorders.[1] The Fe isotopic composition of serum and whole blood reflects an individual´s iron status.[2–4] Patients suffering from hereditary hemochromatosis (HH) and anemia of chronic disease (ACD) show opposite alterations in their whole blood Fe isotopic composition.[3,5] Walczyk and von Blanckenburg showed that blood and muscle tissue have a similar Fe isotopic composition, while that of liver iron is heavier.[6,7] Hotz *et al.* identified the preferential uptake of light iron isotopes in the intestine and the fact that the extent of this fractionation depends on the dietary iron absorption efficiency as key factors governing the whole blood Fe isotopic composition.[2,8] Chronic kidney disease (CKD) also affects the serum Fe isotopic composition.[4] In patients with renal insufficiency, serum Fe isotopic analysis allows iron deficiency anemia (IDA) and erythropoietin-related (EPO-related) anemia to be distinguished from one another.[4]

As the potential of exploiting natural Fe isotope ratio variations in whole blood / serum iron for clinical purposes has been evidenced, developing simple and reliable analytical methods, providing higher sample throughput and thus lower cost, are needed. Both sample acquisition and sample preparation preceding high-precision isotope ratio measurements by MC-ICP-MS take considerable time, especially the chromatographic isolation of the target analyte from the sample matrix that is typically required to ensure accurate correction for instrumental mass discrimination. In a previous work, it has been demonstrated that direct Fe isotopic analysis of acid-digested whole blood, *i.e.* without isolation of the target analyte, can be performed followed by an adequate dilution and correction for instrumental mass discrimination. This approach is very straightforward, but its routine use over longer periods of time might overburden the instrument.[9]

Also blood collection and storage are critical issues for both elemental determination and isotopic analysis. Although in current clinical practice, whole blood sampling is typically carried out by venipuncture, ‘dry microsampling’ techniques, such as the collection of dried blood spots (DBS) on different support types (*e.g.*, filter paper spotting cards or hydrophilic membranes), have become popular for regular clinical examination and in the context of other bioanalytical applications, *e.g.*, neonatal screening,[10] toxicokinetics,[11] drug monitoring[12] or

viral disease management.[13] Dry microsampling facilitates sample acquisition, transport and bioanalysis on a large scale.[14] It is inexpensive, minimally invasive and requires microliters of sample only, mostly finger- or heel-prick blood. DBS has been used for measurements of the ferritin and soluble transferrin receptor contents in blood plasma and blood serum with the aim of iron status assessment[15,16] and for identifying IDA.[17] However, the methods described require a multi-step sample preparation. Several papers report on the combination of DBS whole blood sample collection and ICP-MS for multi-element determination,[18,19] although to the best of our knowledge, iron was not included in the list of elements studied, probably because in whole blood it is not a meaningful clinical parameter. Aramendía *et al.* developed a method for the simultaneous determination of trace element (Cd, Co, Cu and Pb) concentrations and Cu isotope ratios using DBS and split-flow laser ablation single-collector ICP-MS / multi-collector ICP-MS, but the precision attainable with this approach is not sufficient for clinical applications.[20]

Successful analysis after dry microsampling *via* DBS is jeopardized by varying hematocrit levels (HCT %, volume fraction of red blood cells in blood), an inhomogeneous distribution of the sample material on the support and the risk of contamination.[21–23] Blood with a low HCT level has a lower viscosity, thus giving rise to a larger spot size for a given volume of blood.[21] Also between certified reference materials and real samples, different dispersion properties were observed.[20]

An alternative technique for dry microsampling, termed volumetric absorptive microsampling (VAMS), has recently been proposed for quantitative bioanalysis.[24–27] It is based on the absorption of liquid sample into a porous polymeric tip. This device, commercially available under the brand name Mitra™ from Phenomenex (CA, US), overcomes the issues associated with the HCT level and sample inhomogeneity, while it is equally simple and can be integrated into an automated sample preparation procedure.[24,27,28] VAMS has recently been applied to the accurate determination of (ultra)-trace concentrations of prosthesis-related metals (Al, Ti, V, Cr, Co, Ni, Sr and Zr) in whole blood.[29] Moreover, the VAMS hydrophilic polymer with absorbed blood microsamples showed good stability at different storage times and temperature variations for caffeine and paraxanthine determinations,[28] although the maximum storage time for an antibiotic was limited to 10 days.[26] Verougstraete *et al.* observed a good agreement between the hemoglobin A_{1c} level measured after VAMS and in capillary microsamples, but only when using a wet VAMS tip.[30]

The goal of this study was to investigate the potential of using VAMS for the Fe isotopic analysis by MC-ICP-MS of venous and finger-prick blood for further clinical applications. Prior to the Fe isotope ratio measurements, the Fe concentrations in blood sampled *via* VAMS were determined using single-collector sector-field ICP-MS. Extraction conditions and the stability of the sample-loaded VAMS tip were studied and a miniaturized chromatographic Fe isolation procedure was developed. The proposed methodology was optimized using the Seronorm™ Trace Elements Whole Blood L-1 reference material and real venous blood samples. The Fe isotopic compositions of finger-prick and venous blood collected at the same time from 6 donors were compared.

4.3 EXPERIMENTAL

4.3.1 Materials and reagents

Ultrapure water (resistivity ≥18.2 MΩ cm) was obtained from a Milli-Q Element water purification system (Millipore, France). *Pro analysis* grade 14 M nitric acid (Pro-Labo, Belgium) was further purified by sub-boiling distillation in PFA equipment (PicoTrace, Germany). *Optima* grade 12 M hydrochloric acid used in the chromatographic separation was obtained from Fisher Chemicals (UK). Ultrapure 9.8 M hydrogen peroxide used for sample preparation was acquired from Sigma-Aldrich (Belgium). Purissima grade acetone (≥ 99.5%) and trace select grade methanol (≥ 99.9%) were purchased from Sigma Aldrich.

The Fe isotopic reference material IRMM-014 (Institute for Reference Materials and Measurements, IRMM, Belgium) was used for external correction in a standard-sample bracketing approach. The elemental Fe standard solution (Inorganic Ventures, The Netherlands; lot D2-FE03110), previously characterized isotopically[3], was used as an in-house reference to monitor the quality of the isotope ratio measurements. Single-element standard stock solutions (Inorganic Ventures) used for quantification purposes and Ni single-element standard solution (Inorganic Ventures, lot G2-Nl02086), used as an internal standard for correction of instrumental mass discrimination, were prepared from commercially available 1 g L^{-1} stock solutions. Seronorm™ Trace Elements Whole Blood L-1 (SERO AS, Norway, lot 1406263) was used for method optimization and validation.

The VAMS Mitra™ (lot 41106A) devices used for blood microsampling were obtained from Phenomenex (CA, US). The VAMS device consists of a hydrophilic porous material fitted to a plastic holder. This material absorbs a fixed volume of blood when exposed to a liquid blood sample. The absorption volume (~ 10.6 μL) into the hydrophilic polymer tip and the corresponding reproducibility have been experimentally validated by Denniff *et al.*[24] and Spooner *et al.*[27]

AG MP-1 strong anion exchange resin (100-200 mesh) purchased from Bio-Rad (CA, USA) was used for Fe chromatographic isolation.

4.3.2 Samples and sample preparation

Whole blood samples of supposedly healthy individuals (2 females and 9 males, 23-35 years) were obtained from the Ghent University Hospital (Belgium). Ethical approval was obtained for this research from an independent commission connected to the Ghent University hospital and an informed consent was signed by the blood donors. Venous blood samples and the Seronorm reference material were used for method optimization and validation. For 6 individuals, the venous and finger-prick blood samples were collected simultaneously in order to evaluate the possibility of relying on the finger-prick (capillary) blood Fe isotopic composition in the context of biomedical applications.

Venous blood was sampled by venipuncture in EDTA vacutainer tubes suitable for trace element analysis and stored at -20 ºC until sample preparation. Finger-prick blood and also venous microsamples were collected *via* VAMS following the manufacturer's instructions. The venous microsamples were obtained by immersing the VAMS tip into the blood collected in the vacutainer tube. For the finger-prick blood, the first and second blood droplets after the finger-prick were discarded to avoid contamination from sloughing skin, and the third and fourth droplets were separately loaded onto VAMS tips for further analysis.[31] The hydrophilic polymer VAMS tip was dipped into the blood sample until it was fully colored (approximately 6 s). The VAMS device containing the blood microsample was subsequently dried under ambient conditions for about 2 hours and then stored as such for further analysis.

Thereafter, two procedures were applied. First, the VAMS tip was placed in a Savillex® PFA beaker and 1 mL of Milli-Q water was added. After vortexing during 5 min, the tip was

removed and the mixture was acid digested at 110 ºC overnight (~16 h) using 2 mL of 14 M HNO_3 and 500 µL of 9.8 M H_2O_2. As a reference procedure, 10.6 µL of the corresponding venous blood samples were directly pipetted in a Savillex® PFA beaker and subsequently acid digested. The digests obtained after the two procedures were evaporated to dryness and then re-dissolved in 500 µL of 6 M HCl + 0.001% H_2O_2 for chromatographic isolation of Fe.

The chromatographic separation was performed using 1 mL pipette tips filled with 0.5 mL of AG MP-1 (100-200 mesh) strong anion exchange resin. A piece of cotton was placed as bed support and as stopper. The resin was pre-cleaned with 500 µL of 7 M HNO_3, 2 mL of Milli-Q water, 2 mL of 0.7 M HNO_3 and 2 mL of Milli-Q water and conditioned with 4 mL of 6 M HCl + 0.001% H_2O_2. After sample loading, the matrix components were eluted from the column in 2 two steps, firstly with 2 mL of 9 M HCl and secondly with 5 mL of 6 M HCl + 0.001% H_2O_2. The Fe fraction was then eluted with 6 mL of 1 M HCl and collected in a 15 mL Teflon Savillex® beaker. The purified Fe fraction was evaporated to dryness at 90 ºC to remove residual chlorides and re-dissolved in concentrated HNO_3. This procedure was repeated twice. The final residue was re-dissolved in 500 µL of 0.42 M HNO_3. A procedural blank, treated in the same way as the samples, was included in each batch of samples. All sample manipulations were carried out in a class-10 clean room. The Teflon Savillex® beakers were pre-cleaned in sequential steps with 7 M HNO_3 and with 6 M HCl.

4.3.3 Instrumentation and measurements

A Thermo Scientific Neptune MC-ICP-MS instrument (Bremen, Germany) equipped with a large dry interface pump (130 $m^3\ h^{-1}$ pumping speed) and high-transmission 'jet' Ni interface cones ('jet' sampling cone and X-type skimmer) was used for Fe isotope ratio measurements. A PFA concentric nebulizer (100 µL min^{-1}) mounted onto a double spray chamber with cyclonic and Scott-type sub-units was used for sample introduction into the plasma. Measurements were performed at medium mass resolution (pseudo mass resolution[32]), in static collection mode, using six Faraday collectors connected to 10^{11} Ω amplifiers. Instrument settings and data acquisition parameters are shown in Table 4-1 (A). Ni was used as an internal standard at the same concentration level as the target element (300 µg L^{-1}). The in-house isotopic standard solution was included in the sequence after each 5 samples to

check quality of the isotope ratio measurements. All solutions (in-house standards and samples) were measured in duplicate.

Table 4-1. Instrument settings and acquisition parameters for (A) the Neptune MC-ICP-MS instrument and (B) the Element XR SF-ICP-MS instrument

A. MC-ICP-MS Neptune	
RF power (W)	1275
Guard electrode	Connected
Sample and skimmer cones	Jet sampler and X-type skimmer, Ni, 1.1 and 0.8 mm orifice diameter, respectively
Lens settings	Optimized for maximum Fe^+ signal intensity
Ar flow rates (L min^{-1}): plasma gas	15
auxiliary gas	0.75
nebulizer gas	0.9-1.0
Sample uptake rate (μL min^{-1})	100
Resolution mode	Medium (pseudo)
Acquisition mode	Static; multi-collection
Number of blocks	9
Number of cycles	5
Integration time (s)	4.194
Cup configuration	L4: ^{54}Fe; L2: ^{56}Fe; L1: ^{57}Fe; C: ^{58}(Fe + Ni); H1: ^{60}Ni; H3: ^{62}Ni
B. SF-ICP-MS Element XR	
RF power (W)	1250
Guard electrode	Connected
Sample and skimmer cones	Ni, 1.1 mm and 0.8 mm orifice diameter
Lens settings	Optimized for maximum signal intensity
Ar flow rates (L min^{-1}):	
plasma gas	15
auxiliary gas	0.8-0.9
nebulizer gas	1.0-1.1
Sample uptake rate (μL min^{-1})	200
Resolution mode	Low, medium, high
Acquisition mode	E-scan
Dwell time per point (ms)	10
Point per peak	20
Number of runs	5
Number of passes	5

The isotopic composition of the samples is expressed in delta notation (δ^{56}Fe and δ^{57}Fe, ‰) relative to the reference material IRMM-014 and calculated as follows (eqn. 4-1), where *x* is 56 or 57:

$$\delta^{x}Fe_{sample} = \left(\frac{{}^{x}Fe/{}^{54}Fe_{sample}}{{}^{x}Fe/{}^{54}Fe_{IRMM-014}} - 1 \right) \quad (4\text{-}1)$$

Mass bias correction was performed through the combination of internal correction with admixed Ni relying on the revised Russell's law (using a regression line to establish the correlation between the correction factors for Fe and Ni) and external correction in a sample-standard bracketing approach (SSB).[33] 2s-rejection of outliers was applied for the measured isotope ratios.

A Thermo Scientific (Bremen, Germany) Element XR single-collector sector-field ICP-MS instrument was used for determination of element concentrations. For the introduction of sample into the plasma, a 200 μL min^{-1} quartz concentric nebulizer mounted onto a cyclonic spray chamber was used. The instrument settings and data acquisition parameters used are summarized in Table 4-1 (B). External calibration was performed and Ga was used as an internal standard to correct for matrix effects and instrument instability.

4.4 RESULTS AND DISCUSSION

4.4.1 Iron determination

The use of VAMS was first evaluated for the quantitative determination of Fe using the Seronorm reference material and real venous whole blood. A variety of solutions, such as Milli-Q water, 0.7 M HNO_3, 5% acetone, 5% methanol, and hot 7 M HNO_3 (v/v) were tested as extraction solutions. Fig. 4-1 shows the VAMS tips after extraction using different extraction solutions. First, Fe was determined in the supernatant obtained after extraction of the blood microsample from the VAMS tip and centrifugation. As can be seen in Fig. 4-1 (a), quantitative recoveries of Fe were only obtained using hot 7 M HNO_3. These recoveries were 99 with 1% of absolute deviation between the two replicates for the reference material and 94 with 4% of absolute deviation between the two replicates for real blood, both relative to the

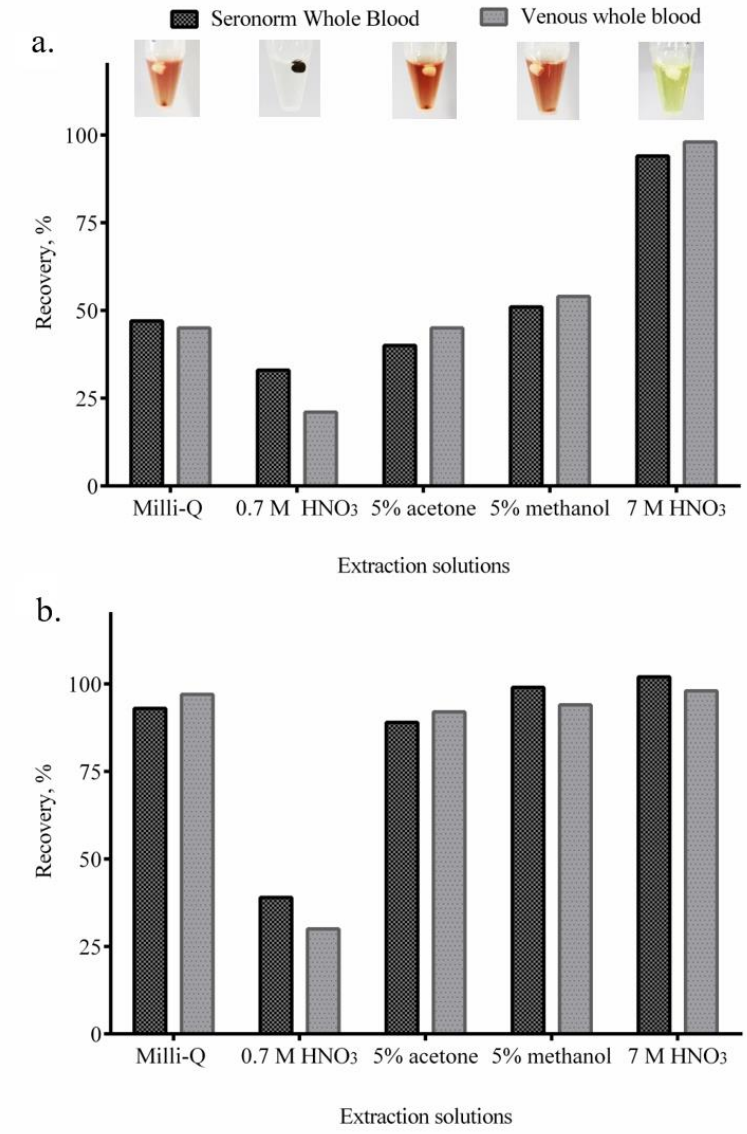

Fig. 4-1 Recoveries for Fe obtained after VAMS tip extraction (a) in the resulting supernatant and (b) after digestion of the extracted mixture for Seronorm whole blood L-1 reference material and a real whole blood sample. Recoveries are expressed as the average of 2 measurement replicates. The absolute deviation between the two values was ≤ 10%.

reference value (*i.e.* the result obtained using the reference procedure). The poor Fe recoveries obtained using the other extraction solutions tested can be related to precipitation of proteins and/or inadequate extraction conditions (Fig. 4-1 a). To evaluate this, the resulting mixture extracted from the VAMS tip was further digested. The results for the Seronorm reference material and for the real blood sample obtained after acid digestion of the extracted mixture from VAMS are shown in Fig. 4-1 (b). As can be seen, the recoveries obtained with Milli-Q water, 5% acetone, 5% methanol and 7 M HNO_3 (hot) were all quantitative. However, a *ca.* two-fold longer extraction time was required for the real blood sample (5 min) compared to

the reference material (2 min) to reach similar recoveries from the VAMS tip for both matrixes. The different extraction efficiencies obtained for the reference material and the real blood are probably related to the viscosity of the sample. This dissimilarity has already been previously observed in the context of extraction of blood from a VAMS tip[28] and also in the case of DBS sample collection on filter paper.[20]

Based on the results obtained, the extraction of sample material from the VAMS tip containing the dry blood sample was accomplished with 1 mL of Milli-Q water and 5 min of agitation. The extract was subsequently subjected to acid digestion. This approach enables accurate determination of Fe in microsamples of blood using SF-ICP-MS and can therefore be applied in future routine applications. The efficiency and corresponding reproducibility of extraction of Fe from VAMS tips was 98 ± 5 % standard deviation (n = 4).

The procedural blank of Fe was 0.5 µg L^{-1} using Milli-Q water, but was increased after acid digestion to 15 µg L^{-1}; this value is still negligible compared to the Fe concentration in a whole blood sample (~ 350 mg L^{-1} in venous blood) and is thus acceptable for further high-precision isotopic analysis.

4.4.2 Iron isotopic analysis

Isolation procedure

It is well known that the presence of matrix components in the sample solution can cause spectral interference and affect the extent of instrumental mass discrimination in MC-ICP-MS and therefore, the target analyte is traditionally chromatographically isolated to guarantee accurate and precise results.[34] This procedure is labour-intensive and time-consuming, thus reducing sample throughput. In order to perform the Fe isotopic analysis of blood microsamples using VAMS, a miniaturized chromatographic isolation approach, using a small amount of anion exchange resin AG-MP1 (0.5 mL), was developed. For studying the chromatographic separation in detail, the analyte element and concomitant matrix elements were determined using SF-ICP-MS in separately collected 1 mL eluent fractions. The elution profile of the target element and concomitant elements is presented in Fig. 4-2 for the Seronorm reference material. As can be seen, the matrix elements were successfully removed,

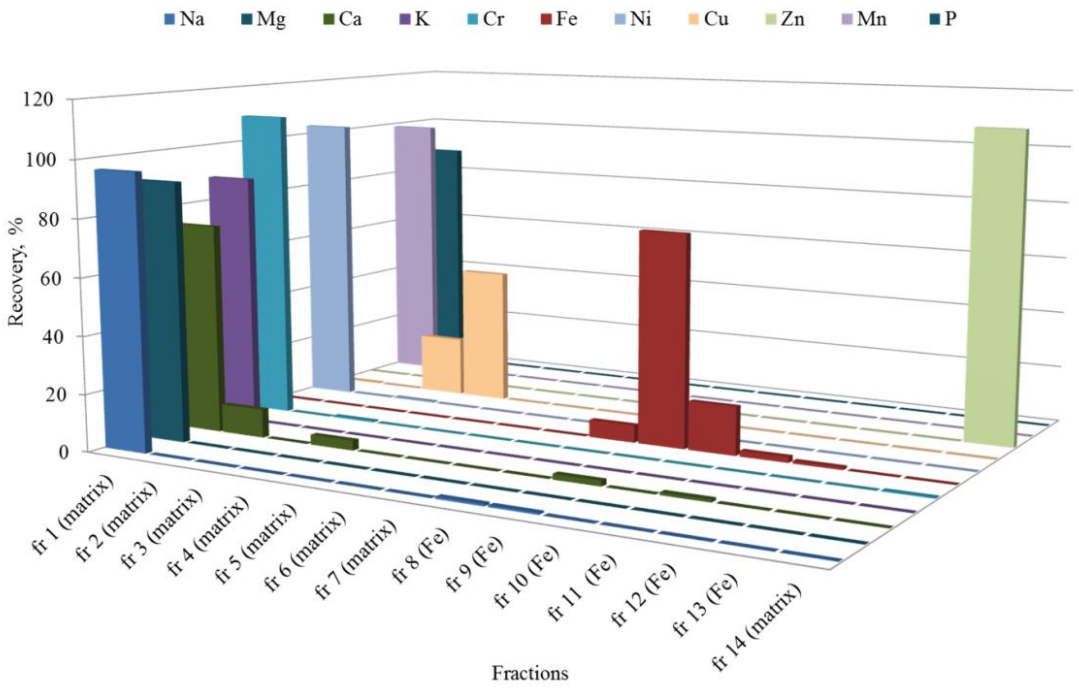

Fig. 4-2 Elution profile for Seronorm Trace Elements Whole Blood L-1 reference material. For fractions (frs) 1-2 (matrix) 1 mL of 9 M HCl and for frs 3-7 (matrix) 1 mL of 6 M HCl + 0.001% H_2O_2 were used for matrix elution; for frs 8-13 (Fe) 1 mL of 1 M HCl is used for elution; for fr 14 (matrix) 5 mL of 0.7 M HNO_3 is used to clean the resin for further use.

while recoveries of Fe were quantitative (101 ± 8%, n = 48 over a period of one year). The average concentration of Fe after the isolation procedure was 349 ± 10 mg L^{-1} (n = 4), which is in excellent agreement with the certified value of 349 ± 7 mg L^{-1} (t-test, $t_{exp} < t_{crit}$, $\rho < 0.05$). For one batch of samples (~ 20 columns), Fe isolation is accomplished in 2 hours compared to 9 hours for the standard procedure for whole blood matrixes,[35] which reduces the total sample preparation time. Moreover, the use of the miniaturized chromatographic isolation approach results in a significant reduction in the consumption of the expensive ultrapure acids (a 2.3-fold lower consumption of HNO_3 and a 3.3-fold lower one of HCl).

Iron isotopic analysis after VAMS

The suitability of VAMS for high-precision isotopic analysis of Fe by MC-ICP-MS was evaluated using the Seronorm reference material and real venous whole blood. Incomplete extraction of Fe from a VAMS tip, due to non-optimized extraction conditions, induced isotope fractionation. A shift of -0.56‰ in $\delta^{56}Fe$ was observed when the recovery of Fe was

less than 72%. This significantly lighter isotopic composition can be explained by the slightly faster elution of the lighter of two Fe isotopes.[34,36,37] The Fe isotopic composition of blood microsamples extracted with Milli-Q water from VAMS devices, followed by acid digestion were in good agreement with the reference values obtained on the basis of the standard approach (for an aliquot of blood that was directly digested). The results obtained for 5 venous blood microsamples and for the Seronorm reference material after VAMS and for the corresponding reference samples are plotted in Fig. 4-3. A paired t-test showed that no significant difference could be established between both methodologies at a 95% confidence level ($t_{exp} = 1.659 < t_{crit} = 2.571$). The individual data for Fe concentrations are shown in the Supplementary Information (Table 4-S1). The repeatability for the Fe isotope ratio measurements, expressed as the standard deviation for three sample replicates, was between 0.03 and 0.08‰ in the case of VAMS. The reproducibility, expressed as the standard deviation, was between 0.05‰ and 0.18‰ for $\delta^{56}Fe$ and $\delta^{57}Fe$, respectively (values obtained for 5 independent measurement sessions).

The results for all of the samples fall on the normal mass-dependent fractionation line ($\delta^{57}Fe = 1.47\ \delta^{56}Fe$). The differences between the results with and without blank correction were 0.05 and 0.07‰ for $\delta^{56}Fe$ and $\delta^{57}Fe$, respectively and thus, no blank correction was required.

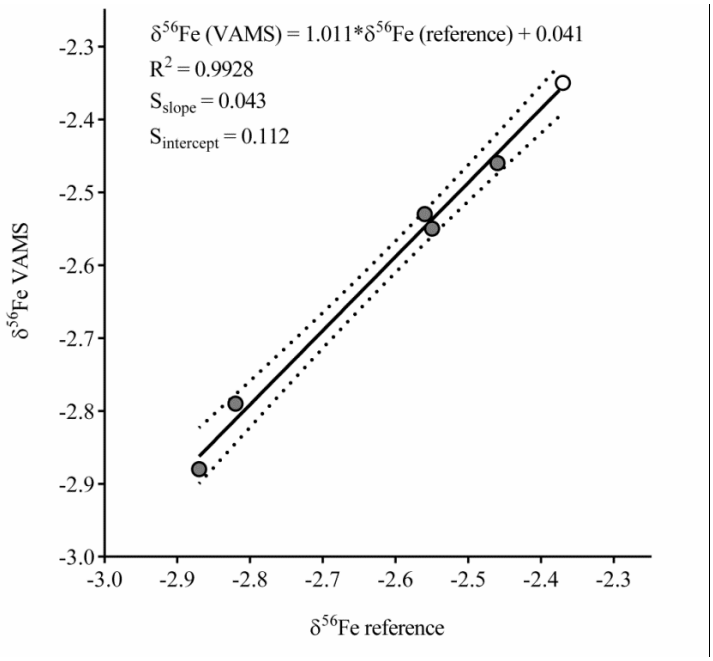

Fig. 4-3 Isotopic composition of 5 venous whole blood samples (filled circles) and Seronorm Whole Blood reference material (open circle) obtained using VAMS and the reference approach. The dashed lines indicate the confidence interval ($\rho < 0.05$).

4.4.3 Stability of blood samples in the VAMS device

The stability of blood samples loaded onto the VAMS device was evaluated according to De Kesel *et al*.[28] For this evaluation, samples were extracted from a VAMS tip after 2 h of drying (considered as the zero time point), after 4 days of storage at 60 °C, 4 °C and -20 °C and after long storage at room temperature (1-4 weeks). This experiment was carried out using one venous whole blood sample, analyzed in triplicate for each time point. The VAMS devices with the dried blood microsamples were placed in closed tips holders, thus avoiding contact between tips and stored as such until analysis. A blank tip was included in each set of samples to evaluate potential contamination originating from the VAMS device. The average Fe concentrations, isotopic compositions and procedural blanks are presented in Table 4-2. No significant differences were observed between the group means at a 5% significance level using one-way ANOVA (JMP statistical software, version 12.1.0, SAS Institute Inc., Cary, NC, USA). Thus, the Fe concentrations and isotopic compositions of dried microsamples were not affected during a period of at least 28 days when the VAMS tips are stored at room temperature. Thus, the VAMS device is suitable for high-precision Fe isotopic analysis and quantitative Fe assay until at least 1 month after sampling. Moreover, the samples were also stable for at least 4 days when they were stored under harsher conditions, such as storage temperatures of 60 °C, 4 °C and -20 °C. These results indicate the potential for long term storage and shipping of VAMS-collected samples under different temperature conditions.

4.4.4 Finger-prick *versus* venous blood

Finger-prick blood is generally considered as capillary blood,[31] although it can actually be a mixture of arterial, venous and capillary blood. In previous works focused on clinical research, the Fe isotopic composition was established for venous whole blood, serum and/or plasma collected by venipuncture and no data are available for capillary blood and/or blood collected using dry microsampling techniques. In neonates, capillary blood shows higher levels of hemoglobin and HCT than venous blood[38] and thus, the Fe isotopic composition could be different between finger-prick and venous blood.[4] The difference in hemoglobin level between capillary and venous blood diminishes in adults.[39–41] Discrepancies between finger-prick DBS and venous blood in adults are reported in the literature, *e.g.*, for HCT, cholesterol and glucose levels,[42] however, the lack of consensus for these differences between

Table 4-2. Fe isotopic compositions and concentrations in blood microsamples extracted from VAMS tips stored under different conditions. Fe concentrations and recoveries are expressed as the average of 3 sample replicates ± SD, %. Delta Fe values are expressed as the average ± SD (n = 3).

	Room temperature (21°C)				**60 °C**	**4 °C**	**-20 °C**
	2h	**7 days**	**14 days**	**28 days**	**4 days**		
[Fe], mg L^{-1}	370 ± 1	340 ± 14	365 ± 27	354 ± 18	358 ± 22	358 ± 15	372 ± 4
[Fe] blank, mg L^{-1}	0.015	0.073	0.079	0.079	0.080	0.178	0.078
Recovery, %	101 ± 1	101 ± 3	102 ± 3	105 ± 7	103 ± 1	92 ± 15	98 ± 3
$\delta^{56}Fe$	-2.35 ± 0.01	-2.34 ± 0.03	-2.39 ± 0.05	-2.42 ± 0.01	-2.36 ± 0.02	-2.40 ± 0.03	-2.40 ± 0.03
$\delta^{57}Fe$	-3.45 ± 0.05	-3.43 ± 0.05	-3.51 ± 0.07	-3.50 ± 0.02	-3.50 ± 0.04	-3.52 ± 0.04	-3.51 ± 0.05

capillary and venous blood could be related with the microsampling technique used and/or the representativeness of the microsample.

To evaluate the suitability of the finger-prick blood Fe isotopic composition for further clinical research (*e.g.*, assessment of an individual's iron status), finger-prick and venous blood samples were collected simultaneously from 6 healthy individuals (1 female and 5 males). The microsampling was performed in duplicate, *i.e.* the third and fourth blood droplet were sampled separately for each individual. Fe concentrations were determined before and after the isolation procedure and matrix elements that can potentially interfere with the determination of Fe isotope ratios, such as Cr, Ca and K, were monitored after the isolation procedure. The contribution of these elements was negligible in all cases. Table 4-3 compiles the Fe recoveries, average concentrations and Fe isotopic composition. No significant differences were established between the finger-prick and venous blood using a paired t-test at a level of confidence of 95% ($t_{exp} = 0.125 < t_{crit} = 2.571$). The use of dried finger-prick blood after VAMS combined with a miniaturized isolation procedure can thus be used for high-precision isotopic analysis of Fe with the final aim of clinical research.

4.5 CONCLUSIONS

Volumetric absorptive microsampling (VAMS) using a commercially available device (Mitra^{TM}) was suitable for high-precision Fe isotopic analysis of whole blood using MC-ICP-MS for clinical applications. Fe was recovered quantitatively after VAMS. Accurate and precise data were obtained using 1 mL of Milli-Q water as extraction solution followed by acid digestion and a miniaturized chromatographic approach for Fe isolation. The Fe isotopic composition and Fe concentrations are not affected during a period of at least 28 days when the VAMS device is stored at room temperature and during a period of at least 4 days when it is stored at 60 °C, 4 °C or -20 °C. By using this methodology, no differences in the Fe isotopic composition or Fe concentration were observed between finger-prick and venous blood. The approach proposed greatly enhances the sample throughput, reduces the amount of reagents required and thus, is beneficial in terms of time and cost. The VAMS-collected finger-prick blood samples were adequate for Fe isotopic analysis and thus, the suitability of this approach for future applications was shown.

Table 4-3. Fe isotopic compositions and concentrations of finger-prick and venous blood from supposedly healthy individuals. Delta Fe values for 2 sample aliquots are shown. The absolute deviation between two value was ≤ 0.09 for δ^{56}Fe and ≤ 0.11 for δ^{57}Fe.

Sample	**Finger-prick blood**					**Venous blood**				
	[Fe], mg L^{-1}	**δ^{56}Fe**		**δ^{57}Fe**		**[Fe], mg L^{-1}**	**δ^{56}Fe**		**δ^{57}Fe**	
f28	370	-2.41	-2.40	-3.49	-3.55	399	-2.35	-2.36	-3.41	-3.48
m27	338	-2.63	-2.63	-3.91	-3.88	381	-2.61	-2.69	-3.82	-3.92
m28	393	-2.97	-3.01	-4.38	-4.45	389	-3.04	-3.04	-4.59	-4.48
m23	416	-2.89	-2.81	-4.28	-4.21	416	-2.91	-2.89	-4.32	-4.28
m26	433	-2.81	-2.72	-4.15	-4.04	423	-2.79	-2.73	-4.11	-4.02
m35	451	-3.08	-3.11	-4.52	-4.58	417	-3.01	-3.04	-4.40	-4.47

4.6 ACKNOWLEDGEMENTS

The Flemish Research Foundation FWO-Vlaanderen is acknowledged for financial support through research project “G023014N”. Marta Costas- Rodríguez thanks FWO-Vlaanderen for her postdoctoral grant.

4.7 REFERENCES

1. Costas-Rodríguez, M., Delanghe, J. & Vanhaecke, F. High-precision isotopic analysis of essential mineral elements in biomedicine: Natural isotope ratio variations as potential diagnostic and/or prognostic markers. *TrAC* **76,** 182–193 (2016).
2. Hotz, K., Augsburger, H. & Walczyk, T. Isotopic signatures of iron in body tissues as a potential biomarker for iron metabolism. *J. Anal. At. Spectrom.* **26,** 1347–1353 (2011).
3. Van Heghe, L., Delanghe, J., Van Vlierberghe, H. & Vanhaecke, F. The relationship between the iron isotopic composition of human whole blood and iron status parameters. *Metallomics* **5,** 1503–1509 (2013).
4. Anoshkina, Y. *et al.* Iron isotopic composition of blood serum in anemia of chronic kidney disease. *Metallomics* **9,** 517–524 (2017).
5. Krayenbuehl, P.-A., Walczyk, T., Schoenberg, R., von Blanckenburg, F. & Schulthess, G. Hereditary hemochromatosis is reflected in the iron isotope composition of blood. *Blood* **105,** 3812–3816 (2005).
6. Walczyk, T. & von Blanckenburg, F. Natural iron isotope variations in human blood. *Science* **295,** 2065–6 (2002).
7. Walczyk, T. & von Blanckenburg, F. Deciphering the iron isotope message of the human body. *Int. J. Mass Spectrom.* **242,** 117–134 (2005).
8. Hotz, K. & Walczyk, T. Natural iron isotopic composition of blood is an indicator of dietary iron absorption efficiency in humans. *J. Biol. Inorg. Chem.* **18,** 1–7 (2013).
9. Anoshkina, Y., Costas-Rodríguez, M. & Vanhaecke, F. High-precision Fe isotopic analysis of whole blood for biomedical purposes without prior isolation of the target element. *J. Anal. At. Spectrom.* **30,** 1816–1821 (2015).
10. Pitt, J. J. Newborn screening. *Clin. Biochem. Rev.* **31,** 57–68 (2010).
11. Stove, C. P., Ingels, A.-S. M. E., De Kesel, P. M. M. & Lambert, W. E. Dried blood spots in toxicology: from the cradle to the grave? *Crit. Rev. Toxicol.* **42,** 230–243 (2012).
12. Edelbroek, P.M., van der Heijden, J. and Stolk, L. . Dried blood spot methods in therapeutic drug monitoring: methods, assays, and pitfalls. *Ther. Drug Monit.* **31,** 327–336. (2009).
13. Smit, P. W. *et al.* Systematic review of the use of dried blood spots for monitoring HIV viral load and for early infant diagnosis. *PLoS One* **9,** e86461 (2014).

14. Demirev, P. A. Dried blood spots: Analysis and applications. *Anal. Chem.* **85,** 779–789 (2013).

15. Flowers, C. H. & Cook, J. D. Dried plasma spot measurements of ferritin and transferrin receptor for assessing iron status. *Clin. Chem.* **45,** 1826–1832 (1999).

16. Ahluwalia, N. *et al.* Ferritin concentrations in dried serum spots prepared by standard compared with simplified approaches: A validation study in Guatemala City. *Am. J. Clin. Nutr.* **81,** 1366–1371 (2005).

17. Cook, J. D., Flowers, C. H. & Skikne, B. S. An assessment of dried blood-spot technology for identifying iron deficiency. *Blood* **92,** 1807–13 (1998).

18. Lehner, A. F. *et al.* Diagnostic analysis of veterinary dried blood spots for toxic heavy metals exposure. *J. Anal. Toxicol.* **37,** 406–422 (2013).

19. Vacchina, V. *et al.* Use of dried blood spots and inductively coupled plasma mass spectrometry for multi-element determination in blood. *J. Trace Elem. Med. Biol.* **28,** 255–259 (2014).

20. Aramendía, M. *et al.* Direct analysis of dried blood spots by femtosecond-laser ablation-inductively coupled plasma-mass spectrometry. Feasibility of split-flow laser ablation for simultaneous trace element and isotopic analysis. *J. Anal. At. Spectrom.* **30,** 296–309 (2015).

21. Denniff, P. & Spooner, N. The effect of hematocrit on assay bias when using DBS samples for the quantitative bioanalysis of drugs. *Bioanalysis* **2,** 1385–1395 (2010).

22. Youhnovski, N., Bergeron, A., Furtado, M. & Garofolo, F. Pre-cut Dried Blood Spot (PCDBS): An alternative to Dried Blood Spot (DBS) technique to overcome hematocrit impact. in *Rapid Commun. Mass Spectrom.* **25,** 2951–2958 (2011).

23. Lenk, G., Hansson, J., Beck, O. & Roxhed, N. The effect of drying on the homogeneity of DBS. *Bioanalysis* **7,** 1977–1985 (2015).

24. Denniff, P. & Spooner, N. Volumetric absorptive microsampling: A dried sample collection technique for quantitative bioanalysis. *Anal. Chem.* **86,** 8489–8495 (2014).

25. Denniff, P., Parry, S., Dopson, W. & Spooner, N. Quantitative bioanalysis of paracetamol in rats using volumetric absorptive microsampling (VAMS). *J. Pharm. Biomed. Anal.* **108,** 61–69 (2015).

26. Parker, S. L., Roberts, J. A., Lipman, J. & Wallis, S. C. Quantitative bioanalytical validation of fosfomycin in human whole blood with volumetric absorptive microsampling. *Bioanalysis* **7,** 2585–2595 (2015).

27. Spooner, N. *et al.* A device for dried blood microsampling in quantitative bioanalysis: overcoming the issues associated with blood hematocrit. *Bioanalysis* **7,** 653–659 (2015).

28. De Kesel, P. M. M., Lambert, W. E. & Stove, C. P. Does volumetric absorptive microsampling eliminate the hematocrit bias for caffeine and paraxanthine in dried blood samples? A comparative study. *Anal. Chim. Acta* **881,** 65–73 (2015).

29. Bolea-Fernandez, E., Phan, K., Balcaen, L., Resano, M. & Vanhaecke, F. Determination of ultra-trace amounts of prosthesis-related metals in whole blood using volumetric absorptive micro-sampling and tandem ICP – mass spectrometry. *Anal. Chim. Acta* **941,** 1–9 (2016).

30. Verougstraete, N. *et al.* Volumetric absorptive microsampling at home as an alternative

tool for the monitoring of HbA1c in diabetes patients. *Clin. Chem. Lab. Med.* DOI: 10.1515/cclm-2016-0411 (2016). doi:10.1515/cclm-2016-0411

31. WHO. *WHO guidelines on drawing blood : best practices in phlebotomy*. *World Health Organization* (World Health Organization, 2010). at <http://www.ncbi.nlm.nih.gov/pubmed/23741774> Last accessed on 25/07/0217.

32. Vanhaecke, F. & Moens, L. Overcoming spectral overlap in isotopic analysis via single- and multi-collector ICP-mass spectrometry. *Anal. Bioanal. Chem.* **378,** 232–240 (2004).

33. Baxter, D. C., Rodushkin, I., Engström, E. & Malinovsky, D. Revised exponential model for mass bias correction using an internal standard for isotope abundance ratio measurements by multi-collector inductively coupled plasma mass spectrometry. *J. Anal. At. Spectrom.* **21,** 427–430 (2006).

34. Vanhaecke, F., Balcaen, L. & Malinovsky, D. Use of single-collector and multi-collector ICP-mass spectrometry for isotopic analysis. *J. Anal. At. Spectrom.* **24,** 863 (2009).

35. Van Heghe, L., Engström, E., Rodushkin, I., Cloquet, C. & Vanhaecke, F. Isotopic analysis of the metabolically relevant transition metals Cu, Fe and Zn in human blood from vegetarians and omnivores using multi-collector ICP-mass spectrometry. *J. Anal. At. Spectrom.* **27,** 1327–1334 (2012).

36. Rodushkin, I., Stenberg, A., Andrén, H., Malinovsky, D. & Baxter, D. C. Isotopic Fractionation during Diffusion of Transition Metal Ions in Solution. *Anal. Chem.* **76,** 2148–2151 (2004).

37. Matthews, A., Emmanuel, S., Levi, L., Gvirtzman, H. & Erel, Y. Kinetic fractionation of Fe isotopes during transport through a porous quartz-sand column. *Geochim. Cosmochim. Acta* **72,** 5908–5919 (2008).

38. Kayiran, S. M., Özbek, N., Turan, M. & Gürakan, B. Significant differences between capillary and venous complete blood counts in the neonatal period. *Clin. Lab. Haematol.* **25,** 9–16 (2003).

39. Rao, L. V., Moiles, D. & Snyder, M. Finger-Stick Complete Blood Counts. *Point Care J. Near-Patient Test. Technol.* **10,** 120–122 (2011).

40. Cable, R. G. *et al.* The difference between fingerstick and venous hemoglobin and hematocrit varies by sex and iron stores. *Transfusion* **52,** 1031–1040 (2012).

41. Patel, A. J., Wesley, R., Leitman, S. F. & Bryant, B. J. Capillary versus venous haemoglobin determination in the assessment of healthy blood donors. *Vox Sang.* **104,** 317–323 (2013).

42. De Kesel, P. M., Sadones, N., Capiau, S., Lambert, W. E. & Stove, C. P. Hemato-critical issues in quantitative analysis of dried blood spots: challenges and solutions. *Bioanalysis* **5,** 2023–2041 (2013).

4.8 SUPPLEMENTARY INFORMATION

Table 4-S1. Iron concentrations of venous whole blood samples after extraction from VAMS tips and using the reference procedure. Data are expressed in mg L^{-1} as average of 2 sample replicates. The absolute deviation between the two values ranged between 7 and 10 mg L^{-1}

	Venous whole blood sample					**Seronorm whole blood L-1**
	1	**2**	**3**	**4**	**5**	**reference material**
Reference procedure	411	370	388	362	387	348
VAMS	427	360	376	361	374	350

CHAPTER 5

NATURAL IRON ISOTOPE FRACTIONATION IN AN INTESTINAL CACO-2 CELL LINE MODEL

Based on publication:

María R. Flórez, Yulia Anoshkina, Marta Costas-Rodríguez, Charlotte Grootaert, Joris Delanghe, John Van Camp and Frank Vanhaecke, Journal of Analytical Atomic Spectrometry, 2017, DOI: 10.1039/C7JA00090A

5.1 ABSTRACT

In this work, Fe isotopic analysis of samples coming from an in vitro intestinal model was performed via multi-collector ICP-mass spectrometry (MC-ICP-MS) to evaluate the isotope fractionation accompanying the iron uptake and transport mechanisms at a cellular level. The Caco-2 cell line has been used, after cell differentiation, as enterocyte model and a bi-cameral experimental setup has been developed and optimized for stimulating intracellular iron fluxes. An Fe : ascorbic acid mixture with a molar ratio of 1:5 was used as a source of non-heme bioavailable iron. Good experimental repeatability and reproducibility were attained with low blank contribution levels, allowing precise and reliable Fe isotope ratio results. Both iron absorption and transport processes were accompanied by Fe isotope fractionation in favor of the lighter isotopes. After 3 hours of exposure, the isotopic composition of the apical solution and the cells did not significantly differ from the original solution added to the cells. After 24 hours of exposure, the trend observed was towards a light Fe isotopic composition in the cells, whereas the apical solutions were enriched in the heavier isotopes. These results were in good agreement with previous *in vivo* and *ex vivo* findings. An overall increase in delta Fe values of the cell layers exposed to iron treatment relative to the corresponding values for the untreated cells also seems to support the assumption of a preferential accumulation of heavy isotopes in enterocyte ferritin. The consistency of the results obtained supports the usefulness of *in vitro* cell culture models as an interesting complementary tool for studying iron metabolic pathways at the intestinal level.

5.2 INTRODUCTION

Iron is an essential micronutrient for almost all living organisms. Particularly, in the human body, iron is involved in oxygen transport and storage, acts as cofactor in some metallo-enzymes, and takes part in many other fundamental processes.[1] However, regulation of the iron metabolism is of capital importance, as iron may exert toxicity when present at high levels and iron deficiency may likewise give rise to metabolic disorders.[2] With a lack of an active iron excretion route, iron homeostasis is mainly maintained through an interplay between iron absorption, recycling and loss (*e.g.*, bleeding). From a mechanistic point of view, iron absorption from the diet takes place at the apical membrane of duodenal enterocytes. Part of this iron is then stored as ferritin (major iron storage protein) within the enterocyte and part is transferred to the basolateral site of the enterocytes through the membrane transporter protein ferroportin. In the blood, transferrin (Tf, a circulating iron transport protein) binds this exported iron and serves as a major vehicle to deliver iron to the periphery. Iron from transferrin is then internalized by cells expressing a transferrin receptor protein.[1,3]

These biochemical mechanisms are accompanied by reduction/oxidation or by bonding reactions. Both may be accompanied by mass-dependent fractionation effects as different isotopes of the same element may engage in these biochemical reactions to a slightly different extent. Light isotopes react more readily owing to a slightly lower activation energy (kinetic effect), while heavier isotopes exhibit a slight preference for strong molecular binding environments (thermodynamic or equilibrium state).[4,5]

It has been established that the Fe isotopic composition of an individual's whole blood/serum provides reliable information on his/her iron status, and therefore, it appears to be a potential marker for diseases related to a dysfunction in the iron regulating axis.[6–11] These impairments in iron regulation have a direct effect on the intestinal iron absorption efficiency and may eventually lead to iron deficiency or iron overload. This was pointed out in an early study by Walczyk and von Blanckenburg,[12] in which they indicated a trend towards a lighter Fe isotopic signature in blood than in Fe-storage organs. This finding was later confirmed by Hotz *et al*. using a pig model.[13] In the latter work, the Fe isotopic composition of the diet and the blood of a pig was compared to that of the intestinal mucosa at different sites. An enrichment in the light Fe isotopes was observed in the main intestinal absorptive points, stressing a preferential uptake of light Fe isotopes in the intestine.

However, the processes occurring at the cellular or molecular level leading to isotope fractionation are still unknown or poorly understood. In this context, *in vitro* studies are valuable for the identification of such biological processes and for studying the incorporation pathways of iron into the cells. Isotope fractionation during the incorporation of metals, such us Cu, Fe and Zn, into bacteria has been evidenced.[14–16] Kappler *et al.*[17] described different extents of Fe isotope fractionation produced by a variety of biological and abiological iron oxidation processes. Recently, Cu and U isotope fractionation has been evidenced in human cell lines, such as the HepG2 (hepatoma-like cells)[18] and SH-SY5Y (neuroblastoma-like cells),[19] respectively. The intracellular Cu was isotopically heavier under hypoxic conditions than under normoxic conditions, in concordance with the ^{65}Cu enrichment found in hepatocellular tumorous tissues compared to the healthy surrounding tissue.[18] The intracellular U in the neuroblastoma cells was enriched in the light ^{235}U isotope relative to the exposure solutions. Different incorporation pathways of U into the cells have been suggested.[19]

In the present work, Fe isotopic analysis of samples obtained from an *in vitro* model of enterocytes was performed *via* multi-collector inductively coupled plasma-mass spectrometry (MC-ICP-MS) to investigate the mechanisms responsible for Fe isotope fractionation at the cellular level of the intestinal enterocytes, as a first metabolic barrier where iron uptake from the intestinal lumen and subsequent incorporation of iron to the peripheral circulation takes place. The Caco-2 cell line is a well-established enterocyte model used for iron absorption studies. Caco-2 cells differentiate spontaneously into bipolar enterocyte-like cells, exhibiting tight intercellular junctions which allow also optimal conditions for transcellular transport studies. This cell line has been extensively used for iron bioavailability tests and manifests a behavior in good agreement with *in vivo* comparative uptake and transport studies.[20–23] An experimental setup was developed to optimize iron fluxes through the epithelial cells and the analytical procedure was evaluated aiming at controlling any source of analytical bias for further investigation of the Fe isotope fractionation through the cells.

5.3 EXPERIMENTAL

5.3.1 Reagents and standards

14 M *pro-analysis* grade HNO_3 (ProLabo, Belgium) was used throughout this work for sample digestion, chromatographic Fe isolation and sample/standard dilution after further purification by sub-boiling distillation in a PFA system. *Optima* grade 12 M HCl used for sample preparation was purchased from Fisher Chemical (UK). Ultrapure water used for all experiments (with a resistivity of 18.2 MΩ·cm at 25°C) was obtained from a Milli-Q Element water purification system (Merck Millipore, USA). *TraceSELECT® Ultra* H_2O_2 9.8 M (Fluka, Sigma-Aldrich, Belgium) was used for sample digestion.

Analytical grade AG® MP-1 strong anion exchange resin (100-200 μm dry mesh size, chloride anionic form, Bio-Rad, Belgium) packed in polypropylene chromatographic columns (Bio-Rad PolyPrep), was used for Fe isolation from the sample matrix.

Single-element standard solutions of various elements (1 g L^{-1}) purchased from Inorganic Ventures (The Netherlands) were used for quantification (Fe and Ga) and mass bias correction purposes (admixed Ni).

An Fe isotopic reference material (IRMM-014, Institute for Reference Materials and Measurements, Belgium) was used for external mass bias correction through the sample-standard bracketing approach. A single-element Fe standard solution in nitrate form (from now on referred to as A&MS-Fe) purchased from Inorganic Ventures (lot D2-FE03110) and previously characterized for its isotopic composition was used for Caco-2 cells uptake and transport experiments and also as an in-house isotopic standard for measurement quality control. All standards and samples were properly diluted with 0.42 M sub-boiled HNO_3 prior to the measurements.

BioXtra, 99.0% crystalline L-Ascorbic acid and human apo-transferrin (apo-Tf), cell culture tested, were purchased from Sigma-Aldrich in powder form.

Iron (II) sulfate heptahydrate, an ACS reagent for analysis grade, was purchased from Carlo Erba Reagents (Italy).

5.3.2 Cell culture and sample harvesting

The human colon adenocarcinoma Caco-2 cell line (HTB37) was obtained from the American Type Culture Collection (MD, USA). Cells were seeded (at a density of 100 000 cells per well) in 24 mm diameter polyester membrane filters of 0.4 µm pore size with a 4.52 cm^2 cell growth area, fitted to 6-well Transwell® polystyrene plates (Costar, Corning, UK), creating a bicameral chamber. The cells were grown in Dulbecco's modified Eagle's medium (DMEM) supplemented with GlutaMAX™ (Gibco, Life Technologies, CA, USA), 10% heat-inactivated fetal bovine serum (FBS, Greiner Bio One, Belgium), 1% non-essential amino acids (NEAA, Gibco, Life Technologies) and 1% penicillin-streptomycin (P/S, Gibco, Life Technologies). Cells were incubated in a humidified atmosphere with 5% CO_2 and at 37°C (Memmert CO_2 incubator, VWR, Belgium). The culture medium was replaced every 2-3 days and cells were allowed to grow and differentiate for 17 days. Cell confluence was regularly checked using a trinocular inverted phase-contrast microscope (AE31, Motic, VWR, Belgium) and the integrity of a tight monolayer was evaluated by monitoring the transepithelial electrical resistance (TEER) prior to the exposure with an automated tissue resistance measurement system (REMS, World Precision Instruments, UK), ensuring that in every bicameral chamber the measured TEER was > 300 $\Omega \cdot cm^2$, indicative of an intact monolayer.

5.3.3 Sample preparation

After 17 post-seeding days, cells were washed twice with Iscove's modified Dulbecco's medium (IMDM, Sigma-Aldrich) and were incubated in IMDM without FBS during 24 hours for iron and serum protein depletion. After this period, the cell monolayer was washed twice with IMDM and an exposure medium with 120 µM of Fe, prepared from the isotopically characterized Fe in-house standard A&MS-Fe in IMDM, was added to the apical surface, together with 600 µM of ascorbic acid (1 : 5, Fe : AA molar ratio). The basal compartment was filled either with IMDM or with a 50 µM apo-Tf solution prepared in IMDM. This setup was used in four of the six wells per plate in every experiment, while the remaining two were used for procedural blanks, with the same basal composition, but with an apical solution containing 600 µM ascorbic acid in IMDM only (no Fe). The first batch of samples in every experiment was collected after 3 hours of exposure (two exposure wells plus one blank well),

while the rest were incubated for 24 hours to allow ferritin production. Apical and basal compartment solutions were separately collected in Teflon Savillex® beakers (Savillex, MN, USA). Cells were washed twice with IMDM to remove any nonspecifically bound iron. Then, the fine polyester membrane containing the cell monolayer was detached from the well insert and also placed in Teflon Savillex® beakers for further acid digestion.

All samples (cells, apical and basal solutions) were digested in the Teflon Savillex® beakers with a mixture of 4 mL of 14 M HNO_3 and 1 mL of 9.8 M H_2O_2. As this mixture was highly reactive, the digestion was first performed at room temperature and with the beakers not completely closed to avoid overpressure, and subsequently, after tightly closing the beakers, on a hotplate at 110°C for 18 hours. The digests thus obtained were evaporated to dryness at 95°C and re-dissolved in 5 mL of 8 M HCl (with the addition of 0.001% H_2O_2 to ensure that Fe is in its higher oxidation state) for subsequent Fe chromatographic isolation.

Iron was isolated from the samples by anion exchange chromatography, based on the procedure described by Van Heghe *et al*.[24] In short, 1 mL of AG MP-1 resin is packed in the polypropylene chromatographic column, supported by a microporous polyethylene frit. A piece of cotton is placed as stopper on top of the resin bed. After the resin has been thoroughly cleaned and conditioned with 8 M of HCl, the sample is loaded into the column. Matrix compounds are eluted with 3 mL of 8 M HCl + 0.001% H_2O_2 and 9 mL of 5 M HCl + 0.001% H_2O_2. Fe is then quantitatively collected in pre-cleaned Teflon Savillex® beakers by passing through 7 mL of 0.6 M HCl. This purified Fe fraction is evaporated to dryness at 95°C and subsequently re-dissolved in 1 mL of 14 M HNO_3. This drying/re-dissolving step is repeated twice to get rid of the chlorine. After that, the final residue was re-dissolved in 0.5 mL of 0.42 M HNO_3.

Cell seeding and exposure, as well as sample collection, were carried out under aseptic conditions inside a class II biological safety cabinet (MSC-Advantage, Thermo Scientific, VWR, Belgium). All solutions used for cell exposure were previously filter-sterilized with 0.22 µm pore membrane filters units (Millex-GP, Merck Millipore). After sample collection, all manipulations were carried out inside a class 10 clean lab. The Teflon Savillex® beakers were previously cleaned with 7 M HNO_3 and 6 M HCl in several steps and further rinsed with Milli-Q water and all the polyethylene metal-free material with 1.4 M HNO_3 followed by Milli-Q water.

5.3.4 Instruments and measurements

For total Fe quantification before and after chromatographic isolation, an Element XR single-collector sector field ICP-MS instrument (Thermo Scientific, Germany) operated at medium mass resolution was used. The sample introduction system consisted of a quartz concentric nebulizer (200 µL min^{-1}) and a cyclonic spray chamber. Samples and calibration standards were properly diluted with 0.42 M sub-boiled HNO_3 and Ga added as internal standard (10 µg L^{-1}) to correct for non-spectral interferences and instrument instability. The instrument settings and data acquisition parameters are summarized in Table 5-1.

Table 5-1. Instrument settings and data acquisition parameters for Fe quantification using a Thermo Scientific Element XR single collector sector field ICP-MS instrument.

Instrument settings	
RF power (W)	1230
Guard electrode	Connected
Sampler cone	Ni; Standard; 1.1 mm aperture diameter
Skimmer cone	Ni; H-type; 0.8 mm aperture diameter
Lens settings	Optimized for maximum analyte signal intensity
Plasma gas flow rate (L min^{-1})	15
Auxiliary gas flow rate (L min^{-1})	0.84
Nebulizer gas flow rate (L min^{-1})	1.015
Sample uptake rate (µL min^{-1})	200
Resolution	Medium (~ 4000 resolving power)
Data acquisition parameters	
Scan mode	E-Scan
Segment duration (s)	0.2
Sample time (s)	0.01
Runs	5
Passes	5
Samples per peak	20
Nuclides monitored	^{54}Fe, ^{56}Fe; ^{57}Fe; ^{69}Ga

Isotopic analysis was performed using a Thermo Scientific Neptune multi-collector ICP-MS instrument. The sample introduction system comprised a low-flow PFA concentric nebulizer (100 µL min^{-1}) and a tandem quartz spray chamber consisting of a cyclonic and a Scott-type sub-unit. The instrument was equipped with a large dry interface pump and an X-type Ni

skimmer and Jet-type Ni sampling cones were used to improve the sensitivity. Measurements were performed at medium mass resolution and in static multi-collection mode, making use of six Faraday cups connected to 10^{11} Ω current amplifiers. The instrument settings and data acquisition parameters are given in Table 5-2.

Table 5-2. Instrument settings and data acquisition parameters for Fe isotopic analysis using a Thermo Scientific Neptune MC-ICP-MS.

Instrument settings	
RF power (W)	1275
Guard electrode	Connected
Sampler cone	Ni; Jet-type; 1.1. mm aperture diameter
Skimmer cone	Ni; X-type; 0.8 mm aperture diameter
Large dry interface pump (m^3 h^{-1})	130
Lens settings	Optimized for maximum analyte signal intensity
Plasma gas flow rate (L min^{-1})	15
Auxiliary gas flow rate (L min^{-1})	0.80
Nebulizer gas flow rate (L min^{-1})	1.003
Sample uptake rate (µL min^{-1})	100
Resolution	Medium
Data acquisition parameters	
Acquisition mode	Static; multi-collection
Number of blocks	9
Number of cycles/block	5
Integration time (s)	4.194
Cup configuration	L4: ^{54}Fe, L2: ^{56}Fe, L1: ^{57}Fe, C: (^{58}Fe+^{58}Ni), H1: ^{60}Ni, H3: ^{62}Ni

The sample-standard bracketing (SSB) approach was applied by alternating the measurement of every sample/A&MS-Fe in-house standard with a measurement of the isotopic standard (IRMM-014) for applying external mass bias correction. The Fe concentration in samples and standards was carefully matched (within ± 5%) to avoid variation in the extent of instrumental mass bias due to differences in the target element concentration. Whenever possible, Fe concentration was adjusted to 300 µg L^{-1}. For those cases where the Fe concentration in the samples was not sufficiently high, samples and standards were adjusted to 200 µg L^{-1}. Ni was added to all samples and isotopic standards at the same concentration and was used as the internal standard for mass bias correction. The A&MS-Fe in-house standard was measured every 5 samples to ensure correct instrument performance.

Off-line mass bias correction was performed by combining internal correction (using the admixed Ni as internal standard) by applying the revised Russell's model for calculating the mass bias factors as described by Baxter *et al.* and the SSB external correction approach.[25] The isotopic composition is expressed in delta notation (δ^{56}Fe and δ^{57}Fe, ‰) relative to the IRMM-014 Fe isotopic reference material, as described elsewhere.[11,26]

5.4 RESULTS AND DISCUSSION

5.4.1 Optimization of the in vitro enterocyte model

Cell viability assays

Caco-2 cells were seeded in 96-microwell plates (10^4 cells per well density) to perform several cell viability assays towards the iron species intended for the exposure to find a suitable concentration, offering a good compromise between cell viability and a sufficient iron content for reliable isotopic analysis. The cells were incubated in DMEM with 10% FBS, 1% NEAA and 1% P/S (200 µL per well) and allow to differentiate for 18 days prior to the experiments. The culture medium was changed every 2-3 days. Established protocols for the MTT (3-[4,5-dimethylthiazol-2-yl]-2,5 diphenyl tetrazolium bromide) test for mitochondrial activity[27] and the sulforhodamine B (SRB) assay for protein content determination[28] were applied to cells exposed for 24 hours to solutions with different Fe concentration (0, 1, 5, 10, 15, 20, 30, 40 and 50 mg L^{-1}) prepared by the appropriate dilution of the A&MS-Fe in-house isotopic standard with IMDM, in the presence of 600 µM of ascorbic acid. Results of the SRB assay show no significant differences in protein content and thus, no evidence of immediate toxicity leading towards protein loss of the cells for any of the concentrations tested after 24 hours. MTT assay results show somewhat more variability, and some decrease in mitochondrial activity was observed for the higher concentrations (30-50 mg L^{-1}), but the decrease was always < 20%. The results for these viability assays can be found in Tables 5-S1 and 5-S2 of the supplementary information.

Enhancement of non-heme iron bioavailability

It is already known that several compounds may inhibit iron absorption, for instance by promoting insoluble iron aggregates, or enhance it, by stabilizing its reduced and more soluble form Fe^{2+}. The soluble species Fe^{2+} is the most suitable for the non-heme iron absorption by brush-border membrane transport proteins of the intestinal enterocytes and, therefore, the most bioavailable form.[1] Ascorbic acid exerts a very pronounced enhancing effect on non-heme iron absorption[29] and it has been frequently used in studies of iron availability involving Caco-2 cells.[30–32] The effectiveness of the ascorbic acid relies on its ability to reduce Fe from ferric to ferrous form and the chelating properties of ascorbate at nearly neutral pH environment to preferentially form Fe^{2+} soluble complexes.

The enhancement of the iron absorption by Caco-2 cells was not evaluated in detail in this work; however, it was tested for further study of the Fe isotope fractionation accompanying the processes involved. For this, the conditions recommended in the literature[32] were applied in the present setup to obtain the Fe in the bioavailable form for the cells, and thus to ensure sufficient intracellular Fe for isotope ratio measurements. Ascorbic acid needs to be added in a sufficient excess to Fe. As no strong inhibitors are expected to be present in the exposure media, an Fe : AA molar ratio of 1 : 5 was appropriate. Under these conditions, the iron uptake increased up to 5-fold, in concordance with previous studies.[32,33]

Control of blank levels

The setup conditions and manipulation of the cell cultures were optimized, not only for assuring a sufficient Fe concentration in the samples, but also to achieve the maximum possible control over the Fe blank levels, which is crucial for the correct interpretation of the isotope ratio data obtained. During cell growth to confluency and differentiation, cells were maintained under normal Fe conditions in DMEM culture medium (originally containing 0.1 mg L^{-1} of Fe, added as $Fe(NO_3)_3 \cdot 9H_2O$) supplemented with 10% FBS, which provides the cells with a total constant Fe dose of approximately 400 µg L^{-1}. Prior to the exposure experiment, the cell layers were carefully rinsed twice with fresh IMDM culture medium (with no Fe inorganic salts added, having an Fe concentration of < 5 µg L^{-1}) and incubated during 24 hours in IMDM to allow Fe depletion. After this depletion time, the medium was discarded and substituted by the corresponding apical and basal exposure media, both

properly prepared in IMDM. The Fe contents in procedural apical and basal blank solutions were monitored after every experiment and were always < 10 µg L^{-1}. Samples were collected in due course in pre-cleaned Teflon beakers for acid digestion. Under these conditions, the average amount of Fe in each compartment of 9 setup blanks seeded on 5 different days was 0.04 ± 0.02 µg Fe (per 1.5 mL of apical solution), 0.06 ± 0.02 µg Fe (per 2 mL of basal solution) and 0.10 ± 0.04 µg Fe (per cell monolayer), expressed as average and standard deviation of 9 replicates measured in different sessions.

Evaluation of the experimental and measurement precision

Under the optimized conditions described above, experimental repeatability and reproducibility were assessed. Repeatability is expressed as the standard deviation of the Fe isotopic composition of the cell monolayer obtained from four different exposure replicates in a single experimental setup, which was between 0.01-0.08‰ for δ^{56}Fe and 0.01-0.15‰ for δ^{57}Fe. The reproducibility values, expressed as the standard deviation of the isotopic composition of the cell monolayer of four exposure replicates determined in two different experimental setups (within 3 months), were 0.03‰ for δ^{56}Fe and 0.06‰ for δ^{57}Fe.

Regarding the measurement precision, the internal precision expressed as the standard deviation for 45 cycles within a single measurement was 0.04‰ for δ^{56}Fe and 0.06‰ for δ^{57}Fe. The external precision, expressed as the standard deviation of 10 measurements of the A&MS-Fe in-house standard during a 16-hours measurement session, was 0.03‰ for δ^{56}Fe and 0.05‰ for δ^{57}Fe. The isotopic composition of the A&MS-Fe in-house standard was measured a total of 45 times during 6 different measurement sessions (on 6 different days) within 5 months. The reproducibility of the measurements thus obtained, expressed as the standard deviation for those 45 measurements, was 0.02‰ for δ^{56}Fe and 0.05‰ for δ^{57}Fe. An average isotopic composition for the A&MS-Fe in-house standard of 0.46 ± 0.02‰ for δ^{56}Fe and 0.67 ± 0.05‰ for δ^{57}Fe was obtained, in good agreement with previous studies.[24,34]

5.4.2 Natural iron isotope fractionation accompanying iron fluxes through the cells

Non-heme extracellular iron is taken up by the intestinal cells as Fe^{2+} (after the action of a membrane protein with ferric reductase activity) through a pathway involving a divalent metal ion transporter protein (DMT1) located in the brush-border at the apical pole of the enterocyte. Once inside the cell, the iron is gathered in the cytosol, where it is forming a pool of exchangeable intracellular transit iron associated with low molecular weight ligands, commonly known as labile iron pool (LIP). Ferritin production is stimulated within the cell in response to intracellular iron enrichment, and thus the iron from the LIP will either be sequestered as ferritin-bounded (after oxidation) within the enterocyte for eventual discarding by cell shedding into the intestinal lumen or transported across the basolateral membrane through the membrane divalent iron exporter protein ferroportin1 into the systemic circulation. Iron release across the basolateral membrane involves the oxidation of iron to its Fe^{3+} form by the membrane-bound ferroxidase hephaestin, to be incorporated into circulating apo-Tf.[1,3,35,36]

In the current *in vitro* enterocyte model, non-heme iron is already offered to the cells in a highly bioavailable stabilized Fe^{2+} form by the addition of ascorbic acid in the apical solution to facilitate the uptake process. Apo-Tf was added to the basal solution in order to stimulate iron transport to the basal chamber. A final concentration of 50 µM of apo-Tf was selected, which would be considered a normal value for human serum and will offer enough iron binding sites (each apo-Tf molecule presents two high-affinity iron binding sites).

The optimized setup for the isotopic analysis of the different culture compartments consisted of a 6-well Transwell® plate with filter inserts creating a two-chamber system. Caco-2 cells were seeded over the surface of the inserts and maintained immersed in DMEM culture medium for 17 days to allow cell differentiation prior to the exposure experiment. After a subsequent 24 hours of iron and serum protein depletion in iron- and serum-free IMDM medium and appropriate assessment of monolayer integrity by TEER measurements, the cell layers were carefully rinsed twice with fresh IMDM medium and a 1.5 mL solution containing 120 µM of Fe as Fe-ascorbate (prepared as described above) was offered to the apical chamber of four of the six wells. The remaining two wells were kept as procedural blanks, and thus, each apical compartment consisted of 1.5 mL of an ascorbic acid solution of 600 µM prepared in IMDM culture medium. 2 mL of a 50 µM solution of apo-Tf in IMDM

medium were added to each basal chamber, and the cells were kept at 37°C in an incubator, in a humidified atmosphere with 5% CO_2. A scheme of the experimental setup is represented in Fig. 5-1.

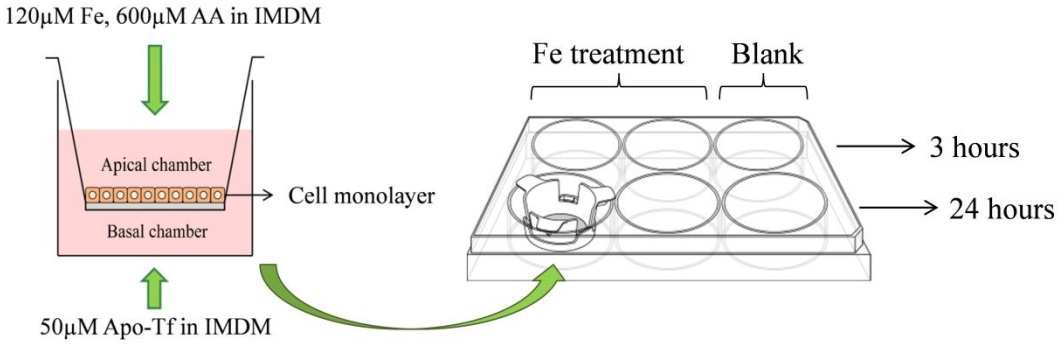

Fig. 5-1 Scheme of the in vitro experimental setup relying on the intestinal Caco-2 cell line model for studying Fe isotope fractionation accompanying intestinal Fe uptake.

Samples (apical and basal media and the cell monolayer) were collected after 3 and after 24 hours of iron exposure. These time points have been selected in order to isolate as much as possible the mechanisms potentially involved in inducing mass-dependent fractionation in the Fe isotopic composition, *i.e.* iron uptake from the apical compartment into the cytosolic iron pool, iron incorporation into ferritin within the cells, and iron transport across the basolateral membrane to the basal compartment. After sample collection, iron was quantified in each compartment, before and after chromatographic analyte isolation, to assure complete recovery. The Fe transport efficiency (expressed in percent) was calculated based on the original Fe concentration in the exposure medium at the start of the experiment and the final Fe concentrations in the apical, cell and basal compartments. At the 3 hours' time point, an uptake of around 30% was observed, while very little transport was recorded. After 24 hours, enough time to allow ferritin production in the cells, the intracellular iron accounted for around 45% of the initially fed iron, while approx. 1% of this iron was found in the basal compartment. This increase in absorbed iron with a very low transport rate could maybe be explained by a cellular response towards changes in the LIP, which is an indicator of the iron status of the cell. The cells on their own have a regulatory mechanism by which, in response to their metabolic requirements, they can modulate the expression of the proteins required for import, storage and export of iron.[37,38] Similar low magnitude percentages of iron transported

Table 5-3. Isotopic composition of Fe (‰) in the three compartments of the setup - samples collected at two different time points (after 3 and after24 hours); each experiment was performed in duplicate (ER1 and ER2). Uncertainties represent the internal precision of the measurements expressed as the standard deviation of all the measurement cycles. The $\delta^{56}Fe$ value of the original exposure medium is 0.53 ± 0.04 ‰.

	3 hours Fe exposure				**24 hours Fe exposure**			
	ER1		**ER2**		**ER1**		**ER2**	
	$\delta^{56}Fe$	**$\delta^{57}Fe$**	**$\delta^{56}Fe$**	**$\delta^{57}Fe$**	**$\delta^{56}Fe$**	**$\delta^{57}Fe$**	**$\delta^{56}Fe$**	**$\delta^{57}Fe$**
Apical	0.51 ± 0.04	0.75 ± 0.06	0.46 ± 0.03	0.68 ± 0.07	0.73 ± 0.04	1.11 ± 0.06	0.77 ± 0.04	1.08 ± 0.07
Caco-2 cells	0.33 ± 0.04	0.50 ± 0.05	0.39 ± 0.03	0.49 ± 0.06	0.15 ± 0.04	0.26 ± 0.06	0.27 ± 0.04	0.39 ± 0.06
Basal*	-0.33 ± 0.06	----------	-0.33 ± 0.06	----------	-1.52 ± 0.06	----------	-1.52 ± 0.06	----------
Untreated Caco-2 cells	-0.55 ± 0.05	----------	----------	----------	-0.86 ± 0.05	----------	----------	----------

* Values of $\delta^{56}Fe$ for the basal compartments are the result of the analysis of the combined solution from both experimental setups at each time point

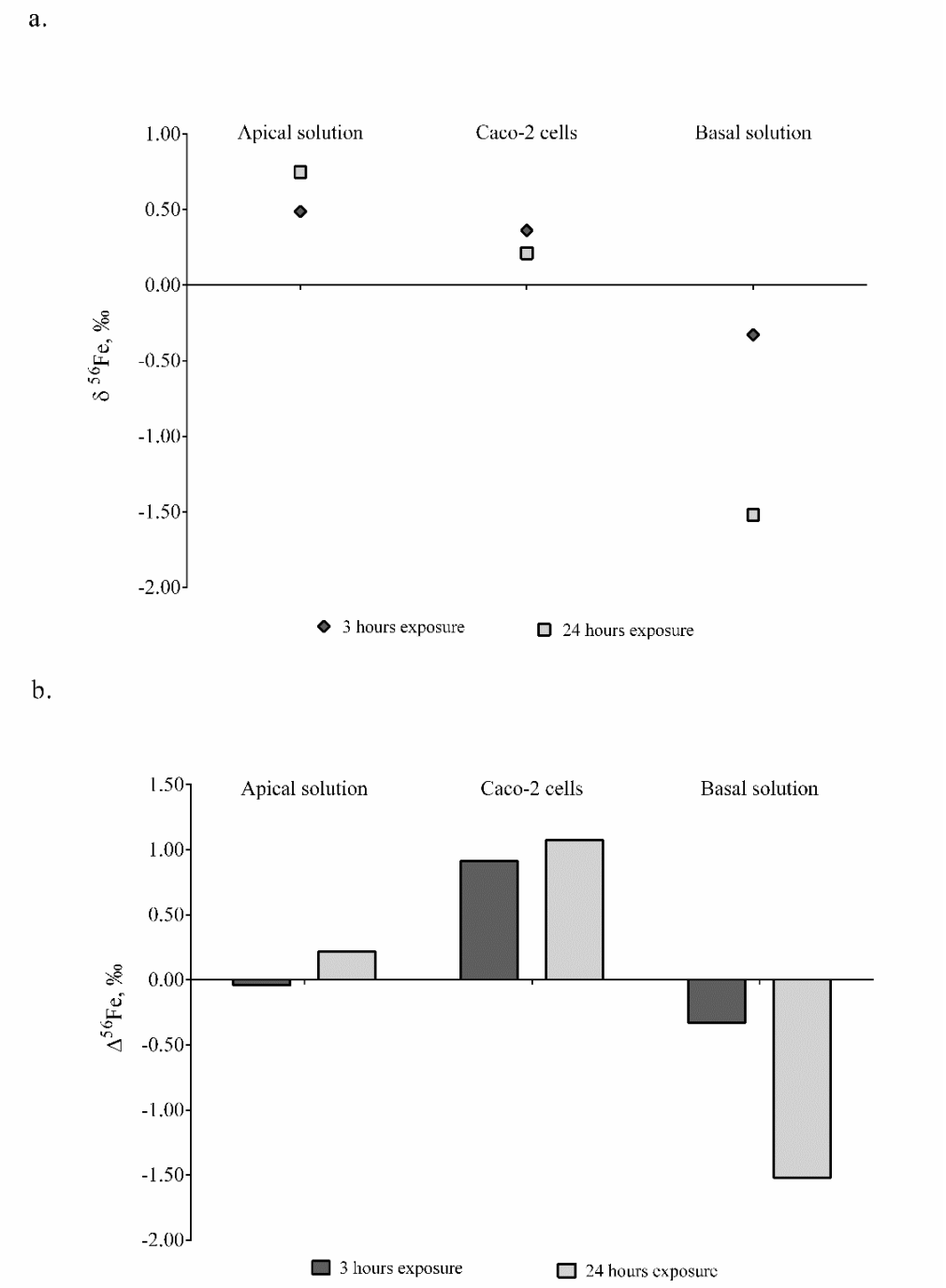

Fig. 5-2 (a) Variations in $\delta^{56}Fe$ values of the apical, basal and cell compartments after exposure to Fe (as $Fe(NO_3)_2$ in the presence of ascorbic acid) and sample collection at different time points (after 3 and after 24 hours). (b) Differences in $\delta^{56}Fe$ values between each culture compartment and its corresponding "time zero". Increments in apical $\delta^{56}Fe$ values are expressed relative to the value of the exposure medium, and cell and basal values are expressed for procedural blank cells and basal solution, respectively. The external precision, expressed as the standard deviation of five replicates of A&MS-Fe in-house standard subjected to sample preparation, was 0.03 ‰ for $\delta^{56}Fe$. The absolute deviation obtained for culture replicates wells ranged between 0.01 and 0.08 ‰.

in Caco-2 cells cultured under normal iron conditions were reported previously for *in vitro* studies of intestinal iron transport across Caco-2 cells.[39,40]

For each time point, two individual experimental setups were used and cells and apical solutions were analyzed separately for their Fe isotopic composition. The basal solutions for both experimental replicates were combined in order to have sufficient Fe concentration for obtaining reliable isotope ratio data. Results for the isotopic analysis are gathered in Table 5-3 and represented in Fig. 5-2a for ease of interpretation. A trend towards a heavier isotopic composition with time is observed in the apical compartment, evidencing a preferential uptake of the lighter isotopes. Both the cells and the solution of the basal compartment exhibit an enrichment in light Fe isotopes. This trend is particularly pronounced in the basal solution, which indicates also a strong preferential transfer of the lighter isotopes across the epithelial cells. These *in vitro* results are in good agreement with previously reported conclusions from *in vivo* and *ex vivo* studies.[13,41] In Fig. 5-2b, the differences in δ^{56}Fe value between the solution of each setup compartment and its corresponding "time zero" are represented, *i.e.* apical solution minus exposure medium, exposure cells minus procedural blank cells and basal solution minus basal blank. The most noteworthy behavior is probably an overall increase in the intracellular Fe isotopic composition relative to the corresponding value for the control setup ($\Delta^{56}Fe = (\delta^{56}Fe)_t - (\delta^{56}Fe)_0 > 0$), which together with the fact of a less pronounced enrichment in light isotopes than in the basal solution, seems to support the statement presented by Hotz *et al.*[13] of a preferential accumulation of heavy Fe isotopes in the form of ferritin within the enterocytes.

5.4.3 Presence/absence of apo-Tf in the basal compartment

Alvarez-Hernandez *et al.*[40] studied iron transport through Caco-2 cells using ^{59}Fe radioisotope as tracer. They demonstrated that, while Caco-2 cells show a constitutive rate of iron transport in the absence of any chelating ligand or serum protein, the presence of apo-Tf as iron "sequestering" protein is needed to stimulate transepithelial iron transfer to the basal compartment. In their study, several chelators with higher affinity for iron than that of the apo-Tf were tested, as well as some other Tf forms. In all those cases, iron transport to the basal compartment was poorly stimulated or no effect was observed compared to the transport in the presence of apo-Tf, suggesting a unique mechanism of interaction of this protein with the basal surface of the Caco-2 cells.

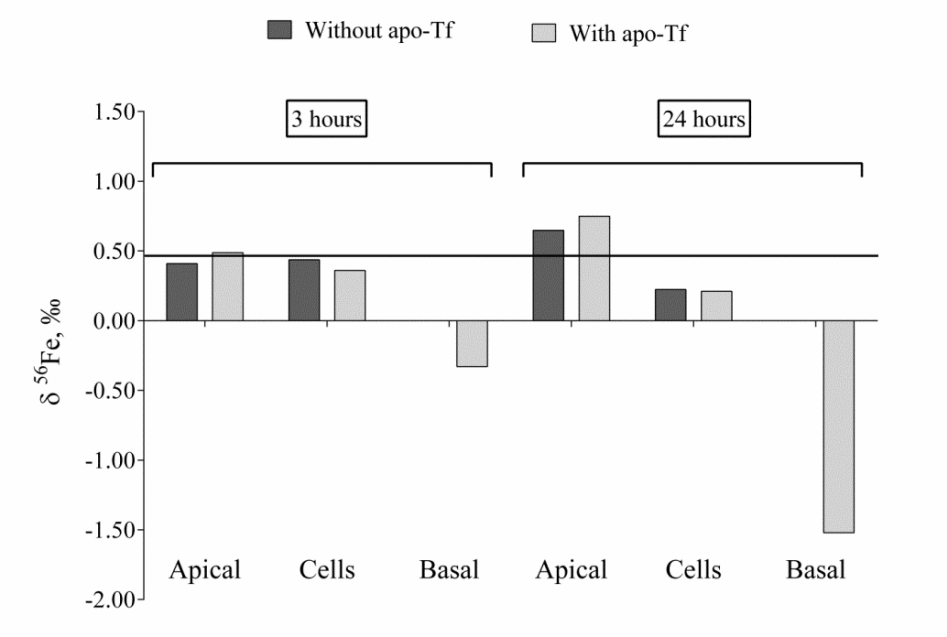

Fig. 5-3 Comparative study of Fe isotopic composition trends after 3 and after 24 hours of exposure to the Fe / ascorbic acid mixture in the presence and absence of apo-Tf for stimulating iron transport to the basal compartment. The standard deviation is 0.03 ‰ for five replicates of in-house standard subjected to sample preparation and measured in the same session.

A similar experiment to that described in the previous section was performed by only eliminating the presence of apo-Tf in the basal solution to block the iron transfer process and evaluate only the isotopic effects accompanying iron uptake. Fig. 5-3 shows a comparative representation of the trend in Fe isotopic composition obtained for each compartment at 3 and at 24 hours in absence and in presence of apo-Tf as stimulating factor for iron transport to the basal compartment. Without apo-Tf in the basal compartment, the Fe concentration observed after 3 h and 24 h in the basal compartment was not high enough for reliable measurement of the Fe isotopic composition *via* MC-ICP-MS. After 3 hours exposure, the isotopic composition of the apical solution and the cells does not significantly differ from that of the A&MS-Fe in-house standard (value indicated in the figure with a solid line). After 24 hours exposure, the trend towards a lighter Fe isotopic composition in the cells and a heavier isotopic composition of the apical solutions was observed in both cases. A possible explanation may rely on the fact that the iron absorption efficiency of the cells is maximal after cell depletion and, after 3 hours exposure, the cells had already incorporated almost 70% of the total iron uptake observed at the end of the experiment. The approximately remaining 30% is absorbed over the subsequent 21 hours of exposure, indicating that the uptake efficiency gradually decays, probably due to the increased iron status of the cells, resulting in a more pronounced isotope fractionation.

5.4.4 Natural iron isotope fractionation of the specific non-heme iron uptake pathway

Ferrous sulfate is traditionally the inorganic iron source of choice for all *in vitro* iron uptake/transport experiments through Caco-2 cells[21,42] as well as *in vivo* iron absorption studies.[43,44] This salt is widely employed as Fe fortificant in many kinds of dried meals as a highly bioavailable iron source due to its high solubility in water. In the development of the enterocyte model used in the current work, the A&MS-Fe in-house standard in nitrate form was used to facilitate the isotopic data interpretation. However, a study offering iron to the Caco-2 cells as $FeSO_4$ at different time points under the optimized conditions was carried out to compare the trend in the isotopic variation occurring across the epithelial cells. The results obtained are represented in Fig. 5-4. As expected, the apical solution tends towards a heavier Fe isotopic composition with time, while the cells and the basal solution are characterized by a lighter isotopic composition, supporting the hypothesis that both uptake and transport processes are accompanied by an Fe isotope fractionation in favor of the light isotopes. From a metabolic point of view, a similar behavior should be expected due to the fact that all iron offered to the cells in an inorganic salt form seems to be transported through the apical membrane by the same specific uptake pathway for non-heme iron. Once it is incorporated into the LIP, the origin or initial form of an iron ion is no longer of relevance.

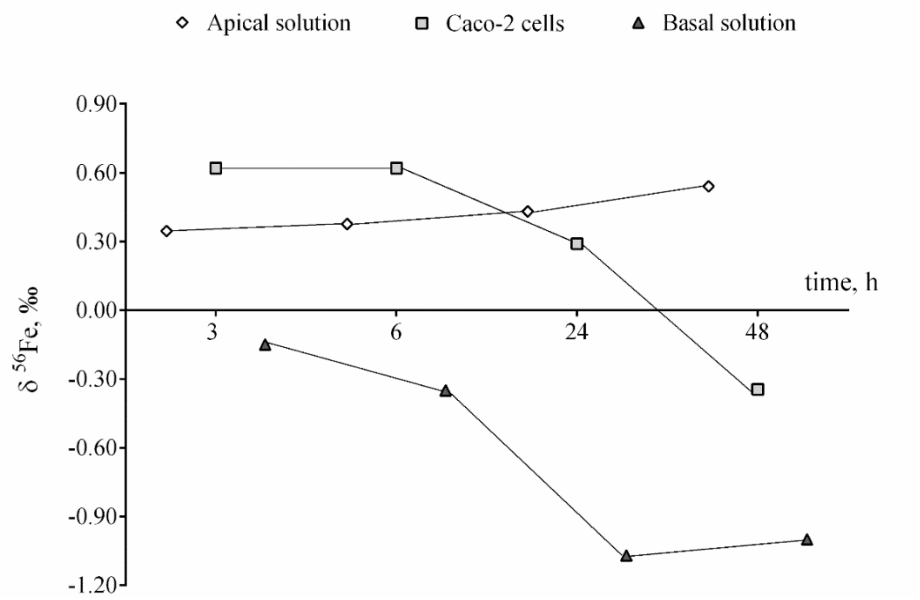

Fig. 5-4 Trend in the $\delta^{56}Fe$ values of the apical, basal and cell compartments upon exposure to Fe as $FeSO_4$ in the presence of ascorbic acid and sample collection at different time points (after 3, 6, 24 and 48 hours). The standard deviation is 0.03 ‰ for five replicates of in-house standard subjected to sample preparation and measured in the same session.

5.5 CONCLUSIONS

In this pilot study, an *in vitro* intestinal model was developed and evaluated as a tool to study the isotope fractionation effects triggered by the iron metabolic uptake and transport mechanisms at a cellular level. The Caco-2 cell line has been used, after cell differentiation, as enterocyte model and a bi-cameral experimental setup has been developed and optimized for stimulating intracellular iron fluxes. Under the optimum conditions, good experimental repeatability and reproducibility were attained with low blank contribution levels, allowing precise and reliable results for Fe isotope ratios. Both iron absorption and transport processes are accompanied by Fe isotope fractionation in favor of the light isotopes. These results are in good agreement with previous conclusions from *in vivo* and *ex vivo* studies, in which the Fe isotopic composition of the blood or intestinal mucosa was lighter than that of the diet. Furthermore, the data generated in this work also support the assumption of a preferential accumulation of the heavier isotopes in enterocyte ferritin. The consistency of the results obtained supports the usefulness of *in vitro* cell culture models as an interesting complementary tool for studying iron metabolic pathways.

5.6 ACKNOWLEDGEMENTS

The Flemish Research Foundation FWO-Vlaanderen (research project “G023014N”) and the Special Research Fund of Ghent University (BOF-UGent) (research project “01B04212”) are acknowledged for financial support. María R. Flórez thanks BOF-UGent for her postdoctoral grant. Marta Costas-Rodríguez thanks FWO-Vlaanderen for her postdoctoral grant.

5.7 REFERENCES

1. Crichton, R. *Iron Metabolism: From Molecular Mechanisms to Clinical Consequences, 3rd Edition*. (John Wiley & Sons, Ltd, 2009).
2. Andrews, N. C. Disorders of iron metabolism. *N. Engl. J. Med.* **341,** 1986–95 (1999).
3. Gulec, S., Anderson, G. J. & Collins, J. F. Mechanistic and regulatory aspects of intestinal iron absorption. *Am. J. Physiol. Gastrointest. Liver Physiol.* **307,** G397-409 (2014).
4. Vanhaecke, F. & Degryse, P. *Isotopic Analysis: Fundamentals and Applications Using ICP-MS*. (Wiley-VCH Verlag GmbH & Co. KGaA, 2012).

5. Vanhaecke, F., Balcaen, L. & Malinovsky, D. Use of single-collector and multi-collector ICP-mass spectrometry for isotopic analysis. *J. Anal. At. Spectrom.* **24,** 863 (2009).

6. Krayenbuehl, P.-A., Walczyk, T., Schoenberg, R., von Blanckenburg, F. & Schulthess, G. Hereditary hemochromatosis is reflected in the iron isotope composition of blood. *Blood* **105,** 3812–3816 (2005).

7. Stenberg, A. *et al.* Measurement of iron and zinc isotopes in human whole blood: preliminary application to the study of HFE genotypes. *J. Trace Elem. Med. Biol.* **19,** 55–60 (2005).

8. Hotz, K., Krayenbuehl, P.-A. & Walczyk, T. Mobilization of storage iron is reflected in the iron isotopic composition of blood in humans. *J. Biol. Inorg. Chem.* **17,** 301–9 (2012).

9. Van Heghe, L., Delanghe, J., Van Vlierberghe, H. & Vanhaecke, F. The relationship between the iron isotopic composition of human whole blood and iron status parameters. *Metallomics* **5,** 1503–1509 (2013).

10. Hotz, K. & Walczyk, T. Natural iron isotopic composition of blood is an indicator of dietary iron absorption efficiency in humans. *J. Biol. Inorg. Chem.* **18,** 1–7 (2013).

11. Costas-Rodríguez, M., Delanghe, J. & Vanhaecke, F. High-precision isotopic analysis of essential mineral elements in biomedicine: Natural isotope ratio variations as potential diagnostic and/or prognostic markers. *TrAC.* **76,** 182–193 (2016).

12. Walczyk, T. & von Blanckenburg, F. Natural iron isotope variations in human blood. *Science* **295,** 2065–6 (2002).

13. Hotz, K., Augsburger, H. & Walczyk, T. Isotopic signatures of iron in body tissues as a potential biomarker for iron metabolism. *J. Anal. At. Spectrom.* **26,** 1347–1353 (2011).

14. Navarrete, J. U., Borrok, D. M., Viveros, M. & Ellzey, J. T. Copper isotope fractionation during surface adsorption and intracellular incorporation by bacteria. *Geochim. Cosmochim. Acta* **75,** 784–799 (2011).

15. Kafantaris, F.-C. A. & Borrok, D. M. Zinc isotope fractionation during surface adsorption and intracellular incorporation by bacteria. *Chem. Geol.* **366,** 42–51 (2014).

16. Amor, M. *et al.* Mass-dependent and -independent signature of Fe isotopes in magnetotactic bacteria. *Science (80-.).* **352,** 705–708 (2016).

17. Kappler, A., Johnson, C. M., Crosby, H. A., Beard, B. L. & Newman, D. K. Evidence for equilibrium iron isotope fractionation by nitrate-reducing iron(II)-oxidizing bacteria. *Geochim. Cosmochim. Acta* **74,** 2826–2842 (2010).

18. Bondanese, V. P. *et al.* Hypoxia induces copper stable isotope fractionation in hepatocellular carcinoma, in a HIF-independent manner. *Metallomics* **7,** 299–308 (2016).

19. Paredes, E. *et al.* Evidence of isotopic fractionation of natural uranium in cultured human cells. *Proc. Natl. Acad. Sci. U. S. A.* **113,** 14007–14012 (2016).

20. Alvarez-Hernandez, X., Smith, M. & Glass, J. Regulation of iron uptake and transport by transferrin in Caco-2 cells, an intestinal cell line. *Biochim. Biophys. Acta - Biomembr.* **1192,** 215–222 (1994).

21. Garcia, M. N., Flowers, C. & Cook, J. D. The Caco-2 cell culture system can be used as

a model to study food iron availability. *J. Nutr.* **126,** 251–8 (1996).

22. Glahn, R. P., Lee, O. A., Yeung, A., Goldman, M. I. & Miller, D. D. Caco-2 cell ferritin formation predicts nonradiolabeled food iron availability in an in vitro digestion/Caco-2 cell culture model. *J. Nutr.* **128,** 1555–61 (1998).

23. Au, A. P. & Reddy, M. B. Caco-2 cells can be used to assess human iron bioavailability from a semipurified meal. *J. Nutr.* **130,** 1329–34 (2000).

24. Van Heghe, L., Engström, E., Rodushkin, I., Cloquet, C. & Vanhaecke, F. Isotopic analysis of the metabolically relevant transition metals Cu, Fe and Zn in human blood from vegetarians and omnivores using multi-collector ICP-mass spectrometry. *J. Anal. At. Spectrom.* **27,** 1327–1334 (2012).

25. Baxter, D. C., Rodushkin, I., Engström, E. & Malinovsky, D. Revised exponential model for mass bias correction using an internal standard for isotope abundance ratio measurements by multi-collector inductively coupled plasma mass spectrometry. *J. Anal. At. Spectrom.* **21,** 427–430 (2006).

26. Malinovsky, D. *et al.* Performance of high resolution MC-ICP-MS for Fe isotope ratio measurements in sedimentary geological materials. *J. Anal. At. Spectrom.* **18,** 687–695 (2003).

27. van Meerloo, J., Kaspers, G. J. L. & Cloos, J. in *Cancer cell culture : methods and protocols.* 237–245 (Humana Press, 2011).

28. Vichai, V. & Kirtikara, K. Sulforhodamine B colorimetric assay for cytotoxicity screening. *Nat. Protoc.* **1,** 1112–1116 (2006).

29. Teucher, B., Olivares, M. & Cori, H. Enhancers of iron absorption: ascorbic acid and other organic acids. *Int. J. Vitam. Nutr. Res.* **74,** 403–19 (2004).

30. Glahn, R. P., Wortley, G. M., South, P. K. & Miller, D. D. Inhibition of Iron Uptake by Phytic Acid, Tannic Acid, and ZnCl 2 : Studies Using an In Vitro Digestion/Caco-2 Cell Model. *J. Agric. Food Chem.* **50,** 390–395 (2002).

31. Yun, S., Habicht, J.-P., Miller, D. D. & Glahn, R. P. An in vitro digestion/Caco-2 cell culture system accurately predicts the effects of ascorbic acid and polyphenolic compounds on iron bioavailability in humans. *J. Nutr.* **134,** 2717–21 (2004).

32. Zhu, L., Glahn, R. P., Yeung, C. K. & Miller, D. D. Iron uptake by Caco-2 cells from NaFeEDTA and FeSO4: Effects of ascorbic acid, pH, and a Fe(II) chelating agent. *J. Agric. Food Chem.* **54,** 7924–8 (2006).

33. Reddy, M. B. & Cook, J. D. Assessment of dietary determinants of nonheme-iron absorption in humans and rats. *Am. J. Clin. Nutr.* **54,** 723–8 (1991).

34. Anoshkina, Y., Costas-Rodríguez, M. & Vanhaecke, F. High-precision Fe isotopic analysis of whole blood for biomedical purposes without prior isolation of the target element. *J. Anal. At. Spectrom.* **30,** 1816–1821 (2015).

35. Winter, W., Bazydlo, L. & Harris, N. The molecular biology of human iron metabolism. *Lab. Med.* **45,** 92–102 (2014).

36. Frazer, D. M. & Anderson, G. J. Iron imports. I. Intestinal iron absorption and its regulation. *Am. J. Physiol. Gastrointest. Liver Physiol.* **289,** G631-5 (2005).

37. Cairo, G. & Recalcati, S. Iron-regulatory proteins: molecular biology and pathophysiological implications. *Expert Rev. Mol. Med.* **9,** 1–13 (2007).

38. Cabantchik, Z. I. Labile iron in cells and body fluids: physiology, pathology, and pharmacology. *Front. Pharmacol.* **5,** 45 (2014).

39. Sánchez, L., Ismail, M., Liew, F. Y. & Brock, J. H. Iron transport across Caco-2 cell monolayers. Effect of transferrin, lactoferrin and nitric oxide. *Biochim. Biophys. Acta* **1289,** 291–7 (1996).

40. Alvarez-Hernandez, X., Smith, M. & Glass, J. The effect of apotransferrin on iron release from Caco-2 cells, an intestinal epithelial cell line. *Blood* **91,** 3974–9 (1998).

41. Walczyk, T. & von Blanckenburg, F. Deciphering the iron isotope message of the human body. *Int. J. Mass Spectrom.* **242,** 117–134 (2005).

42. Kalgaonkar, S. & Lönnerdal, B. Effects of dietary factors on iron uptake from ferritin by Caco-2 cells. *J. Nutr. Biochem.* **19,** 33–9 (2008).

43. Swain, J. H., Newman, S. M. & Hunt, J. R. Bioavailability of elemental iron powders to rats is less than bakery-grade ferrous sulfate and predicted by iron solubility and particle surface area. *J. Nutr.* **133,** 3546–52 (2003).

44. Zimmermann, M. B. *et al.* Comparison of the efficacy of wheat-based snacks fortified with ferrous sulfate, electrolytic iron, or hydrogen-reduced elemental iron: randomized, double-blind, controlled trial in Thai women. *Am. J. Clin. Nutr.* **82,** 1276–82 (2005).

5.8 SUPPLEMENTARY INFORMATION

Table 5-S1. Results of the MTT test for mitochondrial activity of cells exposed to different concentrations of the A&MS-Fe in-house standard, in the presence of 600 µM of ascorbic acid.

Fe concentration	Absorbance			Average	Blank corrected	%
1 mg L^{-1}	0.512	0.722	0.812	0.682	0.613	104
5 mg L^{-1}	0.543	0.692	0.713	0.649	0.580	98
10 mg L^{-1}	0.639	0.524	0.638	0.600	0.531	90
15 mg L^{-1}	0.810	0.627	0.700	0.712	0.643	109
20 mg L^{-1}	0.668	0.629	0.624	0.640	0.571	97
Blank	0.699	0.537	0.680	0.660	0.591	100
Blank	0.729	0.650	0.663			
30 mg L^{-1}	0.649	0.644	0.497	0.597	0.528	89
40 mg L^{-1}	0.501	0.536	0.579	0.539	0.470	80
50 mg L^{-1}	0.618	0.561	0.582	0.587	0.518	88
plate blank	0.073	0.066	0.068	0.069		

Table 5-S2. Results for the sulforhodamine B (SRB) assay for protein content for cells exposed to different concentrations of the A&MS-Fe in-house standard, in the presence of 600 µM of ascorbic acid.

Fe concentration	Absorbance			Average	Blank corrected	%
1 mg L^{-1}	2.742	2.725	2.920	2.796	2.745	110
5 mg L^{-1}	2.733	2.626	2.789	2.716	2.665	107
10 mg L^{-1}	2.818	2.915	2.710	2.814	2.763	111
15 mg L^{-1}	2.774	2.736	2.686	2.732	2.681	108
20 mg L^{-1}	2.847	2.617	2.549	2.671	2.620	105
Blank	2.648	2.545	2.487	2.543	2.492	100
Blank	2.569	2.493	2.518			
30 mg L^{-1}	2.725	2.763	2.764	2.751	2.700	108
40 mg L^{-1}	2.782	2.693	2.677	2.717	2.666	107
50 mg L^{-1}	2.787	2.518	2.694	2.666	2.615	105
plate blank	0.051	0.049	0.052	0.051		

CHAPTER 6

IRON ISOTOPIC COMPOSITION OF AGE-SEPARATED ERYTHROCYTES

6.1 INTRODUCTION

Iron is an essential micronutrient with a unique pathway within the human body. On the one hand, iron is a component of the heme-group in hemoglobin and of iron-sulfur proteins which are required for numerous biological processes.[1] On the other hand, iron is able to catalyze redox reactions generating toxic radicals that are harmful to human cells. Dietary iron is not readily absorbed due to its insolubility at intestinal pH and by its precipitation and/or chelation by many food compounds (*e.g.*, phytates). There are no specific mechanisms for iron excretion from the body. Loss of iron typically occurs through bleeding and normal sloughing of intestinal epithelial cells, where it is retained under the form of ferritin when body iron stores are elevated.

The greatest need for iron mobilization in the body is the erythropoiesis. About 70% of the iron in an adult human body is found under the form of heme in hemoglobin in the red blood cells (RBCs). Although ~25 mg of iron is required per day for hemoglobin production and erythropoiesis, only 1 to 2 mg is absorbed in the gut per day. Therefore, the majority of iron used for the RBC formation comes from iron recycled from the senescent red blood cells by macrophages.[1,2]

Erythropoiesis is a continuous process of proliferation and differentiation which begins from the hematopoietic stem cell and ends with the erythrocyte (red blood cell).[3] Human RBCs, after differentiating from erythroblasts produced in the bone marrow, are released into the blood circulation. A normal RBC progresses through several stages in the circulation, including a short period as a reticulocyte, a long period as a mature RBC, and most probably, a short period at a senescent state[4], after which it is phagocytized by macrophages.[5] On average, in a healthy subject, erythrocytes have a life span of about 120 ± 15 days (~ 117 days in men and ~106 days in women), however, this value may vary between 70 and 140 days.[6] The limited lifespan of RBCs may be due to a variety of age-dependent changes, including biochemical, physical and immunological alterations.[7] However, the molecular mechanism, as well as the signaling pathways of regulation involved into lifespan of RBCs are still unknown. During their life, erythrocytes undergo multiple changes, which affect the properties of the cell directly, such as an increase in the hemoglobin concentration, a moderate elevation in the Na^+ concentration and a decrease in the levels of K^+ and sialic acid, and a decrease in diameter and corpuscular volume due to the release of membrane proteins, all of which result in a gradually increasing cellular density of erytrocytes.[7–10]

Many methods have been reported for the separation of erythrocytes based on age-dependent density changes.[8,11] The separation of RBC according to their density can be achieved by simple centrifugation of RBCs with an angle-head rotor[12] or by using a mixture of water-insoluble compounds with well-defined density ranges.[11,13] The isolated erythrocyte fractions correspond to age ranges.[8,11,14] The separation of the RBCs by centrifugation alone does not provide the resolution achieved using a mixture of phthalate esters, however the latter method provides only two fractions per centrifugation.[8] The methodologies using Stractan (arabinogalactan) and/or Percoll (colloidal silica particles coated with polyvinylpyrrolidone) gradients provide an improved migration of the RBC according to their actual density.[15–18] Besides density separation, aging RBCs can be also separated by size, using counterflow centrifugation (elutriation).[19]

While transferrin-bound iron represents the iron transport compartment, erythrocyte iron represents the Hb-bound iron, which provides information on the functional iron compartment. A clear link has been established between an individual's iron status and the isotopic composition of the iron in human blood and serum.[20–22] The intestinal absorption and transfer of iron from the blood into the liver (for storage purposes) seem to be the main sources of Fe isotopic fractionation.[23,24] The goal of this pilot study was to evaluate the isotopic variations of iron in density-separated fractions of erythrocytes and the potential effect of *in vivo* erythrocyte aging on the Hb-bound iron isotopic composition. For this purpose, isotopic analysis was performed *via* multi-collector inductively coupled plasma mass spectrometry (MC-ICP-MS).

6.2 EXPERIMENTAL

6.2.1 Materials and reagents

Ultrapure water (resistivity ≥ 18.2 MΩ cm) was obtained from a Milli-Q Element water purification system (Millipore, France). *Pro analysis* grade 14 M nitric acid (Pro-Labo, Belgium) was further purified by sub-boiling distillation in PFA equipment (PicoTrace, Germany). *Optima* grade 12 M hydrochloric acid used in the chromatographic separation was obtained from Fisher Chemicals (UK). Ultrapure 9.8 M hydrogen peroxide used for sample preparation was acquired from Sigma-Aldrich (Belgium). Dibutyl phthalate (99%,

ρ = 1.043 g mL^{-1}) and dimethyl phthalate (99%, ρ = 1.190 g mL^{-1}) were purchased from Janssen Chimica (Belgium).

The Fe isotopic reference material IRMM-014 (Institute for Reference Materials and Measurements, IRMM, Belgium) was used for external correction in a standard-sample bracketing approach. The elemental Fe standard solution, further referred to as A&MS-Fe, (Inorganic Ventures, The Netherlands; lot D2-FE03110), previously characterized isotopically[22], was used as an in-house standard to monitor the quality of the isotope ratio measurements. Single-element standard solutions used for quantification purposes and Ni single-element standard solution (lot G2-Nl02086), used as an internal standard for correction for instrumental mass discrimination, were prepared from commercially available 1 g L^{-1} stock solutions (Inorganic Ventures, The Netherland).

AG MP-1 strong anion exchange resin (100-200 mesh) purchased from Bio-Rad (CA, USA) was used for Fe chromatographic isolation.

6.2.2 Samples and sample preparation

Whole blood samples of supposedly healthy individuals (1 female of 29 years and 1 male of 45 years) were obtained from the Ghent University Hospital (Belgium). Ethical approval was obtained for this research from an independent commission connected to the Ghent University Hospital.

Venous blood was sampled by venipuncture in EDTA vacutainer tubes suitable for trace element analysis and immediately centrifuged (3000 rpm for 10 min at 4°C). The supernatant plasma and leukocyte-rich buffy coat were gently aspirated using a Pasteur pipette. Part of the plasma was kept in a pre-cleaned 15 mL metal-free tube for further centrifugation and the rest was discarded. The total volume whole blood occupied by the erythrocytes was approximately 45% for each sample.

An aliquot of 50 µL of erythrocytes obtained from each individual was placed into a pre-cleaned Teflon Savillex® beakers for further acid digestion and used as a control sample (isotopic composition of the total erythrocyte fraction). The erythrocytes were separated

according to their density using two different methods (Fig. 6-1): by direct high-speed centrifugation (Method A) and by using a mixture of phthalates (Method B).

Method A of erythrocyte separation was based on simple centrifugation. The erythrocyte cells were re-suspended in plasma and this mixture was subjected to centrifugation in an angled rotor (to facilitate circulation of the tube content) as first described by Murphy.[12] After centrifugation at 4°C and separation of the buffy coat, as described above, the cells were re-suspended in plasma a second time. After a second centrifugation, the plasma and leukocyte-rich buffy coat were removed. The 1 mL of cells thus obtained were placed in two pre-cleaned 2 mL Eppendorf tubes (Eppendorf AG, Germany, lot E163631P) as analytical replicates. Separation was accomplished by centrifuging the tubes for 15 min at room temperature (10000 rcf, Eppendorf 5415D Centrifuge, Eppendorf AG, Germany). The remaining plasma was carefully aspirated and discarded, and the target fractions were carefully removed. The fractions were taken as the top 10% (v/v) (young cells) and bottom 10% (v/v) (senescent cells), while the remainder was considered as middle aged cells.

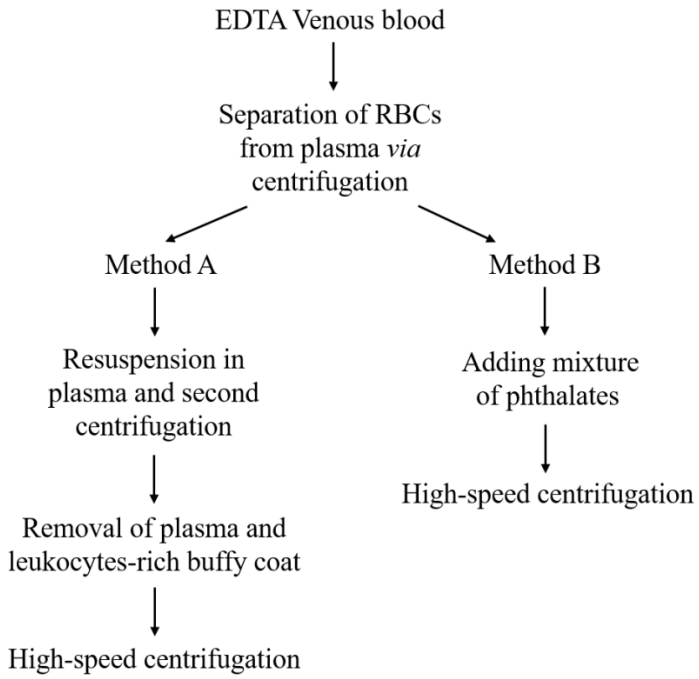

Fig. 6-1 A schematic illustration of the methods used for RBCs separation according to their density.

Method B was based on erythrocyte separation according to their density using phthalate esters as separation solutions.[8,11,14] Phthalate oil mixtures of well-defined density were prepared by mixing two phthalate eaters, dibutyl phthalate and dimethyl phthalate, to achieve

densities of 1.094 and 1.110 g mL^{-1} at 20°C for separation of young and senescent cells, respectively. The specific gravities were chosen according to previous works.[8,14,25] 0.5 mL of phthalate mixture with a specific gravity was added to 1 mL of erythrocytes and the mixture was centrifuged for 10 min at room temperature (10000 rcf, Eppendorf 5415D Centrifuge, Eppendorf AG, Germany). The target fractions were carefully pipetted from above or under the phthalate mixture layer. In Fig. 6-2, the separated senescent (bottom fraction) and young (top fraction) erythrocyte fractions are shown.

The separated fractions (~20-50 µL) and control samples were placed in Savillex® PFA beakers and digested at 110 ºC overnight (~16 h) using 2 mL of 14 M HNO_3 and 500 µL of 9.8 M H_2O_2. The digests obtained were evaporated to dryness and then re-dissolved in 500 µL of 6 M HCl + 0.001% H_2O_2 for chromatographic isolation of Fe.

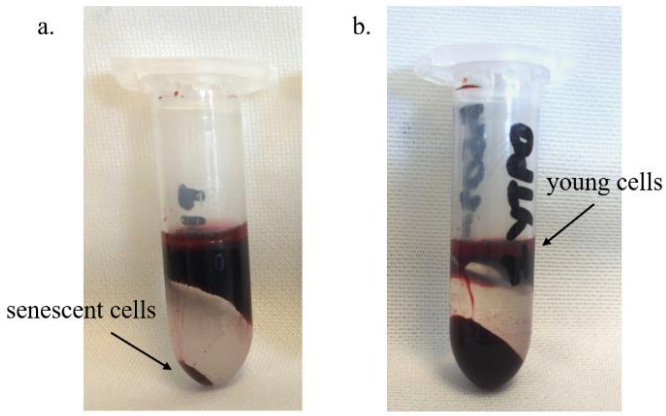

Fig. 6-2 Separated fractions of senescent (a) and young (b) erythrocytes using the mixture of phthalates with specific densities of 1.110 and 1.094 g mL^{-1} at room temperature, respectively.

The chromatographic separation was performed according to Anoshkina *et al.*[26] In brief, 1 mL pipette tips were filled with 0.5 mL of AG MP-1 (100-200 mesh) strong anion exchange resin. A piece of cotton was placed as bed support and as stopper. The resin was pre-cleaned with, subsequently, 500 µL of 7 M HNO_3, 2 mL of Milli-Q water, 2 mL of 0.7 M HNO_3 and 2 mL of Milli-Q water and conditioned with 4 mL of 6 M HCl + 0.001% H_2O_2. After sample loading, the matrix components were eluted from the column in two steps, firstly with 2 mL of 9 M HCl and secondly with 5 mL of 6 M HCl + 0.001% H_2O_2. The Fe fraction was then eluted with 6 mL of 1 M HCl and collected in a 15 mL Teflon Savillex® beaker. The purified Fe fraction was evaporated to dryness at 90 ºC to remove residual chlorides and re-dissolved in concentrated HNO_3. This procedure was repeated twice. The final residue was re-dissolved

in 500 µL of 0.42 M HNO_3. An in-house A&MS-Fe standard and procedural blank, treated in the same way as the samples, were included in each batch of samples. The separation of erythrocytes was carried out in the laboratory of the Department of Clinical Biology, Microbiology and Immunology at the Ghent University Hospital and all further sample manipulations were carried out in a class-10 clean room at the Department of Analytical Chemistry of Ghent University.

6.2.3 Instrumentation and measurements

A Thermo Scientific Neptune MC-ICP-MS instrument (Germany) equipped with a large dry interface pump (130 m^3 h^{-1} pumping speed) and high-transmission 'jet' Ni interface cones ('jet' sampling cone and X-type skimmer cone) was used for Fe isotope ratio measurements. A PFA concentric nebulizer (100 µL min^{-1}) mounted onto a double spray chamber with cyclonic and Scott-type sub-units was used for sample introduction into the plasma. Measurements were performed at medium mass resolution (pseudo mass resolution[27]), in static collection mode, using six Faraday collectors connected to 10^{11} Ω amplifiers. Instrument settings and data acquisition parameters are shown in Table 6-1 (A). Ni was used as an internal standard at the same concentration level as the target element (300 µg L^{-1}). The in-house A&MS-Fe isotopic standard solution was included in the sequence after each 5 samples to check quality of the isotope ratio measurements. All solutions (in-house A&MS-Fe standard and samples) were measured in duplicate.

The isotopic composition of the samples is expressed in delta notation (δ^{56}Fe and δ^{57}Fe, ‰) relative to the reference material IRMM-014 and calculated as follows (eqn. (6-1)), where *x* is 56 or 57:

$$\delta^{x}Fe_{sample} = \left(\frac{{}^{x}Fe/{}^{54}Fe_{sample}}{{}^{x}Fe/{}^{54}Fe_{IRMM-014}} - 1 \right) \quad (6\text{-}1)$$

Mass bias correction was performed through a combination of internal correction with admixed Ni relying on the Russell's law (using a regression line to establish the correlation between the correction factors for Fe and Ni) and external correction in a sample-standard bracketing approach (SSB).[28,29] 2s-rejection of outliers was applied for the measured isotope ratios.

Table 6-1. Instrument settings and data acquisition parameters for (A) the Neptune MC-ICP-MS instrument and (B) the Element XR SF-ICP-MS instrument.

A. MC-ICP-MS Neptune	
RF power (W)	1275
Guard electrode	Connected
Sample and skimmer cones	Jet sampler and X-type skimmer, Ni, 1.1 and 0.8 mm orifice diameter, respectively
Lens settings	Optimized for maximum Fe^+ signal intensity
Ar flow rates (L min^{-1}):	
plasma gas	15
auxiliary gas	0.75
nebulizer gas	0.9-1.0
Sample uptake rate (μL min^{-1})	100
Resolution mode	Medium (pseudo)
Acquisition mode	Static; multi-collection
Number of blocks	9
Number of cycles	5
Integration time (s)	4.194
Cup configuration	L4: ^{54}Fe; L2: ^{56}Fe; L1: ^{57}Fe; C: ^{58}(Fe + Ni); H1: ^{60}Ni; H3: ^{62}Ni
B. SF-ICP-MS Element XR	
RF power (W)	1250
Guard electrode	Connected
Sample and skimmer cones	Ni, 1.1 mm and 0.8 mm orifice diameter
Lens settings	Optimized for maximum Fe^+ signal intensity
Ar flow rates (L min^{-1}):	
plasma gas	15
auxiliary gas	0.8-0.9
nebulizer gas	1.0-1.1
Sample uptake rate (μL min^{-1})	200
Resolution mode	Low, medium, high
Nuclides monitored	^{23}Na (LR), ^{44}Ca (MR), $^{54,56,57,58}Fe$ (MR), ^{52}Cr (MR), ^{39}K (HR), $^{63,65}Cu$ (MR), $^{64,66}Zn$ (MR), ^{60}Ni (MR), ^{69}Ga (LR, MR, HR)
Acquisition mode	E-scan
Dwell time per point (ms)	10
Point per peak	20
Number of runs	5
Number of passes	5

A Thermo Scientific (Germany) Element XR single-collector sector-field ICP-MS instrument was used for determination of element concentrations. For the introduction of sample into the

plasma, a 200 μL min^{-1} quartz concentric nebulizer mounted onto a cyclonic spray chamber was used. The instrument settings and data acquisition parameters used are summarized in Table 6-1 (B). External calibration was performed and Ga was used as an internal standard to correct for matrix effects and instrument instability.

6.3 RESULTS AND DISCUSSION

6.3.1 Analytical method validation

Sample preparation

The sample preparation procedure of the biological samples entailed an acid digestion and further Fe isolation using anion exchange chromatography to minimize spectral and non-spectral interferences. A blank and in-house A&MS-Fe isotopic standard were included in each set of samples. Element determinations were carried out using SF-ICP-MS in all samples and standards before and after the isolation procedure. The recoveries of Fe were quantitative in all cases (96 ± 5 %, n = 23), ensuring absence of on-column isotope fractionation. The efficiency of the anion exchange chromatography procedure was evaluated by monitoring matrix elements, such as Na, Ca, K, Cr in each fraction after isolation. In all cases, the concentrations were lower than 0.5 mg L^{-1} for major matrix elements such as Na and K and negligible compared to the Fe concentration in erythrocytes (~ 800 mg L^{-1}). The use of medium resolution allows to avoid any effect of the occurrence of Ar-containing polyatomic ions on the Fe^{+} ion signals (spectral overlap).

The iron content in the phthalate esters used for the separation of the erythrocytes was evaluated. The contribution was 72 μg L^{-1} and 79 μg L^{-1} from the dimethyl and dibutyl phthalates, respectively. This contribution of iron was not significant relative to the iron amount in the erythrocytes.

The contribution of the procedural blanks, treated in the same way as the samples, was less than 0.1%. As a result, the maximum bias observed between the results with and without blank correction was 0.007 and 0.014 ‰ for $\delta^{56}Fe$ and $\delta^{57}Fe$, respectively. This maximum difference was within two times the standard deviation and thus, no blank correction was done before mass bias correction.

Isotope ratio measurements

The repeatability and reproducibility of the isotope ratio measurements by MC-ICP-MS were evaluated using the A&MS-Fe in-house standard. The repeatability, expressed as two times the standard deviation for 14 replicates of the A&MS-Fe in-house standard within one measurement session, was 0.06 and 0.10‰ for δ^{56}Fe and δ^{57}Fe, respectively. The results obtained during a 22 h measurement session fall on the normal mass-dependent fractionation line (δ^{57}Fe = 1.48 δ^{56}Fe), demonstrating absence of spectral overlap.

The reproducibility, expressed as two times the standard deviation for the A&MS-Fe in-house standard over a period of one year (as intermediate precision), was 0.06 and 0.07‰ for δ^{56}Fe and δ^{57}Fe (n = 116), respectively, and for a period of three years (as a long term precision) was 0.07‰ and 0.12‰ for δ^{56}Fe and δ^{57}Fe (n = 256), respectively.

Table 6-2. Fe isotopic composition of cell fractions obtained using centrifugation only (method A) and using the separation procedure with phthalate esters (method B). Delta Fe values are expressed as the average of two measurement replicates (in ‰). The absolute deviation between the two measurement values has also been included in the table.

Sample			δ^{56}Fe	Absolute deviation	δ^{57}Fe	Absolute deviation
Female control			-2.47	0.03	-3.58	0.04
Male control			-2.66	0.03	-3.93	0.05
Method A						
Female	**Aliquot 1**	young	-2.49	0.005	-3.66	0.01
		middle	-2.48	0.005	-3.69	0.01
		senescent	-2.48	0.03	-3.64	0.005
	Aliquot 2	young	-2.46	0.02	-3.63	0.02
		middle	-2.53	0.015	-3.66	0.02
		senescent	-2.49	0.015	-3.68	0.01
Method B						
Female	**Aliquot 1**	young	-2.46	0.02	-3.63	0.04
		senescent	-2.46	0.01	-3.61	0.02
	Aliquot 2	young	-2.51	0.02	-3.65	0.05
		senescent	-2.44	0.005	-3.57	0.03
	Aliquot 3	young	-2.47	0.03	-3.60	0.015
		senescent	-2.43	0.02	-3.56	0.02
Male	**Aliquot 1**	young	-2.60	0.015	-3.84	0.03
		senescent	-2.67	0.01	-3.90	0.02

6.3.2 Iron isotopic composition of erythrocytes

On average, the senescent cell fractions show an Fe concentration that is 8% higher than those of the young cells. The average Fe isotopic composition of erythrocytes acquired using the two separation methods and control samples are presented in Table 6-2.

A graphical representation of the Fe isotopic composition in the different cell fractions acquired from one subject (female) is shown in Fig. 6-3. The δ^{56}Fe value of the control sample from the female subject (overall erythrocyte Fe isotopic composition) was -2.47 ± 0.06 ‰ (two times the standard deviation). The average δ^{56}Fe value and two times the standard deviation obtained for the young and senescent cell fractions were -2.48 ± 0.03 and -2.48 ± 0.01 ‰, respectively, using Method A (centrifugation only) and -2.48 ± 0.05 and -2.44 ± 0.03 ‰, respectively, using Method B (phthalates mixture). Two-way ANOVA at a 5% significance level (JMP statistical software, version 12.1.0, SAS Institute Inc., Cary, NC, USA) showed that there was no significant difference, neither between the values for the young and the senescent fractions of RBC nor as a function of the separation method used.

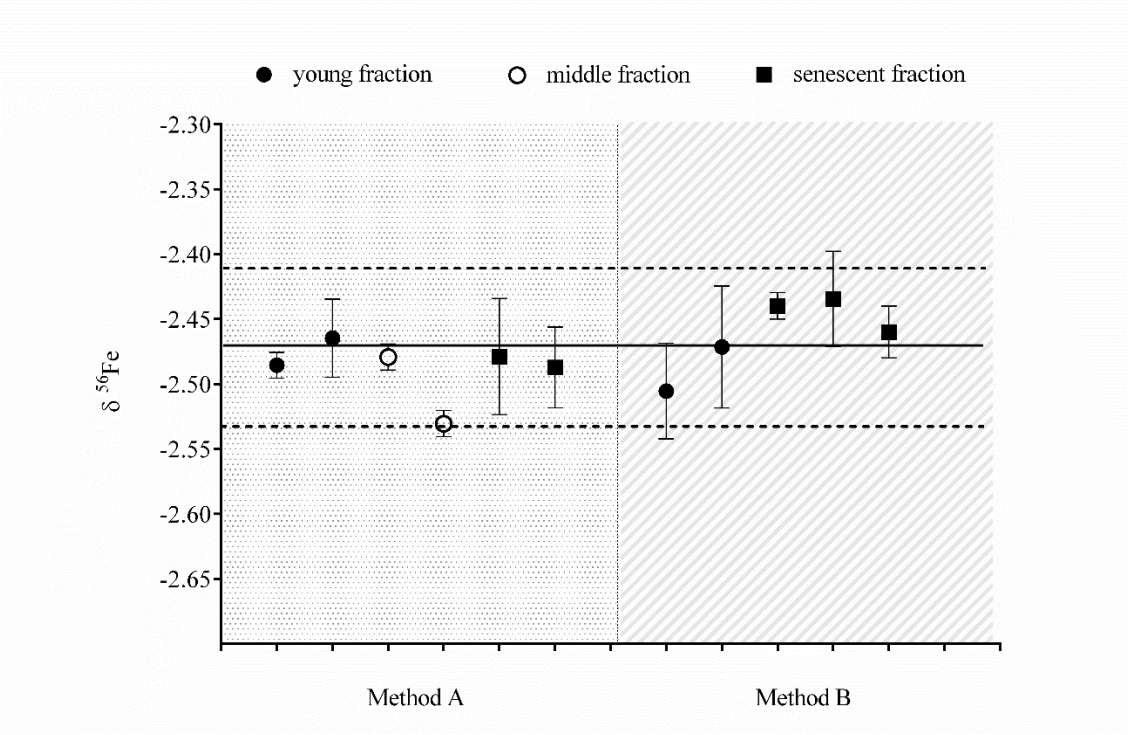

Fig. 6-3 Fe isotopic composition of erythrocyte fractions obtained from one individual and separated according to cell density using centrifugation only (method A) and using the separation procedure with phthalate esters (method B). The solid line indicates the isotopic composition of the total erythrocyte fraction (control sample) and the dashed lines indicate two times the corresponding standard deviation.

In Fig. 6-4, a three-isotope plot of iron ($\delta^{57}Fe$ *vs* $\delta^{56}Fe$) is presented for the RBC fractions obtained. All data points define a single mass fractionation curve, the slope of which matches the theoretical value (1.48 according to exponential law), therefore demonstrating absence of spectral overlap.

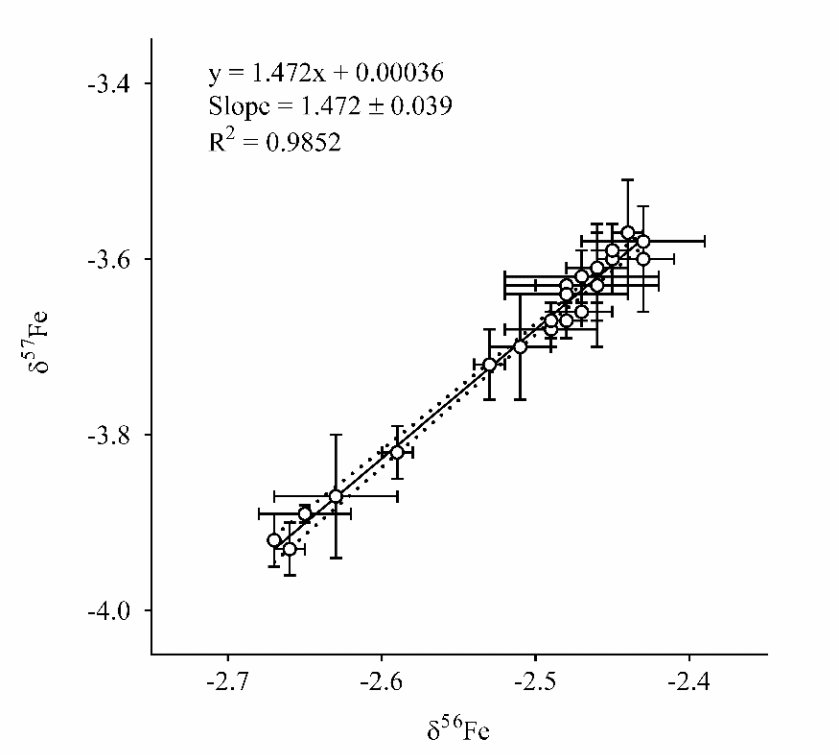

Fig. 6-4 Three-isotope plot constructed based on measurement results for separated RBCs fractions. The solid line indicates the linear regression line and the dashed lines correspond to 95% confidence interval for the line.

These results obtained in this preliminary study suggest that the Fe isotopic composition of erythrocytes does not change within their lifespan. Therefore, the main source of isotopic fractionation is coming from the intestinal iron absorption, with preferential uptake of lighter iron isotopes, and from the transfer of iron under the form of ferritin in liver hepatocytes, which are known to be enriched with heavier iron isotopes. This finding is in concordance with the results of previous studies on the iron isotopic composition of whole blood/serum.[22,30]

6.4 CONCLUSIONS

In this preliminary study, the erythrocytes were separated according to their density using two methods, based on centrifugation only and on using a mixture of phthalates. The results obtained for the young and senescent red blood cells suggest absence of differences in the Fe isotopic composition between them. Thus, the *in vivo* aging process of the enterocytes does seem to influence the Fe isotopic composition of whole blood. This supports the hypothesis that Fe fractionation mainly occurs during intestinal absorption and during the transfer of iron to the liver as main iron storage location, under the form of ferritin in the liver hepatocytes. All Fe isotope ratio data plot on a single mass-fractionation line, indicating the suitability of the analytical method.

6.5 REFERENCES

1. Korolnek, T. & Hamza, I. Macrophages and iron trafficking at the birth and death of red cells. *Blood* **125,** 2893–2897 (2015).
2. Papanikolaou, G. & Pantopoulos, K. Iron metabolism and toxicity. *Toxicol. Appl. Pharmacol.* **202,** 199–211 (2005).
3. Koury, M. J. & Ponka, P. New insights into erythropoiesis: The Roles of Folate, Vitamin B12, and Iron. *Annu. Rev. Nutr.* **24,** 105–131 (2004).
4. Cohen, R. M. *et al.* Red cell life span heterogeneity in hematologically normal people is sufficient to alter HbA1c. *Blood* **112,** 4284–91 (2008).
5. Kruse, A., Uehlinger, D. E., Gotch, F., Kotanko, P. & Levin, N. W. Red blood cell lifespan, erythropoiesis and hemoglobin control. *Contrib. Nephrol.* **161,** 247–54 (2008).
6. Franco, R. S. Measurement of red cell lifespan and aging. *Transfus. Med. Hemother.* **9,** 302–307 (2012).
7. Linderkamp, O., Friederichs, E., Boehler, T. & Ludwig, A. Age dependency of red blood cell deformability and density: studies in transient erythroblastopenia of childhood. *Br. J. Haematol.* **83,** 125–9 (1993).
8. Cohen, N. S., Ekholm, J. E., Luthra, M. G. & Hanahan, D. J. Biochemical characterization of density-separated human erythrocytes. *BBA - Biomembr.* **419,** 229–242 (1976).
9. Högman, C. F. & Meryman, H. T. Storage parameters affecting red blood cell survival and function after transfusion. *Transfus. Med. Rev.* **13,** 275–96 (1999).
10. Lutz, H. U. & Bogdanova, A. Mechanisms tagging senescent red blood cells for clearance in healthy humans. *Front. Physiol.* **4,** 387 (2013).
11. Danon, D. & Marikovsky, V. Determination of density distribution of red blood cells population. *J. Lab. Clin. Med.* **64,** 668–74 (1964).

12. Murphy, J. R. Influence of temperature and method of centrifugation on the separation of erythrocytes. *J. Lab. Clin. Med.* **82,** 334–41 (1973).

13. Parker, J. C. Dog red blood cells. Adjustment of density in vivo. *J. Gen. Physiol.* **61,** 146–57 (1973).

14. Bartolucci, P. *et al.* Erythrocyte density in sickle cell syndromes is associated with specific clinical manifestations and hemolysis. *Blood* **120,** 3136–3141 (2012).

15. Rennie, C. M., Thompson, S., Parker, A. C. & Maddy, A. Human erythrocyte fractionation in 'percoll' density gradients. *Clin. Chim. Acta* **98,** 119–125 (1979).

16. Fabry, M. *et al.* Dense cells in sickle cell anemia: the effects of gene interaction. *Blood* **64,** (1984).

17. Clark, M. R. Selected ionic and metabolic characteristics of human red cell populations separated on stractan density gradients. *Prog. Clin. Biol. Res.* **195,** 381–8 (1985).

18. Lutz, H. U., Stammler, P., Fasler, S., Ingold, M. & Fehr, J. Density separation of human red blood cells on self forming PercollR gradients: correlation with cell age. *BBA - Gen. Subj.* **1116,** 1–10 (1992).

19. Bosch, F. H. *et al.* Characteristics of red blood cell populations fractionated with a combination of counterflow centrifugation and Percoll separation. *Blood* **79,** 254–60 (1992).

20. Stenberg, A. *et al.* Measurement of iron and zinc isotopes in human whole blood: preliminary application to the study of HFE genotypes. *J. Trace Elem. Med. Biol.* **19,** 55–60 (2005).

21. Krayenbuehl, P.-A., Walczyk, T., Schoenberg, R., von Blanckenburg, F. & Schulthess, G. Hereditary hemochromatosis is reflected in the iron isotope composition of blood. *Blood* **105,** 3812–3816 (2005).

22. Van Heghe, L., Delanghe, J., Van Vlierberghe, H. & Vanhaecke, F. The relationship between the iron isotopic composition of human whole blood and iron status parameters. *Metallomics* **5,** 1503–1509 (2013).

23. Walczyk, T. & von Blanckenburg, F. Natural iron isotope variations in human blood. *Science* **295,** 2065–6 (2002).

24. Hotz, K., Augsburger, H. & Walczyk, T. Isotopic signatures of iron in body tissues as a potential biomarker for iron metabolism. *J. Anal. At. Spectrom.* **26,** 1347–1353 (2011).

25. Sparrow, R. L., Healey, G., Patton, K. A. & Veale, M. F. Red blood cell age determines the impact of storage and leukocyte burden on cell adhesion molecules, glycophorin A and the release of annexin V. in *Transf. Apher. Sci.* **34,** 15–23 (2006).

26. Anoshkina, Y., Costas-Rodríguez, M. & Vanhaecke, F. Iron isotopic analysis of finger-prick and venous blood by multi-collector inductively coupled plasma-mass spectrometry after volumetric absorptive microsampling. *J. Anal. At. Spectrom.* **32,** 314–321 (2017).

27. Vanhaecke, F. & Moens, L. Overcoming spectral overlap in isotopic analysis via single- and multi-collector ICP-mass spectrometry. *Anal. Bioanal. Chem.* **378,** 232–240 (2004).

28. Woodhead, J. A simple method for obtaining highly accurate Pb isotope data by MC-ICP-MS. *J. Anal. At. Spectrom.* **17,** 1381–1385 (2002).

29. Baxter, D. C., Rodushkin, I., Engström, E. & Malinovsky, D. Revised exponential

model for mass bias correction using an internal standard for isotope abundance ratio measurements by multi-collector inductively coupled plasma mass spectrometry. *J. Anal. At. Spectrom.* **21,** 427–430 (2006).

30. Hotz, K. & Walczyk, T. Natural iron isotopic composition of blood is an indicator of dietary iron absorption efficiency in humans. *J. Biol. Inorg. Chem.* **18,** 1–7 (2013).

CHAPTER 7

IRON ISOTOPIC COMPOSITION OF BLOOD SERUM IN ANEMIA OF CHRONIC KIDNEY DISEASE

Based on publication:

Yulia Anoshkina, Marta Costas-Rodríguez, Marijn Speeckaert, Wim Van Biesen, Joris Delanghe and Frank Vanhaecke, Metallomics, 2017, Vol. 9, Issue 5, P. 517-524

7.1 ABSTRACT

Chronic kidney disease (CKD) is a general term for disorders that affect the structure and function of the kidneys. Iron deficiency (ID) and anemia occur in the vast majority of CKD patients, most of whom are elderly. However, establishing the cause of anemia in CKD and therefore, making an informed decision concerning the corresponding therapeutic treatment is still a challenge. High-precision Fe isotopic analysis of blood serum samples of CKD patients with and without ID/anemia was explored *via* multi-collector inductively coupled plasma-mass spectrometry (MC-ICP-MS) for such purpose. Patients with CKD and/or iron disorders showed a heavier serum Fe isotopic composition than did controls. Many clinical parameters used for diagnosis and follow-up of anemia correlated significantly with the serum Fe isotopic composition. In contrast, no relation was observed between the serum Fe isotopic composition and the estimated glomerular filtration rate as a measure of kidney function. Among the CKD patients, the serum Fe isotopic composition was substantially heavier in the occurrence of ID anemia, while erythropoietin-related anemia did not exert this effect. The Fe isotopic composition can thus be useful for distinguishing these different types of anemia in CKD patients, *i.e.* ID anemia *vs* erythropoietin-related anemia.

7.2 INTRODUCTION

Impaired kidney function can occur due to (i) a kidney injury or acute renal failure caused by dehydration, extensive blood loss and/or the use of medicines or (ii) long-term damage of the kidneys (chronic kidney disease, CKD) caused by a variety of reasons.[1] CKD is generally associated with multiple comorbid conditions, such as anemia, cardiovascular diseases, mineral misbalances, diabetes mellitus, and a disturbed bone metabolism. Variations in the CKD expression depend on its cause and pathology, severity and rate of progression.[2] At an early stage, the disease is often asymptomatic and detected during examination for other purposes only.[3] The prevalence of CKD is considerably higher in the elderly; more than 30% of the end stage renal disease patients are 70 years or older.[3–7] The combination of the deteriorating overall health condition in the old age and the silent condition of CKD complicates the diagnosis and determination of the cause(s) of the disease. The definition of CKD is typically based on the presence of kidney damage, as detected by an increased urinary albumin excretion (> 30 mg per day), and a decreased kidney function during 3 or more months, as established by monitoring the estimated glomerular filtration rate (eGFR).[2] The eGFR is calculated using the Chronic Kidney Disease Epidemiology Collaboration (CKD-EPI) equation, which is based on the serum creatinine level, adjusted for gender and race and expressed in mL min^{-1} per 1.73 m^2.[8] Significant kidney dysfunction may be present despite a normal serum creatinine level because the latter can also be affected by many factors that are independent of kidney injury or kidney function (such as age, gender, race, muscle mass, nutritional status, infection and use of some types of medication).[9–11] Therefore, the eGFR is considered a more reliable clinical parameter for establishing the stage of CKD. According to the guidelines of The Kidney Disease: Improving Global Outcomes (KDIGO) organization, the stages of CKD based on eGFR values are: ≥ 90 (stage 1), 60-89 (stage 2), 45-59 (stage 3a), 30-44 (stage 3b), 15-29 (stage 4), and < 15 mL min^{-1} per 1.73 m^2 (stage 5).[12]

The vast majority of CKD patients develop iron deficiency (ID) and anemia.[13] ID can occur as a result of malnutrition (decreased dietary iron intake), malabsorption, blood loss during hemodialysis, frequent blood sampling, gastrointestinal bleeding, multiple vascular access surgeries, hepcidin fluctuations, *etc,*[14] resulting in a reduction of the serum iron concentration and transferrin saturation (TSAT), while the erythroid iron level is still preserved.[13,15] Persistent ID leads to iron deficiency anemia (IDA) as a more severe condition, characterized by a reduction in total body iron content and in erythrocyte production.[13,15,16] IDA can be

caused by true iron deficiency, *e.g.*, in cases with blood loss from hemodialysis or blood sampling, low nutritional iron content or malabsorption.[16,17] However, IDA can also be caused by inflammation, where iron stores can be normal, but the iron is not available for erythropoiesis. This situation is termed functional ID, which is a major component of anemia of chronic disease (ACD).[18] Another common cause of anemia in CKD is the impaired production of erythropoietin (EPO) as a result of kidney damage and/or decreased kidney function and, as consequence, a decreased production of RBC precursors in the bone marrow, leading to a reduced level of erythroid iron.[5,13,15,16,19] Patients with this type of anemia (sometimes also termed non-IDA) show a normal iron store and supply. The diagnostic criteria for ID and anemia vary between published studies.[13,17,20–26] Based on a compilation of data available in the literature, the diagnostic cut-off value for anemia used in this study was established at $\leq$ 12.5 g dL^{-1} for hemoglobin (Hb) for males, while that for ID was a TSAT $\leq$ 20%.

The presence of ID and anemia aggravates the progression of kidney disease[16] and specific treatments are required depending on the underlying causes. However, the determination of the cause of anemia in CKD and thus, making adequate decisions concerning the patient's treatment, is still a challenge. In general, routine diagnostic tests have low specificity. For instance, the level of ferritin, traditionally used as a measure of the iron store, increases with age (or more accurately with the iron accumulation) and as a result of chronic inflammatory disorders.[27] About 50% of the patients following EPO-therapy do not reach a normal Hb level due to the presence of ID and/or functional ID.[12]

Recently, it has been demonstrated that the Fe isotopic composition of whole blood can be useful to assess a healthy individual's iron status.[28–30] In addition, patients suffering from hereditary hemochromatosis (HH), showed a heavier whole blood Fe isotopic composition than did a gender-matched reference population,[28,29,31] while patients suffering from ACD showed a lighter whole blood Fe isotopic composition.[29] The isotopic analysis of blood serum, wherein transferrin is the main carrier of iron, is interesting due to its higher iron turnover rate (< 5 days) than that of whole blood erythrocytes (~120 days).

This study investigated the potential use of the serum Fe isotopic composition for revealing iron metabolism changes in CKD patients and for distinguishing between different types of anemia, such as IDA and EPO-related anemia. High-precision Fe isotopic analysis was accomplished *via* multi-collector inductively coupled plasma-mass spectrometry (MC-ICP-

MS) after acid digestion and chromatographic isolation of the target element. The relation between the serum Fe isotopic composition and relevant clinical parameters used for diagnosis and monitoring of CKD and iron disorders was evaluated.

7.3 EXPERIMENTAL

7.3.1 Materials and reagents

Ultrapure water (resistivity ≥ 18.2 MΩ cm) was obtained from a Milli-Q Element water purification system (Millipore, France). *Pro analysis* grade 14 M nitric acid (Pro-Labo, Belgium) was further purified by sub-boiling distillation in PFA equipment (PicoTrace, Germany). *Optima* grade 12 M hydrochloric acid used in the chromatographic separation was obtained from Fisher Chemicals (UK). Ultrapure 9.8 M hydrogen peroxide used for sample preparation was acquired from Sigma-Aldrich (Belgium).

The Fe isotopic reference material IRMM-014 (Institute for Reference Materials and Measurements, IRMM, Belgium) was used for instrumental mass discrimination in a standard-sample bracketing approach. The elemental Fe standard solution (Inorganic Ventures, The Netherlands; lot D2-FE03110), previously characterized isotopically,[32] was used as an in-house reference to monitor the quality of the isotope ratio measurements. Single-element standard stock solutions (Inorganic Ventures) used for quantification purposes and Ni single-element standard solution (Inorganic Ventures, The Netherlands; lot G2-Nl02086), used as an internal standard for correction of instrumental mass discrimination, were prepared from commercially available 1 g L^{-1} stock solutions. Seronorm™ Trace Elements Serum L-1 reference material (SERO AS, Norway, lot 0903106) was used for method validation.

Polypropylene chromatographic columns filled with AG MP-1 strong anion exchange resin (100–200 mesh, chloride form) purchased from Bio-Rad (Belgium) were used for Fe chromatographic isolation.

7.3.2 Samples

A total of 82 serum samples from males (55-84 years), acquired from the Ghent University Hospital, were analyzed. 44 serum samples were from patients suffering from CKD before undergoing dialysis (stages 3a, 3b, 4 and 5) without chronic inflammation. Among these samples, 14 were from patients with CKD without ID or anemia, 9 from patients with CKD and ID, 10 with CKD and EPO-related anemia, and 11 from patients with CKD and IDA (Table 7-1). 6 samples were obtained from patients with only ID and 7 with IDA (no CKD). Patients with chronic inflammation (*i.e.* ACD) were not included in this study. The gender-matched reference population was composed of 25 serum samples from supposedly healthy individuals. Patients and control group did not receive EPO treatment or iron supplementation. This research project was approved by an independent commission for medical ethics connected to the Ghent University Hospital and was performed in accordance with the guidelines for good clinical practice and the statement of Helsinki, emplaced to protect volunteers participating in experiments. All individuals signed an informed consent form concerning this study.

7.3.3 Sample preparation

Venous blood was drawn between 0900 and 1000 h, allowed to clot, and centrifuged (1000 g for 10 min at room temperature). In order to avoid variations in the serum Fe isotopic composition related to dietary iron intake, all samples were collected from individuals in fasted state.[33] The supernatant serum was collected for analysis and was split into two aliquots, one for the determination of the clinical parameters (at Ghent University hospital) and another of about 500 µL for Fe isotopic analysis (at the Department of Analytical Chemistry). The main biomedical indicators of iron status and kidney function are provided in Appendix A. Samples were stored at -20 ºC in pre-cleaned Eppendorf tubes until sample preparation.

Ferritin was assayed using electrochemiluminescence immunoassay on a Roche Modular E 170 analyzer (Roche Diagnostics). Serum sTfR was assayed by fixed-time immunonephelometry on a BN II nephelometer (Siemens). Transferrin saturation was calculated from measurements of the serum iron concentration by spectrophotometry

(ferrozine method) and the serum transferrin concentration by immunoturbidimetry using commercial reagents on a Cobas 8000 analyzer (Roche Diagnostics). Assuming that two iron atoms bind to one molecule of transferrin, the serum transferrin saturation (%) was calculated according to equation 7-1[34]:

$$\left(\frac{Serum\ iron\ (\mu mol\ L^{-1})}{Serum\ transferrin\ (g\ L^{-1})}\right) \times 3.98 \qquad (7\text{-}1)$$

For isotopic analysis, the serum samples were digested in Savillex® PFA beakers using 2 mL of 14 M HNO_3 and 0.5 mL of 9.8 M H_2O_2 at 110 ºC overnight (16 h). The digest thus obtained was evaporated to dryness and the residue was re-dissolved in 5 mL of 8 M HCl + 0.001% H_2O_2 and submitted to the chromatographic isolation procedure.

Fe isolation was accomplished using a modified protocol of Maréchal *et al.*[35] and Van Heghe *et al.*[32] Bio-Rad Poly-Prep columns were filled with1 mL of AG MP-1 (100-200 mesh) strong anion exchange resin. The resin was pre-cleaned with, subsequently, 3 mL of 7 M HNO_3, 5 mL of Milli-Q water, 5 mL of 0.7 M HNO_3 and 5 mL of Milli-Q water and conditioned with 5 mL of 8 M HCl + 0.001% H_2O_2. After sample loading, the matrix was eluted with 3 mL of 8 M HCl + 0.001% H_2O_2; next, Cu was eluted with 9 mL of 5 M HCl + 0.001%H_2O_2. Finally, Fe was eluted with 7 mL of 0.7 M HNO_3 and this fraction was collected in a Teflon Savillex® beaker. The Fe fraction was evaporated to dryness at 90 ºC to remove residual chloride and re-dissolved in concentrated HNO_3. This procedure was repeated twice. The final residue was re-dissolved in 500 µL of 0.42 M HNO_3. A procedural blank, treated in the same way as the samples, was included in each batch of samples. All sample manipulations were carried out in a class-10 clean room.

7.3.4 Instrumentation and measurements

A Thermo Scientific Neptune MC-ICP-MS instrument (Germany) was used for Fe isotope ratio measurements. The sample introduction system consisted of a 100 µL min^{-1} PFA concentric nebulizer and a high-stability dual spray chamber with cyclonic and Scott-type sub-units. Medium mass resolution (pseudo mass resolution[36]) was used to be able to measure the Fe^+ signal intensities free from spectral overlap. Measurements were performed in static collection mode, using six Faraday collectors connected to 10^{11} Ω amplifiers. Instrument

settings and data acquisition parameters are shown in the Supplementary Information (Table 7-S1). Procedural blanks were measured at the beginning of the measurement session to evaluate their contribution to the Fe^+ signal intensities. An in-house Fe standard solution, previously characterized isotopically,[32] was measured every 5 samples to monitor the quality of the isotopic measurements. All solutions were doped with Ni as internal standard. The concentrations of Fe and admixed Ni were adjusted to 300 μg L^{-1} in all samples and isotopic standards. Mass bias correction relied on a combination of external correction in a sample-standard bracketing approach (SSB) and internal correction with Ni using the Baxter-revised Russell's law.[37] The isotope ratios were obtained after the 2s-rejection of outliers. The isotopic composition is expressed in delta notation (δ^{56}Fe and δ^{57}Fe, ‰) and calculated according to equation 7-2, where *x* is 56 or 57:

$$\delta^{x}Fe_{sample} = \left(\frac{{}^{x}Fe/{}^{54}Fe_{sample}}{{}^{x}Fe/{}^{54}Fe_{IRMM-014}} - 1 \right) \quad (7\text{-}2)$$

A Thermo Scientific Element XR sector field ICP-MS instrument (Germany) was used for quantitative determination of the Fe concentration of the samples for quality control purposes (see section 7.4.1). For sample introduction into the plasma, a 200 μL min^{-1} quartz concentric nebulizer mounted onto a cyclonic spray chamber was used. The instrument settings and data acquisition parameters are shown in Supplementary Information (Table 7-S1). External calibration (calibration curve) was relied on for quantification, combined with Ga as an internal standard to correct for matrix effects and instrumental instability.

7.3.5 Statistical Methods

IBM® SPSS Statistics 23 (SPSS Inc. Chicago Illinois, USA) and GraphPad Prism®(GraphPad Software Inc., CA, USA) packages for Windows were used for the statistical analysis of the data. The non-parametric Kruskal-Wallis test was used for comparison of the results obtained for the different groups of patients. Bivariate analysis was used for assessing potential correlations between the serum Fe isotopic composition and a series of clinical parameters. Multiple regression analysis was performed to identify the parameters governing the serum iron isotopic composition variability.

7.4 RESULTS AND DISCUSSION

7.4.1 Method validation

Reliable Fe isotope ratio measurements of blood serum by MC-ICP-MS require the efficient decomposition of the matrix by acid digestion, and isolation of the target element to minimize spectral and non-spectral effects. Both steps have to be performed without Fe isotope fractionation and to assure this, a quantitative Fe recovery is mandatory. In each set of samples, an in-house Fe standard, the Seronorm^{TM} Trace Elements Serum L-1 reference material and a blank were included. The quantitative determination of Fe *via* sector field ICP-MS was performed before and after the isolation procedure. The recoveries of Fe were quantitative in all cases (99 ± 5%). The presence of matrix elements, potentially interfering with the Fe isotope ratio measurements, such as Cr, Ca, and K, were determined in the purified Fe fractions. The content of these elements was negligible in all samples after chemical separation. The procedural blank was ≤ 1 % of the Fe concentration present in the serum samples. The differences between the results with and without blank correction were 0.05 and 0.07‰ for δ^{56}Fe and δ^{57}Fe, respectively and thus, no blank correction was performed.

The combined uncertainty obtained for Seronorm reference material during one year was 0.03 and 0.12‰ for δ^{56}Fe and δ^{57}Fe, respectively (n = 9). All results fall on the normal mass-dependent fractionation line ($\delta^{57}Fe = 1.48 \cdot \delta^{56}Fe$), demonstrating absence of spectral overlap.

7.4.2 Fe isotopic composition in serum samples

The blood serum samples originated from patients suffering from CKD with and without ID, IDA or EPO-related anemia, from patients with ID and IDA without CKD and from supposedly healthy individuals. Thus, 7 groups of patients were established on the basis of their clinical condition (Table 7-1). The serum Fe isotopic composition obtained for each group, expressed in delta notation and calculated against the IRMM-014 reference material, is presented in Table 7-1.

The reference population was formed by 18 aged male individuals (55-84 years) and 7 young males (~30 years) without inflammation, kidney disease and iron disorders. Since no

significant differences were observed between the aged and young cohorts (δ^{56}Fe values of -2.68 ± 0.21‰ and -2.64 ± 0.13‰, respectively), these 25 individuals were considered as reference population. This is in concordance with an earlier reported finding for whole blood samples from male individuals.[28,38] The median δ^{56}Fe value obtained for the reference population (after removal of one outlier, using the 2s-criterion) was -2.67 ± 0.20 ‰.

Table 7-1. Isotopic composition of Fe in blood serum from a reference population and from patients with CKD and/or a disorder of iron metabolism. δFe values are expressed as median ± interquartile range; *p* is the level of significance from the Kruskal-Wallis test that was used to compare each group patients to the reference population.

Diagnosis	Description	δ^{56}Fe	δ^{57}Fe	n	*p*
Reference population	eGFR > 90 mL/min/1.73 m² Hb > 12.5 g dL^{-1} 20% < TSAT < 45%	-2.67 ± 0.20	-3.90 ± 0.38	24	
CKD, no anemia, no ID	eGFR < 60 mL/min/1.73 m² Hb > 12.5 g dL^{-1} 20% < TSAT < 45%	-2.34 ± 0.35	-3.35 ± 0.56	13	0.0023
CKD, no anemia, ID	eGFR < 60 mL/min/1.73 m² Hb > 12.5 g dL^{-1} TSAT < 20%	-1.87 ± 0.52	-2.85 ± 1.04	9	0.0006
CKD, EPO-related anemia, no ID	eGFR < 60 mL/min/1.73 m² Hb < 12.5 g L^{-1} 20% < TSAT < 45%	-2.47 ± 0.37	-3.46 ± 0.58	10	0.0058
CKD, IDA	eGFR <60 mL/min/1.73 m² Hb < 12.5 g dL^{-1} TSAT < 20%	-1.36 ± 0.57	-2.13 ± 0.45	11	< 0.0001
ID (no CKD)	eGFR > 90 mL/min/1.73 m² Hb > 12.5 g dL^{-1} TSAT < 20%	-2.02 ± 0.36	-2.90 ± 0.81	5	0.0021
IDA (no CKD)	eGFR > 90 mL/min/1.73 m² Hb < 12.5 g dL^{-1} TSAT < 20%	-1.29 ± 0.67	-1.81 ± 0.78	7	< 0.0001

The median δ^{56}Fe value for the overall population of CKD patients was -2.01 ± 0.50 ‰, that is +0.66‰ higher than for the reference population. Fig. 7-1 provides box-plots for the δ^{56}Fe values of patients suffering from CKD, patients suffering from disorders of iron metabolism and a reference population. All patient groups showed a heavier Fe isotopic composition than the reference population. The δ^{56}Fe values increased (*i.e.* iron became enriched in the heavier iron isotopes) in the following order: reference population < CKD ≈ CKD + EPO-related anemia < CKD + ID ≈ ID < CKD + IDA ≈ IDA.

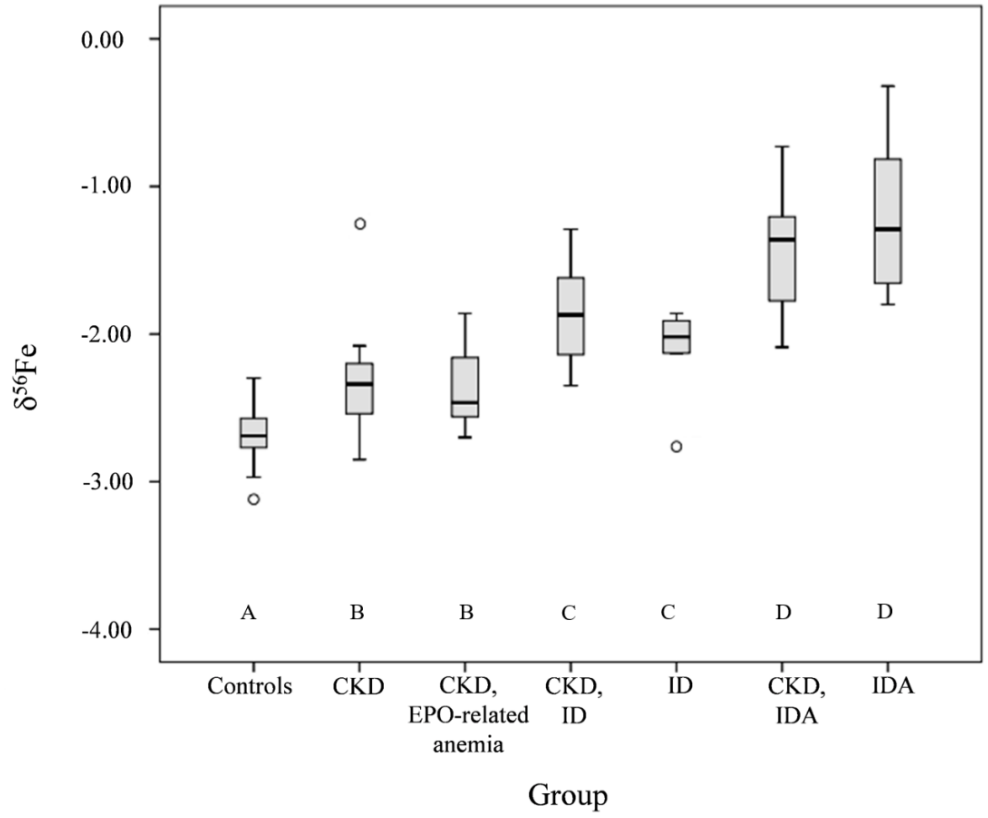

Fig. 7-1 Serum Fe isotopic composition in patients suffering from CKD and iron disorders. The box-plots compile the median, quartiles and extreme values. The box-plots are annotated with letters. When two groups were given a different letter, there is a significant difference between the corresponding δ^{56}Fe values ($p \leq 0.05$). The open circles are outliers.

As can be seen in Table 7-1, the differences between each group and the reference population were significant (Kruskal-Wallis test). Among the CKD patients, the groups with ID and IDA showed a δ^{56}Fe value higher by +0.47‰ and +0.98‰, compared to the CKD group without iron disorder. A similar shift towards a heavier serum Fe isotopic composition in the case of ID and IDA is also seen in the cohort without CKD (Fig. 7-1). The differences in the δ^{56}Fe values were +0.65‰ for ID and +1.38‰ for IDA compared to the reference population. The IDA group also provided higher δ^{56}Fe values than the ID group, as is the case in the CKD population. The heavy serum Fe isotopic composition of patients with ID and IDA is independent of the renal insufficiency, but is related to the low iron status, characterized by a depleted store of iron. This is in agreement with a previously reported finding for whole blood.[29,31] Iron deficiency in the general population is mainly caused by blood loss and/or impaired intestinal absorption of dietary iron with the subsequent reduction in the level of serum iron. Isotopically heavier iron stored in the liver or coming from the labile iron pool (LIB) is used to compensate for the reduced uptake. Also the iron uptake in the intestine is

upregulated, which is accompanied by a lower degree of isotope fractionation (known to favor the uptake of the lighter isotopes).

The serum Fe isotopic composition of the CKD patients with anemia but without iron depletion did not significantly differ from that of the CKD group with normal iron metabolism (Fig. 7-1). In this case, the anemia is the result of a reduced production of EPO in the kidneys and, as a consequence, a downgraded erythropoiesis in the bone marrow without shortage of iron supply, and no compensation by heavier iron stores from the liver takes place (Tf < 3.6 g/L, 20 < TSAT <50, 54 < Fer < 260 ng mL^{-1}). However, our data also show that in patients with CKD stage 3 or higher, heavier Fe isotopes prevail, and this is independent of the iron status. In the case of CKD, the blood filtration and reabsorption processes are affected, while the disease also might have an effect on the level of components involved in iron homeostasis (*e.g.* hepcidin).[39,40] It has been suggested recently that the kidneys are not only involved in the synthesis of hepcidin, but also in the elimination of this peptide[41,42], which can consequently affect intestinal iron absorption and release from store site (LIB, macrophages, and hepatocytes).[43] The combination of these factors might influence the Fe isotope fractionation and therefore to have an effect on the serum Fe isotopic composition. However, due to the complicated iron metabolism in patients with CKD,[39] further research is warranted to explore the source and cause of this shift.

7.4.3 Correlations with clinical parameters

A timely determination of the causes of anemia is important in the complex therapy of patients with stage 3-5 renal disease, especially in the elderly, but this can still be difficult for a number of technical and biological reasons.[44] There are no specific clinical or biochemical parameters to make the differential diagnosis of anemia in patients with CKD stage 3 or higher. A large set of biochemical parameters (about 10) are frequently determined for this purpose. The clinical conclusion concerning iron status is traditionally based on a combination of parameters, related to iron metabolism, and hematologic indices. Correlations between the serum Fe isotopic composition and the clinical parameters routinely used for diagnosis and follow-up of the CKD progression and those for iron status were evaluated. These clinical parameters and a summary of the information they provide are compiled in Table 7-2 (the individual correlations are provided in Supplementary Information,

Fig. 7-S1-S8). The individual data are provided in the Supplementary Information (Supplementary Information, Table 7-S2). Serum EPO measurement was not considered due to its poor ability to assess EPO-related anemia. Endogenous EPO is characterized by a short biological half-life, making the serum EPO level not very informative due to its biological variation.[45]

Table 7-2. Correlation between the serum Fe isotopic composition and clinical parameters used for the diagnosis of CKD and iron disorders.

Clinical parameter	Information	Correlation (95% confidence level)	
		Spearman's rho coefficient	2-tailed level of significance
Serum creatinine (SCr), mg dL^{-1}	Kidney filtration function	0.112	0.299
Estimated glomerular filtration rate (eGFR), mL min^{-1}per 1,73 m^2	Flow rate of fluid filtered through the kidney	-0.250	0.035
Serum Fe concentration, µg dL^{-1}	Concentration of circulating iron	-0.671	< 0.0001*
Hemoglobin (Hb), g dL^{-1}	Iron-containing oxygen-transporting metalloprotein in the red blood cells	-0.641	< 0.0001*
Ferritin (Fer), ng mL^{-1}	Iron storage status	-0.705	< 0.0001*
Transferrin (Tf), g L^{-1}	Body iron requirement	0.632	< 0.0001*
Total iron-binding capacity (TIBC), µg dL^{-1}	Potential capacity of transferrin molecules to bind serum iron	0.618	< 0.0001*
Transferrin saturation (TSAT), %	Actual amount of iron bound by transferrin	-0.786	< 0.0001*
Soluble transferrin receptor (sTfR), mgL^{-1}	Functional iron status	0.716	< 0.0001*
C-reactive protein (CRP), mg L^{-1}	Inflammation	0.331	0.043

* Significant correlation

As can be seen in Table 7-2, no obvious correlations were observed between the Fe isotopic composition and the CKD parameters, such as serum creatinine or eGFR. Also with C-reactive protein (CRP), no correlation was established. In contrast, the serum Fe isotopic

composition was clearly correlated with the iron status parameters. Transferrin, the total iron binding capacity (TIBC) and the level of soluble transferrin receptor (sTfR) reflect the body´s iron requirements. sTfR is related to erythropoiesis and is increased in patients with IDA. δ^{56}Fe values increase when these parameters increase. In the absence of inflammation, ferritin and TSAT (calculated based on the serum iron level and the iron-binding capacity), on the other hand, reflect the body´s iron store. δ^{56}Fe values increase when the levels of ferritin and TSAT decrease. Reduced ferritin and TSAT indicate activation of the iron stores to provide the required circulating iron and stimulation of intestinal iron uptake. The storage of iron, mainly in the liver, is known to be enriched in the heavy Fe isotopes,[28,31] while an increased intestinal uptake is characterized by a lower level of isotope fractionation, tentatively explaining the heavier serum Fe isotopic composition observed for ID and IDA patients (with/without CKD). In the case of EPO-related anemia, the uptake of iron from the gastrointestinal tract is down-regulated due to an increased hepcidin production and/or decreased renal clearance rate.[39,46] In addition to the parameters mentioned above, many other biochemical indexes are currently explored to evaluate the iron status,[20,22,27,44,47–51] such as the ratio of sTfR to the logarithm of the ferritin concentration, the ratio of the transferrin level to the logarithm of ferritin and the Thomas-plot (reticulocyte hemoglobin content *vs* the ratio of sTfR to the logarithm of the ferritin concentration). Investigation of a bone marrow biopsy is the gold standard method to assess stainable iron, but is highly invasive.[52] The benefit of the sTfR is that its level is unaffected by inflammation or infections, so that it allows to discriminate true from functional iron deficiency. The combination of information on the iron store (level of serum ferritin) and the Fe supply (soluble transferrin receptor) shows potential advantages for discriminating iron deficiency anemia from different other types of anemia, however it still can be affected by inflammatory status due to the use of the ferritin concentration.[47,48] This index correlated significantly with the iron isotopic composition (Spearman's rho coefficient 0.773, $p < 0.0001$). The higher values of sTfR/log Fer ratio, established for CKD patients with ID and IDA, correspond to a heavier serum Fe isotopic composition (ranging between -2.35‰ and -0.73‰).

In Fig. 7-2, a three-isotope plot of Fe (δ^{57}Fe *vs* δ^{56}Fe) is provided for the CKD patients and the reference population. As can be seen, the cohort of CKD patients with ID and IDA is clearly separated from those with EPO-related anemia (except one outlier), which coincides with the CKD-only cohort.

Multiple regression analysis was also performed to reveal the major drivers of the Fe isotope ratio variability. It was shown that delta value was only independently related to TSAT (β value of -0.026, p = 0.0002), sTfR (β value of 0.24, p = 0.0049) and ferritin (β value of -0.001, p = 0.0061). The multiple regression equation obtained was:

$$\delta^{56}Fe = -1.81\ (\pm\ 0.23) - 0.026\ (\pm\ 0.005)\cdot TSAT + 0.24\ (\pm\ 0.07)\cdot sTfR - 0.001(\pm\ 0.000)\cdot Fer \qquad (7\text{-}3)$$

The Fe isotopic composition in the population studied was governed by the TSAT, sTfR and Fer. This equation explained 70.1% of the variability in the Fe isotopic composition. The multiple adjusted R^2 obtained for the predictors (*i.e.* TSAT, sTfR and Fer) was 0.84 (F = 53, p < 0.000, n = 72) and the standard error of the estimate was 0.36.

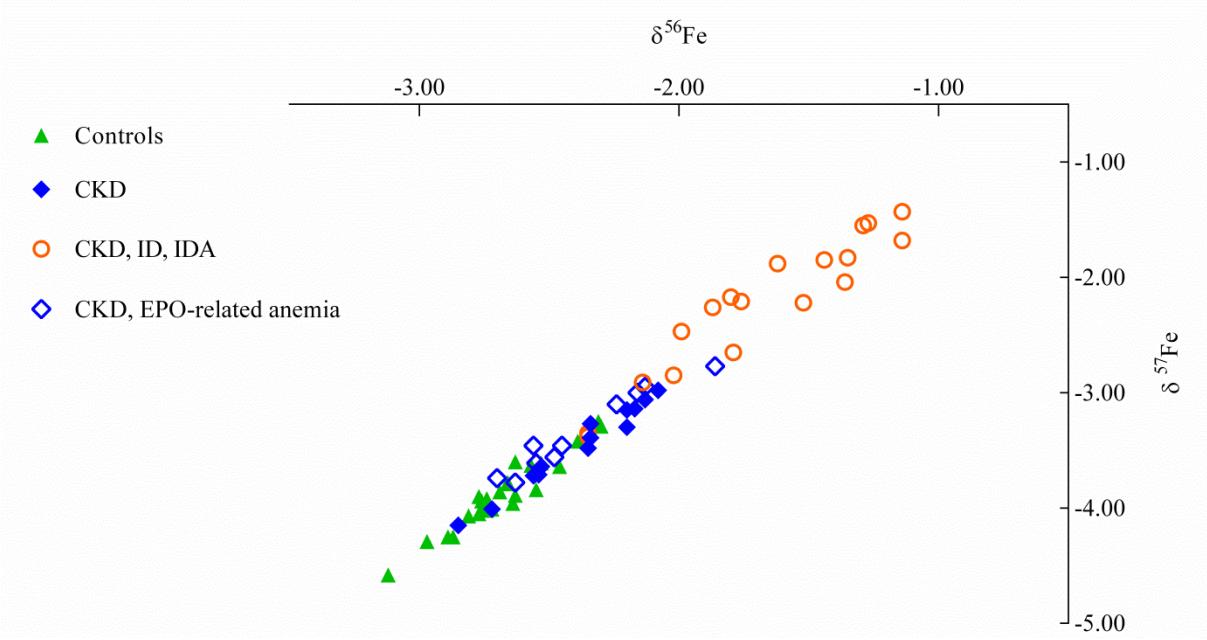

Fig. 7-2 Serum Fe isotopic composition for samples from the reference population, CKD patients, CKD patients complicated by ID and IDA and CKD patients with EPO-related anemia. The precision expressed as 2 s.d. is 0.07‰ for $\delta^{56}Fe$ and 0.12‰ for $\delta^{57}Fe$.

Thus, the serum isotopic composition of Fe shows a significant response to iron status in CKD. In this pilot study, the serum Fe isotopic composition was demonstrated to be a useful complimentary tool for revealing Fe-related complications in CKD without chronic inflammation.

7.5 CONCLUSIONS

High-precision Fe isotopic analysis of blood serum by MC-ICP-MS provided relevant clinical information on the iron status of patients with CKD stage 3 or higher. Patients suffering from CKD complicated with iron disorders (ID, IDA) showed a significantly heavier serum Fe isotopic composition than did patients suffering from CKD only. CKD patients suffering from EPO-related anemia did not show a significant difference in serum Fe isotopic composition compared to the cohort with CKD only. No significant correlations were found between the serum Fe isotopic composition and eGFR or serum creatinine levels, but δFe values showed strong positive correlation with Tf, TIBC, and sTfR levels and strong negative correlation with serum Fe concentration, Fer, Hb, and TSAT values. The Fe isotopic composition was also significantly correlated with sTfR/log Fer index, which is gaining interest as a sensitive index for ID/IDA. The factors governing the Fe isotopic composition in the population studied were TSAT, sTfR and Fer. The results obtained in this exploratory study indicate that Fe isotopic analysis can be a useful complimentary tool for distinguishing between IDA and EPO-related anemia in CKD patients.

7.6 ACKNOWLEDGEMENTS

The Flemish Research Foundation FWO-Vlaanderen is acknowledged for financial support through research project “G023014N”. Marta Costas- Rodríguez thanks FWO-Vlaanderen for her postdoctoral grant.

7.7 AUTHOR CONTRIBUTIONS

FV, MS and JD designed the study. YA carried out the sample preparation, elemental and isotopic analysis and data treatment. MS and JD performed the sampling and the determination of clinical data. YA wrote the initial manuscript. MCR contributed to data interpretation and writing. YA, MCR, MS, WVB, JD and FV participated in the discussion of the results and reviewed the final manuscript.

7.8 REFERENCES

1. Chawla, L. S. & Kimmel, P. L. Acute kidney injury and chronic kidney disease: an integrated clinical syndrome. *Kidney Int.* **82,** 516–524 (2012).
2. Levey, A. S. & Coresh, J. Chronic kidney disease. *Lancet* **379,** 165–180 (2012).
3. Cirillo, M. *et al.* Low glomerular filtration in the population: prevalence, associated disorders, and awareness. *Kidney Int.* **70,** 800–806 (2006).
4. Prakash, S. & O'Hare, A. M. Interaction of aging and chronic kidney disease. *Semin. Nephrol.* **29,** 497–503 (2009).
5. Corsonello, A. *et al.* Special considerations for the treatment of chronic kidney disease in the elderly. *Expert Rev. Clin. Pharmacol.* **9,** 727–37 (2016).
6. Shih, C.-T. *et al.* Changes in levels of copper, iron, zinc, and selenium in patients at different stages of chronic kidney disease. *Genomic Med. Biomarkers, Heal. Sci.* **4,** 128–130 (2012).
7. O'Hare, A. M. *et al.* Age affects outcomes in chronic kidney disease. *J. Am. Soc. Nephrol.* **18,** 2758–65 (2007).
8. Levey, A. S. *et al.* A new equation to estimate glomerular filtration rate. *Ann. Intern. Med.* **150,** 604–612 (2009).
9. Rossing, P. Doubling of serum creatinine: is it sensitive and relevant? *Nephrol. Dial. Transplant* **13,** 244–6 (1998).
10. Edelstein, C. L. Biomarkers of Acute Kidney Injury. *Adv. Chronic Kidney Dis.* **15,** 222–234 (2008).
11. Waikar, S. S., Betensky, R. A., Emerson, S. C. & Bonventre, J. V. Imperfect Gold Standards for Kidney Injury Biomarker Evaluation. *J. Am. Soc. Nephrol.* **23,** 13–21 (2012).
12. Stevens, P. E. & Levin, A. Evaluation and management of chronic kidney disease: Synopsis of the kidney disease: Improving global outcomes 2012 clinical practice guideline. *Ann. Intern. Med.* **158,** 825–830 (2013).
13. Hörl, W. H. Clinical aspects of iron use in the anemia of kidney disease. *J. Am. Soc. Nephrol.* **18,** 382–93 (2007).
14. Wish, J. B. Assessing iron status: beyond serum ferritin and transferrin saturation. *Clin. J. Am. Soc. Nephrol.* **1,** S4–S8 (2006).
15. Camaschella, C. Iron-Deficiency Anemia. *N. Engl. J. Med.* **372,** 1832–1843 (2015).
16. Babitt, J. L. & Lin, H. Y. Mechanisms of anemia in CKD. *J. Am. Soc. Nephrol.* **23,** 1631–4 (2012).
17. *Assessing the iron status of populations: including literature reviews. Report of a Joint World Health Organization/Centers for Disease Control and Prevention Technical Consultation on the Assessment of Iron Status at the Population Level*. (World Health Organization, 2007). at <http://www.who.int/nutrition/publications/micronutrients/anaemia_iron_deficiency/9789241596107/en/> Last accessed on 25/07/0217.
18. Thomas, D. W. *et al.* Guideline for the laboratory diagnosis of functional iron

deficiency. *Br. J. Haematol.* **161,** 639–648 (2013).

19. Astor, B. C., Muntner, P., Levin, A., Eustace, J. A. & Coresh, J. Association of Kidney Function With Anemia. *Arch. Intern. Med.* **162,** 1401 (2002).

20. Bermejo, F. A guide to diagnosis of iron deficiency and iron deficiency anemia in digestive diseases. *World J. Gastroenterol.* **15,** 4638 (2009).

21. Goddard, A. F., James, M. W., McIntyre, A. S. & Scott, B. B. Guidelines for the management of iron deficiency anaemia. *Gut* **60,** 1309–16 (2011).

22. Urrechaga, E., Borque, L. & Escanero, J. Assessing iron status in CKD patients: new Laboratory parameters. *Chronic Kidney Dis.* **30,** 225–250 (2012).

23. Locatelli, F. *et al.* Kidney Disease: Improving Global Outcomes guidelines on anaemia management in chronic kidney disease: A European Renal Best Practice position statement. *Nephrol. Dial. Transplant.* **28,** 1346–1359 (2013).

24. National Clinical Guideline Centre. *Anaemia Management in Chronic Kidney Disease*. *Anaemia Management in Chronic Kidney Disease: Partial Update 2015* (Royal College of Physicians (UK), 2015). at <http://www.ncbi.nlm.nih.gov/pubmed/26065064>. Last accessed on 25/07/0217.

25. National Institute for Health and Care Exellence. *Chronic kidney disease: managing anaemia. Guidance and guidelines. NICE*. (NICE, 2015). at <https://www.nice.org.uk/guidance/ng8?unlid=6344784542016101117293 1>. Last accessed on 25/07/0217.

26. Practice Guidelines for Iron Deficiency and Anemia in CKD. *Https://www.compact-renal.com/2016/05/19/practice-guidelines-iron-deficiency-anemia-ckd/*. (2016). at <https://www.compact-renal.com/2016/05/19/practice-guidelines-iron-deficiency-anemia-ckd/>. Last accessed on 25/07/0217.

27. Rimon, E. *et al.* Diagnosis of iron deficiency anemia in the elderly by transferrin receptor-ferritin index. *Arch. Intern. Med.* **162,** 445–9 (2002).

28. Krayenbuehl, P.-A., Walczyk, T., Schoenberg, R., von Blanckenburg, F. & Schulthess, G. Hereditary hemochromatosis is reflected in the iron isotope composition of blood. *Blood* **105,** 3812–3816 (2005).

29. Van Heghe, L., Delanghe, J., Van Vlierberghe, H. & Vanhaecke, F. The relationship between the iron isotopic composition of human whole blood and iron status parameters. *Metallomics* **5,** 1503–1509 (2013).

30. Costas-Rodríguez, M., Delanghe, J. & Vanhaecke, F. High-precision isotopic analysis of essential mineral elements in biomedicine: Natural isotope ratio variations as potential diagnostic and/or prognostic markers. *TrAC* **76,** 182–193 (2016).

31. Hotz, K., Krayenbuehl, P.-A. & Walczyk, T. Mobilization of storage iron is reflected in the iron isotopic composition of blood in humans. *J. Biol. Inorg. Chem.* **17,** 301–9 (2012).

32. Van Heghe, L., Engström, E., Rodushkin, I., Cloquet, C. & Vanhaecke, F. Isotopic analysis of the metabolically relevant transition metals Cu, Fe and Zn in human blood from vegetarians and omnivores using multi-collector ICP-mass spectrometry. *J. Anal. At. Spectrom.* **27,** 1327–1334 (2012).

33. von Blanckenburg, F. *et al.* An iron stable isotope comparison between human erythrocytes and plasma. *Metallomics* **6,** 2052–61 (2014).

34. Thomas, L. *Clinical laboratory diagnostics : use and assessment of clinical laboratory results*. (TH-Books, 1998).

35. Maréchal, C. N., Télouk, P. & Albarède, F. Precise analysis of copper and zinc isotopic compositions by plasma-source mass spectrometry. *Chem. Geol.* **156,** 251–273 (1999).

36. Vanhaecke, F. & Moens, L. Overcoming spectral overlap in isotopic analysis via single- and multi-collector ICP-mass spectrometry. *Analytical and Bioanalytical Chemistry* **378,** 232–240 (2004).

37. Baxter, D. C., Rodushkin, I., Engström, E. & Malinovsky, D. Revised exponential model for mass bias correction using an internal standard for isotope abundance ratio measurements by multi-collector inductively coupled plasma mass spectrometry. *J. Anal. At. Spectrom.* **21,** 427–430 (2006).

38. Jaouen, K. *et al.* Is aging recorded in blood Cu and Zn isotope compositions? *Metallomics* **5,** 1016–24 (2013).

39. Hamada, Y. & Fukagawa, M. Is hepcidin the star player in iron metabolism in chronic kidney disease? *Kidney Int.* **75,** 873–874 (2009).

40. Martines, A. M. F. *et al.* Iron metabolism in the pathogenesis of iron-induced kidney injury. *Nat. Rev. Nephrol.* **9,** 385–398 (2013).

41. Kulaksiz, H. *et al.* Pro-hepcidin: expression and cell specific localisation in the liver and its regulation in hereditary haemochromatosis, chronic renal insufficiency, and renal anaemia. *Gut* **53,** 735–43 (2004).

42. Malyszko, J., Malyszko, J. S., Pawlak, K. & Mysliwiec, M. Hepcidin, iron status, and renal function in chronic renal failure, kidney transplantation, and hemodialysis. *Am. J. Hematol.* **81,** 832–837 (2006).

43. Shah, S. V., Rajapurkar, M. M. & Baliga, R. The Role of Catalytic Iron in Acute Kidney Injury. *Clin. J. Am. Soc. Nephrol.* **6,** 2329–2331 (2011).

44. Goodnough, L. T., Skikne, B. & Brugnara, C. Erythropoietin, iron, and erythropoiesis. *Blood* **96,** 823–33 (2000).

45. Fisher, J. W. Erythropoietin: physiology and pharmacology update. *Exp. Biol. Med. (Maywood).* **228,** 1–14 (2003).

46. Ashby, D. R. *et al.* Plasma hepcidin levels are elevated but responsive to erythropoietin therapy in renal disease. *Kidney Int.* **75,** 976–81 (2009).

47. Punnonen, K., Irjala, K. & Rajamäki, A. Serum transferrin receptor and its ratio to serum ferritin in the diagnosis of iron deficiency. *Blood* **89,** 1052–1057 (1997).

48. Malope, B. I., MacPhail, A. P., Alberts, M. & Hiss, D. C. The ratio of serum transferrin receptor and serum ferritin in the diagnosis of iron status. *Br. J. Haematol.* **115,** 84–89 (2001).

49. Thomas, C., Kirschbaum, A., Boehm, D. & Thomas, L. The diagnostic plot: a concept for identifying different states of iron deficiency and monitoring the response to epoetin therapy. *Med. Oncol.* **23,** 23–36 (2006).

50. Leers, M. P. G., Keuren, J. F. W. & Oosterhuis, W. P. The value of the Thomas-plot in the diagnostic work up of anemic patients referred by general practitioners. *Int. J. Lab. Hematol.* **32,** 572–81 (2010).

51. Castel, R. *et al.* The transferrin/log(ferritin) ratio: a new tool for the diagnosis of iron

deficiency anemia. *Clin. Chem. Lab. Med.* **50,** 1343–9 (2012).

52. Wang, W., Knovich, M. A., Coffman, L. G., Torti, F. M. & Torti, S. V. Serum ferritin: Past, present and future. *Biochim. Biophys. Acta - Gen. Subj.* **1800,** 760–769 (2010).

7.9 SUPPLEMENTARY INFORMATION

Table 7-S1. Instrument settings and acquisition parameters for MC-ICP-MS Neptune (A) and SF-ICP-MS Element XR (B)

(A) Neptune MC-ICP-MS	
RF power (W)	1275
Guard electrode	Connected
Sample and skimmer cones	Thermo jet sampler and X-type skimmer, 1.1 and 0.8 mm of orifice diameter, respectively; Ni
Lens settings	Optimized for maximum Fe^{+}signal intensity
Ar flow-rates (L min^{-1}):plasma gas	15
auxiliary gas	0.75
nebulizer gas	0.9-1.0
Sample uptake rate (μL min^{-1})	100
Resolution mode	Medium (pseudo)
Acquisition mode	Static; multi-collection
Number of blocks	9
Number of cycles	5
Integration time (s)	4.194
Cup configuration	L4: ^{54}Fe; L2: ^{56}Fe; L1: ^{57}Fe; C: ^{58}(Fe+Ni); H1: ^{60}Ni; H3: ^{62}Ni
(B) Element XR SF-ICP-MS	
RF power (W)	1250
Guard electrode	Connected
Sample and skimmer cones	Ni, 1.1 mm and 0.8 mm orifice diameter
Lens settings	Optimized for maximum signal intensity
Ar flow-rates (L min^{-1}):	
plasma gas	15
auxiliary gas	0.8-0.9
nebulizer gas	1.0-1.1
Sample uptake rate (μL min^{-1})	200
Resolution mode	Low, medium, high
Acquisition mode	E-scan
Dwell time per point (ms)	10
Point per peak	20
Number of runs	5
Number of passes	5

Table 7-S2. Iron isotopic composition and clinical parameters in renal insufficiency and Fe disorders patients. SCr – serum creatinine, eGFR - estimated glomerular filtration rate, Hb – hemoglobin, [Fe] – Fe concentration in serum, Fer– ferritin, Tf – transferrin, TIBC - total iron-binding capacity, TSAT - transferrin saturation, sTfR - soluble transferrin receptor, CRP - C-reactive protein. Delta Fe values are expressed as average ± 2 s.d.

Diagnosis	Sample label	$\delta^{56}Fe$	SCr mg dL^{-1}	eGFR mL min^{-1} per 1.73 m^2	Hb g dL^{-1}	[Fe] µg dL^{-1}	Fer ng mL^{-1}	Tf g L^{-1}	TIBC[a] µg dL^{-1}	TSAT %	sTfR mg L^{-1}	CRP mg dL^{-1}
CKD, no anemia, no ID	1	-2.08 ± 0.03*	1.70	42.9	13.6	90	42	2.39	294	30	1.49	2.4
	2	-2.72 ± 0.01*	2.72	29.8	15.0	-	-	-	-	37	1.15	0.7
	3	-2.34 ± 0.04	2.55	36	15.1	93	91	2.39	294	31	1.67	2.8
	4	-2.54 ± 0.17*	2.05	31.9	14.3	102	95	3	369	27	1.19	5
	5	-2.53 ± 0.11*	2.35	25.5	13.0	76	253	1.94	238	31	1.2	8.3
	6	-2.34 ± 0.04	3.14	17.3	12.7	50	177	1.79	220	22	1.8	6
	7	-2.20 ± 0.08*	2.11	29.7	12.5	86	115	2.21	272	31	1.03	1.1
	8	-2.85 ± 0.05	1.62	40.9	13.1	88	176	2.16	265	32	1.46	2.1
	9	-2.13 ± 0.05	1.58	38.2	13.7	-	-	-	-	31	1.03	3.6
	10	-2.20 ± 0.05*	1.24	53	13.6	91	65	3.06	376	24	1.32	4.2
	11	-2.35 ± 0.12*	1.51	46	14.4	83	54	2.53	311	26	0.82	2.1
	12	-2.17 ± 0.04	1.96	36.2	12.7	73	177	2.64	324	22	1.24	<0.6
	13	-1.30 ± 0.04*	1.89	32.4	12.7	69	125	2.6	319	21	1.89	4.4
	14	-2.56 ± 0.06*	1.47	40.4	12.8	71	155	2.42	297	23	1.84	<0.6
CKD, no anemia, ID	15	-2.02 ± 0.02*	1.65	41.9	13.2	101	42	-	-	15	1.92	2.7
	16	-2.35 ± 0.03*	1.69	36.6	14.9	64	91	2.98	366	17	1.73	3.5
	17	-2.35 ± 0.14*	1.78	34.7	13.1	59	46	2.38	292	20	1.68	1
	18	-2.14 ± 0.03	2.19	27	17.7	68	130	3.19	392	17	-	2.5
	19	-1.29 ± 0.03	1.46	34	13.2	54	72	2.52	310	17	1.61	6.3

Diagnosis	Sample label	$\delta^{56}Fe$	SCr mg dL^{-1}	eGFR mL min^{-1} per 1.73 m^2	Hb g dL^{-1}	[Fe] µg dL^{-1}	Fer ng mL^{-1}	Tf g L^{-1}	TIBC[a] µg dL^{-1}	TSAT %	sTfR mg L^{-1}	CRP mg dL^{-1}
	20	-1.87 ±0.04*	1.43	43	12.7	28	75	3.55	436	6	3.02	11.1
	21	-1.44 ± 0.03	1.31	53	14.5	40	53	3.09	380	11	1.43	11.3
	22	-1.80 ± 0.03	1.31	51	13.1	20	13	3.15	387	5	-	1.8
	23	-1.62 ± 0.03	1.41	50	15.2	50	95	2.45	301	17	1.65	3.5
CKD, EPO-related anemia, no ID	24	-1.86 ± 0.04	1.60	39.8	12.1	102	54	2.74	336	30	1.24	3
	25	-2.48 ± 0.05	1.68	38.9	12.3	56	68	2.26	278	20	1.44	0.7
	26	-2.63 ± 0.02*	2.87	21.1	11.6	79	260	2.34	288	27	1.58	-
	27	-2.16 ± 0.03*	1.65	37	10.9	73	-	-	-	28	1.28	0.1
	28	-2.55 ± 0.13*	1.49	44.5	11.5	119	-	-	-	28	1.10	1.5
	29	-2.13 ± 0.04	2.19	30.5	11.2	98	220	2.58	317	30	1.05	<0.6
	30	-2.45 ± 0.04	2.49	28.7	11.1	43	-	-	-	21	2.83	18.5
	31	-2.56 ± 0.05*	2.48	23.3	11.6	66	60	2.72	334	20	1.37	0.2
	32	-2.24 ± 0.04	2.99	18.4	11.7	56	173	2.57	316	32	1.51	2
	33	-2.70 ± 0.05	6.44	8.3	9.9	61	243	2.03	249	24	1.26	0.9
CKD, IDA	34	-1.14 ± 0.05	1.73	40.5	10.9	41	33	2.83	348	11	1.76	-
	35	-1.52 ± 0.03	1.95	31	10.8	42	33	3.21	394	10	2.00	14.2
	36	-1.76 ± 0.06	1.67	42.1	11.2	31	-	3.03	372	8	2.74	0.4
	37	-0.73 ± 0.04	2.28	27	8.1	19	23	2.93	360	5	4.00	7.1
	38	-1.79 ± 0.03	2.26	28	10.0	39	10	3.30	405	10	2.23	6.5
	39	-2.09 ± 0.03	1.36	34	11.9	44	177	2.42	297	15	1.37	13
	40	-1.36 ± 0.03*	2.11	28	11.6	47	13	2.95	362	13	-	2

Diagnosis	Sample label	$\delta^{56}Fe$	SCr mg dL^{-1}	eGFR mL min^{-1} per 1.73 m^2	Hb g dL^{-1}	[Fe] µg dL^{-1}	Fer ng mL^{-1}	Tf g L^{-1}	TIBC[a] µg dL^{-1}	TSAT %	sTfR mg L^{-1}	CRP mg dL^{-1}
	41	-1.99 ± 0.06	1.44	50	9.4	11	180	1.83	225	5	2.26	31.4
	42	-1.14 ± 0.04	1.41	50	12.4	24	9	3.12	383	6	1.12	-
	43	-1.35 ± 0.04	1.43	49	9.4	39	11	3.83	471	8	2.20	<0.6
	44	-1.27 ± 0.03	0.95	54	11.5	25	111	1.90	233	11	2.69	8.3
ID	45	-2.76 ± 0.04	0.92	>90	13.8	49	446	2.13	262	18	1	0.7
	46	-2.13 ± 0.08*	0.81	>90	14.4	53	130	2.47	303	17	1.97	21
	47	-1.91 ± 0.09*	1.12	70	13.4	60	22	2.88	354	16	1.34	0.7
	48	-2.11 ± 0.05*	0.98	83	12.6	74	87	3.11	382	19	1.21	3.9
	49	-1.93 ± 0.05*	0.84	89	13.1	52	36	3.45	424	12	1.49	2.5
	50	-1.86 ±0.04	0.69	88	14.2	37	12	3.39	416	9	-	-
IDA	51	-1.29 ± 0.12*	1.26	61	11.9	28	20	3.01	370	7	-	2.8
	52	-1.80 ± 0.06*	0.95	82	11.9	41	10	3.41	419	9	2.66	<0.6
	53	-0.77 ± 0.03	0.88	86	8.6	18	6	3.00	369	4	4.42	4.5
	54	-1.80 ± 0.03	0.76	76	10.3	45	37	3.05	375	12	-	-
	55	-0.32 ± 0.03	0.83	>90	10.3	16	9	2.89	355	5	3.18	2.8
	56	-0.86 ± 0.06	0.98	70	7.5	9	7	3.21	394	2	3.82	<0.6
	57	-1.51 ± 0.04	1.05	67	7.5	18	10	3.36	413	4	3.82	4.5
Normal values			*0.6 - 1.2*	*> 90*	*> 12.5*	*65 - 177*	*15-200*	*2 - 3.6*	*280 - 436*	*20 - 45*	*1.8 - 4.6*	*< 0.6*

[a] TIBC calculated according to H. Yamanishi et al. Clin. Chem 2003, 175-178.

- No data available

* Data based on duplicate measurement

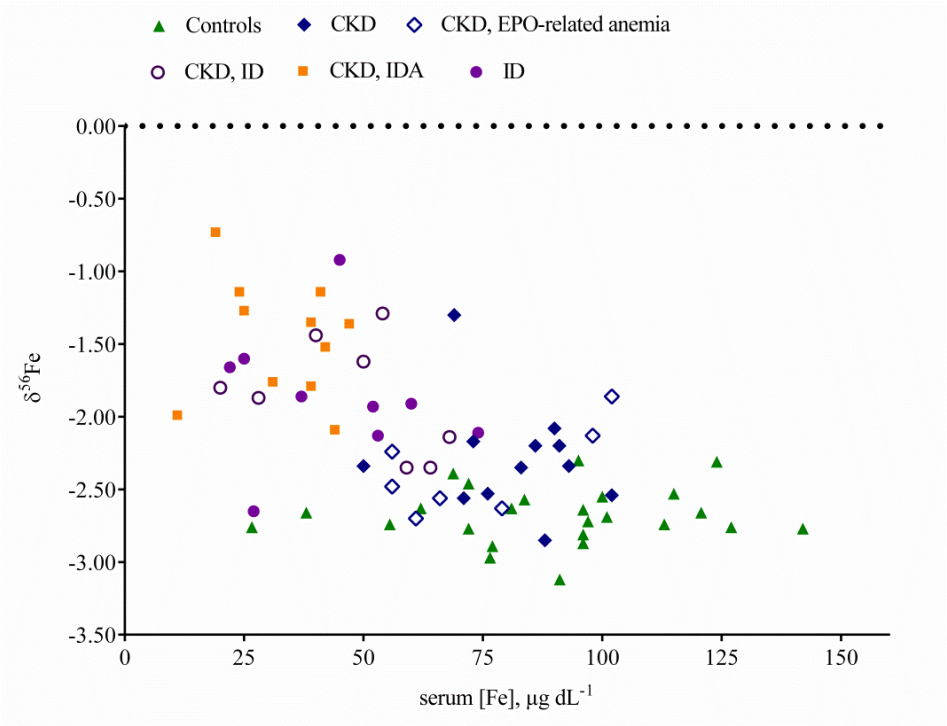

Fig. 7-S1 Isotopic composition of Fe in blood serum as a function of serum Fe concentration from a reference population and from patients with CKD and/or a disorder of iron metabolism.

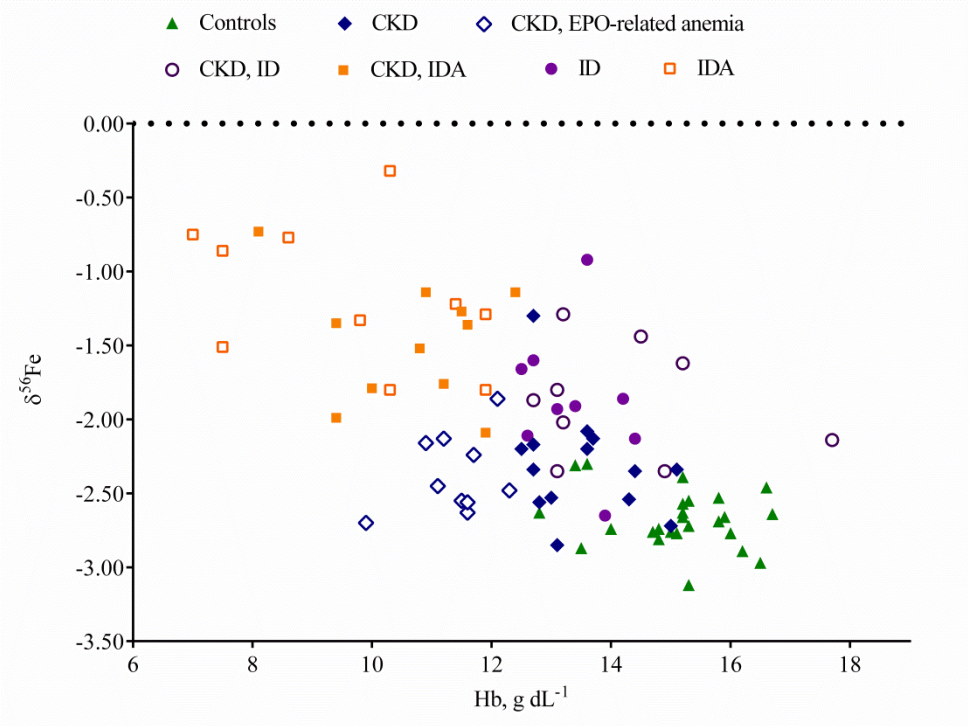

Fig. 7-S2 Isotopic composition of Fe in blood serum as a function of hemoglobin concentration from a reference population and from patients with CKD and/or a disorder of iron metabolism.

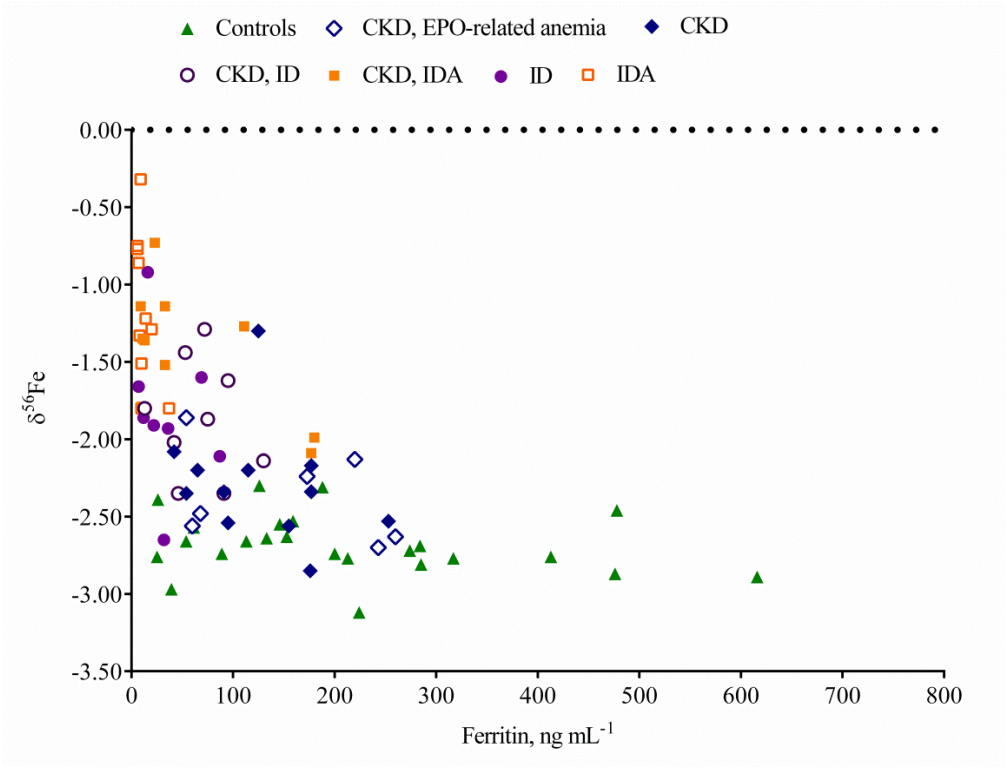

Fig. 7-S3 Isotopic composition of Fe in blood serum as a function of serum ferritin concentration from a reference population and from patients with CKD and/or a disorder of iron metabolism.

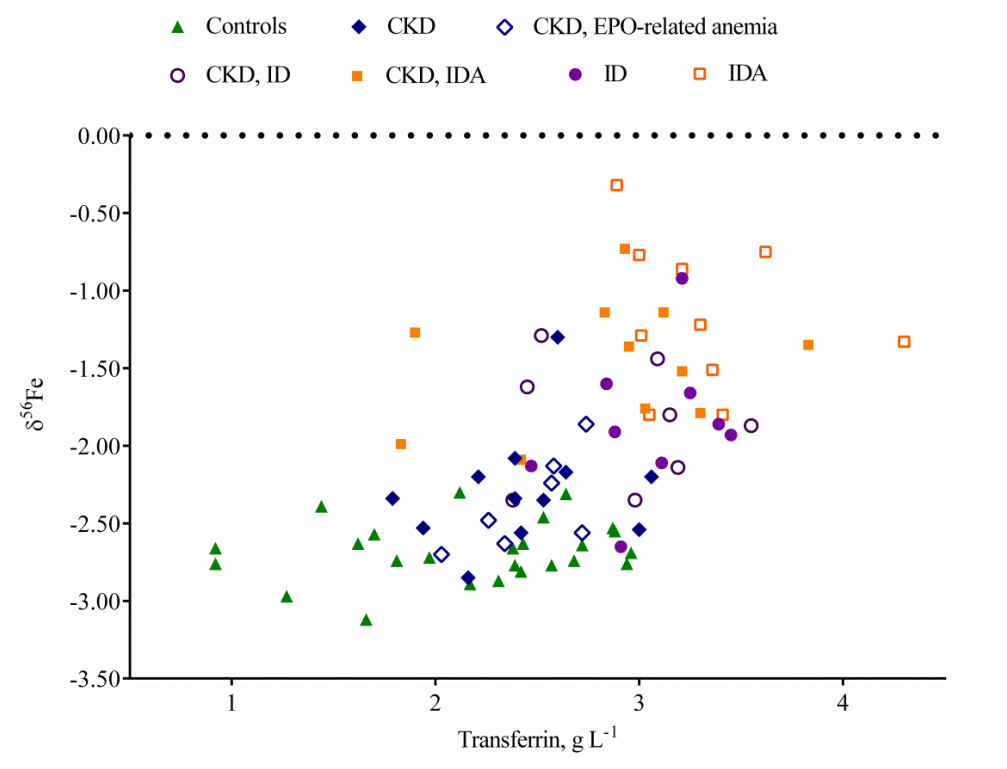

Fig. 7-S4 Isotopic composition of Fe in blood serum as a function of serum transferrin concentration from a reference population and from patients with CKD and/or a disorder of iron metabolism.

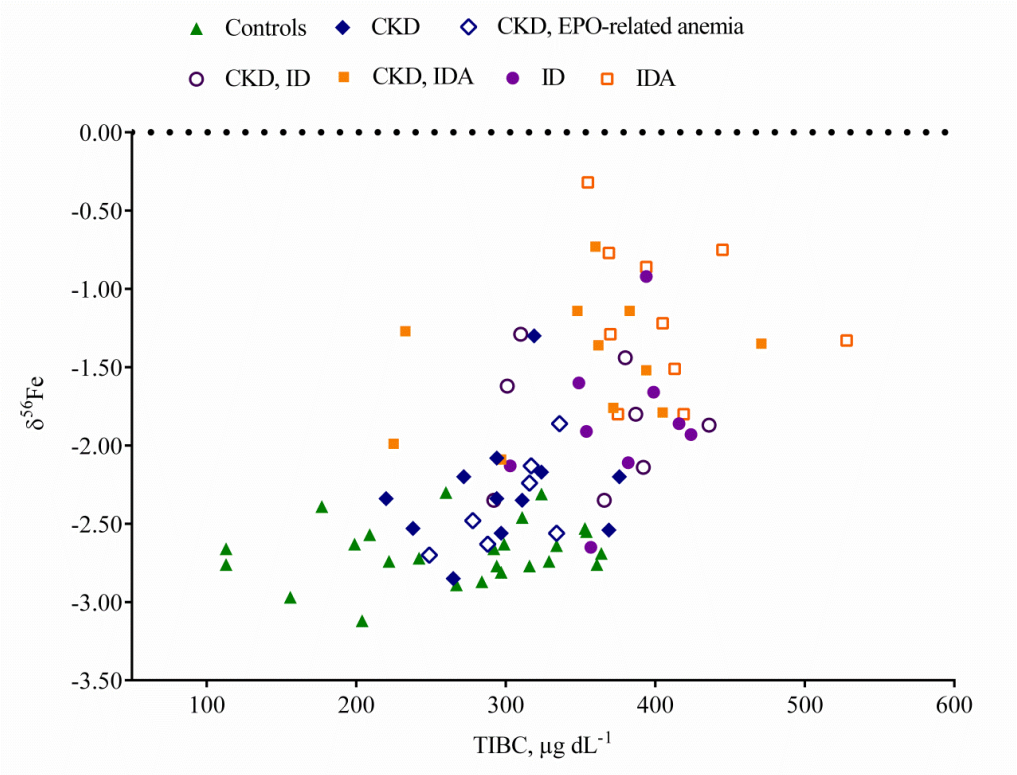

Fig. 7-S5 Isotopic composition of Fe in blood serum as a function of total iron-binding capacity (TIBC) from a reference population and from patients with CKD and/or a disorder of iron metabolism

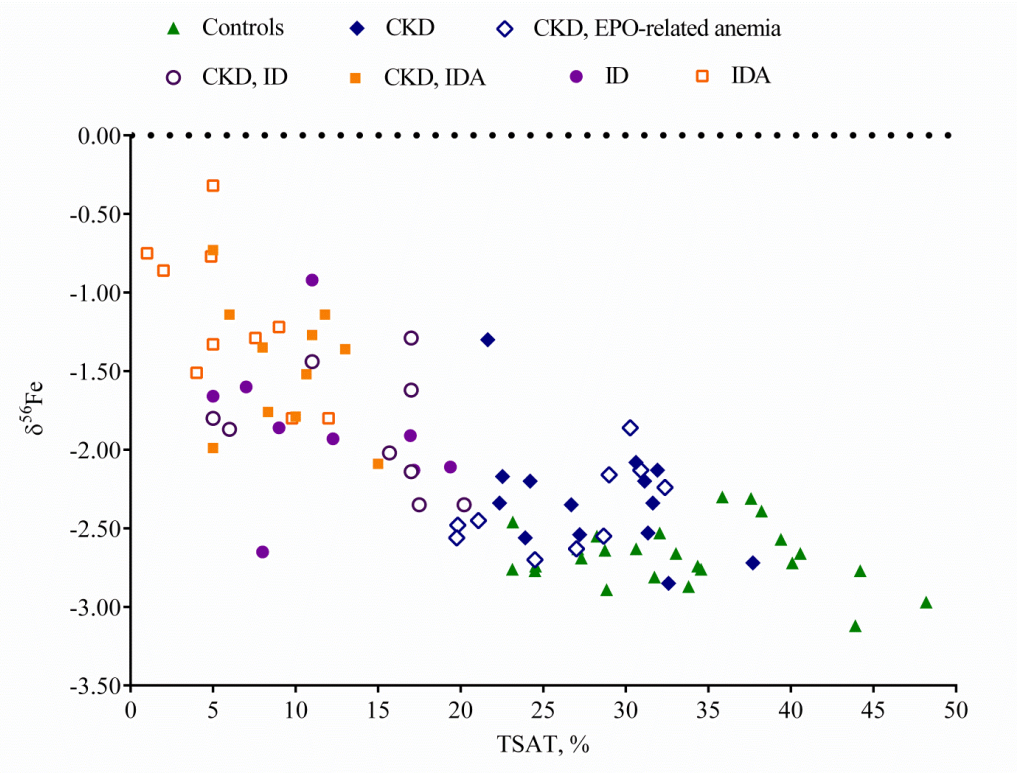

Fig. 7-S6 Isotopic composition of Fe in blood serum as a function of transferrin saturation (TSAT) from a reference population and from patients with CKD and/or a disorder of iron metabolism

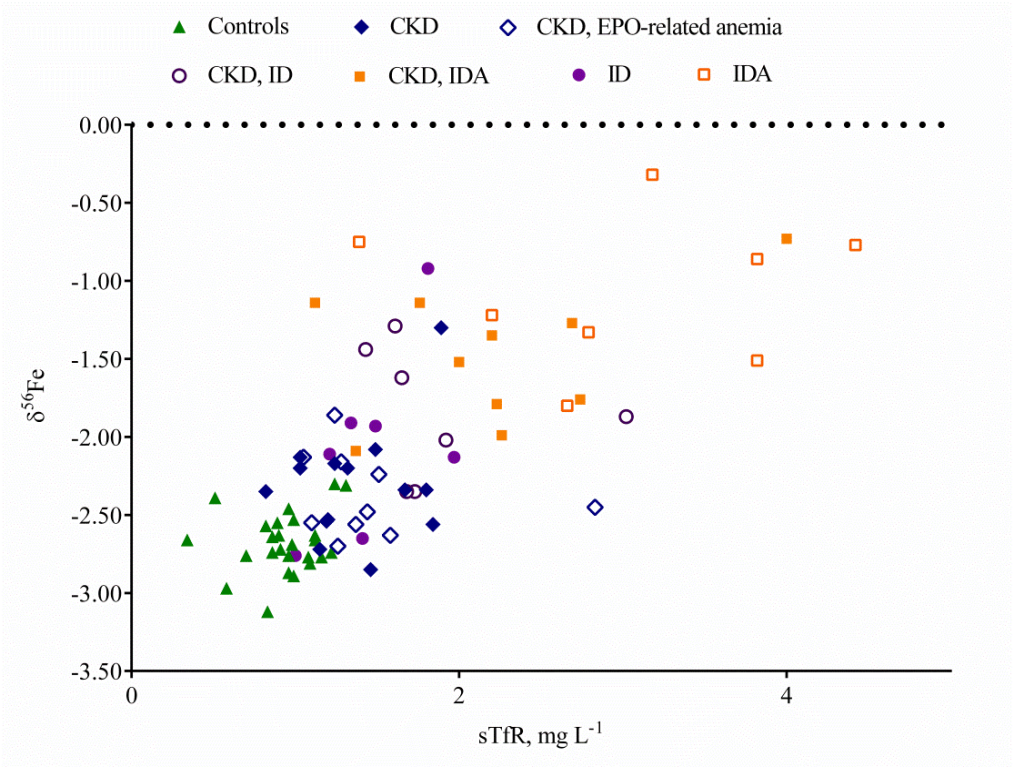

Fig. 7-S7 Isotopic composition of Fe in blood serum as a function of soluble transferrin receptor from a reference population and from patients with CKD and/or a disorder of iron metabolism.

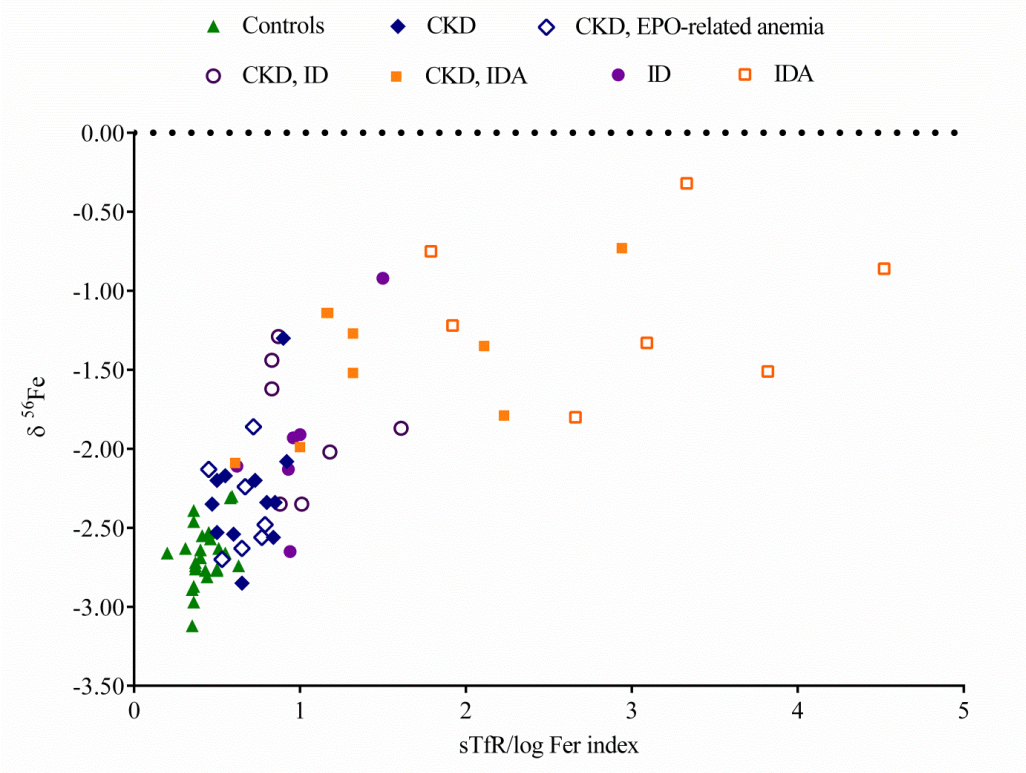

Fig. 7-S8 Isotopic composition of Fe in blood serum as a function of soluble transferrin / log ferritin index from a reference population and from patients with CKD and/or a disorder of iron metabolism.

SUMMARY AND CONCLUSIONS

By developing two analytical approaches that allow the sample preparation prior to high-precision isotopic analysis of Fe *via* multi-collector - inductively coupled plasma - mass spectrometry (MC-ICP-MS) to be simplified and therefore, the sample throughput to be increased, a first goal of this PhD was achieved. A second goal of this PhD then consisted of application of the analytical methods developed for high-precision isotopic analysis of Fe in human whole blood and serum in a real-life biomedical context.

It is clear that MC-ICP-MS provides significantly more precise isotope ratio data than other ICP-MS techniques, but the availability of the equipment is an important issue. In **Chapter 2**, the suitability of single-collector SF-ICP-MS in the context of a human absorption study using isotopically enriched iron isotopic tracers was demonstrated. A good agreement between the results for the enrichments in ^{57}Fe and ^{58}Fe in whole blood samples as obtained using SF-ICP-MS and MC-ICP-MS was achieved. Since a minimum of 5% oral iron absorption is expected for any worthwhile supplementation strategy, SF-ICP-MS can be considered as a suitable technique for the routine determination of iron absorption in human iron supplementation studies, offering the possibility to track down changes down to 0.3% and 0.6% for $^{57/54}$Fe and $^{58/54}$Fe, respectively. However, it cannot be used for the measurement of natural Fe isotope ratio variations due to the significantly lower precision.

In **Chapter 3**, the direct isotopic analysis of whole blood iron after acid digestion and adequate dilution (0.75 - 1.5 mg L^{-1} of Fe) of the sample digest without chromatographic Fe separation from the matrix was demonstrated to be a viable alternative to the traditional sample pre-treatment preceding MC-ICP-MS measurements. Results obtained in such way have to be corrected for instrumental mass discrimination using a combination of internal correction with ^{62}Ni/^{60}Ni as an internal standard and external correction in a standard-sample bracketing approach. As a result, chromatographic Fe isolation preceding the MC-ICP-MS Fe

isotope ratio measurements can be avoided. This simple methodology allows to increase the sample throughput and reduce the amount of acids, cost and time required. However, long term use of this method has to be further evaluated as it might lead to overburdening of the instrument. The suggested approach can, however, already be relevant for specific clinical applications that require a prompt response.

In **Chapter 4**, another methodology, using the volumetric absorptive microsampling (VAMS) technique for blood sampling and a miniaturized anion exchange protocol for the separation of iron from the blood matrix, was developed. Accurate and precise isotope ratio data were obtained using 1 mL of Milli-Q water as extraction solution for liberating the iron from the VAMS tip, followed by acid digestion. The stability of the VAMS-collected whole blood was evaluated under different storage conditions and it has been shown that the Fe isotopic composition and Fe concentrations are not affected during a period of at least 28 days when the VAMS device is stored at room temperature and during a period of at least 4 days when it is stored at 60 °C, 4 °C or -20 °C. The validated methodology was used to assess the Fe isotopic composition of finger-prick blood, which was compared to that of simultaneously collected venous whole blood. No differences in the Fe isotopic composition or Fe concentration were observed between finger-prick and venous blood. This approach greatly enhances the sample throughput and highly reduces the amount of reagents required and therefore, it is beneficial in terms of time and cost. The results obtained for the VAMS-collected finger-prick blood samples demonstrated this approach to be suitable for further clinical applications.

For a better understanding of the origin of the Fe isotope fractionation in the human body, some *in vitro* and *in vivo* models were studied. An enterocyte model using the Caco-2 cell line was used to study intestinal iron absorption as a major source of isotope fractionation in the human body. In **Chapter 5**, the preferential uptake of lighter iron isotopes from a non-heme iron source at the luminal (apical) membrane and the preservation of the heavier isotopes in ferritin form inside the cells during transport across the basolateral membrane of erythrocytes were demonstrated. These results were in good agreement with previously reported data showing that the Fe isotopic composition of the blood and intestinal mucosa was lighter than that of the diet. The optimum experimental conditions obtained in this study provided results with a low contribution from the blank and good repeatability and reproducibility, thus, providing reliable results for the Fe isotopic compositions of the separate compartments.

Another possible source of natural Fe fractionation, is the multiple biochemical changes that erythrocytes undergo during their life span. The possible effect of these changes on the isotopic composition of whole blood was investigated and the corresponding results reported in **Chapter 6**. The erythrocytes were separated according to their density, which corresponds to their age due to their gradual decrease in diameter and corpuscular volume. This separation was accomplished using two methods, one based on centrifugation and another using a mixture of phthalates. The results obtained for young and senescent red blood cells using both methodologies suggest the absence of measurable differences in the Fe isotopic composition between them and thus, the results indicate that no significant fractionation takes place as a result of *in vivo* aging of erythrocytes. These findings support the hypothesis that fractionation mainly occurs during intestinal absorption and during processes of iron release and uptake by ferritin.

The possibility of using the Fe isotopic composition of blood serum as a tool for identification of Fe-related disorders was demonstrated in **Chapter 7** for patients with kidney insufficiency. It has been demonstrated that high-precision Fe isotopic analysis of blood serum by MC-ICP-MS provided relevant clinical information on the iron status of a male cohort of patients with CKD stage 3 or higher and without chronic inflammation. Patients suffering from CKD complicated with the iron disorders ID and IDA showed a significantly heavier serum Fe isotopic composition than did patients suffering from CKD only. The isotopic composition of serum obtained from CKD patients suffering from EPO-related anemia did not show a significant difference compared to the cohort with CKD only. Delta Fe values showed strong correlations with the individual's iron status parameters such as (i) serum transferrin concentration, total iron-binding capacity, and soluble transferrin receptor, reflecting the iron supply, and (ii) the concentrations of ferritin and hemoglobin and the transferrin saturation, reflecting the iron store. A three-isotope plot clearly demonstrated the utility of the serum Fe isotopic composition to distinguish between IDA and EPO-related anemia.

The promising results promote a raise of the interest in natural variations of the isotopic composition of essential metals, such as iron, in human (bio)fluids and tissues related to disorders. Based on results for the Fe isotopic composition in human body fluids and tissues in health and disease, obtained in previous studies and this one, it can be concluded that the differences between individuals reflect the differences in iron absorption efficiency (which, in turn, can be altered due to different disorders). The preferential uptake of lighter iron isotopes

was demonstrated along a variety of studies, carried out previously or in the context of this PhD and based on a comparison of the isotopic compositions of food and whole blood, on animal models or on an intestinal cell model.

Studying natural isotopic variations for essential mineral elements in the context of biomedical applications is an important research line at the A&MS group of Ghent university. The final aim of this research line is to develop alternative approaches or potential biomarkers for the early diagnosis of diseases that can otherwise only be revealed at a later stage or using more invasive methods (such as a biopsy) and/or for prognosis. Information on isotope fractionation in the human body can also provide a more profound insight into the metabolism of metabolically relevant transition metals, such as iron. Studying the processes involved in the quite complex human iron metabolism in detail using *in vitro* and *in vivo* models provides important information on the sources of Fe isotopic variation, which can be further used to explain alterations in the isotopic composition of Fe in human blood/serum from patients suffering from disorders affecting iron metabolism. Although the methods developed in this PhD can still not be immediately used as a diagnostic tool in daily clinical practice, the findings contribute to a better understanding of human iron metabolic processes under specific medical conditions, such as iron deficiency anemia and EPO-related anemia. Although, this research has made significant steps forward, further research is required to further explore the sources of Fe isotopic variations related to different medical conditions. For instance, studying ID and anemia caused by inflammation (functional ID and ACD) would be a logical further step to take to evaluate the utility of Fe isotopic analysis for studying Fe-related complications in patients with renal insufficiency. Moreover, studying the change in the serum / whole blood Fe isotopic composition in response to specific disorders for both genders will provide information on threshold values for diagnosis. In general, the combination of extensive *in vivo* and *in vitro* experimental research, theoretical modeling, the use of mass balances and of mixing calculations are also necessary to improve our insight into iron metabolism and related disorders.

ACKNOWLEDGEMENTS

"The journey of a thousand miles begins with one step"

LaoTzu

Writing this thesis was a summarizing step of the last four years. However, this PhD was not only my merit and would not be accomplished without the input and help from a lot of people.

First and foremost, I would like to express my gratitude to my supervisor, Prof. Dr. Frank Vanhaecke, for giving me the opportunity to start a PhD in his group. The time when I was visiting A&MS group for just a week in April 2013 changed my life completely. I was so amazed by the lab and people working there, that there were no doubts about starting a PhD. Dear Frank, thank you for the support and your believe in me! Even in situations, when I was so down due to difficulties related to several projects, you always found words or jokes to cheer me up. There are no words to express my gratitude to such an outstanding supervisor. You always made right suggestions that were very useful to sharpen the ideas and conclusions drawn from the obtained results. You always will be a role model of a great leader for me.

I would like to thank Prof. Dr. Karel Strijckmans for the professional guidance of the department and help in solving administration issues.

I sincerely say a word of gratitude to Prof. Dr. Joris Delanghe for the medical explanations, for the opportunity to perform RBCs separation in his lab at UZ Gent, helping with sample collection and regular need of centrifugation of blood any time during these last four years, as well as giving a critical sight on interpretation of the results.

I express my gratitude towards all the people involved in projects that I participated in during the last four years. I want to acknowledge Prof. Dr. Marijn Speeckaert for the help in sample

collection and discussion for CKD project. I would like also to thank Prof. Dr. John Van Camp and Dr. Charlotte Grootaert for collaboration in Caco-2 cell line project. It was a pleasure to learn something totally new.

I want to thank all the PhD students, postdoctoral fellows and staff members I worked with since October 2013 at the S12. Many thanks to Chantal, Tine and Ingrid for the help solving any administrative and bureaucratic problems. Harry, Jorge and Davy were always ready to solve and prevent technical problems, and keeping the good functioning of our ICP-MS devices. I also want to acknowledge Philip for quick response on solving computer related issues. During past four years I had pleasure to meet and work with such wonderful people in A&MS group. Lieve, Karen, Sara, Eduardo, Balázs, Stepan, Augustina, Veerle, Lana, Sanwang, Michaela, Ana, Steven, Asha, Kris, Rosa, Stijn, Andrey, Thibaut, Marta, Lara, Charo, Winfried, you are great guys. Guys from the other groups in S12, we had a nice conversation during lunch breaks and it was always a lot of fun during team-building activities. Alessia, thank you for support, friendship and a great company in the thorny way of learning Dutch. I wish to all of you a big success in your life path! And thanks to technologies, I can always refresh my memories about our team-building, Amadeus-time, pizza nights and bowling by looking at the photos. It has been a pleasure for me to be a member of the A&MS group and Analytical chemistry department.

I would like to thank individually Andrey Izmer for helping me out from the very beginning, starting from that one week of my visit in A&MS. Based on his stories and experience, I got a great portion of the enthusiasm. Lieve Balcaen, you were the first person I met in S12 and I still remember how nervous I was. I want to say apart words of gratitude to Marta Costas-Rodríguez. Thank you for helping to survive days of Neptune measurements in the beginning of my way in A&MS, being involved in the topics, and input in publications. Stepan Chernonozhkin, the world is so small! It was such a surprise and pleasure to have a person in next-door office who is basically your neighbour (in Russian distance scale) in the Motherland Russia. Balázs Klencsár, thank you for the help with statistics and lesson of HPLC! I was very lucky to have such great office mates as Lana, Michaela and Sanwang. Thank you, girls! Kris, thank you for the technical support with Neptune and organization of events in S12 (together with Sylvia) and talks during the coffee breaks. Apart, special thanks for Stepan, Balázs, Thibaut, Stijn and Jens for being volunteers to bravely donate some blood in order to help me with VAMS project.

Apart from the colleagues, I want to thank sincerely my friends and family. Anastasia Portasenok and Rita Santos Sobral, you were the ones who listened to all my ideas as much as all my complains during this time. Thank you for supporting and cheering me up! There are no enough words to say how thankful I am to my family, who always supported me in all endeavors. It is hard to be 6000 km away from the family, but I always feel your care about me. Мама, спасибо за поддержку и бесконечную веру в меня!

And last, but not least, I want to say that I did not exaggerate in the beginning of this text saying that living in Belgium has changed my life. It indeed has been changed. Aside from great professional experience, my life has gained another momentum after meeting Jens. Thank you for your continued support and believe in me. You are the person who has always been by my side, no matter what! So I have another reason to thank the universe for being in Belgium.

Yulia Anoshkina

Ghent, August 2017

APPENDIX A

THE MAIN BIOMEDICAL INDICATORS OF IRON STATUS AND KIDNEY FUNCTION

Clinical parameter	Indication for	Commonly used methods
Transferrin saturation (TSAT), %	percentage of iron bound to transferrin.	Calculated from[1]: $$TSAT = \frac{Serum\ iron\ (\mu mol\ L^{-1})}{TIBC\ (\mu mol\ L^{-1})} \cdot 100$$ or $$TSAT = \frac{Serum\ iron\ (\mu mol\ L^{-1})}{Serum\ transferrin\ (g\ L^{-1})} \cdot 3.98$$
Total iron-binding capacity (TIBC), µg dL^{-1}	maximum amount of iron needed to saturate plasma or serum transferrin	Colorimetric assay of amount of iron that can be bound to unsaturated transferrin *in vitro*; determination from transferrin concentration measured immunologically (serum or plasma)[1,2] the theoretical ratio of TIBC to Tf is: TIBC (µmol L^{-1}) = 25.1·Tf (g L^{-1}) or TIBC (µg dL^{-1}) = Tf (g L^{-1}) /0.008
Ferritin (Fer), ng mL^{-1}	"size" of the iron stores	Immunoassay, *e.g.*, enzyme-linked immunosorbent assay (ELISA) or immunoturbidometry (serum or plasma)[1]

Clinical parameter	Indication for	Commonly used methods
Transferrin (Tf), g L^{-1}	body iron requirement	Immunoassay, *e.g.*, ELISA or immunoturbidometry (serum or plasma)
Soluble transferrin receptor (sTfR), mgL^{-1}	functional iron status	Immunoassay, *e.g.*, ELISA or immunoturbidometry (serum or plasma)[1]
Hemoglobin (Hb), g dL^{-1}	iron-containing oxygen-transporting metalloprotein in the red blood cells	Cyanmethemoglobin using colorimeter or spectrophotometer or as azide-methhemoglobin using, *e.g.*, HemoCue® (whole blood)[1]
Serum Fe concentration, µg dL^{-1}	concentration of circulating iron	Colorimetry
Serum creatinine (SCr), mg dL^{-1}	kdney filtration function	Colorimetric or fluorometric tests (serum or plasma)
Estimated glomerular filtration rate (eGFR), mL min^{-1}per 1,73 m^2	flow rate of fluid filtered through the kidney	Calculated according to:[3] MDRD (Modification of Diet in Renal Disease) equation for standardized serum creatinine: $GFR = 175 \cdot Scr^{-1.154} \cdot age^{-0.203} \cdot 1.212$ (if black race) $\cdot 0.742$ (if female) CKD-EPI (Chronic Kidney Disease Epidemiology Collaboration) equations: *a) White or other race:* female and Scr ≤ 0.70 mg dL^{-1} : $GFR = 144 \cdot (Scr/0.7)^{-0.329} \cdot (0.993)^{age}$ female and Scr > 0.70 mg dL^{-1} : $GFR = 144 \cdot (Scr/0.7)^{-1.209} \cdot (0.993)^{age}$ male and Scr ≤ 0.90 mg dL^{-1} : $GFR = 141 \cdot (Scr/0.9)^{-0.411} \cdot (0.993)^{age}$ male and Scr >0.90 mg dL^{-1} : $GFR = 141 \cdot (Scr/0.9)^{-1.209} \cdot (0.993)^{age}$ *b) Black race* female and Scr ≤ 0.70 mg dL^{-1} : $GFR = 166 \cdot (Scr/0.7)^{-0.329} \cdot (0.993)^{age}$ female and Scr > 0.70 mg dL^{-1} : $GFR = 166 \cdot (Scr/0.7)^{-1.209} \cdot (0.993)^{age}$ male and Scr ≤ 0.90 mg dL^{-1} : $GFR = 163 \cdot (Scr/0.9)^{-0.411} \cdot (0.993)^{age}$ male and Scr >0.90 mg dL^{-1} : $GFR = 163 \cdot (Scr/0.9)^{-1.209} \cdot (0.993)^{age}$ *where age is expressed in years and standardized serum creatinine (Scr) in mg dL^{-1}*

Clinical parameter	Indication for	Commonly used methods
C-reactive protein (CRP), mg L^{-1}	inflammation	Immunoassay (*e.g.*, ELISA), colorimetry (serum or plasma)

1. *Assessing the iron status of populations: including literature reviews. Report of a Joint World Health Organization/Centers for Disease Control and Prevention Technical Consultation on the Assessment of Iron Status at the Population Level*. (World Health Organization, 2007). at <http://www.who.int/nutrition/publications/micronutrients/anaemia_iron_deficiency/9789241596107/en/>
2. Yamanishi, H., Iyama, S., Yamaguchi, Y., Kanakura, Y. & Iwatani, Y. Total iron-binding capacity calculated from serum transferrin concentration or serum iron concentration and unsaturated iron-binding capacity. *Clin. Chem.* **49,** 175–178 (2003).
3. Levey, A. S. *et al.* A new equation to estimate glomerular filtration rate. *Ann. Intern. Med.* **150,** 604–612 (2009).

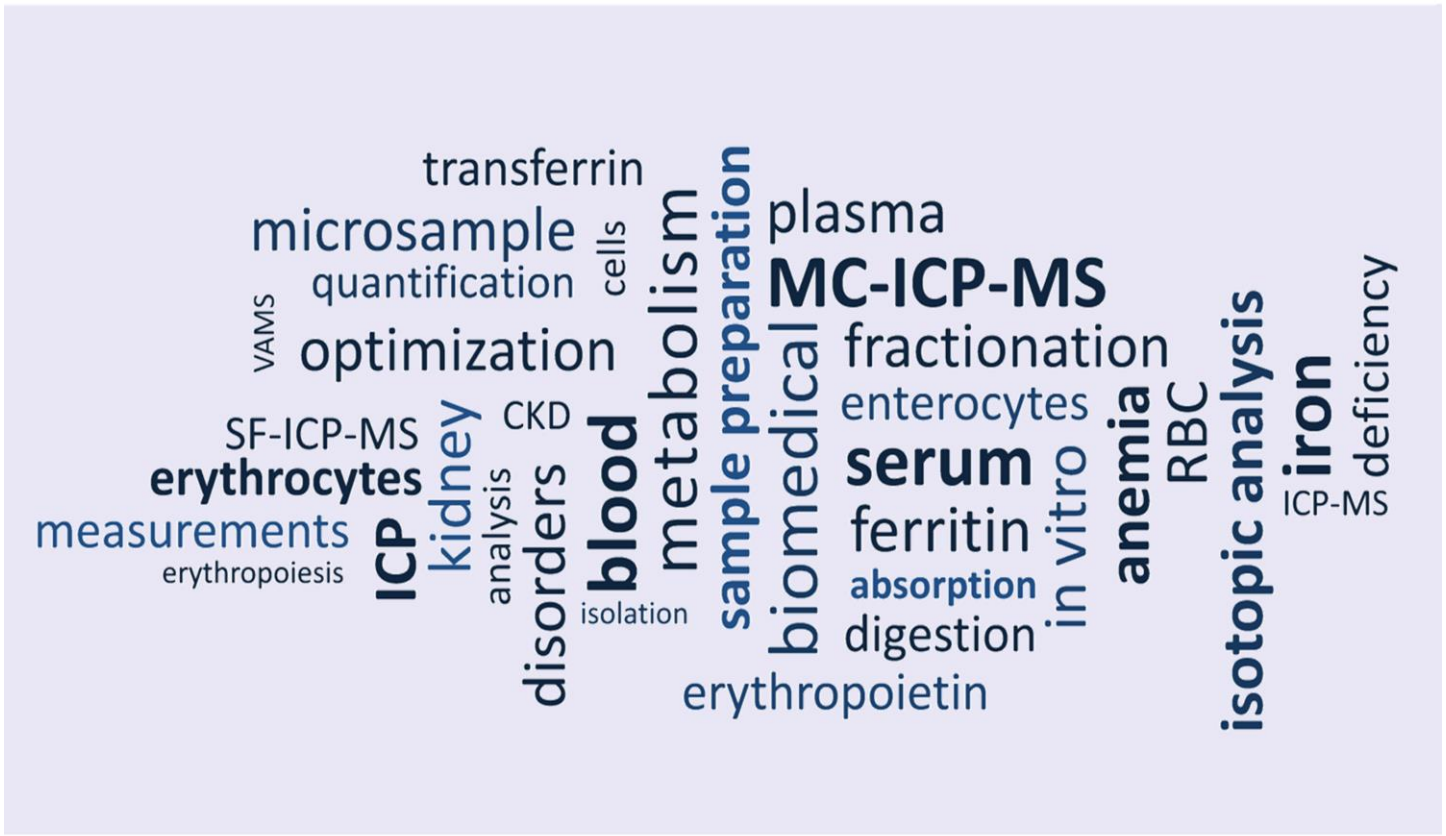

GHENT UNIVERSITY

A&MS Atomic and Mass Spectrometry

FACULTY OF SCIENCES